January 2017

Epigenetic Remodeling As A Mediator Of Environmental Toxicant Exposure In The Brain

Christopher David Walden

Follow this and additional works at: https://commons.und.edu/theses

EPIGENETIC REMODELING AS A MEDIATOR OF ENVIRONMENTAL
TOXICANT EXPOSURE IN THE BRAIN

by

Christopher David Walden
Bachelor of Science, University of North Dakota, 2010

A Dissertation

Submitted to the Graduate Faculty

of the

University of North Dakota

in partial fulfillment of the requirements

for the degree of

Doctor of Philosophy

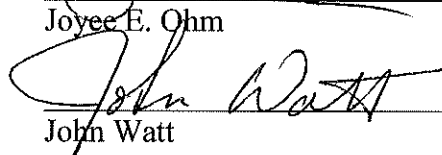Grand Forks, North Dakota

August
2017

This dissertation, submitted by Christopher David Walden in partial fulfillment of the requirements for the Degree of Doctor of Philosophy from the University of North Dakota, has been read by the Faculty Advisory Committee under whom the work has been done and hereby approved.

_____
Jonathan D. Geiger
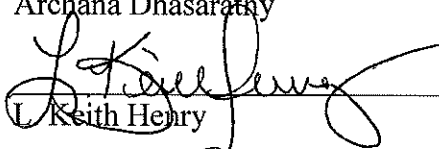
_____
Joyce E. Ohm

_____
John Watt

_____
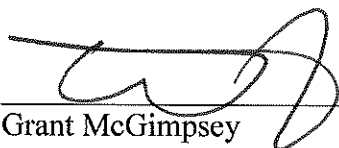Archana Dhasarathy

_____
L. Keith Henry

_____
Diane Darland

This dissertation is being submitted by the appointed advisory committee as having met all of the requirements of the School of Graduate Studies at the University of North Dakota and is hereby approved.

_____
Grant McGimpsey
Dean of the Schoool of Graduate Studies
Vice President for Research & Economic Development

_____
July 27, 2017
Date

PERMISSION

Title   Epigenetic remodeling as a mediator of environmental toxicant exposure
          in the brain

Department   Biomedical Sciences

Degree   Doctor of Philosophy

In presenting this dissertation in partial fulfillment of the requirements for a graduate degree from the University of North Dakota, I agree that the library of this University shall make it freely available for inspection. I further agree that permission for extensive copying for scholarly purposes may be granted by the professor who supervised my dissertation work or in his absence, by the Chairperson of the department or the dean of the School of Graduate Studies. It is understood that any copying or publication or other use of this dissertation or part thereof for financial gain shall not be allowed without my written permission. It is also understood that due recognition shall be given to me and to the University of North Dakota in any scholarly use which may be made of any material in my dissertation.

<div align="right">

Christopher David Walden
August 4, 2017

</div>

TABLE OF CONTENTS

LIST OF FIGURES

LIST OF TABLES

ACKNOWLEDGMENTS

I express my sincerest gratitude and appreciation for the effort in my training on the part of my advisory committee and my fellow lab mates; with whose guidance has developed my abilities as a scientist.

To my children Alexander, Matthew, Maximus, and Annabelle, for whom I pursued this degree; and to my steadfast wife Rachel, whose support made it possible for me to complete my work

ABSTRACT

Natural toxins and artificial toxicants are abundant throughout our environment and may play an integral role in remodeling our epigenome and in the development of neural diseases. Exposure to heavy metals and organic pollutants, such as DDT and its derivatives, have been linked to neural disease. Additionally, there are links between direct exposure, in both adults and children, to short-lived pesticides and neural diseases. While the link has been established, understanding the root cause has yet to be elucidated. One increasingly relevant field offering promise in achieving this goal is epigenetics. Epigenetic remodeling is one potential mechanism by which environmental exposures may lead to human disease. Epigenetic remodeling events have been increasingly implicated in the underpinnings of a variety of brain disorders including neurodegenerative disorders and cancer. We hypothesize that environmental exposures and associated epigenetic remodeling events may occur early in life during the critical development stages and play a role in long term development of many neural diseases. We examine the current status of the field and highlight areas in need of attention and propose a model toxicant for understanding the effects of early epigenetic remodeling events and the impact of disease by examining the ability of the environmental toxicant Paraquat to remodel the epigenome both *in vitro* and *in vivo*, and investigate whether exposures in early development may be linked to disease.

CHAPTER I

EARLY NEURAL DEVELOPMENT CHANGES MAY AFFECT THE LONG TERM HEALTH OF THE NERVOUS SYSTEM.

Introduction

Neurodegenerative disorders and brain cancers are increasingly prevalent and present significant medical and societal problems that are expected to increase as our population ages and the onset of these diseases increases. While the true cost of malignant gliomas, including indirect and societal costs has not yet been fully evaluated, outdated values of treatment are greater than $100,000 US per patient per year [1]. Indeed, the Agency for Healthcare Research and Quality puts a valuation on the direct cost of medical treatment in 2011 at 88.7 billion US dollars within the United States alone [2]. Alzheimer's is the most prominent neurodegenerative disease with a 71% increase in number of deaths from Alzheimer's from 2010 to 2013. The cost of Alzheimer's disease is estimated at 236 billion US dollars in healthcare and long term care related costs. Parkinson's disease is another prominent neurodegenerative disease with an economic burden on the United States of approximately 14 billion US dollars in 2010 [3]. The economic burden of disease is one factor that is more easily quantified than other burdens induced by neural diseases. Each of these diseases has a specific set of symptoms that create undue burden on these patients. Mean survival from glioblastoma multiforme is approximately 12 months and current therapies extend life by 6 months over standard chemotherapy and radiation [4, 5]. Other less aggressive gliomas that offer better prognosis for survival with treatment still retain the burden of cognitive deficit and loss of function depending on the brain region affected [6, 7]. Alzheimer's

and Parkinson's have their own unique symptoms with some crossover including cognitive deficit. These diseases are almost all progressive and as of yet they are incurable largely because the root causes have not been elucidated. While these diseases are often considered multifactorial the epidemiological data implicates an environmental component in these diseases.

Epidemiological Links Between Environmental Exposure and Disease

Epidemiological evidence implicates a role for toxic environmental exposure in the development of neural disease. Exposure to commercial pesticides increases the odds ratio of childhood onset gliomas with greater odds ratio if exposed during the gestational period [8]. A study conducted in China for children exposed to pyrethroid pesticides determined that children with high levels of pesticide metabolite in the urine had the highest odds-risk ratio of 3.26 with a 95% confidence interval of 1.73 to 6.14 in having a childhood brain tumor [9]. In the same study, the parents that had been self-reported to be exposed to mosquito and cockroach killing pesticides had an increased odds-risk ratio for their children developing childhood brain tumors. Meta-analysis of epidemiological studies indicate an increased risk of childhood brain tumors if either parent is exposed during or before pregnancy with a higher risk from prenatal paternal exposure to agricultural pesticides [10]. Prenatal exposures to lead and p,p'-DDE (a metabolite of DDT, a persistent organic pollutant) have a higher risk for behavioral abnormalities in children [11]. Chlorpyrifos exposure in adolescent Egyptian pesticide applicators show decreased function in neurobehavioral tests as compared to their controls [12]. In the same study, the control group show greater levels of chlopyrifos metabolite in urine samples than that of US adolescents indicating ready availability from environmental

exposure. Acute exposure risk in children as well as assessment of the field of environmental toxicants in high level exposure has been detailed in a recent review [13]. The authors highlight a growing need to understand the full impact of toxicants on the health of children, highlighting a need for work in low dose chronic exposures.

Adult exposure to pesticides presents its own set of risks to the exposed individual. Adults having high urinary levels of organochlorine pesticides increases the odds-risk ratio for cognitive decline [14]. In adults exposed to pesticides for ectoparasite control, used in sheep farming, there was an increased risk of neurodegenerative disease including parkinsonism, dementia, and neuropathy [15]. Often there is an increased risk of neurodegenerative disease associated with living in a rural environment, and often this has been attributed to pesticide exposure [16-18]. A detailed examination in California examined the links between specific pesticides and Parkinson's disease. Utilizing pesticide use reporting system data, mandated by California law, the authors were able to examine pesticide interactions with specific genetic variants offering insight into susceptibility of specific populations to Parkinson's disease [19]. This study offered a unique perspective into the length of exposure not commonly available to epidemiological data. These studies implicate pesticide exposure in an increased risk for neurodegenerative disorders or cognitive decline in adult exposure.

There appears to be a delineation of effect according to exposure period in these epidemiological studies; prenatal and early childhood exposure may increase risk of childhood brain tumors as well as neurobehavioral impairments, whereas adult exposure may lead to an increased risk for neurodegenerative disease. This may be the result of the developmental period versus the matured brain, and it may be an artifact of how these

studies were designed, but this hypothesis merits additional investigation. Oxidative

stress, produced by many environmental toxicants, has been implicated in

neurodegenerative disease and in adult neurons the ability to compensate for increased

stress may be reduced from compensatory capability in development [20]. Oxidative

damage has been linked to increased risk of cancer as well [21, 22]. It may be likely that

early development may be prime for toxicant disruption of normal differentiation

pathways leading to the development of a cancerous phenotype. Alternatively, this may

be an effect of the focus of epidemiological studies and the lack of longitudinal exposure

studies. This calls to our attention the need to develop longitudinal studies of high risk

for toxicant exposure cohorts to understand fully the critical exposure windows for

developing neural disease and if early exposure versus late exposure may be the deciding

factor for increased risk of neural cancer or neurodegenerative disease (figure 1). Our lab

is interested in focusing on the early development exposures and the effect on future

disease generation.

Barker Hypothesis of Disease

The idea that an early development stress leads to disease later in the life of the

affected individual is not new. The Barker Hypothesis was originally proposed by David

Barker in 1990 where he hypothesized that intrauterine growth retardation, low birth

weight, and premature birth have a causal relationship to the origins of health disparities

in later life including cardiovascular disease and insulin resistant diabetes [23]. The

supporting evidence for the Barker Hypothesis, alternatively known as the Thrifty

Phenotype Hypothesis, comes from both epidemiological and animal studies and

primarily focuses on metabolically oriented diseases [24]. Animal studies allow for the

carefully controlled environment without other confounding variables inherent in epidemiological studies. Male and female mice that have been immune challenged prior to mating have been shown to sire larger, faster growing offspring conferring a potential fitness advantage [25]. Other studies have shown that male rats with reduced protein intake developed a diabetic phenotype which abated after reconditioning with normal protein diet indicating there is a critical window for reprogramming [26]. Neonate rats can be preprogrammed in a thrifty phenotype response with corticosterone exposure in early life that leads to more severe diabetic phenotype when rendered diabetic [27]. All of these studies indicate that there is a window of opportunity during which environmental events can impact disease and health state later in life.

The Barker hypothesis, however, is not limited to metabolic diseases; early exposure of cohorts to famine increased risk of gastrointestinal cancers with the youngest cohort having the greatest risk when compared to later adolescent stage cohorts [28]. We can expand this hypothesis based upon epidemiological evidence to include other early development perturbations and their effect on disease. This hypothesis is especially attractive as many neural diseases do not have a clear origin and may be attributable to such early events not previously considered. A review of literature focusing on early life exposures and DNA methylation, an epigenetic mark, hypothesizes that DNA methylation may be a mechanism by which the Barker Hypothesis may work [29]. Indeed, with the expansion of the epigenetics field and how critical epigenetics is to the study of the brain; there is cause to investigate early exposure events in addressing the origins of neural diseases.

Neuroepigenetics

Neuroepigenetics is a newly emerging field that focuses on how epigenetic mechanisms can impact neuronal and neuroglial function. Being that epigenetics involves the study of heritable, reversible modifications that control gene function, the focus on neural epigenetics only began emerging after the realization that some of the epigenetic control mechanisms need not be inherited to be altered and have an impact [30]. J. D. Sweatt even highlights that the field of neuroepigenetics has helped to redefine the epigenetics field as a whole for this reason. This includes DNA methylation which was once thought to be an inherited epigenetic mark. Considering that neurons are post mitotic; their DNA methylation profile should have a stable DNA methylation signature. The field has since shown that the methylation profile is dynamic and incorporates other cytosine markers.

Currently, the focus of neuroepigenetics is largely on neurons and the transcriptional control that epigenetics allows in these post-mitotic cells which allows them the ability to adapt to current environments. There is increasing evidence that neuroepigenetics is involved in development, learning and memory and environmental stress response in neurons. There is some evidence that astrocytes, a critical support cell within the nervous system, are also utilizing some of the same mechanisms and impacting neuronal epigenetics. Here we will briefly overview the major epigenetic components and their relevance in the neural system.

DNA modifications

DNA methylation is a hallmark epigenetic mark that is probably the most well understood mark in terms of function. DNA methylation is the addition of a methyl

group to the 5' carbon in cytosine bases. This mark is typically associated with cytosine guanine pairs (CpG) and has knownregulatory function in association with regions of DNA 200 base pairs or larger that contain greater than 50% CpGs termed CpG Islands and have an observed over expected ratio of cytosine and guanine greater than 60% [31]. The importance of CpG islands first emerged within the context of cancer and understanding that hyper-methylation led to inactivation of tumor suppressor genes [32]. However, it is evident that the regions 2000 or 4000 base pairs up and downstream, termed CpG shores and shelves respectively, are important in gene regulation [33, 34]. These regions may also be important in the differentiation of tissues and cell types and therefore important in identifying the cells of origin of cancer [35]. Research has shown that when an island region is heavily methylated and within or near a promoter region, there is a strong correlation with down regulation of the associated gene [32, 36-38]. The presence or absence of DNA methylation can also alter binding sites of transcription factors which plays a role in the impact of DNA methylation [39].

In the mammalian brain, the majority of DNA methylation changes occur outside of CpG islands during development [40, 41]. In fragile X syndrome the methylation outside of CpG islands in the FMR1 gene can predict anatomical structure of the brain [42]. Neural Progenitor cells exhibit a strong correlation between DNA methylation and histone mark changes compared to embryonic stem cells which have poor correlation [43]. This may be due to the differentiation of the neural progenitor cells being further along in the differentiation process, as the highest correlation exists between increased DNA methylation and the loss of open chromatin marks. This suggests that some of the previously available genes are being "closed" off for neural progenitor cells. There may

be interplay with proteins capable of recognizing and binding the methylation marks as well.

There are a number of methyl binding proteins, but one protein of known significance in the human brain is methyl-CpG binding protein 2 (MECP2), as the absence or mutation of this protein produces Rett Syndrome [44]. Rett syndrome produces severe cognitive deficits as well as craniofacial deformities and cranial neuropathy. Females with Rett syndrome are heterozygous for the non-functional MECP2 and mouse models have been established to evaluate the development of abnormalities [45]. The deficits associated with non-functional MECP2 can be rescued in an animal model with the reintroduction of functional MECP2 [46]. MECP2 is also capable of recognizing other cytosine modifications such as 5-hydroxymethylcytosine [47]. This emphasizes the importance of evaluating other DNA modifications in addition to 5-methylcytosine.

DNA methylation is a stable mark and was originally thought to be semi-permanent epigenetic mark, erasable only though DNA damage and repair mechanisms [48]. However, with recent advances, DNA methylation has been discovered to be more dynamic in the context of a single cell. With the discovery of Tet enzymes and their ability to hydroxylate the methyl group, new research has our understanding of potential molecular mechanisms by which the methyl group can be removed [49]. 5-methylcytosine is hydroxylated to form 5-hydroxymethylcytosine and subsequently converted to a number of other intermediaries and replaced with an un-methylated cytosine in a base excision repair pathway [50]. This implies that 5-hydroxymethylcytosine is only intermediate and plays no particular role as an epigenetic

mark. In the human brain however, there is evidence that 5-hydroxymethylcytosine is itself and epigenetic mark and can be associated with increased gene expression [51, 52]. This is thought to be an important feature in the post mitotic neurons as a mechanism with which to regulate gene expression and may play a critical role in synapse formation and memory function [53]. 5-HMC is more prevalent the brain and is developmentally correlated, as the mark wanes as aging occurs [47, 54].

Another important finding is that DNA methyltransferase 1 (DNMT1) cannot recognize the 5-hydroxymethylcytosine form and subsequently will not add a methyl group to the daughter strand during replication [55]. It may also play a role in altering the methylation profile as DNMT1 is required to maintain DNA methylation [56]. DNMT1 has been shown to be recruited during gene transcription to maintain the methylation profile as it exists [57]. If DNMT1 is unable to recognize 5-hydroxymethlcytosine, the methylation mark may be ultimately removed during normal replication. Interestingly, DNMT1 may not be the only protein unable to recognize 5-hydroxymethylcytosine, raising the possibility of inhibiting recruitment, an idea that deserves more attention. Case in point is the correlation between 5-HMC presence and MECP2 occupancy; such a correlation might suggest that MECP2 does not recognize 5-HMC [47]. In contrast, MBD3, part of the Nucleosome Remodeling and Deacetylase complex (NURD), requires 5-HMC to be present to bind chromatin and the loss of this function alters gene expression profiles [52].

We are now beginning to assess the effect of environmental influences on changes in DNA methylation, especially in regards to pesticide exposure. Using a stress model in mice, physical restraint for a period of 30 minutes, investigators found changes in 5-

hydroxymethylcytosine in adult hippocampus [53]. The majority of these changes exhibited increased levels of 5-hydroxymethylcytosine with approximately 20% being loss of the mark. Oxidative stress influences DNA methylation levels of cells exposed *in vitro* to hydrogen peroxide with a global reduction of 5-methylcytosine [58]. While this study did not evaluate the global levels of 5-hydroxymethylcytosine, they were able to assess a loss in TET activity. In contrast to this another group evaluated global 5-hydroxymethylscytosine levels in the presence of redox-active quinones and found an increased TET function and increasing levels of 5-hydroxymethylcytosine [59]. The authors found that redox active quinone induction of 5-hydroxymethylcytosine was iron dependent. This offers a potential window of understanding duringwhich environmental toxins may be the most prominent in altering the epigenome. Exposure to long lived pollutants such as organochlorines shows an increased association with hyper-methylation of MGMT, a DNA repair enzyme often hyper-methylated in glioblastoma multiforme [60]. Of the two pollutant groups assessed, organochlorine pesticides and polychlorinated biphenyls, the association curve was dependent upon the group assessed. Organochlorine pesticides group has a decreasing association of MGMT hyper-methylation with higher serum concentrations, while polychlorinated biphenyls exhibited a peak of MGMT hyper-methylation in midlevel serum concentrations. Additional *in vitro* evaluation of pesticide exposure has shown that some pesticides are capable of inducing DNA methylation changes after a 12 hour exposure utilizing chip arrays originally designed for cancer epigenome measurements [61]. This study highlights both that pesticides are capable of inducing DNA methylation changes *in vitro* but also highlights the limitations of utilizing chip arrays. Chip arrays offer a glimpse into the

methylation status after testing experimental variables, however they are limited in the sites they can query. As these arrays were initially set up for cancer analysis, the majority of sites queried are near CpG islands limiting the capability to study regions outside of the CpG islands. As CpG islands are often a protected structure from DNA methylation changes, these are least likely to be impacted immediately in an environmental exposure model [62]. This also raises the question of what may be potentially missed by conventional use of the arrays; which may include non-CpG methylcytosine or hydroxyl-methylcytosine marks.

Additional cytosine modifications may be playing an influence in gene regulation and deserve more attention. Among those marks are halide methylcytosines such as 5-chlorocytosine and 5-bromocytosine. Both of these marks are irreversible marks and can be recognized as a methylated cytosine by DNMT1 [55]. These marks can be introduced through reactive species such as hypochlorous acid and once initiated are capable of silencing gene expression [63, 64]. There is some evidence that these marks may play a role in cancer, but have not been evaluated within the mammalian brain [65, 66]. Another mark that may have bearing on the gene expression profile are methylation of non-CpG cytosines [67]. The evidence indicates that these marks are prevalent in the brain but their effect is unclear [68, 69]. However, there is some indication that non-CpG methylation are critical in gene expression as MECP2 requires methylated CpA dinucleotides to be present in order to localize and regulate gene expression [70] With the advancing field of neuroepigenetics, these marks and others deserve more attention and their interplay with other epigenetic marks and machinery in regulating gene expression.

Polycomb Repressive Complexes

Polycomb repressive complexes are large multimeric protein complexes that bind DNA and are often associated with repressing gene expression [71]. There are two main polycomb complexes: Polycomb Repressive Complex 1 (PRC1) and Polycomb Repressive Complex 2 (PRC2). The distinction between the two main complexes is in their function. PRC1 operates in a maintenance capacity, keeping repressed regions in a closed conformation in the removal or replacement of other repressive marks and ubiquinates histone tails [72]. PRC2 is often associated with dynamic gene repression and methylates histone tails [73, 74]. Each complex incorporates a defined set of proteins, but the composition of the complex does not require all of the defined set being present and often homologs of a particular protein fill in for specific roles [75]. PRC1 is often identified by major constituents: B Lymphoma Mo-MLV Insertion Region 1 (BMI1) and RING1 A/B, while PRC2 is often identified by major constituents: Enhancer of Zest 2 (EZH2), Suppressor of Zeste 12 (SUZ12) and Embryonic Ectoderm Development (EED) proteins [76, 77].

PRC1 maintains the ability to ubiquitinate histone tails through the RING1 A/B subunit [78]. PRC1 subunit BMI1 stabilizes the RING1 A/B complex and facilitates ubiquitination [79, 80]. BMI1 contains a ubiquitin-like pocket with which it can oligomerize or bind polycomb subunit PHC2 enhancing the ability of PRC1 to ubiquitinate H2A [80]. BMI1 is often studied in the context of gliomas, especially Glioblastoma Multiforme as BMI1 plays a critical role in cancer maintenance and is hypothesized to play a role in maintaining glioblastoma stem cells [81]. This hypothesis is supported as BMI1 maintains neural stem cells in their stem cell phenotype, and may

be the crux of the cancer stem cell phenotype [82]. PRC1 also plays a significant role in other functions as well, evidenced by the finding that BMI1 can confer resistance to oxidative stress [83]. In the same study, the authors describe that BMI1 expression is reduced in an aging brain. This may tie back into the idea that late life exposure to environmental toxicants induce neurodegeneration as opposed to cancer.

PRC2 is a critical complex in the differentiation and function of neuroectodermally derived cells. PRC2 functions by introducing H3K27me3 marks onto the histone tails where the complex associates. These marks are critical for the differentiation of neurons and the loss of these marks leads to a dedifferentiated state of the neuron and ultimately neurodegeneration [84]. The loss of this repressive mark increases gene expression of those genes marked by H3K27me3 [84, 85]. EZH2 is the primary component of PRC2 that catalyzes the H3K27me3 mark [86]. For EZH2 to be functionally active it must be incorporated into the complex and another PRC2 component, PHF1, is required for EZH2 to efficiently catalyze the mark [87]. PRC2 components are critical to the function of PRC2 in the development of the neurectoderm; removing a single component can have severe consequences. Knocking out EZH2 in the midbrain alters the differentiation profile of midbrain neurons to a forebrain phenotype [85]. EZH2 is necessary for proper radial migration of pyramidal neurons [88]. EED is the chromatin binding protein of PRC2 and removal of EED induces a failure of PRC2 to assemble and function in maintaining repressive marks [89, 90]. EED knockout models prevent the development of normal brain structure as neural progenitor cells are prevented from astroglial differentiation [91]. EED is regulated in its stem cell

maintenance paradigm through transcription factors STAT3 and OCT-3/4 which control expression of the EED gene [90].

Polycomb repressive complexes are critical for proper neural development from progenitor cells to differentiating and migrating neurons. As we have seen, disruptions in these complexes can lead to deleterious or cancerous effect and begs the question, are the polycomb complexes susceptible to environmental influence? As previously mentioned, oxidative stress can be induced by a number of pesticides, and in the case of polycomb complexes; oxidative stress causes a shift in polycomb group proteins to DNA damage regions and EZH2 as well as EED are more tightly bound to the DNA [92]. In this same study the authors found that DNMT1 would translocate to CpG islands with another polycomb member SIRT1 indicating the potential to alter DNA methylation. Cigarette smoke extract was able to induce an increase in EZH2 protein in human broncho-epithelial cells, a model system for understanding cigarette induced lung cancer [93]. In a mouse model of lung cancer, urethane was able to induce increases in EZH2 and consequently global levels of H3K27me3 [94]. Each of these studies highlight that toxins can influence polycomb proteins, however, these studies affect mature models and also show limitations in the breadth of toxins explored. A study in drosophila, the model system where polycomb complexes were discovered, examines the epigenetic inheritance in exposing an F1 generation to an antibiotic and the resultant decreases of polycomb gene expression that were carried out to F3 generation [95]. If reductions in polycomb expression are capable of crossing transgenerational lines, then they may also be affecting an organism throughout its lifetime. In another model, examining the links between breast cancer and Diethylstilbestrol and Bisphenol-A exposure, the authors were

able to identify increases in adult mice of EZH2 expression and H3K27me3 marks after having been exposed during gestation [96]. These studies highlight the potential to alter polycomb complex response in an early development environment. What effect such an alteration might have, has limited direct study, but might be inferred from knockout and over expression models, an area that needs further investigation. In addition, pesticide exposure is prevalent in society and little is known about the effect of these environmental exposures on polycomb complexes composition or localization.

Histone Modifications

Histones, proteins that package DNA, have highly modifiable tails that are subject to methylation, acetylation, ubiquination, phosphorylation and other modifications [97]. Histone modifications are incorporated through enzymes that covalently modify the amino acid residue in histone tails [86, 98, 99]. These enzymes offer a means of regulating the chromatin landscape and can be incorporated into transcription complexes and repressive complexes [86]. These complexes are often a target in therapies as they have few side-effects in treatment and are effective in their treatment paradigm [100]. Cancers targetable through histone deacetylase inhibitors are thought to be epigenetically addicted and often respond well to their treatment. Such targets are attractive enough that there has been investigation into their use in treating neurodegenerative diseases [99, 101, 102].

Histone modifications play a role in gene regulation as some marks are associated with an open chromatin feature such as methylation of H3K4 and acetylation of H3K27 tails [103, 104]. Open chromatin is thought to be more available for gene transcription allowing for the occupation by RNA polymerase II [105]. RNA polymerase II is also

thought to play a role in maintaining the open chromatin state [106]. In opposition, methylation of H3K27 is associated with a closed chromatin state, as is methylation of H3K9 [107]. Interestingly H3K27 tri-methylation plays an integral role in development by its incorporation into bivalent domains [108]. Bivalent domains are those regions of chromatin that exhibit both closed and open chromatin marks and have low gene expression in early progenitor cells [109]. It is thought that these regions allow for the stem cell to enter a differentiation pathway and increase expression of key genes while turning off those other bivalent domains not necessary in the differentiation pathway.

Histone modifications play a significant role in neurodevelopment as they are immediate moderators of gene expression. Caspase 3 is down-regulated in mature brains due not to changes in transcription factors, but to increased DNA methylation and decreased histone acetylation, reducing the accessibility of the chromatin [110]. This is biologically important as a mature brain will require less pruning of unneeded neurons that usually occurs during development requiring less apoptotic activator. Also in development, AF9, of the AF9/MLLT3 translocation in leukemia, controls TBR1 gene through demethylation of H3K79 at the TBR1 promoter preventing gene expression [111]. TBR1 suppression allows for the development of the six layer cortex as TBR1 is the last expressed transcription factor in a sequential set of transcription factors in differentiation cortical neurons [111]. H3K4me2 differentially marks the gene body of tissue specific genes and is acquired during differentiation of progenitor cells in the mouse brain [112, 113]. These marks are associated with genes that are being expressed in a tissue specific manner and as would be expected, are dynamic through development as gene expression profiles change during differentiation [114]. These studies highlight

the importance of histone modifications during development and off site histone modifications may present developmental abnormalities. In humans with spina bifida, histone H3K79me2, which has shown to be important for cortical development, is globally down regulated [115]. This study does not evaluate at which locations H3K79me2 is down regulated and such an evaluation would help to determine if the modifications absence is causative or correlative. A study that highlights the need for appropriate levels and composition of histone acetylation in the development of a healthy brain is the knockout of BRPF1 in mice; BRPF1 interacts with a histone acetyltransferase complex enhancing its function [116]. The knockout of BRPF1 reduces brain structure with thinner cortical layers and a reduction in the available progenitor cells, these mice are also behaviorally abnormal and have a short lifespan of less than 30 days [117]. These studies indicate the importance of proper covalent histone modifications for proper brain development.

Histone tail modifications are dynamic and play a role in gene regulation. As a result, researchers have hypothesized that there might be shifts in the levels of these marks in response to environmental cues or toxins. Developmental arsenic exposure alters the histone marks in adult mouse brain tissues and these marks are differentially affected based upon the sex of the animal [118]. Two important considerations arise from this study: that sex alters the impact of the toxicant, and that epigenetic changes are observed in adult animals long after the exposure event. The study focused on global H3K4me3 and H3K9Ac marks and found that arsenic exposed females experienced a loss in these marks while their male counterparts experienced a gain. Another heavy metal, cadmium, has been shown to reduce global levels of repressive mark H3K27me1 in

mouse embryonic stem cells [119]. While this study did not identify the specific location of the changes in the genome, global loss of a repressive mark suggests that there may be persistent changes in gene expression. Exposure to ethanol in neural stem cells and the fetus induce changes in H3K27me3 and H3k4me3 marks that persist after the acute exposure [120]. The effects of the ethanol exposure were also greater after the acute exposure window implying that these remodeling events may be slow to develop a phenotype, an important consideration when designing exposure studies. Histone modifications are also subject to pesticides and other environmental exposures. Rat dopaminergic neurons exposed to Paraquat for 24 hours exhibited a loss of histone deacetylase protein expression and subsequently a gain in histone acetylation [98]. Dieldrin exposure also increased histone acetylation in both rat dopaminergic neurons and mouse models [121]. Dieldrin is a pesticide that has been discontinued in use since the late 1980's but persists in the environment and has a strong association with Parkinson's disease [122]. Increased acetylation in response to both Paraquat and Dieldrin might suggest a common mechanism in response to pesticide exposure. What is needed is a detailed examination of where the acetylation events occur both in terms of specific histone residues and whether these changes occur in specific regions in the genome. Reactive quinones have been shown to form a histone modification at a number of sites both on the tails and within the histone body. These modifications, while unknown how they might react with the epigenetic machinery, have been shown to produce reactive oxygen species within the nucleus, raising the potential for mutagenesis [123]. These studies suggest that the epigenome may be susceptible to environmental insults.

Micro-RNAs

Micro-RNAs (miRNA) are a subset of non-coding RNA, ranging from 15-30 nucleotides, which bind target sequences and inhibit translation of the bound mRNA through the RISC (miRNA Induced Silencing Complex) complex. The production of miRNAs has recently been reviewed and involved a multistep enzymatic and translocation from the nucleus process [124]. The study of miRNAs is an emerging field and the details of how they regulate gene expression are beginning to emerge, and also indicate that miRNAs play a crucial role in development of the central nervous system. In a zebrafish dicer knockout model, dicer cleaves precursor miRNA stands into miRNA that bind the RISC complex, there is agenesis of the brain which can be rescued with miRNA-430 [125]. MiRNAs are locally expressed in distinct regions of the brains and can evade detection with standard techniques [126]. The distinct localization of miRNAs indicates that specific cell types require different miRNAs in their function and development. Finding that miRNAs require specialized detection methods could mean missing information in interpreting the importance of miRNAs in specific brain regions. Indeed a recent review of the miRNAs in the adolescent life stage highlights that there is a need for further investigation into miRNAs not only in specific brain regions but also in developmental stages [127].

MiRNAs exhibit differences in the sexes, a recurring theme in epigenetic mechanisms and an important consideration in evaluating the context of differential epigenetic marks [128]. Similar to thesex differences described above, arsenic exposure in pregnant dams differentially affected male and female offspring, with several miRNA being downregulated in males and no impact in females. REST, a transcription factor in

part responsible for differentiation of neural stem cells, is affected by the expression of miRNA-9; one of the down regulated miRNAs in the male mice [129, 130]. Complete loss of REST during development allows for DNA damage events to go unchecked and knockout mice are susceptible to developing gliomas [131]. In contrast, late stage loss of REST induces a neurodegenerative phenotype in mice [132]. This distinction may hearken back to epidemiological studies as to why there is a demarcation in developing brain tumors versus neurodegeneration based on age of exposure. Paraquat exposure in neural progenitor cells prevents differentiation and upregulates a number of miRNAs [133]. This study did not evaluate the specific effects of the differentially expressed miRNAs, however, miRNA-34 was among the highest in differential expression, and is implicated in cellular senescence and as a biomarker of multiple system atrophy [134, 135].

Paraquat as a model toxicant

Paraquat has been used in agricultural practices for a number of years since its introduction to mainstream agriculture in the 1960's. Paraquat is an effective nondiscriminatory herbicide that functions through inhibition of the chloroplast electron transport chain [136]. The use of this herbicide is still prevalent throughout the world, including in the United States. Accidental and intentional ingestion is often fatal and there is no known antidote [137, 138]. Patients who have had a high dose exposure expire from multi-organ failure and develop pulmonary fibrosis in moderate to severe poisonings [139]. Paraquat has some ability to cross the skin in small doses but has otherwise not been reported to be mutagenic [140]. However, levels of Paraquat have been reported in meconium of fetuses from mothers where Paraquat is heavily used,

indicating the exposure of fetuses to Paraquat [141]. Some patients that initially survive

ingestion of large quantities of Paraquat exhibited and die from seizures thereafter,

identifying a neurologic component to Paraquat poisoning [142]. Epidemiologic data in

adult humans does indicate Paraquat increases the risk of Parkinson's disease in certain

populations with specific genetic variants, including dopamine transporter variants and

other comorbidity factors such as traumatic brain injury and behavioral stressors [19, 143,

144].

Paraquat Mechanism of Action

Paraquat has been studied as a model toxicant for the etiology of Parkinson's

syndrome[145]. Initial use of Paraquat in research was due to similar chemical structure

as that of another Parkinsonian inducing toxicant MPP+, a well-established parkinsonian

inducing agent [141, 146]. Paraquat inhibits the electron transport chain in animal cells

through either Complex I or Complex III (figure 2) [147, 148]. Inhibition of the electron

transport inhibits the production of ATP [149]. Paraquat is also capable of redox cycling,

which leads to the production of superoxide radicals that can readily pass through the

mitochondrial membranes [150, 151]. Outside of the mitochondria, the superoxide

radicals are capable of entering a Fenton reaction with available sources of iron and

ultimately becoming hydroxyl radicals [152, 153]. Additionally, superoxide dismutase

converts superoxide radicals into hydrogen peroxide which can dissociate and become

hydroxyl radicals [154]. At high concentrations, Paraquat disrupts the mitochondrial

membrane potential, reducing the ability of mitochondria to produce ATP [155]. The

inhibition of mitochondrial function is reported to have multiple downstream effects

including the release of Cytochrome C. This may induce apoptosis, lead to the production of superoxide radicals, and lead to an increase in the miss-folding of proteins [156-161].

Paraquat in Model Systems

Studies have introduced evidence that Paraquat may be taken up in the intestines and eventually enter the brain from the environment. Caco-2 cells, a model for intestinal uptake in humans, uptake Paraquat through amino acid and choline transporters [162]. Paraquat has been shown to cross the blood brain barrier via arginine and lysine amino acid transporters [163]. In the brain, dopaminergic neurons are sensitive to toxicant stress [164-166]. Dopaminergic neurons uptake Paraquat through dopamine transporters and amino acid and ion transporters [167]. Dopamine facilitates an increased uptake of Paraquat, increasing the availability of toxin within the dopaminergic neuron [167]. Glial cells, including astrocytes and microglia, uptake of Paraquat as well [160]. Microglia convert Paraquat into a monovalent cation increasing uptake through dopamine transporters [167]. The quantity of Paraquat within the central nervous system after 10 mg/kg Paraquat injections peaks initially at 0.6 uM and wanes after several hours to 0.2 uM concentrations [163]. These concentrations are much lower than concentrations required to reduce cell viability directly at *in vitro* testing conditions [148, 160, 162, 167, 168].

Discrepancies in the Paraquat Model System

Many experimental studies use *in vitro* concentrations ranging from 5 uM to 5 mM with much work being done at 250 uM to 1000 uM range *in vitro*. In this concentration range, many cell types lose viability above 200 uM, however, some cell types can lose viability in concentrations as low as 50 uM [133]. Many of these viability

studies involve the use of mitochondrial function as a proxy for viability, a potential

problemin a model system where Paraquat acts by inhibiting mitochondrial function. As

introduced above, these concentrations are much higher than what is proposed to be

found available to the neural systems. This would indicate that there needs to be a frame

shift in concentrations used in *in vitro* work, as concentrations in the brain are found to be

less than 1uM in mouse models.

There are also discrepancies in the mouse model as to the effect of Paraquat on

the dopaminergic system. There are multiple dosing models used with a 1 injection per

week exposure to 10mg/kg intraperitoneal injection over three weeks being among the

most common. Some studies have suggested that the methodology for assessing

dopaminergic cell loss are inaccurate. However, utilizing stereoscopy as the gold

standard, studies have both shown significant loss and no loss in dopaminergic neurons

[159, 169]. The discrepancy does appear to have some relationship to the age of the mice

used in the experiments. Those that argue against dopaminergic cells loss often utilize

young mice usually starting at 7-10 weeks of age and sacrifice shortly after exposure and

find no significant loss of dopaminergic neurons [169]. However, other groups utilizing

older animals (ranging from 2-3 months to 18 months of age) have observed significant

dopaminergic cell loss [145, 170]. This may be in part due to the loss of compensatory

capability of older brains to deal with oxidative stress [171]. Still others use models with

a longer and increased dosing schedule and find reductions in dopaminergic neurons up

to 30-40% in the longest dosing group [172]. What may be missed in most of these

studies, however, is the implication that Paraquat may not be a fast acting toxicant like

MPP+. Paraquat exposure at postnatal days 5-9 leads to significant dopaminergic cell

loss at the age of 6.5 months [170]. Additionally, with a secondary injection of Paraquat at the end point of the study, the effect of Paraquat was exacerbated. It may be that Paraquat is priming the model system for deficit with a second stressor a stronger correlation with epidemiological data. Additionally, if epigenetic components are at play those effects may not be measured immediately and may take additional time to develop. This discrepancy needs to be evaluated as there are a number of research groups that show evidence of dopaminergic cell loss [170, 172, 173]. However, dopaminergic cell loss may be just a facet of Paraquat as a model toxicant.

While there may be some discrepancy in how Paraquat effects dopaminergic neurons, most studiesagree that Paraquat is able to cross the blood brain barrier [163, 169, 174]. The concentration at which Paraquat crosses the blood brain barrier appears to be a fraction of the total amount given to the animal. The majority of Paraquat is excreted in urine and feces, but at low concentrations Paraquat is available to neural systems [175].

Paraquat at Sub-Lethal Concentrations

Many studies focus on Paraquat at high concentrations and their effect on the dopaminergic system. However, there are groups that are investigating a more environmentally relevant level of Paraquat.   In the c. Elegans model, Paraquat has been observed to induce an inverted U-shaped curve in longevity with a maximal 1.5 fold increase in longevity [176]. Paraquat is lethal in c. Elegans at 4 mM and above as the organism cannot compensate for the increased oxidative stress. However, at concentrations from 100 to 1000 uM, c. Elegans display an increase in longevity with a peak at 100-200 uM, while ultra-low doses below 100 uM have limited effect. The

increase in longevity is thought to be part of an reactive oxygen species signaling mechanism and indeed longevity is also affected in models with mutations in metabolic processing such as *Nuo-6* and *Isp-1* that affect the through low level oxidative stress by interruption of the electron transport chain which electron transport chain [177]. Additional studies have linked a paraqaut-like mechanism to induced longevity in c. Elegans while simultaneously retarding development [178, 179]. Inhibiting the electron transport chain or inducing mitochondrial stress can increase the longevity in d. Melanogaster models as well [178]. However, where a discrepancy lay is in the mammalian models. Disrupting superoxide homeostasis in mouse models has a deleterious or no effect on longevity [178]. However, longevity can be induced by decreasing H_2O_2 levels by overexpressing a catalase, *Mcat* [180]. This model survives past wild type models due to reduced overall reactive oxygen species and associated damage and is enhanced with additionally overexpressing super oxide dismutases. The residing difference between the two models may be the incapability of C. Elegans to replace cells and the need to adapt to increased oxidative stress [178]. This has been proposed as a model for neurogenic stress as neurons cannot be easily replaced and may therefore require stress adapting mechanisms. Additionally, even at these longevity inducing levels, Paraquat is able to induce oxidative damage [177]. However, little is known about the oxidative damage to other constituents such as DNA and lipids, nor do we fully understand the effect on epigenetic machinery at these low levels.

Epidemiological evidence indicates the possibility of low level exposure to Paraquat during fetal development in those mothers who have been exposed to environmental levels of Paraquat [141]. The levels of Paraquat detected in the meconium

of fetuses is similar to levels detected for *in vivo* brain exposures. The effect of developmental exposure in the developing brain is only recently being examined. To affect longevity in the c. Elegans model mitochondrial stress is required during a critical developmental window, outside of which no effect on longevity from mitochondrial stress can be induced [181]. Additional evidence to the effect of low level Paraquat exposure in the developing brain comes from a study of embryonic derived 3D-rat brain cultures [182] . In this study, Paraquat was used at much lower than typical concentrations: 0.1, 0.5 and 1 uM. These levels are more akin to the levels found in the brains of *in vivo* treated animals and may offer insight into how low levels of Paraquat affect development. This study showed that initial loss of neuronal proteins could be recovered after several days out of exposure, however, not all proteins were able to recover full expression, indicating a long lived down regulation of the proteins. mRNA of the proteins assessed also exhibited similar patterns. Another important finding of this study is the continued astrogliosis after removal of Paraquat, as well as a delayed activation of microglia. From the studies in c. Elegans and developmental models it is clear that environmental influence through mitochondria may need further consideration for environmental exposures.

Mitochondria as the Environmental Influence Gateway

Mitochondria have been increasingly implicated in playing a significant role in a number of diseases, while our understanding of their interaction within the cellular systems is beginning to emerge [183]. Inhibition of the electron transport chain can induce neural progenitor cells to overcome growth restrictions by inactivating p53 providing a potential gateway for oncogenesis [21]. Mitochondrial inhibition appears to

have a role in neurodegenerative diseases as well through increased reactive oxygen

species and reduced mitochondrial function [184]. Several environmental toxicants

inhibit the electron transport chain including Paraquat, Rotenone, and MPP+ (a derivative

of MPTP) [148]. Mitochondrial stress can have an impact on reactive oxygen species

levels within a cell and lead to DNA damage and ultimately apoptosis or cell cycle

deregulation [185].

Mitochondria play a significant role in disease states and can communicate with

the other components of the cell to regulate function. In the longevity models mentioned

above, mitochondria communicate with the nucleus and activate histone demethylases

specific for H3K27me3 increasing gene expression of H3K27me3 associated genes

[179]. Additionally longevity activating mitochondrial stress increases MET-2 activity

and H3k9me1/2 marks in the chromatin [186]. The mitochondrial DNA itself may act as

a chromatin regulator as the interactions between nuclear and mitochondrial DNA have

been found to be significant although the functional purpose is not yet known [187].

Disruption of mitophagy can lead to DNA damage and cellular senescence in stem cells;

evidence of the importance for proper mitochondrial regulation [188].

Mitochondrial Epigenetics

Mitochondria are considered the frontline sensors for environmental exposure and

one hypothesis by which this may occur may be through epigenetically modifying the

mitochondrial DNA; specifically DNA methylation and hydroxymethylation. There is

some controversy regarding the concept of mitochondrial DNA methylation. This in part

stems from the much lower presence of DNA methylation or 5-Hydroxymethylation in

the mitochondrial DNA versus nuclear DNA [189]. There also does not appear to be a

consensus on the functional relevance of such modifications as of yet, but this may be a

byproduct of the infancy of the field [190]. There are technical limitations in measuring

DNA modifications in the mitochondrial epigenome, one being the repetitive nature of

the mitochondrial DNA sequence making mapping techniques difficult. In addition,

limitations are present in the assay technology as it has been used, requiring careful

consideration of appropriate controls [191]. There has been an overestimation of the

level of mitochondrial DNA methylation due to the circular nature of mitochondrial DNA

as well as non-specific binding with antibody sequestering technologies [189, 191].

However, there are independent DNA modification machinery within the mitochondria

and the utilization of more sensitive techniques have shown the levels of mitochondrial

DNA modifications are significant [192-194]. One study has even been able to link

mitochondrial DNA methylation to environmental exposure of metal rich particulates

[195]. Another study has been able to identify an inverse correlation of mitochondrial

DNA methylation at two loci and the age of the subject indicating a potential aging

biomarker [196]. What is also unclear is if histones and their marks play a significant

role in mitochondrial epigenetics. While histone proteins have been found in

mitochondria, to date no known histone modifying mechanisms have been identified in

the mitochondria [197]. Additionally, histones are not known to associate with the

mitochondrial DNA. However, recent evidence has found Mof, a histone

acetyltransferase, within the mitochondria which binds mitochondrial DNA and plays a

role in mitochondrial transcription [198]. It is clear that there is much work to be done in

the field of mitochondrial epigenetics to elucidate the functional relevance of any

epigenetic marks including the effect on mitochondrial gene expression as well as the

interplay between mitochondrial and nuclear epigenomes. The advent of these needed

advances may bring about a greater understanding in how the mitochondria relay

environmental information into the development and maintenance of living cell systems.

Paraquat may offer an opportunity, as a known mitochondrial disruptor, to examine if

there are epigenetic remodeling events as a direct result of exposure and if those changes

lead to any functional relevance.

Developing an Early Exposure Model

The etiology of neural disease remains elusive as many of these diseases are considered

multifactorial. Neuroepigenetics provides an opportunity to evaluate how environmental

influence over time can impact these neural diseases. There is a clear need to understand

how environmental influence impacts neural disease as evidenced by the epidemiological

studies outlined in this manuscript.
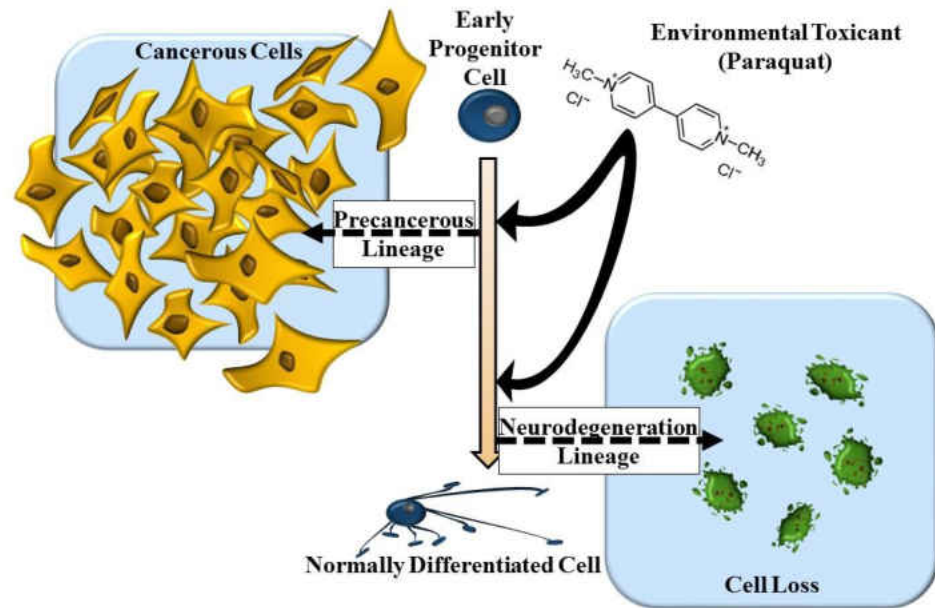
Figure 1. Environmental exposure in early development may drive future disease events. We propose that an early development environmental toxicant exposure, such as Paraquat, can alter the normal differentiation pathway in epigenetic remodeling events. Epigenetic remodeling events may be the key to later disease states in a Barker hypothesis model, where early events direct later disease states.
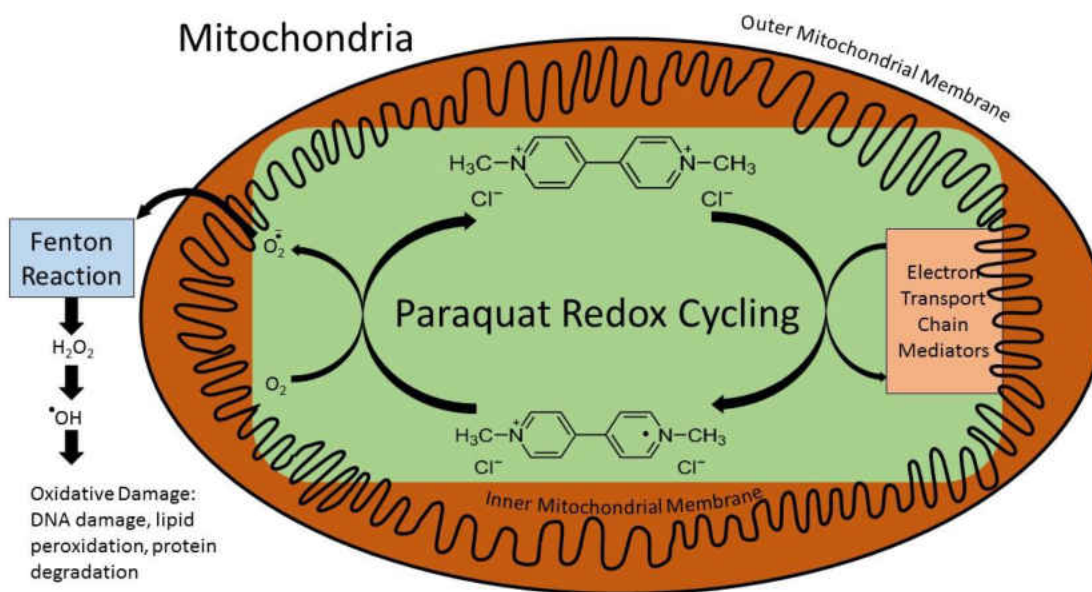
Figure 2. Current understanding of the mechanism of action for Paraquat.
Paraquat enters redox cycling producing superoxide radicals and also inhibiting electron transport chain components. Superoxide radicals pass through the mitochondrial membrane through pores and are converted to hydrogen peroxide chemically through available iron in a Fenton reaction or enzymatically through superoxide dismutase. Hydrogen peroxide can form hydroxyl radicals which can then lead to DNA damage, lipid peroxidation and protein degradation.

CHAPTER II

METHODS

Animal Model

C57bl6 mice (Harlan labs), were treated with 10mg/kg Paraquat or saline with intraperitoneal injection. Paraquat was made fresh prior to each injection time point, 1 mL of injection stock was collected for mass spectrometry. Mice were treated twice weekly for six weeks. Mice were bred after 1 week of injections. Gravid mice were allowed to reach gestational term. Pups were collected and brains removed for mass spectrometry or glial cell cultures. Pup brains for mass spectrometry were snap frozen and pulverized to homogeneity. Pup brain cultures are as described later. Blood samples were taken from pups after decapitation.

Adult mice were treated for a total of 12 injections and six weeks. Mice were euthanized with CO_2. Mice were then trans-cardiac perfused with saline and calcium chloride. In second study blood was collected prior to trans-cardiac perfusion. Blood samples were collected with heparin sulfate tubes and centrifuged to collect sera. Sera was then frozen for mass spectrometry. In the initial study, mice were then perfused with 4% paraformaldehyde and hemispheres retained for histology. Remaining hemisphere was reserved for later DNA and RNA extraction. Histology hemisphere was immersed in 4% paraformaldehyde for 72 hours. In second study mouse brains were removed and one hemisphere immersed in 4% paraformaldehyde for 72 hours. The remaining hemisphere

was snap frozen and pulverized for later RNA and DNA extraction as well as mass spectrometry. Two 30% sucrose exchanges were performed on histology sections. Initial study brains were then paraffin embedded and cut at 7-10 micron sections. Second study brains were frozen in OCT freezing medium and cut with a cryostat at 20 micron thickness. Tissue sections were then stained for tyrosine hydroxylase.

Assay for Transposase Accessible Chromatin (ATAC-seq)

Astrocytes were cultured as described above for 48 hours prior to treatment in T-25 culture flasks. Cells were treated with Paraquat at 0.5, 5 and 50 uM concentrations for 24 or 72 hours. ATAC-seq protocol was used as described by Buenrostro et. al. [199]. Cells were collected by trypsin mediated release and centrifuged at 200 x g for 5 minutes. Cell pellet was re-suspended in 1 mL complete medium and 20 uL was diluted into 200 uL final volume. 10 uL of final volume dilution was counted on a hemacytometer. 25,000 cells from dilution were centrifuged at 500 x g for 5 minutes at 4° C. Cells were washed in 50 uL 1 X Dulbecco's Phophate buffered saline (DPBS). Cells were centrifuged at 500 x g at 4° C for 5 minutes in 0.2 mL PCR tubes. Supernatant was removed and 50 uL Lysis buffer (10 mM Tris-HCl, pH 7.4, 10mM NaCL, 3 mM $MgCl_2$, 0.1% IGEPAL CA-630) was added to each sample. Each sample was gently re-suspended by pipette. Samples were centrifuged at 500 x g for 10 minutes at 4° C. Supernatant was removed and 50 uL of transposase mixture (25 uL 2x reaction buffer (buffer TD from Illumina Nextera Library Prep Kit), 2.5 uL tranposase (TN5 transposase from Illumina Nextera Library Prep Kit) and 22.5 uL of sterile RNase and DNase free water) was added to each sample, now nuclei. Samples were gently re-suspended by pipette and then incubated at 37° C for 30 minutes. Samples were then immediately purified with Minelute PCR purification kit from Qiagen.

Briefly, 250 uL of buffer PB without pH indicator was added to each sample and centrifuged in provided spin columns. 700 uL of buffer PE with ethanol added was added to the column and centrifuged as a wash step. An additional drying step of 1 minute centrifugation was performed. Samples were eluted after a 1 minute incubation in 10 uL buffer EB. Samples were then frozen at -80° C until primer indexing was performed.

Samples were thawed and 35 uL PCR mastermix was added (10 uL nuclease free water, 25 uL NEBNext High-Fidelity 2x PCR Master Mix) and indexed primers were added according to Table 1 at 2.5 uL per primer. Samples were PCR amplified as per Table 2. 5 uL of sample was removed after last cycle of PCR amplification and qPCR amplified to determine the remaining number of cycles, N. 9.5 uL qPCR master mix was added to each sample (4.4 uL nuclease free water, 0.09 uL SYBR Green I, and 5 uL NEB Next High-Fidelity 2x PCR Master Mix). 0.25 uL forward and reverse primer were added to each sample as indexed in Table 1. qPCR was performed in cycles as per Table 2. Remaining N cycles were determined by plotting reaction fluorescence by cycle number and using ¼ of maximal fluorescence of linear function of the graph (figure 3). The remaining 45 uL of original PCR amplified library was continued in PCR cycles as per Table 2 and Table 3. PCR reactions were purified with Qiagen Minelute PCR purification kit as described previously. Samples were then sequenced.

Cell Culture

Astrocyte Paraquat Exposure (Chapter III)

Primary human astrocytes were obtained from Sciencell. Cells were cultured on corning T75 cell culture flasks with 2 ug/cm^2 Poly-D Lysine (Sigma-Aldrich) for

adherence in Astrocyte Medium (Sciencell) with provided supplements. Cells were cultured for at least 24 hours prior to treatment with Paraquat (Sigma-Aldrich). Paraquat exposures of length 24 hours and 72 hours were of a single exposure of concentrations indicated in results.

Long Term Cell Culture (Chapter IV)

Astrocytes, brain vascular pericytes, and Schwann cells (Sciencell) were cultured as recommended by the manufacturer in Human Astrocyte, Human Brain Vascular Pericyte, and Human Schwann Cell media, respectively (Sciencell). Culture dishes were coated with 2 ug/cm^2 Poly-D-Lysine (Sigma) and incubated at least 1 hour prior to use at 37º C. Dishes were then washed once and medium added prior to seeding with cells. Cells were seeded at a density of 5,000 cells/cm^2. Cells were passaged at 90% confluence and plated on Poly-D-Lysine coverslips for immunofluorescence as well as new culture dishes for subsequent passages. Cells were passaged by 0.25% trypsin digestion with EDTA and quenched with complete medium. Cells were centrifuged and pellets suspended in complete medium. Cells were plated at 5,000 cells/cm^2 for each subsequent passage. DNA and RNA were collected from the remainder cell population.

Maternal Paraquat Exposure (Chapter VI)

1-3 day old pups were collected and euthanized; pup heads were dipped in 70% ethanol and decapitated. Brains were immediately excised in a sterile environment. Skin was pulled from the nose to the back of the cranium. Cranium was peeled away with a forceps to expose brain tissue. Cortex of the brain was immersed in dissection medium (1mM EDTA, 1mM EGTA stock 100uM, 1X PBS, 1mg/mL glucose). Cortex was

dissected from brain with forceps by applying pressure at bregma and pushing forward to peel cortex. Corti were minced by individual brain for individual pup cultures or pooled in groups of 3 or 4 pups and minced together in dissection medium. Minced tissue was aspirated from dissection medium and collected at the bottom of a pipette. Tissue was submerged in 4 mL of 0.25% trypsin with EDTA and incubated at 37ºC for 20 minutes. Tissue/trypsin was inverted approximately every 3-4 minutes to mix. 10 mL complete medium (DMEM/F12, 10 mL antibiotic/antimycotic, 10% FBS, 5% Horse Serum) was prepared in a new conical tube. Tissue was aspirated and collected at the bottom of pipette. Tissue alone was added to previously prepared complete medium conical tube and incubate for 2 minutes. Tissue was aspirated and transferred to 10 mL of new complete medium. Tissue was triturated 30 times or until homogeneous mixture of tissue and medium was present. Triturated tissue was transferred to culture flasks (3-4 brain cultures into a t-75 flask; 1 brain culture into a t-25 flask) and incubated for 24 hours at 37º C. Spent medium was removed and 15 mL fresh complete medium was added. After 7 days approximately half of medium was removed and 7.5 mL complete medium was added. At 10 to 14 days cultures were assessed for total microglia by observation and cultures were harvested for plating or RNA and DNA extraction.

Microglia were collected by flask shaking at 200 rpm for 45 minutes at 37ºC. Culture medium was aspirated and flasks were washed with cold dissection medium. Dissection medium was aspirated and collected with culture medium. Fresh culture medium was added to flasks and replace into incubator at 37ºC for adherent cultures. Microglia were centrifuged and suspended in fresh culture medium. Suspended

microglia were aliquoted for RNA and DNA collection and seeding for subsequent experiments.

Adherent cultures were trypsin digested with 0.25% trypsin with EDTA for 5 minutes at 37°C and collected in complete medium to quench trypsin. Cells were centrifuged and pellet suspended in complete medium. Cell suspension was aliquoted for DNA and RNA collection or seeding for subsequent experiments.

Cell Viability

Cell Mitochondrial Viability Assays

96 well plates were prepared for primary cell cultures by incubating wells in 50 uL of 15 ug/ml Poly-D-Lysine solution for at least one hour prior to subculture. Poly-D-Lysine solution was aspirated prior to seeding with cells in culture medium. Cells in culture medium were plated at seeding density of 5000 cells/well and 200 uL/well of culture medium. Culture dishes were then incubated overnight prior to treatment to allow cells to adhere and acclimate. Preparation of Paraquat treatment included preparing a 1 mM stock solution of Paraquat dichloride into complete medium and performing 2 fold dilutions until minimal concentration of 0.5 uM was achieved. For human Microglia and murine viability assays, Paraqaut was prepared at 1mM and diluted to subsequent concentrations. Cells were incubated in 200 uL of indicated concentration for 72 hours. 3 hours prior to end time point 100 uL of medium was aspirated and 10 uL of 5 mg/mL 3-(4,5-Dimethyl-2-thiazolyl)-2,5-diphenyl-2H-tetrazolium bromide (MTT) was added. At end time point all medium was aspirated and 100 uL of isopropyl alcohol was added to solubilize formazan. 96 well plate was read on epoch plate reader and results were compared as a percentage of

control. Each concentration was tested in 6 wells of each 96 well plate and plates were replicated 4 times with different lots and passages of cells for astrocytes. Statistical significance was determined with a one-way ANOVA followed by Dunnet's post-test. * indicate p-value less than 0.05

Cell Viability Assay

Triple stain method was used to assess live/dead cell count in concentrations at 0.5, 5.0, 50.0, and 1000.0uM Paraquat in primary human astrocytes as previously described [200]. 500uM H_2O_2 was used as positive control. Cells were cultured in 35mm Poly-D-Lysine coated glass bottom dishes for at least 24 hours prior to treatment. Cells were treated with indicated concentrations of Paraquat for either 24 or 72 hours. Cells were counted and imaged on a Zeiss Axiovert 200M. Total cell numbers were assessed with hoescht 33342 stain to stain nuclei. Calcien is cell permeable and metabolized by mitochondria producing a green fluorescent substrate if mitochondria are still functioning. Ethidium Homodimer is not cell permeable under normal physiological conditions and staining of nuclei with Ethidium Homodimer indicate loss of membrane integrity. Calcien and ethidium homodimer were added 1 hour before end point at concentrations of 0.5mg/mL and 8uM respectively. Hoescht 33342 was added 30 minutes prior to end point at 10mg/mL. Cells were considered alive if there was no red nuclear staining and had some indication of green fluorescence. Each condition was assessed in 10 fields in the same pattern for all conditions. Each set of conditions was repeated four times for each time point. Statistical significance was determined by a Two-Way ANOVA with Dunnet's post-test. * indicate p-value less than 0.05.

Immunofluorescence

In Vitro Paraquat Treatment

Cells were cultured on Poly-D-Lysine coated coverslips for 24 hours and treated with vehicle, Paraquat (0.5uM, 5 uM, 50 uM, 1000 uM) or 500 uM H_2O_2 and cultured for either 24 or 72 hours. Cells were then fixed with 0.4% paraformeldahyde and incubated at 37°C for 30 minutes. Cells were washed with 1X PBS with calcium and magnesium. For H2AX immunofluorescence, coverslips were blocked in blocking solution consisting of 1X calcium and magnesium PBS, 1.5% donkey serum, 1% natural goat serum, 1% BSA and 0.1% Triton X-100 at room temperature for two hours. Coverslips were incubated in 1:100 anti-phosphorylated-H2AX antibody and 1:1000 anti-glial acidic fibrillary protein antibody in blocking buffer overnight at 4°C. Coverslips were washed three times in 1X calcium and magnesium PBS and incubated at room temperature in 1:100 anti-mouse alexafluor 488 and 1:200 anti-rabbit alexafluor 555 secondary antibodies for two hours. Coverslips were mounted with vectasheild mounting medium and sealed with coverslip sealant. Coverslips were imaged and images were quantified with Image J.

Images were imported into Image J and quantified for total cells, number of positive points (as defined below) in each image and number of cells positive for H2AX mark. Positive points were defined by setting a threshold based on control images for alexafluor 488 channel and measured by internal functions to ImageJ. Set threshold was used for all subsequent image analysis for a given experiment. H2AX positive cells were determined if nuclei had a positive mark. Total positive points for a given image were divided by marked positive nuclei to give a ratio of average positive points per affected cell. Affected

cells were divided by total cells to give a ratio of positive cell to total cells. Data were graphed in Graphpad v.6 and statistical analysis was performed with a one-way ANOVA followed by Dunnet's post-test. * indicate a p-value less than 0.05.

For 8-oxo-dG immunofluorescence, protocol was followed as previously published. Coverslips were washed in 1X calcium and magnesium free PBS (CMF PBS). Coverslips were then incubated in 0.1% Triton X-100 in CMF PBS at room temperature for 15 minutes. Coverslips were washed in CMF PBS and incubated for 1 hour at 37°C in TEN buffer (10mM Tris HCL, 1mM EDTA, 400mM NaCl) with 100ng/mL RNase A cocktail mix. Coverslips were washed in CMF PBS and incubated at room temperature for 10 minutes in 100 mM Tris HCl, 50uM EDTA with 10 ug/mL proteinase K. Coverslips were washed in CMF PBS and incubated in 2 M HCl acid for 5 minutes at room temperature followed by quenching with 2.5 volumes 1 M Tris base for 7 minutes at room temperature. Coverslips were washed and incubated in blocking buffer as above with the exchange of calcium and magnesium PBS for CMF PBS, for two hours at room temperature. Coverslips were then incubated in CMF blocking buffer with 1:100 anti-8-oxo-dG antibody overnight at 4°C. Coverslips were then washed in CMF PBS and and incubated for two hours in CMF blocking buffer with 1:100 anti-mouse alexafluor 488 antibody. Images were quantified in Adobe Photoshop v.6.0. DAPI fields were used to outline measurements for FITC channel intensities. Intensities were measured for 16 cells in each condition for each replicate and average intensity was plotted in Graphpad v.6.0. Statistical analysis was performed with a One-way ANOVA followed by bonferoni's post test.

Long Term Cell Culture

Cells were seeded at 5,000 cells/cm^2 on Poly-D-Lysine coated german glass coverslips and incubated for 2-3 days. Cells were then fixed in 4% paraformeldahyde at 37° C for 30 minutes. Cells were then washed in 1X Dulbecco's Phosphate Buffered Saline three times. Blocking solution of 10% FBS in PBS with additional 0.5% triton X-100 was added and incubated at 37° C for 30 minutes. Cells were washed 3 times in PBS. Primary antibodies were diluted in blocking solution: anti-GFAP (Daka), anti-S-100 (ABCAM), anti-smooth muscle actin (Sigma); and incubated at 4° C overnight. Cells were washed in 1X PBS three times. Secondary antibodies were diluted in blocking solution: anti-mouse Alexafluor (Cell Signaling), anti-Rabbit Alexafluor (Cell Signaling); and incubated overnight at 4° C. Cells were washed 3 times in 1X PBS and mounted on slides with vectashield mounting medium. Coverslips were sealed with clear nail polish and imaged at five random fields. Cell phenotype was assessed by positively marked cells over total cells. Cells were considered positive if appropriate cell marker was identified as well as nuclear staining.

Pup brain glial cell culture

Pup brain tissues were cultured as described above and plated on poly-D-Lysine coated coverslips. Astrocyte cultures and microglia were cultured on coverslips for 48 hours. Cells were then fixed with 4% paraformeldahyde for 30 minutes. Coverslips were washed three times in 1X PBS with calcium and magnesium. Cells were then blocked in blocking buffer (3% donkey serum, 2% natural goat serum, 2% bovine serum albumin, 0.1% triton X-100 in 1X PBS with calcium and magnesium) for two hours at room temperature. Blocking buffer was removed and coverslips were incubated in primary antibody in

blocking buffer (1:1000 anti-GFAP for Astrocytes; 1:200 anti-IBA1 for microglia) overnight at 4°C. Coverslips were then washed three times in 1X PBS with calcium and magnesium. Coverslips were then incubated in secondary antibody (anti-rabbit alexaflour-555 1:200) in blocking buffer for two hours. Coverslips were mounted with mounting medium containing DAPI. Coverslips were imaged for seven fields in each coverslip. N=3 for each condition. Images were counted by two investigators that were blinded to image identities. Images are false colored green for ease of visualization through Adobe Photoshop v6.0. Intensity of microglia images were performed in Adobe Photoshop v.6.0. Intensity was assessed for DAPI and TRITC channels and the ratio of TRITC intensity over DAPI intensity were calculated. Statistical T-test was performed in positive count data and intensity data. * indicates p-value less than 0.05.

DNA Methylation Arrays and Analysis

DNA was isolated and an aliquot of 2000ng was submitted to the University of North Dakota Epigenomics and Bioinformatics Core for Illumina Infinium 450K DNA methylation arrays. 450k methylation array data was imported, controlled for quality, and normalized with SWAN normalization through RnBeads R program package [201]. Data was then exported and analyzed with R program to determine CpG site characteristics and associated genes based upon Illumina annotation. Statistical analysis for over/under representation was determined in R with Fisher's exact test with a cutoff p value of 0.05.

Extraction of RNA and DNA

DNA and RNA isolation were performed with manufacturer kits RNeasy and DNeasy Blood and Tissue (Qiagen) according to manufacturer protocols. Briefly, cell populations were divided equally into two parts and centrifuged at 200xg for 5 minutes. Media was aspirated and cells were washed in DPBS once if isolating DNA. RNA was isolated immediately followed by DNA isolation. DNA and RNA quantity and quality were assessed with a nanodrop 1000 spectrophotometer. 260/280 values for DNA quality and RNA quality ranged from 1.8 to 2.1.

Cell cultures were aspirated of medium and treated with up to 2 mL of .25% trypsin with .5 mM EDTA. Cell suspension was then collected and added to an equal volume of 5% FBS in Dulbecco's phosphate buffered saline to neutralize trypsin. Cell suspension was split evenly between two centrifuge tubes and centrifuged at 200xg for 5 minutes. Supernatant was aspirated and pellet was washed and centrifuged at 200xg for five minutes if DNA extraction was performed or aspirated and 350 uL of Buffer RLT added from Qiagen RNeasy Mini Kit.

DNA extraction was performed with alcohol precipitation as follows. Supernatant was removed from last centrifugation and pellet was lysed in 270 uL DNA Lysis Buffer (50mM Tris, 50 mM EDTA, in 2% SDS). 30 uL of proteinase K was added and samples were incubated overnight at 60° C. The following morning samples were heat treated to denature proteinase K at 100° C for 10 minutes. Samples were transferred to a medium gel phase lock tube and 300 uL of phenol: chloroform: isoamyl alcohol (25:24:1) was added and mixed by inversion. Samples were incubated for up to a minute and centrifuged at 13,000 rpm for 5 minutes at 4° C. Upper aqueous layer was transferred to a new labeled

1.5 mL conical tube and 30 uL of 7.5 M ammonium acetate was added, as well as 600 uL of ice cold ethanol. Samples were incubated for 3 hours at -20° C. Samples were then centrifuged for 20 minutes at 13,000 rpm and 4°C. Supernatant was decanted and aspirated off and pellet was washed in 75% ethanol with an additional centrifugation at 13,000 rpm for 5 minutes at 4° C. Supernatant was aspirated and pellet allowed to dry for 5-10 minutes before being suspended in 50 uL of DNase free sterile water. Samples were quantitated on Nanodrop 1000 apparatus with 260/280 values ranging from 1.6 to 2.1.

Extraction of RNA from samples was performed according to the manufacturer's protocol and are briefly described here. RLT buffer suspended samples were homogenized with a sterile 20 guage syringe needle five times. 75% ethanol was added and mixed via pipette and transferred to kit included column. Samples were centrifuged at 8,000xg for 15 secs and elute discarded. 700 uL buffer RW1 was added to column and centrifuged for 15 seconds at 8,000xg after which elute was discarded. 500 uL of buffer RPE (with 4 volumes of ethanol added as described per kit manual) was added with a 15 second centrifugation at 8,000xg and elute discarded. A second wash of 500 uL of buffer RPE was performed with centrifugation at 8,000xg for 2 minutes. A clean elute tube was placed on column and a dry centrifugation step at 8,000xg for 1 minute was performed. 50 uL of provided RNase free water was added to column and incubated for 1 minute. Sample collection tube was placed in place of elute tube. Final centrifugation step was performed at 8,000xg for 1 minute. Samples were quantitated on Nanodrop 1000 with 260/280 values ranging from 1.8 to 2.2.

Mass Spectrometry

Injection stock samples were evaluated for Paraquat. 10 uL of sample was collected and diluted into 80% methanol with addition of 1 ug of Paraquat standard. Samples were then washed twice with 1 volume hexane and centrifuged for 5 minutes at 2000 x g. Samples were then submitted for LC/LC-mass spectrometry at UND mass spectrometry core. Results are displayed as concentrations of individual injection stocks.

Approximately 10 mg of tissue and 10 uL of serum were processed for mass spectrometry. For tissue, 10 ng of standard were added to each sample in 80% methanol. For sera samples 10 ng of standard was added and samples were dilute to 80% methanol. Samples were pulse sonic ated for 7 seconds. Samples were centrifuged for 10 minutes at 2000 x g. Samples were then washed with hexane twice followed by centrifugation at 2000 x g for 5 minutes. Samples were then submitted for mass spectrometry. Tissue sample extraction was repeated twice with similar results. Results are displayed with initial results and * indicate statistical significance as per T-test.

Reactive Oxygen Species Detection

Whole cell reactive oxygen species assay

Cells were seeded at 5,000 cells per well and cultured for two days in respective complete medium. Cultures were pre-treated with 1% DMSO and 10uM H_2DCFDA in HBSS for one hour. H_2DCFDA medium was removed and replaced with Paraquat conditioned HBSS with 0 uM, 0.5 uM, 5 uM, 50 uM and 1000 uM concentrations of Paraquat. Hydrogen peroxide was used at a concentration of 500 uM as positive control for reactive oxygen species detection. Cultures were read in 5-15 minutes from initial treatment and six hour intervals thereafter until 24 hours. Cultures were incubated at 37º

C with 5% CO_2 between reads. Reads were performed on a Biotek Synergy HT plate reader with excitation/emission at 485/528 and a bottom read with sensitivity of 60. Results are displayed as fold change over control. Each concentration was tested in 6-8 wells of each 96 well plate. Plates were replicated at least 3 times with astrocytes from different lots or passages. Statistics were performed as Two Way ANOVA with Bonferroni's post-test.

Mitochondrial Reactive Oxygen Species

Astrocytes were cultured as described above for 24 to 48 hours prior to treatment in 35 mm poly-d-lysine coated glass bottom dishes. Cells were incubated in 1 uM Mitosox red, 50 nM Mitotracker green and 10 mg/mL Hoescht 33345 for 30 minutes prior to initial treatment with Paraquat. Cells were then treated with Paraquat at 0.5, 5.0, 50.0, 1000.0 uM concentrations for 0.5 or 16 hours. Antimycin A was used as a positive control at 1 uM concentration. 10 fields per dish were imaged on a Zeiss Axiovert 200M. Images were analyzed in Adobe Photoshop version 6.0. Each experiment was replicated a total of 4 times. Statistical analysis of results were completed with a One-way ANOVA with Bonferroni's post-test. * indicate $p < 0.05$.

8-oxo-dG detection

Astrocyte cultures were seeded at 5,000 cells/cm^2 and cultured for 48 hours prior to treatment with Paraquat. Cells were treated with Paraquat at 0.5, 5, 50 and 1000 uM. Complete medium was used as control and 500 uM H_2O_2 was used as positive control. Cells were incubated for two hours. Cells were then fixed in 4% paraformeldahyde for 30 minutes. Coverslips were washed three times in 1X calcium and magnesium free PBS.

RNA Sequencing and Alternative Splicing

Libraries were created using Illumina Tru-Seq strand specific library preparation kits and sequenced on the Illumina HiSeq 2500. The fastq files were aligned against the MM10 reference genome using HISAT2 [202]. Reads were assigned to genes and counted using Rsubread [203] and differential calls made by DESeq2. Differential gene expression lists (tables 5-8) were submitted for gene ontology analysis through Panther Gene ontology database, and Ingenuity Pathway Analysis through Qiagen IPA software.

Sequencing data from second experiment was sequenced with paired end reads allowing for alternative splicing analysis. We used multivariate analysis of transcript splicing to find alternative splicing events [204]. Microglia and astrocyte cultures were analyzed separately with comparison between control and Paraquat treatments.

TABLE 1. ATAC-SEQUENCING SAMPLE LIST AND PRIMER INDEX

Lot	[PQ] uM	Time (hours)	Forward Primer	Reverse Primer
A	0	24	N502	N701
A	0.5	24	N504	N701
A	5	24	N502	N702
A	50	24	N504	N702
B	0	24	N502	N703
B	0.5	24	N504	N703
B	5	24	N502	N704
B	50	24	N504	N704
C	0	24	N502	N705
C	0.5	24	N504	N705
C	5	24	N502	N706
C	50	24	N504	N706
A	0	72	N503	N701
A	0.5	72	N517	N701
A	5	72	N503	N702
A	50	72	N517	N702
B	0	72	N503	N703
B	0.5	72	N517	N703
B	5	72	N503	N704
B	50	72	N517	N704
C	0	72	N503	N705
C	0.5	72	N517	N705
C	5	72	N503	N706
C	50	72	N517	N706

TABLE 2. PCR AMPLIFICATION STEPS

Initial PCR amplification

No. of Cycles	Temp (deg. C)	Time (s)
1	72	300
1	98	30
5	98	10
	63	30
	72	60

Amplification Saturation

No. of Cycles	Temp (deg. C)	Time (s)
1	98	30
20	98	10
	63	30
	72	60

Finishing Cycles

No. of Cycles	Temp (deg. C)	Time (s)
1	98	30
N	98	10
	63	30
	72	60
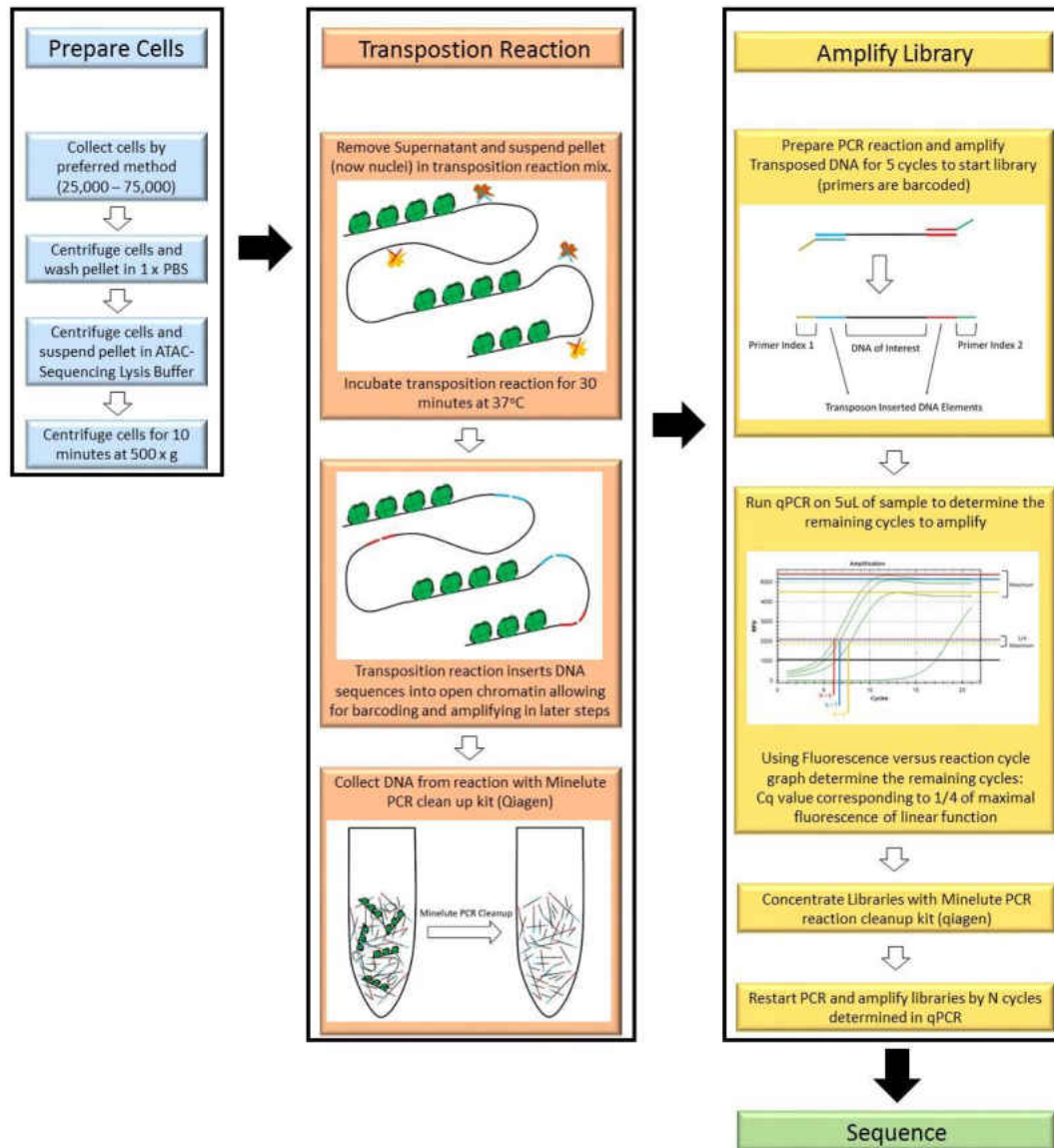
Figure 3. An overview Assay for Transposase Accessible Chromatin Sequencing (ATAC Sequencing). ATAC Sequencing is a current technology to assess the accessibility of chromatin in low numbers of cells. Nuclei are extracted and DNA tag fragments are inserted into open regions of chromatin allowing for sequencing and identification of shifts in chromatin accessibility in response to treatment with Paraquat.

TABLE 3. FLUORESCENCE VALUES OF RTQPCR AND FINISHING (N) CYCLES

Lot	[PQ] uM	Time (hours)	Max Fluorescence	Base Fluorescence	¼ of linear Fluorescence	N cycles
A	0	24	4000	800	800	7
A	0.5	24	4600	1000	900	7
A	5	24	4400	800	900	7
A	50	24	4400	600	950	8
B	0	24	4600	800	950	7
B	0.5	24	4400	600	950	7
B	5	24	4600	800	950	7
B	50	24	4600	600	1000	7
C	0	24	4800	800	1000	8
C	0.5	24	4600	600	1000	7
C	5	24	4800	800	1000	7
C	50	24	4600	800	950	7
A	0	72	4200	800	850	7
A	0.5	72	4600	1000	900	6
A	5	72	4400	800	900	7
A	50	72	4400	800	900	6
B	0	72	4600	800	950	7
B	0.5	72	4200	800	850	7
B	5	72	4600	600	1000	8
B	50	72	4800	800	1000	7
C	0	72	4600	600	1000	8
C	0.5	72	4600	800	950	7
C	5	72	4800	800	1000	6
C	50	72	4200	600	900	7

CHAPTER III

PRIMARY HUMAN ASTROCYTES INDUCE DNA DAMAGE RESPONSE AND REDUCE OXIDATIVE DAMAGE MARKERS WHILE SURVIVING ACUTE LOW CONCENTRATION EXPOSURES OF PARAQUAT

Introduction

Many diseases of the human brain are debilitating, progressive, and have limited therapeutic options. The origin of neural diseases have yet to be fully elucidated and recent evidence implicates both neurodegenerative and neuro-oncologic diseases to be multifactorial [205-207]. Current epidemiological evidence implicates environmental components may be involved in the onset of neural diseases [8-19]. The epidemiological evidence also illuminates the potential link between early exposure and later onset of disease through an increased risk of neural disease after early development exposure. We hypothesize that this delayed effect of environmental stressors on the etiology of neural disease may be attributable to epigenetic remodeling events.

One potential hypothesis in the development of neural disease is that the production of reactive oxygen species induced by pesticide exposure lead to irreversible damage events [171]. There are several agricultural pesticides that work through the induction of oxidative stress [148, 151]. Inhibition of mitochondrial function, several of which are studied in the context of neurodegenerative disease [148, 158]. One such pesticide that is capable of both, is the herbicide Paraquat, which is available throughout the world and currently used in agricultural practices.

Paraquat has been studied in the context of Parkinson's disease models [172]. Parkinson's disease presents with a number of motor deficits including bradykinesia, stooped posture, and masklike facial expression resulting from disruption in the basal ganglia pathways by the loss of dopaminergic neurons [208]. Cognitive deficits may also be present in cases of

Parkinson's disease which are reflected in a whole brain pathology that can be associated with the disease [208, 209]. Patients suffering cognitive deficit are often marked after death by the presence of Lewy bodies throughout the brain [210]. Often, the onset of symptoms is considered late stage of the disease and irreparable damage has already occurred [208]. The disease itself and its origin might start much earlier in life than previously predicted.

Etiology of Parkinson's disease has yet to be elucidated as there are limited genetically heritable influences that have been found to play a role in Parkinson's disease. Genetic mutations in genes such as LRRK2 and PARK2 have been linked to cases with a family history as well as sporadic cases but do not account for the majority of Parkinson's disease cases [211, 212]. Studies focused on pesticide exposure and agricultural links have also shown a strong correlation with development of Parkinson's disease [18, 19]. Parkinson's disease is prominent among epidemiological reports that find correlations between exposure of toxins and onset of neurodegenerative diseases. One factor not accounted for regularly in Parkinson's disease models is the potential presence of pesticides in early life. It may be possible that early pesticide exposure alters the response of normal cells to later stressors and can lead to a neurodegenerative response.

Here we examine the role of pesticides in normal human astrocytes. Astrocytes are a critical support cell within the central nervous system and have potential to influence the loss of more sensitive neurons [213]. Our model system is based on primary fetal derived human astrocytes and their exposure to low concentrations of Paraquat. Low concentrations of Paraquat may be more representative of concentrations present in the neural systems of *in vivo* models. Our primary focus is on the changes that occur in surviving astrocytes. We examine the capability of primary human astrocytes to survive and the reactive oxygen species response to Paraquat. We further examine chromatin accessibility of treated cells to identify potential

epigenetic remodeling events. We find that primary astrocytes are capable of surviving low

concentrations of Paraquat and also do not exhibit a detectable sustained change in reactive

oxygen species. We also find that Paraquat induces a reactive state in primary astrocytes that is

concentration dependent.

Primary human astrocytes can survive low concentrations of Paraquat

Cell viability of primary human astrocytes to determine sub-lethal concentrations

was first assessed using a 3-(4,5-Dimethylthiazol-2-yl)-2,5-Diphenyltetrazolium Bromide

(MTT) assay. The MTT assay has been used as a standard for cell viability in Paraquat

exposure models and works through the conversion of MTT to formazan in the

mitochondria. In these experiments, astrocytes were exposed for 72 hours to

concentrations of Paraquat ranging from 1000 uM to 0.5 uM. Our data is consistent with

other groups that show that high concentrations of Paraquat induce a loss of formazan

signal, and is also consistent with other primary cell types in having a greater sensitivity

than immortalized counterparts (figure 4A). Astrocytes significantly lose viability at 62.5

uM and higher concentrations of Paraquat. There does appear to be a slight increasing

trend in low concentrations of increased viability, but is not statistically significant. The

MTT assay has been a gold standard in Paraquat studies to assess cell viability and

effectively measures mitochondrial function. Our data indicate that at concentrations

below 62.5 uM Paraquat, there is no significant effect on mitochondrial function. While

the MTT assay has been used a proxy for cell death and or proliferation we sought to

assess cell survival using a triple stain live/dead assay to confirm our results.

Using the mitochondrial function data, three concentrations were chosen below

the significant loss in cell viability: 0.5, 5 and 50 uM. These concentrations offer a range

to assess the impact of sub-lethal concentrations of Paraquat, and mirror what is found physiologically in *in vivo* studies for brain Paraquat concentration. Also chosen was a relatively high concentration of 1000 uM Paraquat as concentrations similar to this value have been previously reported to have detrimental effects on the cell population. 500 uM H_2O_2 was chosen as a positive control due to the reactive oxygen species producing nature of Paraquat. In the cell viability assays, primary astrocytes were exposed at the above mentioned concentrations for 24 and 72 hours. Cell death was assessed by the uptake and nuclear staining of ethidium homodimer (red) and cell viability was assessed with calcein metabolism (green). Hoescht staining demarcated nuclei of all cells. Survival results are reported as a ratio of calcein positive cells over total cells (hoescht stained nuclei). Cell viability is significantly reduced in cells exposed to 1000 uM Paraquat and 500 uM H_2O_2 at 24 and 72 hours (figure 4B). A discrepancy exists between the live/dead and mitochondrial viability assays in that at 1000 uM Paraquat there is about 50% cell survival (approximately 65% of control) and mitochondrial viability shows about 10% viability. To differentiate the difference we assessed the total number of cells assayed at 24 and 72 hours as a percent of control and have a significant reduction in the total number of cells at these time points for both 1000 uM Paraquat and 500 uM H_2O_2 indicating that some of the mitochondrial viability loss is from the reduced number of cells (figure 4C). Of note is that the sub-lethal concentrations are indeed not lethal when considering the number of cells and survival of the cells are not statistically different than control.

Sub-lethal Paraquat exposure in primary astrocytes fails to induce cytosolic Reactive Oxygen Species (ROS) above levels of control but transiently increases mitochondrial ROS.

Paraquat is known to produce reactive oxygen species through Electron Transport Chain (ETC) complex inhibition. We evaluated the effect of sub-lethal Paraquat on reactive oxygen species production in the whole cell by H_2DCFDA, a fluorogenic compound that reacts indiscriminately with all reactive oxygen species. At sub-lethal concentrations Paraquat is unable to exhibit reactive oxygen species levels above control levels. However, in the lethal concentration, 1000 uM Paraquat, reactive oxygen species levels are significantly increased, although not to the same level as H_2O_2 (figure 5A). We also sought to evaluate the levels of reactive oxygen species in the mitochondria as Paraquat is reported to produce superoxide radicals within the mitochondria. Primary astrocytes were incubated in mitosox red, a fluorescent probe more specific to superoxide radicals, and mitotracker green as well as heoscht to demarcate cellular localization. Astrocytes were then exposed for 0.5 and 16 hours as an initial response and to define the mitochondrial Reactive oxygen species contribution after significant increase in total cell reactive oxygen species in the lethal dose. Antimycin A, an inhibitor of the ETC, was chosen as a positive control. There is a significant increase in level of mitochondrial reactive oxygen species at 0.5 hours for 0.5 uM Paraquat that is not present in the remaining concentrations including 1000 uM Paraquat (figure 5B,C). At 16 hours, other than the increase in total cell reactive oxygen species for 1000 uM Paraquat, no Paraquat treatment condition has significant reactive oxygen species signal in comparison to the control. The reactive oxygen species signal in primary astrocytes is only transient in the mitochondria for the lowest concentration and the highest concentration induces an

reactive oxygen species signal without significant reactive oxygen species signal in the mitochondria.

Acute Paraquat exposure induces significant DNA damage response in primary human astrocytes at higherconcentrations

We next evaluated the DNA damage response at sub-lethal concentrations by immunostaining for phosphorylated H2AX, an established DNA damage response marker (Figure 6). Cells were also stained for Glial Fibrillary Acidic Protein (GFAP) as an astrocyte marker (figure 6A). H2AX staining was significantly present in more cells at 50 uM Paraquat despite not having a greater H2AX signal in each positive cell in both 24 and 72 hour time points (figure 6B,C). Additionally, H2AX signal was detected in more cells than control for both 1000 uM Paraquat as well as 500 uM H_2O_2. The H2AX signal in each positive cell was no greater than control for 1000 uM at 24 hours, however, at 72 hours there was a significant increase in signal per cell. The opposite was found for H_2O_2, with the signal per cell at 72 hours no longer being significantly greater than control. Additionally the signal at 72 hours for 1000 uM Paraquat was greater than the 24 hour signal for 500 uM H_2O_2.

Gene expression analysis in acute Paraquat exposure of primary human astrocytes displays a batch effect among experiments

Our initial gene expression analysis of acute Paraquat exposure in primary human astrocytes (figure 7) indicated a significant batch effect in samples more dependent on replicate than experimental conditions. Additionally, replicates clustered out independent of time in culture suggesting that the replicate samples are from very distinct groups of astrocytes potentially masking any measurable effect from acute Paraquat exposure. In subsequent experiments, we repeated the acute exposure paradigm and assessed control

conditions based on the number of GFAP expressing cells and the ability to maintain a consistent population.

Loss of Glial Fibrillary Acidic Protien (GFAP) in control conditions indicate acute exposure experiments need to be better controlled and repeated

We initially assessed the number of GFAP positive cells in the H2AX data set from the initial experiments and in GFAP labeled cells from the repeat experiment (figure 8). In the initial acute Paraquat exposure experiments there is a loss in GFAP positive cells over the 72 hour window that occurs in lower concentration Paraquat conditions. In the 1000 uM Paraquat 24 hour condition, there is a significant increase in GFAP positive cells, however, at 72 hours 1000 uM Paraquat is not significantly different than 24 hour control conditions. With 500 uM H_2O_2 exposure the response is similar to the low concentration Paraquat exposures as well as control conditions. This appears to indicate that the initial experiments may not be as well controlled as they could be.

When we repeated the acute Paraquat exposure experiments, careful consideration was taken to control for as many variables as feasible. Three separate donors were used as replicates to allow for biological variability, but the repeat experiment was performed on all three donor cell groups simultaneously with the same reagents to reduce technical variability. We also used the earliest passage possible without sub-culturing to reduce potential differences in these cells which may have been induced by variability in sub-culturing technique. Previous experiments were performed in cells that had been sub-cultured once.

GFAP positive cells were assessed in the repeat experiment for all three donor types. In control conditions, the 72 hour time window no longer induces a drop in the

58

percent of GFAP positive cells. Additionally we see a concentration dependent increase in GFAP positive cells at 24 hours for all concentrations of Paraquat and for 500 uM H_2O_2. The increase in GFAP positive cells is transient in Paraquat treated cells while 500 uM H_2O_2 treated cells maintained higher numbers of GFAP cells.

Nuclear oxidative damage marker is reduced in low concentration Paraquat exposure but not in high Paraquat concentrations

To reaffirm and compliment initial studies we assessed reactive oxygen species response in primary human astrocytes using an oxidative damage marker 8-oxo-dG. We assessed nuclear 8-oxo-dG staining as nuclear damage events would be most likely to drive apoptotic events or may generate mutations that drive oncologic events. Primary human astrocytes were exposed to Paraquat (0.5, 5, 50 and 1000 uM) or 500 uM H_2O_2 for two hours in order to characterize an early astrocyte response which complements our mitochondrial reactive oxygen species studies. In 8-oxo-dG nuclear staining at two hours, there was reduced staining in 0.5 and 5 uM Paraquat conditions from control, while 50 uM and 1000 uM Paraquat were unchanged as compared to vehicle treated cells (figure 9). . 500 uM H_2O_2 induced an increase in nuclear 8-oxo-dg staining.

Initial results may be skewed by reactivity of the cell populations as indicated in figure 8; nuclear 8-oxo-dG staining does confirm a response to Paraquat in low concentration acute exposure. In seeing a reduced intensity at the two lowest concentrations, we might expect that these cells have initiated a DNA damage response or reactive oxygen species mediating response that confers protection of the nuclear DNA from oxidative damage. However, this response is itself ablated at higher concentrations and returns to control condition levels. This may implicate that the stress response is overwhelmed and we are beginning to see nuclear oxidative damage return to normal

59

levels. However, at 1000 uM Paraquat there is no significant increase in oxidative

damage implicating that Paraquat induced oxidative damage is limited. Another

possibility remains that low level Paraquat exposure induces a stress response that ablates

natural oxidative DNA damage better than control conditions but at higher Paraquat

concentrations this condition is lost as the cell is beginning to respond to mitochondrial

dysfunction.

Discussion

We set out to understand the impact of low Paraquat concentrations in primary

human astrocytes as we expected that the astrocytes will alter their epigenetic profile and

survive toxicant exposure. We assessed basic parameters of survival in astrocytes

exposed to Paraquat and found that acute exposure of 50 uM Paraquat and below the

astrocyte cultures are capable of surviving. We further assessed reactive oxygen species

response in low concentrations and have found that only the lowest concentration, 0.5 uM

Paraquat was able to induce a transient mitochondrial reactive oxygen species response.

However, the total reactive oxygen species response over a 24 hour period was not

significantly different than control conditions in the low concentrations. Yet without a

significant reactive oxygen species response we were able to detect DNA damage marker

H2AX in 50 uM Paraquat treated cells at 24 and 72 hours. The DNA damage response

we detect is in the absence of a significant reactive oxygen species response. H2AX

demarcates double stranded DNA breaks. In our exposure model the significant H2AX

response may be attributable to a change in transcription as opposed to DNA damage

repair [214, 215].   The other possibility remains that our measurement methods are not

sensitive enough to detect reactive oxygen species with lower concentrations of Paraquat exposures.

When we assess nuclear 8-oxo-dG, a marker for oxidative DNA damage, in the replicate experiment, we report a decrease in nuclear 8-oxo-dG signaling for the lowest Paraquat concentrations which may indicate an activation of DNA repair mechanisms or suppression of oxidative stress by Paraquat. However, at higher concentrations nuclear 8-oxo-dG returns to control levels ablating any protective effect. The effect on nuclear 8-oxo-dG signaling may be in part to a response seen in other organisms that increases viability and lifespan [216]. We hypothesize that we may be inducing a mild stress state that allows for repair mechanisms to work without creating additional burdens. One potential investigational pathway for the reduction of nuclear 8-oxo-dG staining would be to examine the protein expression and translocation of transcription factors involved with oxidative stress pathways. Additionally, we may be able to check transcription of targets for oxidative stress transcription factors to verify downstream effects of oxidative stress pathways. In the event that oxidative stress pathways are not activated we would pursue mechanisms of reactive oxygen species suppression including investigating activity of electron transport chain members. Electron transport chain activity has been linked to the production of reactive oxygen species, with both increased and decreased activity inducing higher reactive oxygen species levels.

While we have yet to report significant gene expression changes, the replicate experiment proves to be encouraging in that the astrocytes clearly respond to Paraquat exposure at sub-lethal concentrations. Future studies are planned pending results from the ATAC-seq experiments and would include first evaluating changes in gene

expression associated with Paraquat exposure followed by evaluating the DNA methylation changes that might be associated with acute Paraquat exposure. With changes in gene expression data and DNA methylation we may be able to pinpoint specific epigenetic remodelers to target in our assessment of the effect of Paraquat in epigenetic remodeling. An additional future direction is to target chronic long term exposure of primary astrocyte in Paraquat exposure.
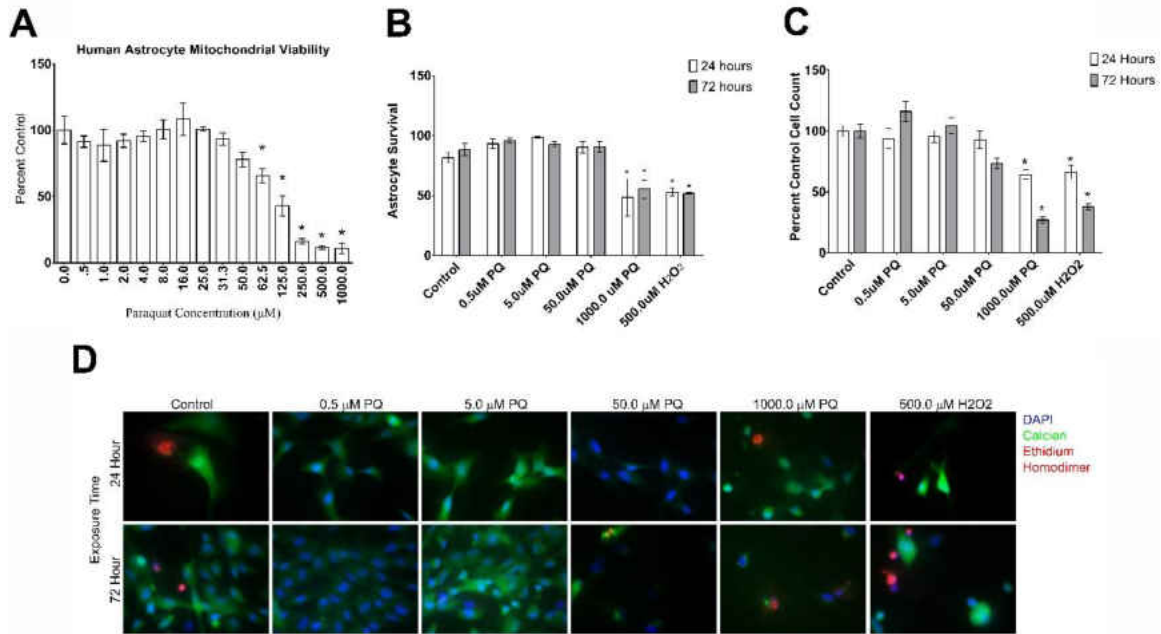
Figure 4. Primary human astrocytes can survive low concentrations of Paraquat.
A) MTT viability assay of primary human astrocytes exposed to a two-fold dilution from
1000 uM Paraquat to vehicle. Significant loss in viability begins at 62.5 uM and
continues at higher concentrations, below 50 uM no significant loss of viability exists. B)
Survivability results from primary astrocytes exposed to vehicle, Paraquat (0.5, 5, 50, and
1000 uM) or 500 uM H_2O_2 as determined by triple stain viability. Significant loss of
survivability exists at 24 and 72 hours in both 1000 uM Paraquat and 500 uM H_2O_2. C)
Total cells surveyed as percent of control in triple stain results. At 72 hours, 1000 uM
Paraquat and 500 uM H_2O_2 exposed cells exhibit significantly fewer cells than that of
control counterparts. D) Fluorescent images of triple stain assay at tested concentrations
and time points. Hoescht 33345 (blue) indicate nuclei; Calcien (green) indicates
fluorescent product of mitochondrial respiration, and ethidium homodimer (red) indicates
nuclei of dead cells as ethidium homodimer is not cell permeable. The cell images also
indicate that the primary astrocytes appear to be thriving in the presence of Paraquat as at
5 and 0.5 uM Paraquat the morphology appears the same as the controls (figure 1D).
However, at 5 uM there does appear to be some differences in morphology. 1000 uM
Paraquat treatment cells are distinctly different than that of the control group.

63
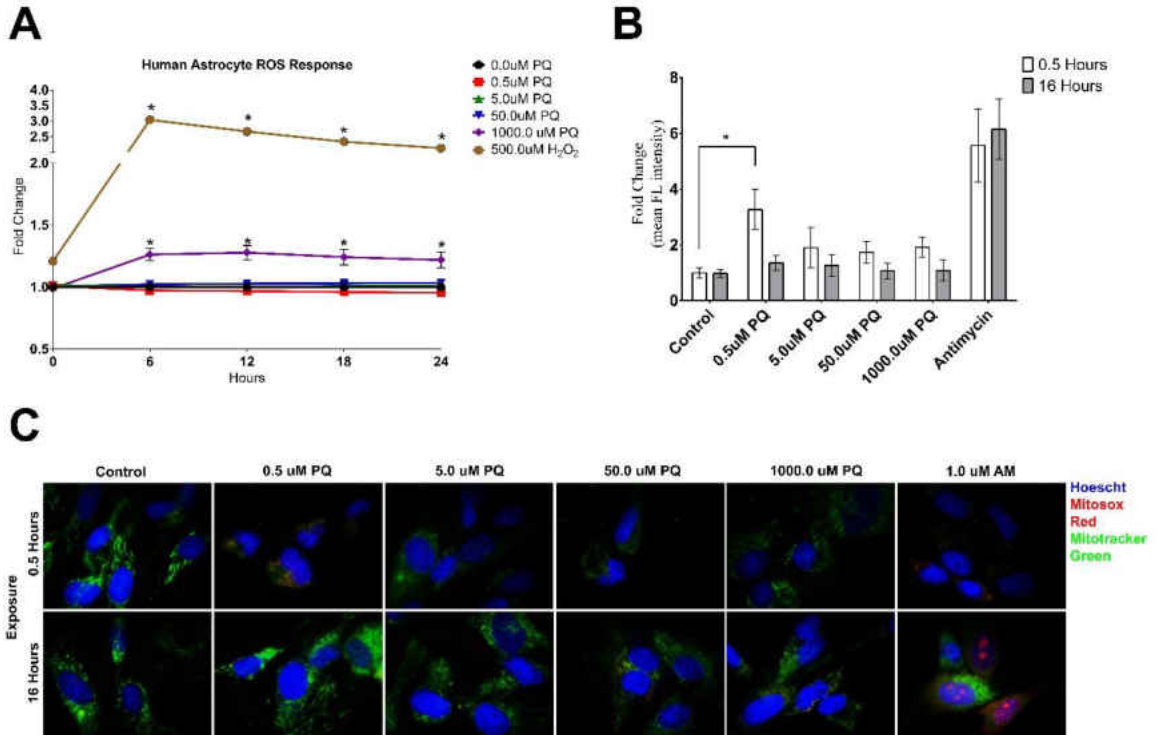
Figure 5. Sub-lethal Paraquat exposure in primary astrocytes fails to induce cytosolic Reactive Oxygen Species (ROS) above levels of control but transiently increases mitochondrial ROS. A) H_2DCFDA non-discriminate measurement of reactive oxygen species at six hour intervals in primary astrocytes exposed to Paraquat (0.5, 5, 50 and 1000 uM) or 500 uM H_2O_2. 1000 uM Paraquat is the only concentration with significant detection of reactive oxygen species. 500 uM H_2O_2, used as a positive control initiates a much higher response than that of the highest concentration of Paraquat tested. B) Measurement of mitochondrial reactive oxygen species with 1 uM mitosox red, 50 nM mitotracker green and 10 mg/mL Hoescht 33345 in primary astrocytes exposed to Paraquat (0.5, 5, 50, 1000 uM) or 1 uM antimycin A as a positive control. Antimycin A, an electron transport chain inhibitor, induces significant increase over control of mitochondrial reactive oxygen species. 0.5 uM Paraquat significantly increases mitochondrial reactive oxygen species at 30 minutes but is attenuated at 16 hours compared to control. The remaining concentrations do not induce significant change in reactive oxygen species over control. C) Images of cells in B.
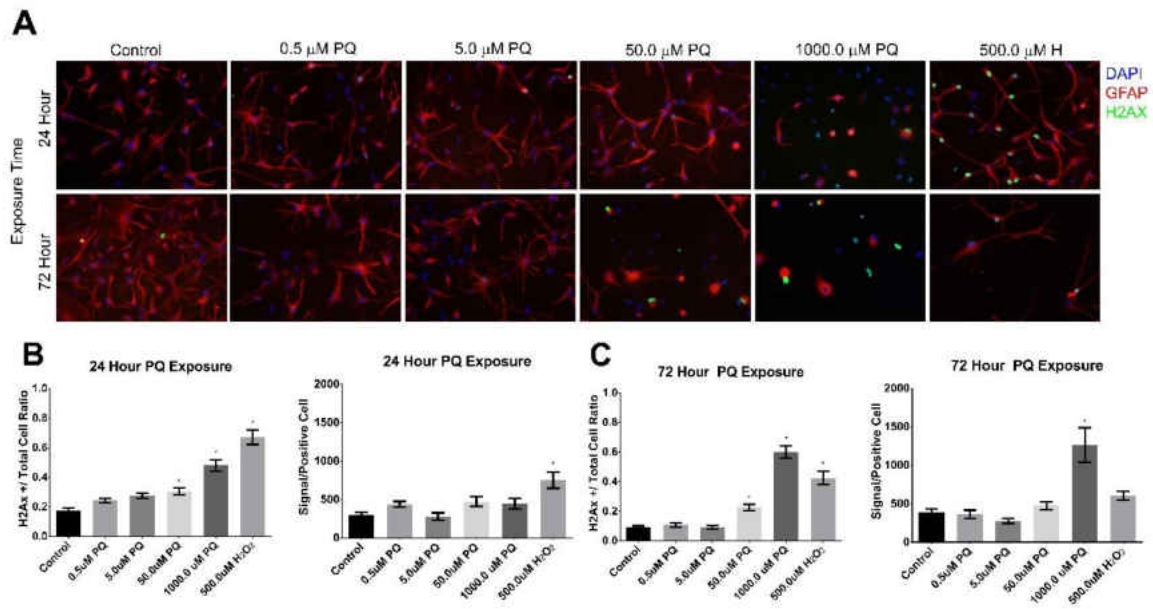
Figure 6. Acute Paraquat exposure induces significant DNA damage response in primary human astrocytes in high sub-lethal to lethal concentrations. A) Fluorescent images of primary astrocytes exposed to vehicle, Paraquat (0.5, 5, 50, and 1000 uM) or 500 uM H_2O_2. DAPI (blue) indicate nuclei; GFAP (red) indicate glial acidic fibrillary protein, a cytoskeletal protein found in astrocytes; and H2AX (green) indicate phosphorylated H2AX histones, a marker for DNA damage. B) Ratio of H2AX positive cells over total cells (left) and total signal per positive cell (right) at 24 hours of exposure. H2AX positive cell ratio indicates 50.0 uM and 1000 uM Paraquat and 500 uM H_2O_2 have significantly greater number of DNA damage responding cells. H2AX signal per H2AX positive cell is significantly more in only positive control, 500 uM H_2O_2. C) Ratio of H2AX positive cells over total cells (left) and total signal per positive cell (right) at 72 hours of exposure. H2AX positive cell ratio is significantly more than control in 50 uM, and 1000 uM Paraquat as well as 500 uM H_2O_2, with 1000 uM Paraquat having a higher ratio than 500 uM H_2O_2. H2AX signal per H2AX positive cell is significantly more in 1000 uM Paraquat and 500 uM H_2O_2.
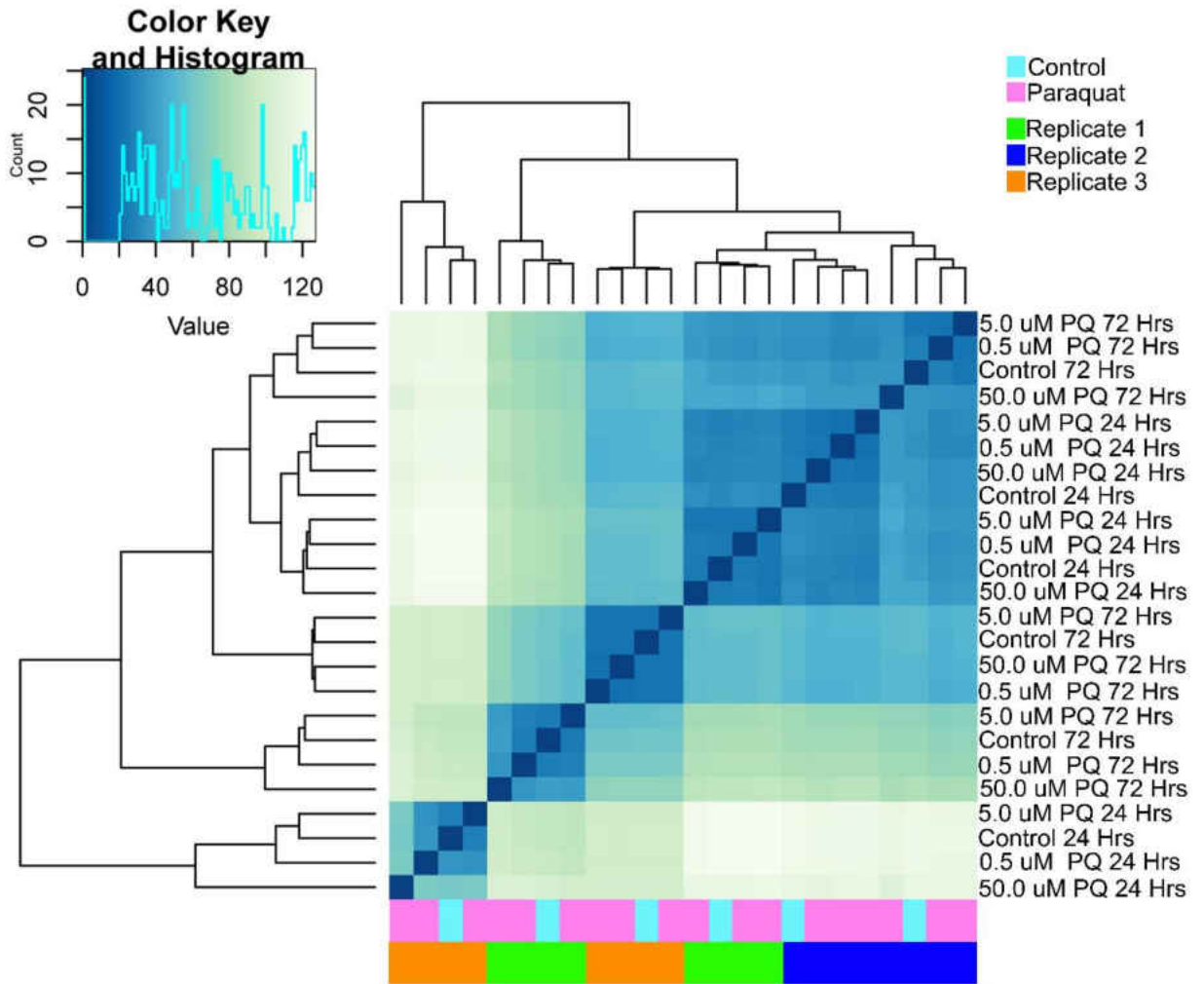
Figure 7. Gene expression analysis in acute Paraquat exposure of primary human astrocytes displays a batch effect among experiments. RNA was collected from primary human astrocytes exposed to Paraquat (0.5, 5, and 50 uM) for 24 or 72 hours. RNA sequencing was performed on collected samples and results are indicated in distance clustering plot. Clustering indicates that data seperates into clusters of individual experiments irrespective of time in culture and treatment condition.
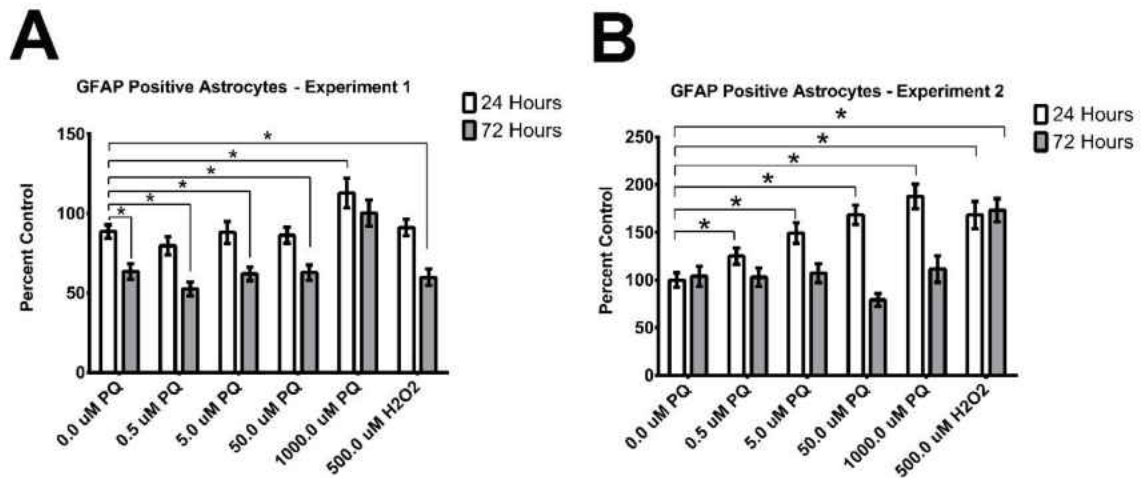
Figure 8. Loss of Glial Fibrillary Acidic Protein (GFAP) in control conditions indicate acute exposure experiments need to be better controlled and repeated. The number of GFAP positive cells were counted in the first series (A) and the second series (B) of experiments. Cells were cultured on coverslips for 48 hours prior to treatment with Paraquat (0.5, 5, 50, and 1000 uM) or 500 uM H_2O_2. Cells were treated with an acute exposure for 24 or 72 hours, fixed in 4% paraformaldehyde, and stained for GFAP. In control conditions there is a drop in the number of GFAP expressing cells for experiment 1 (A) over 72 hours, which is not present in experiment 2 (B). This indicates that experiment 2 was better controlled as the cells are stable over the 72 hour period. Additionally in experiment 2, there is a transient, concentration dependent increase in GFAP expressing cells.

Nuclear 8-Oxo-dG Intensity
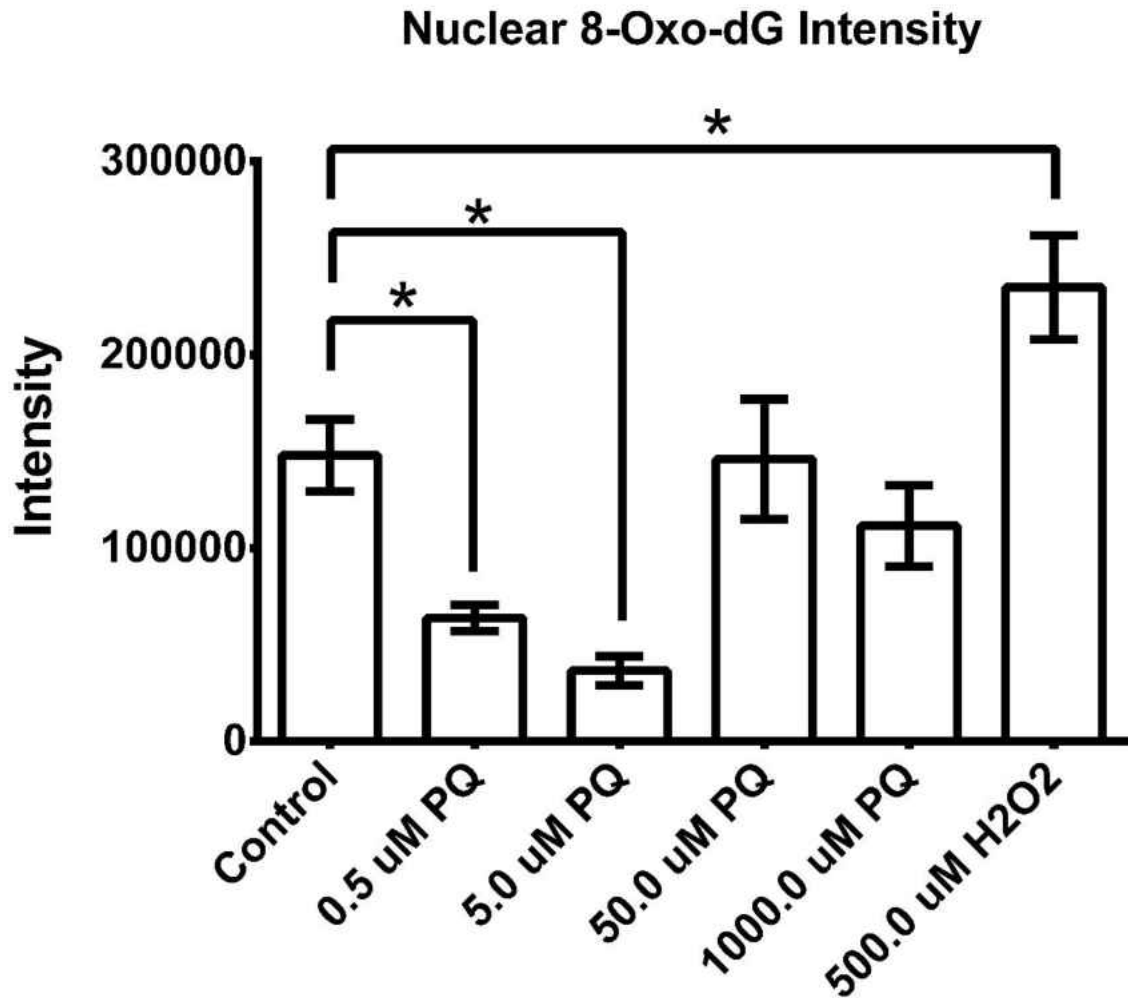
Figure 9. Nuclear oxidative damage marker is reduced in low concentration Paraquat exposure but not in high Paraquat concentrations. Primary human astrocytes were cultured on poly-D-lysine coated coverslips for 48 hours prior to treatment. Astrocyte cultures were treated with Paraquat (0.5, 5, 50 and 1000 uM), 500 uM H_2O_2, or complete medium for two hours. Cells were then fixed with 4% paraformeldahyde, and stained with anti-8-oxo-dG antibody. Images were captured for seven fields in each condition in each astrocyte donor type and intensity of 8-oxo-dG staining was measured for the nuclear area as defined by DAPI stained nuclei. Results indicate average intensity per nuclei. 0.5 and 5 uM have reduced intensity in nuclear staining of 8-oxo-dG compared to control while 50 and 1000 uM remain at control levels. 500 uM H_2O_2 positive control has significantly more nuclear staining for 8-oxo-dG than that of control. Statistical differences were determined by One-way ANOVA followed by Bonferroni's post-test. * indicates p-value < 0.05.

CHAPTER IV

GLIAL CELL MITOCHONDRIAL FUNCTION AND REACTIVE OXYGEN SPECIES RESPONSE TO PARAQUAT IS DEPENDENT ON CELL TYPE

Introduction

The human nervous system is comprised of a heterogeneous mix of cell types (figure 10) with multiple origins. Neurons, astrocytes and oligodendrocytes all arise from neural progenitor cells while brain vascular pericytes and microglia arise from cell lineages outside of the central nervous system [217-221]. The cell lineage of brain vascular pericytes is not clear. Brain vascular pericytes can arise from the same neural progenitors as astrocytes and neurons and integrate in non-neural lineage brain vascular pericytes, generating a mixed origin population of brain vascular pericytes [220, 221]. Microglia are considered myeloid in origin and migrate into the central nervous system during development [222]. Schwann cells are myelinating cells of the peripheral nervous system, and these cells arise from neural progenitor cells but migrate outside of the central nervous system conferring a difference in accessibility to environmental toxicants [223, 224].

Each of these cell types have unique functions in the nervous system. Neurons vary in function and morphology that is entirely dependent upon the context of the region of the brain in which they are found. The primary function of neurons are to communicate signals in circuits established during development. Astrocytes are a

ubiquitous cell type found throughout the nervous system. Their function is primarily to support neuronal function and do so by secreting trophic factors and facilitating neuronal synapses [225]. They also maintain an immune capacity and function in the event of trauma to develop glial scarring preventing further neuronal death [226].

Microglia are the primary immune cell of the central nervous system and can recruit additional immune mediating cells in the event of disease [227, 228]. Microglia interact closely with astrocytes to facilitate the immune response [229]. Microglia also act to clean up the neural environment [230]. Oligodendrocytes and Schwann cells act in a similar capacity but in two distinct locations [231]. Both cell types act to myelinate axons and facilitate neuronal signaling, but oligodendrocytes are limited to the central nervous system while their counterparts, Schwann cells inhabit the peripheral nervous system. Brain vascular pericytes are a major component of the blood brain barrier [232]. Brain vascular pericytes facilitate communication between microglia and the immune cells outside of the central nervous system [233]. Considering many of these cell types have different cell lineages and functional significance we propose that different cells will respond differently to the same stimulus.

We chose Paraquat as our stimulus to assess the effect in different primary cells types because of the links between environmental exposure and neurodegenerative diseases [8-19]. Others have reported *in vitro* effects of Paraquat on neurons and other immortalized cell lines [98, 149, 156, 157, 162]. Our study examines the effect of Paraquat in primary glial cell types in two species. We examine human microglia, brain vascular pericytes and Schwann cells and murine astrocytes and microglia to address that different cell types respond differently to the same stimulus. We assessed mitochondrial

70

viability and reactive oxygen species response, two parameters reported to be affected by Paraquat. We found that Paraquat exposure differentially affects mitochondrial function dependent on cell type. However, we found that in human cells Paraquat induced a similar reactive oxygen species response while in murine cells there was a differential response. Additionally we found that an immortalized microglia cell line, BV2, had a differential reactive oxygen species response than the primary microglia counterparts.

Mitochondrial Viability

Mitochondrial viability is cell dependent in Paraquat exposure

Mitochondrial viability was assessed in fetal derived primary human Brain Vascular Pericytes (BVP) (figure 11 A), Schwann cells (hSC) (figure 11 B) and Microglia (hM) (figure 11 C, D) primarily to assess the effect of Paraquat on cells and secondarily as a proxy for cell viability. All cell types were cultured for 24 to 48 hours prior to treatment and subsequently treated with Paraquat for 72 hours. Mitochondrial viability was assessed through MTT assay.

BVP exhibit a significant decrease of about 65% in mitochondrial viability at 125 uM Paraquat. Concentrations below this value do not show a significant decrease in mitochondrial viability. Concentrations above 125 uM show the most reduced viability at approximately 90% loss in mitochondrial viability.

hSC exhibit a significant loss in mitochondrial viability at 125 uM Paraquat with approximately 50% of the population remaining viable. At 250 uM Paraquat, 25% of the hSC population remain viable. Although not statistically significant, there also appears to be a downward trend in viability at 16 uM Paraquat on up to 62.5 uM Paraquat. Concentrations below 16 uM are not different from the control population.

IL1B stimulates growth in hM [234] and also stimulates an inflammatory response in hM [235]. hM do not actively divide without stimulation, requiring the addition of IL1B in hM cultures to prolong culture conditions. In an effort to assess chronic Paraquat exposure over multiple population doublings *in vitro* we first sought to characterize the effect of IL1B in the response of hM to Paraquat mitochondrial viability (figure 11 D). We also sought to address the effect of Paraquat on mitochondrial viability in unstimulated hM (figure 11 C). Cells were treated with the same paradigm as above with reduced number of different concentrations to account for the limited availability of hM. Unstimulated hM exhibit a significant loss with the addition of Paraquat with 65 to 75 percent remaining viable in concentrations of Paraquat at 64 uM and below. At 1000 uM, unstimulated hM retain 10 percent viability. In the hM viability assays, 500 uM H_2O_2 was used as a positive control to induce cell viability loss. In unstimulated hM, 500 uM H_2O_2 retain viability at 10%. Stimulated hM also have a significant decrease in mitochondrial viability in all Paraquat treatment conditions with the exception of 32 uM Paraqaut. The decrease is less than that of unstimulated hM with a gain of 10 to 15 percent in viability between matched concentration sets in unstimulated versus stimulated hM. The exception to this is at 1000 uM Paraquat where no gain is observed and potentially a decrease may be observed. In the H_2O_2 treated stimulated hM, viability is significantly decreased from the control stimulated hM but only reduced to 60 percent viability compared to a 10 percent viability in unstimulated hM.

We also sought to assess the effect of Paraquat storage in sterile water at 4° C for a period of 3 months. We used BVP as the cell type to screen with as these cells grow quite well. Cells were treated with the same paradigm as above, with fewer conditions

centered around the potential cutoff point of 50 uM Paraquat. 72 hours exposure to 0.5

uM and 5 uM Paraquat had no difference from control in either freshly prepared or 3

month old Paraquat preparation. 50 uM Paraquat was significantly reduced in fresh

Paraquat preparation and reduced but not significant in the 3 month old preparation. The

50 uM Paraquat conditions were not significantly different from one another in the both

preparations. The 1000 uM Paraquat was significantly reduced from control conditions

in both preparations and the conditions were not significantly different from one another.

500 uM H_2O_2 was also significantly reduced in both preparations that were not

significantly different from one another.

Murine glial cells have a differential mitochondrial response to acute Paraquat exposure.

We also sought to assess the effect of Paraquat on mitochondrial viability in

primary murine neonate derived astrocytes (mA) and microglia (mMG) *in vitro*. mA and

mMG were derived from 1 to 3 day old pups on the C57bl6 background. Cells were

cultured from mixed brain cultures and incubated for 24 to 48 hours prior to Paraquat

treatment. Cells were then exposed to Paraquat for 72 hours and mitochondrial viability

was assessed with MTT.

mA mitochondrial viability at 0.5 and 5 uM Paraquat conditions is unchanged

from control (figure 12 A). At 32 uM Paraquat and above there is a significant loss of

mitochondrial viability to 25% remaining or less as the concentration increases. 500 uM

H_2O_2 also has a significant loss in mitochondrial viability with nearly all viability lost.

mMG showed an increase in mitochondrial viability at 0.5 uM Paraquat with

approximately 25% increase over control. 5 uM Paraquat was not significantly different

than the control condition, while 32 uM Paraquat and above all exhibit a significant loss

in viability with less than 20 percent remaining in each of the higher concentrations. 500 uM H_2O_2 also showed a significant loss in mitochondrial viability remained with more mitochondrial viability than that of the 1000 uM Paraquat.

Reactive Oxygen Species Response

Paraquat induced reactive oxygen species response is similar in different human glial cells.

Paraquat has been reported at high concentrations to have a significant reactive oxygen species response in many cell types. We sought to assess the levels of reactive oxygen species in BVP and hSC at concentrations below the significant loss in mitochondrial viability (figure 13). Cells were cultured for 48 hours prior to treatment with Paraquat or H_2O_2, a positive control. Reactive oxygen species levels were assessed with H2DCFDA pretreatment followed by Paraquat exposure. Reads were conducted at 6 hour intervals. At concentrations of 0.5 uM, 5 uM, and 50 uM Paraquat; there was no measurable difference from control conditions in either BVP or hSC. At 1000 uM Paraquat there was a significant and sustained reactive oxygen sspecies signal measured at 6 hours in both BVP and hSC. 500 uM H_2O_2 had a significant signal that was sustained from six hour read onwards in both BVP hSC. The reactive oxygen species response in both cell types is similar at 500 uM H_2O_2 at 2.5 to 3 fold increase over control. The 1000 uM Paraquat shows some difference in respect to cell type with BVP showing a 1.4 fold increase over control (figure 13 A) and hSC showing a 1.6 fold increase over control (figure 13 B).

Paraquat induced reactive oxygen species response in murine glial cells is cell dependent.

We also sought to assess murine glial cells in reactive oxygen species response to Paraquat at sub-lethal and lethal concentrations. Primary murine cells were isolated from neonatal pups as described above and cultured for 48 hours prior to treatment. Cells were pretreated with H_2DCFDA and then treated with Paraquat at 0.5, 5, 50 and 1000 uM Paraquat. 500 uM H_2O_2 was used as a positive control in primary murine cells. There is a distinct reactive oxygen species response between the mA (figure 14 A) and the mMG (figure 14 B). 0.5, 5 and 50 uM Paraquat in mA and mMG were not detectable above control conditions and 500 uM H_2O_2 showed a 2.5 to 3.0 fold change over control conditions. However, the cells differed in their response to the lethal concentration of 1000 uM Paraquat. mA showed an increasing trend above control conditions which was only significant at 18 hours. mMG showed an increased reactive oxygen species level that initiated and was significant at 6 hours and continued to climb up until 18 hours. mA only showed at 18 hours a 1.2 fold increase over control conditions while the mMG showed as high as 1.8 fold increase over control conditions.

Published literature which includes data assessing whole cell *in vitro* reactive oxygen species find reactive oxygen species production at lower concentrations than we are reporting here with primary cells. We sought to verify our conditions against a published cell line with a H_2DCFDA protocol and selected BV2 microglia, a C57bl6 neonatal derived immortalized cell line reported to be similar in function to primary cells [236]. BV2 microglia were cultured for 48 hours prior to treatment. Cells were then subjected to the same protocol as above. BV2 microglia show a reactive oxygen species response similar to the published results but different than that of primary cells (figure 14

C). BV2 microglia have a robust and sustained response at 3 hours with 1000 uM

Paraquat; earlier than that of the primary counterpart. The maximal reactive oxygen

species response to 100 uM Paraquat is at 2.5 fold over control much higher than the

maximal primary cell response. In 50 uM Paraquat treatment the reactive oxygen species

response is significant at 5 hours and continues to climb until 18 hours nearly matching

the 1000 uM Paraquat response. 5 uM Paraquat response becomes significant at 18 hours

at approximately 1.3 fold above control conditions. Both of these concentrations in the

mMG primary cells did not have a response above control conditions. 0.5 uM Paraqaut

did not elicit a response above control conditions matching the primary mMG cells.

Discusssion

In our study evaluating different glial cell types and their response to direct

exposure to Paraquat we found that the different glia respond differently in two basic

parameters: mitochondrial function and reactive oxygen species response.

Mitochondrial function is completely dependent on cell type as human glial cells respond

differently than the murine counterparts (figures 4A, 11 and 13) and differently from one

another. Schwann cells and brain vascular pericytes survive acute Paraquat exposure at

higher concentrations than that of other neuroglia including astrocytes. Schwann cells

offer the capacity to provide a protective function to neurons in biologically averse

environments. This function might provide for internal mechanisms allowing schwann

cells to compensate for toxicants. This may apply to brain vascular pericytes as well, as

blood brain barrier function is maintained in the presence of Paraquat [163]. Blood brain

barrier maintenance is critical for protection of the neural environment.

Interestingly microglia mitochondrial response is different in the two species as murine microglia have increased mitochondrial function at 0.5 uM while the human counterpart exhibits the opposite with reduced mitochondrial function. This study is limited in the interpretation that can be drawn as our mitochondrial assay measures the ability of cells to convert MTT to formazan which can be a function of increased mitochondria through increased cells or mitochondrial biogenesis or increased mitochondrial efficiency.

There remains a possibility that murine microglia have been activated by Paraquat stimulus and the activated microglia survive and proliferate in low Paraquat concentrations. Activation status may play a role in microglial response to Paraquat as the human microglia lose mitochondrial function without IL1B but regain mitochondrial function at 32 uM Paraquat in the presence of IL1B. This may reflect a threshold that must be reached before mitochondrial function is ramped up that is lower in murine microglia.

One significant difference in the microglia is the difference in 500 uM H_2O_2 exposed cells. IL1B treated human microglia show much reduced mitochondrial function compared to untreated human microglia and primary murine microglia. Microglia have the potential to survive reactive oxygen species in an inflammatory state but the murine microglia are reduced to levels similar to high Paraquat exposure. This is in contrast to activated human microglia. Two potential explanations exist; that the murine microglia in our model are not activated in the culturing method, or human microglia have unique adaptive responses for oxidative stress environments. In either case there is a significant difference in how human versus murine microglia respond to insults. This warrants

further investigation as microglia have been implicated in the development and progression of both cancer and neurodegeneration.

While high Paraquat is reported to induce reactive oxygen species in the microenvironment, the IL1B treated microglia don't show a different response than that of untreated human microglia, indicating that at high concentrations, the mechanism that exists to preserve mitochondrial function in the presence of H_2O_2 cannot compensate for Paraquat loss in mitochondrial function. This may offer a clue as to the protective mechanism in human microglia. One critical piece of information that is necessary for better understanding the impact of Paraquat on human microglia is the reactive oxygen species response. We can see in the murine microglia that the reactive oxygen species response is significant in the highest level of Paraquat, much earlier and higher as compared to the murine astrocytes response. Understanding the human microglia reactive oxygen species response, especially at 32 uM Paraquat might offer insight into potential stress response pathways.

BV2 microglia have been reported as a good proxy for microglia as they are proliferative and display many of the same qualities as primary microglia making them easier to propagate and use in experiments. Our data shows, however that BV2 microglia respond differently to similar levels of reactive oxygen species than their non-immortalized primary cell counterparts. Not only do the BV2 respond earlier than the primary counterpart, they also respond at much lower concentrations. Some Paraquat literature is based on reactive oxygen species work in BV2 microglia which may arbitrarily raise attention to reactive oxygen species damage and response mechanisms [160]. Our data also shows primary cells having reduced mitochondrial function at much

lower concentrations of toxicant exposures than that of published literature on many cell lines [148, 160, 162, 167, 168]. We also show that murine astrocytes have lower threshold of mitochondrial inhibition than human astrocytes, but the reverse is true for microglia. Human microglia have reduced mitochondrial function at the lowest Paraquat concentration we tested. Two conclusions can be made from this; cells can survive low acute exposures of Paraquat, but mitochondrial function of these cells is impacted at much lower concentrations in glia than previously reported [160].

A caveat to the data presented here exists in the *in vitro* nature of the cells. With monotype cell cultures we ignore the impact other cells have in Paraquat exposure. Microglia are reported to convert Paraquat to a monovalent cation, the only form that can traverse the dopamine transporter [167]. Astrocytes have been reported to express the dopamine transporter [237]. This might be affecting the bioavailability of Paraquat to astrocytes. Additionally, astrocytes may play a role in activating microglia [238]. This could fundamentally change the microglia response to Paraquat. However, despite these points, *in vitro* culture is necessary in the study of epigenetics as each cell type has a distinct epigenetic profile and mixed populations can mask epigenetic remodeling events.

Our data begins to assess that different cells respond differently to the same environmental stimulus, further investigation is warranted into how each of these cell types are responding. Further work is necessary in understanding the genetic response of the different glial cells to Paraquat exposure. Additionally we need to assess if Paraquat is unique in its effect on the different glial cells or if there is one programmed response in each cell type to a range of environmental toxicants. Additional co-culture studies would

be necessary to determine some of the interactions between the cells and how that plays a

role in the response to environmental toxicants.
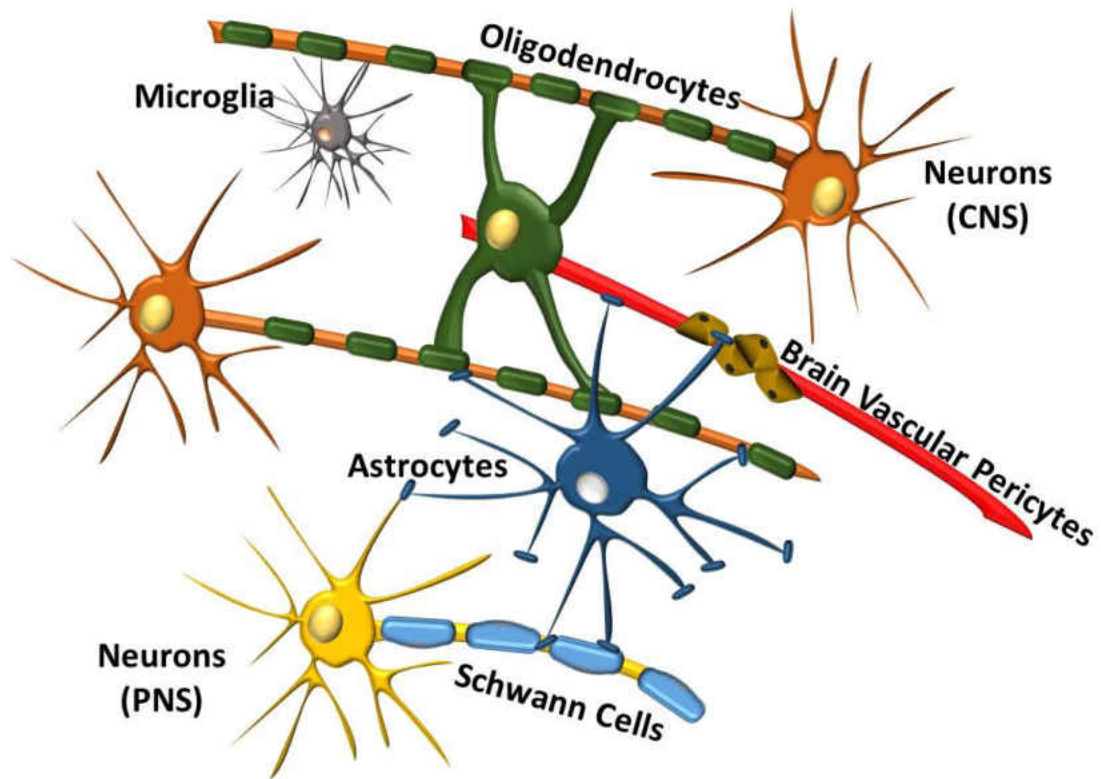
Figure 10. Heterogeneity of the nervous system. Schematic of the main cell types within the nervous system. The heterogeneity of the human nervous system indicates the need for assessing other cell types considering the interactions that can take place between the cell types.
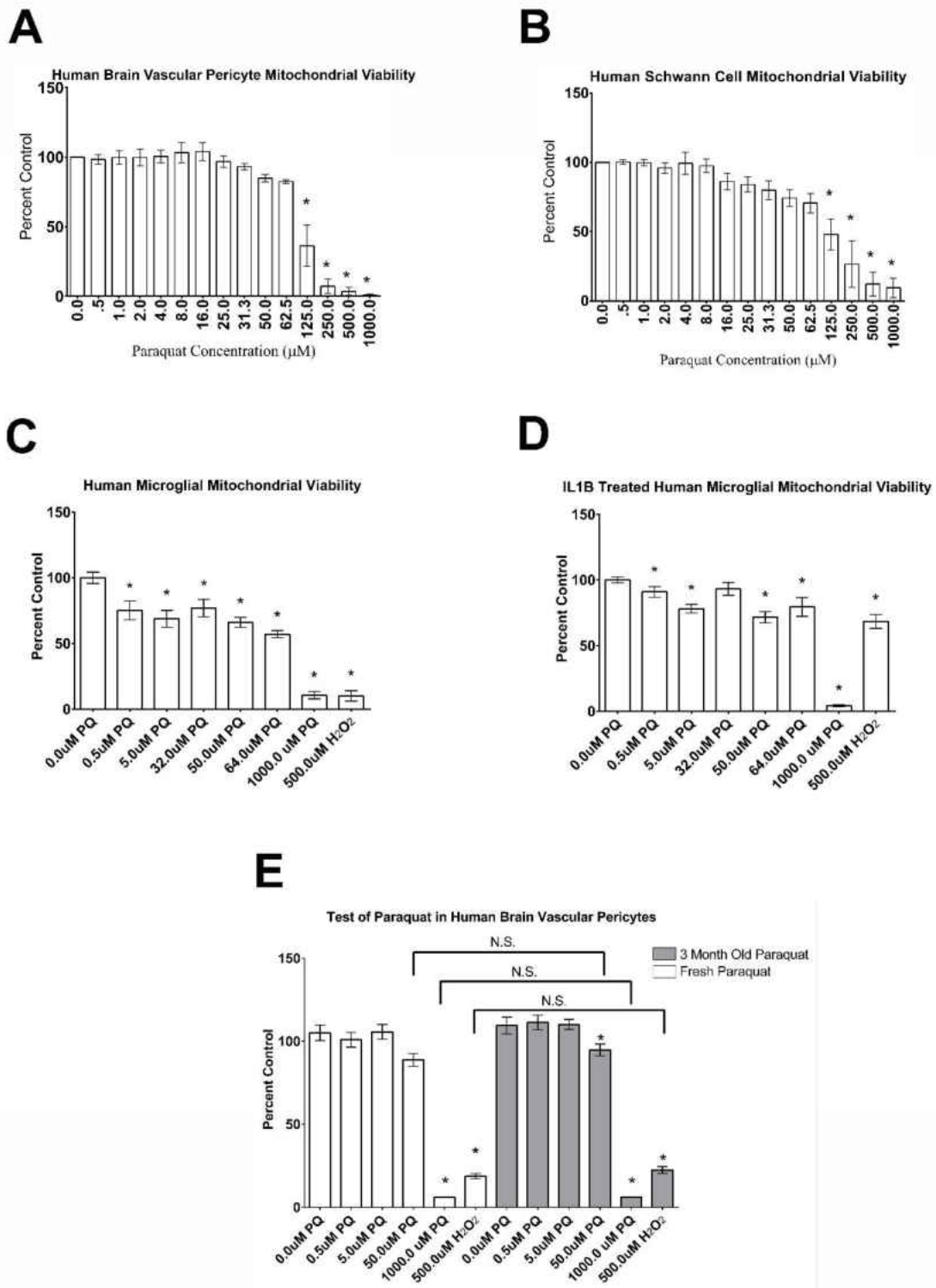
Figure 11. Mitochondrial viability is cell dependent in Paraquat exposure.
Mitochondrial viability in the presence of Paraquat in additional glial cell types: A) brain
vascular pericytes, B) Schwann cells, and microglia in the C) absence or D) presence of

Figure 11 Cont. IL1B. E) Paraquat still affects mitochondrial function equally well after 3 months in water. Cell types were exposed to single concentration of Paraquat for 72 hours and results were determined by quantification of metabolized MTT. * indicate $p < 0.05$as determined by one-way ANOVA followed by bonferroni's post-test.

A

Murine Astrocyte Mitochondrial Viability

B

Murine Microglia Mitochondrial Viability
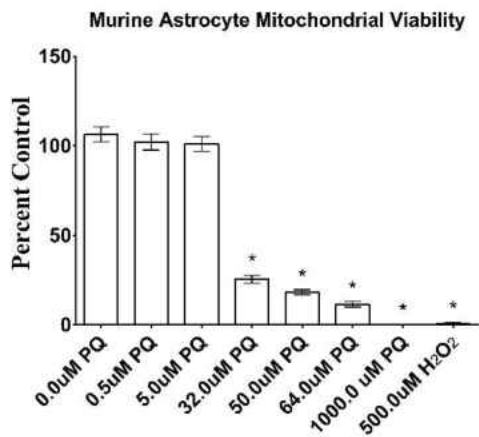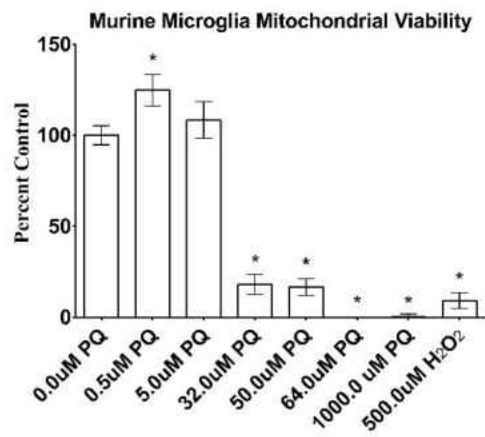
Figure 12. Murine glial cells have a differential mitochondrial response to acute Paraquat exposure. Mitochondrial viability of murine A) astrocytes and B) microglia after 72 hours of Paraquat exposure as determined by metabolized MTT. Murine astrocytes have a significant loss in viability at 32 uM Paraquat and higher concentrations. Concentrations at 5 uM and below show no significant loss in mitochondrial viability. Murine Microglia exhibit a loss in mitochondrial viability at 32 uM and higher concentrations of Paraqaut. However, at 0.5 uM Paraquat, microglia mitochondrial viability is significantly higher than that of control conditions. * indicate $p < 0.05$ as determined by one-way ANOVA followed by bonferroni's post-test.
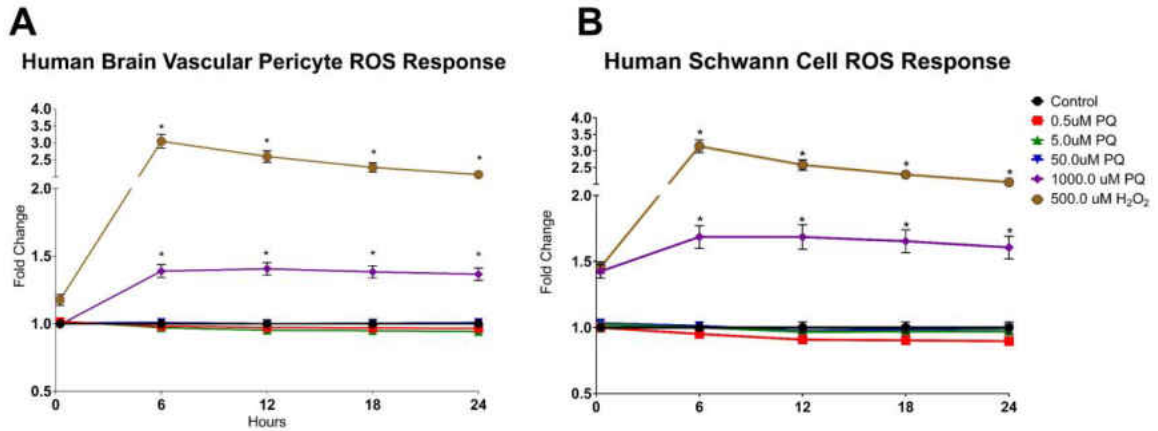
Figure 13. Paraquat induced reactive oxygen species response is similar in different human glial cells. Reactive oxygen species were assessed over 24 hours at six hour intervals in A) brain vascular pericytes and B) Schwann cells exposed to Paraquat. Reactive oxygen species were assessed with H_2DCFDA and fluorescence was measured. 1000 uM Paraquat induces a sustained reactive oxygen species response in both cell types whereas concentrations at 50 uM and below have no significant impact on reactive oxygen species response. * indicate $p < 0.05$ as determined by two-way ANOVA followed by bonferroni's post-test.
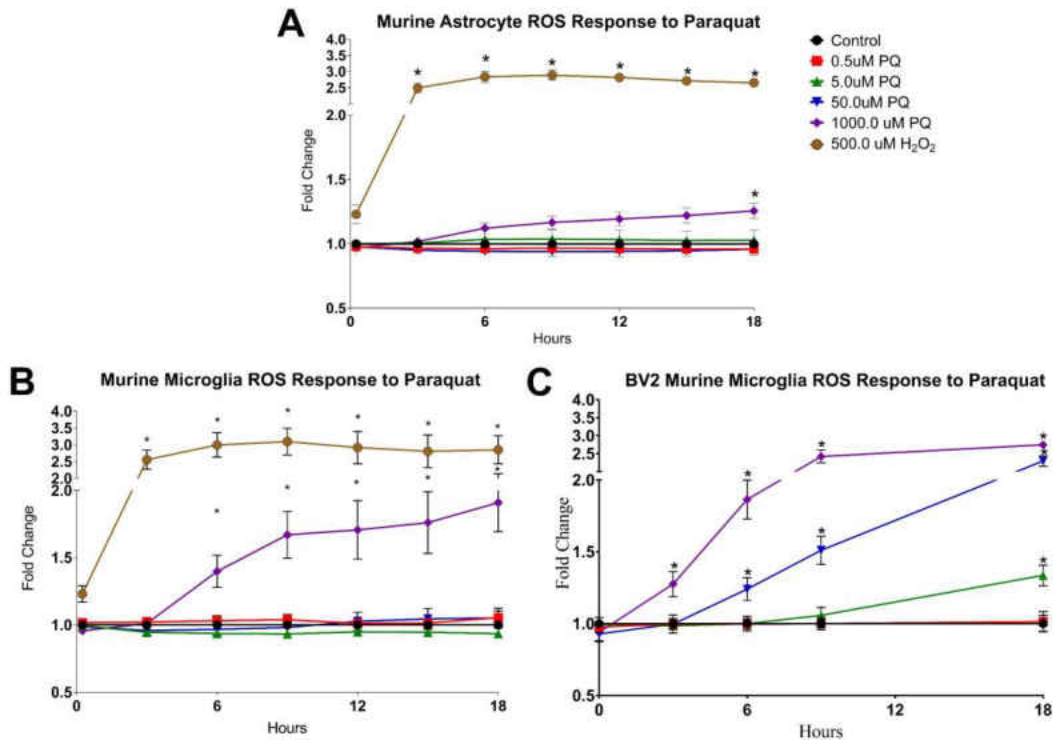
Figure 14. Paraquat induced reactive oxygen species response in murine glial cells is cell dependent. Reactive oxygen species were assessed over 18 hours at three hour intervals in murine A) astrocytes and B) microglia exposed to Paraquat. Reactive oxygen species response in C) immortalized BV2 murine microglia to Paraquat assessed over 18 hours with 3 hour intervals up to 9 hours and a final read at 18 hours. Reactive oxygen species were assessed with H_2DCFDA and fluorescence was measured. Primary murine astrocytes have a significant reactive oxygen species response to Paraquat at 1000 uM and 18 hours of exposure. All other Paraquat concentrations tested in primary astrocytes have no significant impact. Primary murine microglia have a significant reactive oxygen species response that initiates between 3 and 6 hours at 1000 uM Paraquat. All other Paraquat concentrations tested in primary microglia show no significant impact. BV2 immortalized microglia have a significant reactive oxygen species response in concentrations as low as 0.5 uM Paraquat. Higher concentrations tested have an earlier initiation of reactive oxygen species response as well as a greater fold change over control conditions. * indicate $p < 0.05$ as determined by two-way ANOVA followed by bonferroni's post-test.

CHAPTER V

LONG TERM CULTURE INDUCES DNA METHYLATION CHANGES PREVENTING STUDY OF LONG TERM PARAQUAT EXPOSURE *IN VITRO* IN PRIMARY NEURAL CELLS

Introduction

Primary samples are critical to our understanding of environmental exposure driven epigenetic reprogramming. Cell lines often have altered molecular machinery that allows for the continued propagation of the cell line which allows immortalized cell lines to respond differently to treatment conditions [239-242]. The use of primary samples has driven the field of developmental biology as a natural state to study molecular machinery [41, 243, 244]. A field that has increased the understanding in both disease and development fields is the field of epigenetics [245, 246]. As mentioned in the introductory chapter, epigenetic modifications target a number of unique gene regulatory elements including histone modification and polycomb repressor complexes [247, 248] as well as DNA base modifications specifically 5-methylcytosine and 5-hydroxymethylcytosine [249, 250].

DNA base modifications are often the first measure of epigenetic changes in a cell because they are considered to be stable and are easy to quantitate using various loci specific and genome wide techniques. DNA base modifications facilitate gene expression control through a number of mechanisms that can increase or decrease gene expression with the former being more often the case [251]. 5-methylcytosine modifications are facilitated through enzymes that directly covalently modify cytosine residues with in DNA structure. DNMT1 facilitates the maintenance of appropriated methyl modifications as cells replicate [252, 253]. DNMT3a and DNMT3b facilitate de

novo methylation and are may function in concert with other known epigenetic regulatory complexes including the polycomb group [254-256]. DNA demethylation events are indirect as currently no known direct DNA demethylase exists [257]. TET family proteins oxidize the methyl group forming an intermediate form; 5-hydroxymethylcytosine [258]. Subsequent degradation events occur in the conversion through 5-formylcytosine to 5-carboxylcytosine [259]. The resultant product has been proposed to be removed through base excision repair or enzymatically [260, 261]. The inability of DNMT1 to recognize 5-hydroxymethylcytosine as a substrate also prevents the propagation of a cytosine modification thereby providing a second avenue for demethylation [55].

Recent work has been established to evaluate the differences in epigenetic profiles of primary cell populations induced in culture. Much of this work resides in stem cell populations in understanding how better to expand these populations for therapeutic purposes or in the context of understanding how to improve *in vitro* fertilization success rates [262, 263]. Mesenchymal stem cells are perceived to be of high therapeutic potential in their ability to differentiate into numerous cell types [264-266]. Mesenchymal stem cells exhibit decreased overall DNA methylation in long term culture [267]. Mesenchymal stem cells also contain specific DNA methylation sites termed CpG clock sites that can be utilized to identify culture passage of tested mesenchymal stem cells [268, 269]. Hematopoetic stem cells (HSC) and their progenitors have been shown to gain methylation in short term culture, illustrating that different cell types display different responses to long term culture [270].

Little is known about the effects of long term culture on the epigenome in differentiated primary cell types. The importance of understanding how long term culture affects primary cell populations is implicit in the evaluation of the difference between disease points and the corresponding cell of origin when comparing epigenetic marks. Of particular interest to our and other groups is the role of epigenetic remodeling events that occur in the neural environment and the long term ramifications of these changes [271, 272]. As with other cancers; neural cancers exhibit greatly altered epigenetic profiles with DNA methylation when compared to normal primary cells [155, 273, 274]. Additionally neural cell populations in patients with neurodegenerative diseases also exhibit altered DNA methylation profiles [275, 276]. Understanding the etiology of these diseases from an epigenetics perspective requires a baseline of epigenetic profile from the native state of the cell type. Here we evaluate the effects of long term culture in primary human astrocytes, brain vascular pericytes, as well as schwann cells on DNA methylation to better evaluate the best baseline cell population for comparison. We find through Illumina 450k beadchip arrays significant differences in DNA methylation between initial culturing and subsequent passages in all three cell types.

Prolonged cell culture induces phenotype changes in primary cells

To evaluate the effect of long term culture we cultured primary human astrocytes, brain vascular pericytes, and schwann cells for 21 days collecting representative samples at each subculture point (figure 15 A). We first sought to evaluate cellular phenotype across passage points. Astrocytes are commonly identified by cytoskeletal marker glial fibrillary acidic protein (GFAP) which was used for initial assessment of purity [277].

As the astrocyte cell population are cultured across passages GFAP expression is less prominent and few cells express detectable levels of GFAP at passage 4 (figure 15 B). Brain vascular pericytes are marked by immunostaining of α-smooth muscle actin (α-SMA) a cytoskeletal filament specific to pericytes [278].   The expression of α-SMA is retained throughout the latest passage observed (figure 15 B) in all cells imaged indicating a single cell type present in culture. However, at passage 4 brain vascular pericyte morphology has shifted from small stellate cells to a flat amoebic morphology. Schwann cells can be marked by a number of cytological markers. S100 is a common marker for Schwann cells, but not specific to Schwann cells exclusively [279, 280]. To uniquely identify Schwann cells, GFAP expression in conjunction with S100 was used as multiple neural cell populations express GFAP [281]. The expression of GFAP and S100 in the cultured cells appears to be heterogeneous among cells but each cell expresses either protein to some degree. Overall GFAP expression appears to decrease over passaging while S100 increases in expression in later passages. Schwann cells also appear to undergo a morphological shift in passage 4 exhibiting a more flattened morphology then preceding passages.

Prolonged culture induces DNA methylation changes in primary human cell types

Utilizing the Illumina 450K beadchip array we examined DNA methylation in astrocytes, brain vascular pericytes, and Schwann cells from the earliest passage available (p.2) to a later passage (p.5). Data represent sites that are differentially methylated between early and later passages (figure 16 A). For all three cell types the majority of differences include losses of methylation across passage points. The majority of differential methylation shifts from hypermethylated or hypomethylated to

hemimethylated, with few sites shifting from one extreme to the other. Astrocytes

exhibit differential methylation in intermediate passage 3 which is exacerbated and

propagated in passages 4 and 5. However, there is no clear distinction between passage 4

and 5. This indicates that there are two shifts in methylation status of Astrocytes with the

more dramatic being the shift between passage 3 and 4. The sites that exhibit differential

methylation at the early passage are further exacerbated in the shift in methylation at later

passages. Brain Vascular Pericytes hold their initial methylation pattern out to passage 4

before the appearance of a large shift in sites that are differentially methylated. Schwann

cells exhibit a shift at passages later than passage 3, however, with the passage 4 data not

present no distinction about when this shift occurs can be made.

We next characterized the persistence of these changes across the passage points

for astrocytes, brain vascular pericytes and Schwann cells (figure 16 B). In each of the

cell types there are a number of differentially methylated sites that are retained

throughout the passages. Of the earliest initiation in differential DNA methylation,

astrocytes retain 73% and 97% of increased and decreased methylation respectively

whereas pericytes retain 12% and 61% increased and decreased methylation respectively.

Schwann cells retain 43% increased and 61% decreased of the initiating differential

methylation. After passage 4 of both astrocytes and brain vascular pericytes, the

differential methylation is altered across greater number of sites and the retention of those

sites holds at 97% and 67% increased and decreased for astrocytes and 37%and 77%

increased and decreased for brain vascular pericytes. Of note there are a number of sites

that are dynamic between passages, likely reflecting a dynamic role for DNA

methylation. To further understand the importance of these sites we examined where these sites occur.

Changes in DNA methylation occur outside of CpG islands and transcription start sites but occur more frequently on specific chromosomes

We were interested in the implications of changes in DNA methylation across passages and their significance in location. To examine the differential methylation we examined those sites that exhibited increased or decreased methylation with a delta beta value greater than 0.2 or less than -0.2 from P2 to P5.   Utilizing beadchip array annotation we first sought to characterize sites more susceptible to change at the chromosomal level (figure 17 A). Here we note that there are a number of chromosomes that have over and under representation as determined by fisher's exact test in both increased and decreased methylation. Astrocytes have 4 chromosomes that are overrepresented in increased methylation; less than that of brain vascular pericytes and schwann cells with 5 and 7 respectively. In chromosomes underrepresented for increased methylation; astrocytes have 7 chromosomes which is similar to that of brain vascular pericytes and schwann cells at 9 and 8 respectively. While a number of chromosomes are differentially methylated similarly between cell types there are clear and distinct differences between cell types in 9 of the 23 chromosomes. At each of these chromosomes there is a difference in over/under representation as well as the magnitude of the observed over expected ratio. One caveat to this data is the lack of equal representation on the 450K array. While the results were weighted by the number of sites available, some chromosomes are only represented by low numbers of sites such as the Y chromosome with only 93 sites available on the array. In these cases however, the sampling was too low to be determined significant. Decreased methylation has similar

representation in several of the chromosomes that display over or under representation in increased methylation. Chromosomes 2, 5 and 13 are overrepresented in both increased and decreased methylation suggesting that these chromosomes are particularly vulnerable to differences in methylation in long term culture. Additionally chromosomes 19, 20 and X are significantly underrepresented in both increased and decreased methylation indicating greater stability in long term culture. Notably, the number of chromosomes that are significantly over and underrepresented in decreased methylation sites, is more than that of increased methylation in all three cell types; likely reflective in the much greater number of sites that have decreased methylation.

We next considered the representation of these differentially methylated sites in relation to the transcription start site (figure 17 B). Each site is capable of representing more than a single gene which is reflected in the annotation. To address the crossover, sites that were representative of more than one position relative to the start site were counted if the relationship was for an independent gene. Increased methylation is overrepresented in sites annotated with the gene body for all three cell types and within the 3' untranslated region for astrocytes. The remaining regions, including the promoter region and 1st exon displayed fewer than expected sites of increased methylation. In sites that exhibited a decrease in methylation much of the 5' region of the gene body was under represented in all three cell types. The 3' untranslated region and gene body were overrepresented for decreased methylation in brain vascular pericytes as well as Schwann cells. Astrocytes only exhibit overrepresentation of the gene body in decreased methylation. This would suggest that the area around the transcription start site is stable and likely to be unaffected by the differences in DNA methylation attributable to long

term culture. The latter halves of annotated gene bodies are more susceptible to change in long term culture.

Another regulatory feature in DNA methylation that we sought to characterize were CpG islands and adjacent regions called shores and shelves. Our goal was to further characterize these sites and determine if such changes may have implications in long term studies (figure 17 C). CpG Islands associated with promoters are often hypermethylated in cancers [282, 283]. Long term culture of primary cells has been proposed as a model for inducing a cancerous phenotypes [284]. Here we show that in the neural associated cell types studied, CpG islands actually have less than expected numbers of CpG dinucleotides demonstrating increased methylation with long term culture, regardless of cell type. Additionally, long term culture of these neural associated cells only show higher than expected increased methylation in open sea regions. In examining decreased methylation across these primary cells, the loss in methylation is more than expected in regions outside of the CpG Island and its shores. CpG shores are indicative of cell of origin as well as play a role in driving gene expression [35]. However, CpG shelves also play a role in driving gene expression; low island methylation and high shelf methylation has greater correlation with gene expression than that of island methylation or shelf methylation alone [33]. In all three cell types we exhibit loss of methylation in the shelf regions at a greater than expected ratio which may indicate a role in gene expression control over the long term culture of these primary cells. Additionally the stability of the CpG Island in both decreased methylation and increased methylation changes indicates a robust CpG island methylation signature of these cell types across culturing time points.

Cellular proliferation and metabolic function gene ontologies are over-represented in long term culture induced methylation changes

We also assessed differential methylation in the context of gene ontology to address unique ontology groups that arise in long term culture of primary human cells. To address gene ontologies we identified genes that had at least one site differentially methylated between the earliest passage P2 and the subsequent passages P3, P4, P5. Gene lists were analyzed using Panther. Data shown represent ontologies that had over representation with a p-value less than 0.05. Panther offers a number of ontology groups with which to analyze gene lists; we examined biological processes and pathway analysis.

Among all cell types, as we would expect from the retention of differentially methylated sites, there are a number of ontologies describing changes in these cells that appear initially and are retained across passage points. There are increased numbers of overrepresented genes and ontologies that appear in later passages due to more differential methylation in later passages. In each cell type there are changes in DNA methylation that are over-represented in notable ontologies. Astrocytes have changes in DNA methylation over-represented in a number of developmental ontologies that appear in P3 (figure 18 A). The astrocyte population is fetal derived. This may be reflected in the genes that are among the first to be affected in long term culture of primary human cells. Primary cells become senescent with multiple passages, however, this typically occurs at later passage points [269]. Changes in DNA methylation are over-represented that may be reflective of this phenomenon, including those that focus on cell death and apoptosis; which is first observed in P3. Additionally changes in DNA methylation are over-represented in induction of apoptosis ontology which appears in later passages

(figure 18 A,B). DNA methylation changes are also over-represented by biological

process ontologies in late passage that involve cell adhesion to matrix and other cells

(figure 18 B). Analyzing changes in DNA methylation by pathway ontology finds over-

representation of genes in WNT signaling, Integrin signaling, and cadherin signaling

pathways (figure 18 C).   Each of these ontologies include genes that have been

implicated in regulating cellular growth, senescence and cell interactions with cellular

environment and other cells.

Brain vascular pericytes ontology analysis reveals that the majority of genes

impacted by changes in DNA methylation are over-represented in ontologies in both

early and late passages that involve regulation (figure 18 D, E). While the over-

representation is similar to astrocytes, the lack of gene representation in development or

apoptotic feature ontologies in the brain vascular pericytes is notable. Brain vascular

pericytes also exhibit changes in methylation of CpG sights associated with genes known

to play a role in adhesion (figure 18 E). Genes impacted by changes in DNA methylation

are over-represented in the WNT signaling pathway as well as cadherin and integrin

signaling pathways (figure 18 F).

Schwann cells cultured for multiple passages exhibit changes in genes which are

associated with gene over-representation in a number of gene ontologies including

development related ontologies (figure 18 G). Genes impacted by changes in DNA

methylation that are over-represented in apoptotic or cell death ontologies are few in

number. Similarly to brain vascular pericytes and astrocytes, Schwann cells have a

number of genes over-represented in ontologies representative of cell to cell interactions

and matrix adhesion (figure 18 G,H). Analysis of genes impacted by changes in DNA

methylation finds over-representation in WNT, cadherin, and integrin signaling pathways (figure 18 I). Of note is the over-representation of genes in the apoptosis signaling pathway in an earlier passage that is not retained through to P5. The same holds true of genes over-represented in the biological process: induction of apoptosis (figure 18 G,H).

Discussion

We report that primary human astrocytes, brain vascular pericytes, and Schwann cells demonstrate changes in cellular morphology and expression of cell markers during subsequent sub-culturing events. In addition to phenotypic changes, we also report changes to DNA methylation in all three cell types. The culturing conditions for these cells were without treatment and indicate that sub-culturing events or prolonged culture can induce changes in DNA methylation in the absence of an experimental manipulation. Most of these changes are demethylation events, which may have implications for increased chromatin accessibility. While this data does not address the question of how chromatin accessibility changes, it can offer insight into the relevance of such changes.

An important aspect of the culture induced changes arises with regard to the location of the genome in which the changes occur. Many of the changes are outside of key gene regulatory regions, with the exception decreased DNA methylation of island shelves. Shelf regions have been implicated in altering gene expression [33]. Shelf regions have also been implicated in playing a role in cellular identity [35]. However, despite the changes to the shelf regions, the islands and associated shores have few changes. Many of the changes occur outside of gene regulatory regions in what is termed as open sea DNA. Changes in DNA methylation outside of the regulatory regions may have no bearing on gene expression and the significance of these changes is unknown.

Investigation into gene expression may highlight the role culture induced DNA methylation may play in gene expression. We would expect that many of these changes have no direct impact on gene expression, but we have not performed RNA seqencing on these samples.

Changes in culture induced DNA methylation changes may have a significant impact on chromatin accessibility. DNA methylation plays a role in recruiting members of the polycomb repressive complexes and with a significant loss of DNA methylation many of the impacted regions may be now accessible. With current methods such as ATAC-sequencing, we may be able to define chromatin accessibility shifts. These shifts may be important in exposing DNA to damage events. Future investigations are warranted in understanding the DNA damage response and damage events that occur in prolonged culture. This has important implications in expanding *in vitro* cultures for therapeutic purposes. If expanding *in vitro* cultures induces significant changes in methylation and alters the chromatin accessibility, therapeutic uses may be limited as the cells may not respond correctly in a new host. We may also be introducing cells that have potential DNA damage and could lead to future cancer events.

Another consideration in expanding cultures relates to genes affected by culture induced changes in DNA methylation. The changes we report in DNA methylation affect genes associated with multiple distinct and overlapping gene ontologies, but significant among them are WNT signaling and cellular adhesion ontologies. Genes over-represented in WNT signaling and cellular adhesion ontologies can play a role in cellular senescence [285]. Culturing primary cells often induces replicative senescence and the DNA methylation changes we report may be the initiating stages of replicative

senescence [286]. To address if prolonged culture induces cellular senescence in primary human astrocytes, brain vascular pericytes and Schwann cells, we suggest looking at cellular senescence markers throughout the passages. It is important to identify if these cells are entering senescence, as we can use the associated DNA methylation changes to determine the maximal number of passages for expanding cultures.

In our environmental toxicant exposure studies, we find that culture induced DNA methylation changes provide enough of a barrier that prevents using a chronic exposure long term culture model. We see significant changes in approximately 4% of interrogated CpG sites. This represents a significant portion of the sites we can assay and may mask a number of changes induced by environmental exposure. A potential alternative would be to use whole genome bisulfite sequencing to identify all CpG sites. However, our data does not represent the whole genome and a repeat study of culture induced changes would be necessary to identify sites that change with culture. Again this may prevent identifying critically changed sites from environmental exposure. The culture induced changes we report here warrant utilizing *in vivo* models despite technical limitations which may include isolating specific cell types.
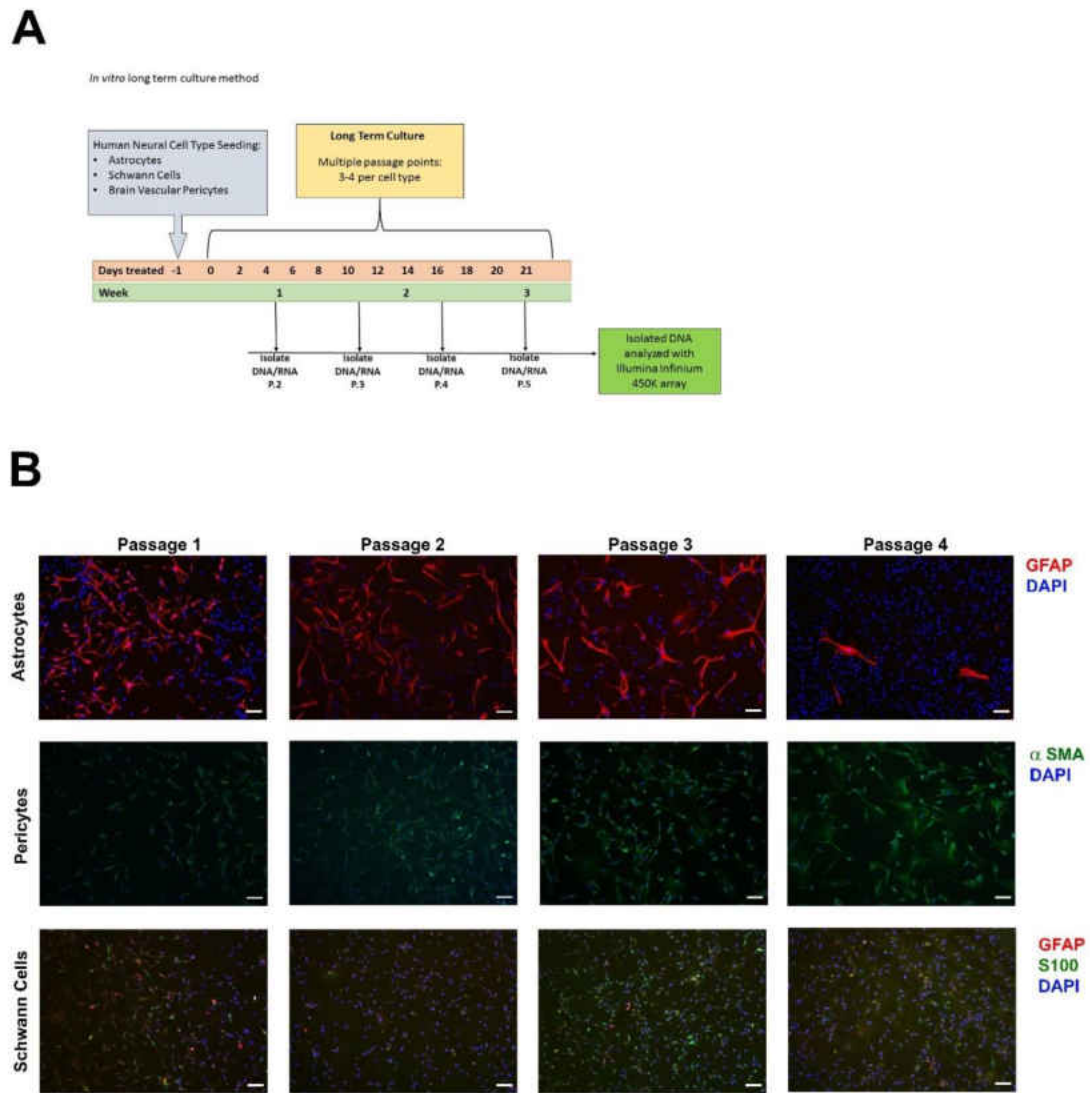
Figure 15. Prolonged cell culture induces phenotype changes in primary cells. A) Schematic of protocol for long term culture of primary human cell types, astrocytes, brain vascular pericytes and schwann cells. Primary cell types were cultured for 21 days through 4 passages and samples collected at each passage point for DNA methylation analysis and immunocytochemistry. B) Cells cultured at each passage were fixed in 4% paraformeldahyde and immunolabelled for astrocytes (GFAP), brain vascular pericytes (a-SMA) and schwann cells (S100, GFAP). Immunolabelling indicates phenotypic change in cell types in morphology or expression of indicated markers.
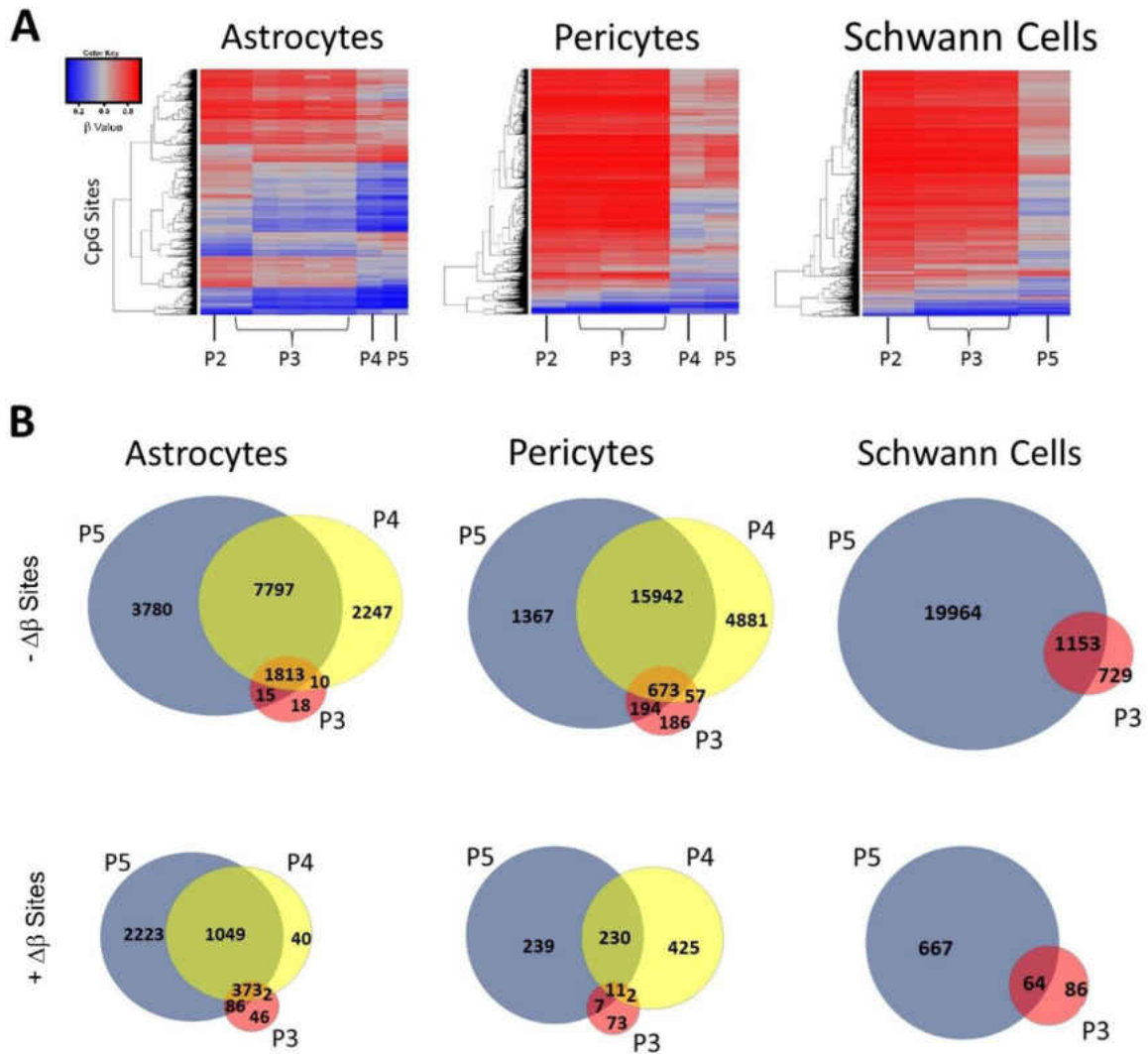
Figure 16. Prolonged culture induces DNA methylation changes in primary human cell types. Primary human cell types were cultured through P5 and DNA was collected at each sub-culture point. DNA methylation was assayed with Illumina 450k Beadchip Array. Data are represented in heatmap (A) for all differentially methylated sites between passage points and venn diagrams (B) of differentially methylated sites common between passage points. $+\Delta\beta$ indicates an increase in methylation at CpG sites, and $-\Delta\beta$ indicates loss of methylation at CpG sites. Primary cell types include Astrocytes, Brain Vascular Pericytes and Schwann cells. Methylation data were SWAN normalized and filtered for adjusted p-value less than 0.05 utilizing RnBeads protocol.

Figure 17. Changes in DNA methylation occur outside of CpG islands and transcription start sites but occur more frequently on specific chromosomes. Differential methylation was determined with a cutoff with absolute Δβ value of 0.2 and characterized based upon Illumina annotation of 450k Beadchip array. Data represent the number of observed sites over expected sites based upon total sites assayed. Characterization of sites include chromosome representation (A), relationship to transcription start site (B), and relationship to CpG island (C). + Δβ sites indicates sites that gained methylation, whereas - Δβ indicates sites of loss in methylation. * indicates an over/under representation greater than 0.5 as determined by Fishers exact test.
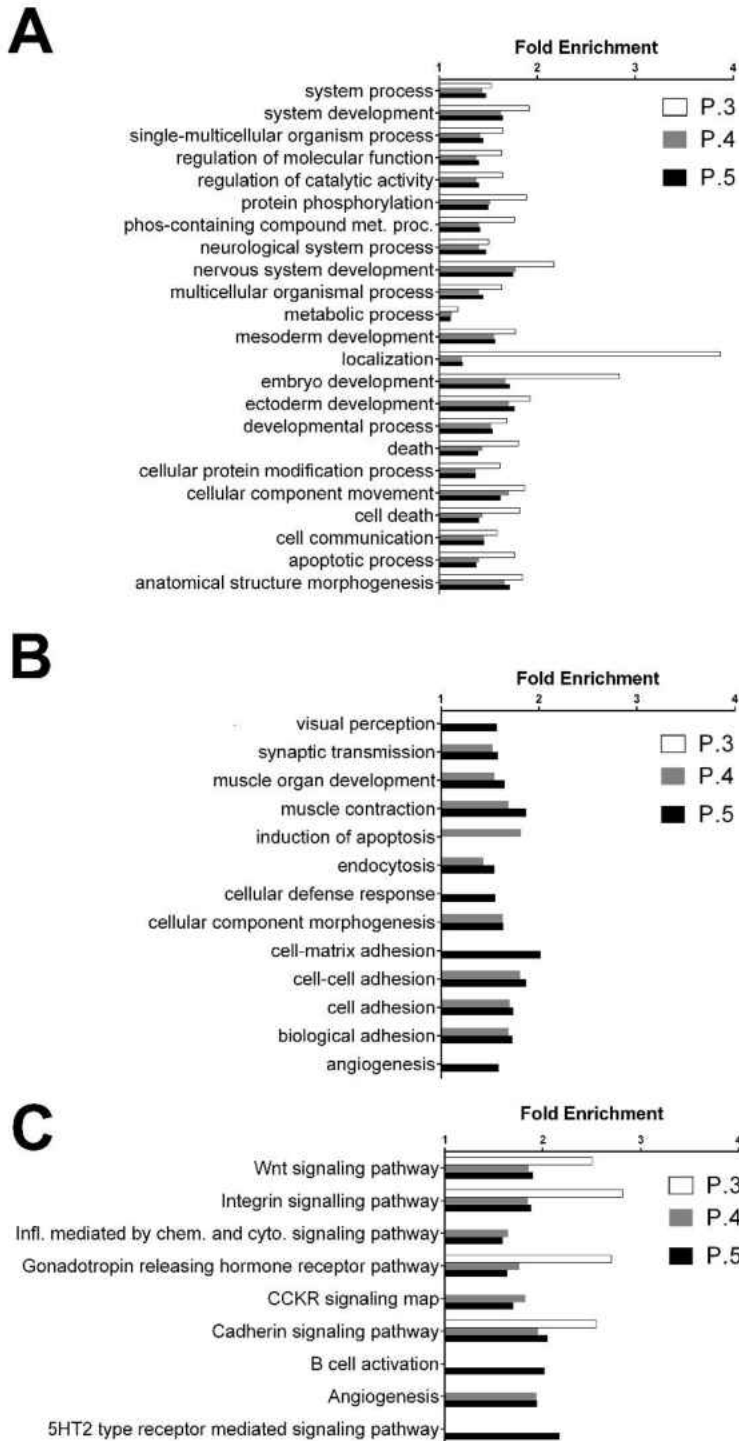
Figure 18. Cellular proliferation and metabolic function gene ontologies are over-represented in long term culture induced methylation changes.

Brain Vascular Pericytes
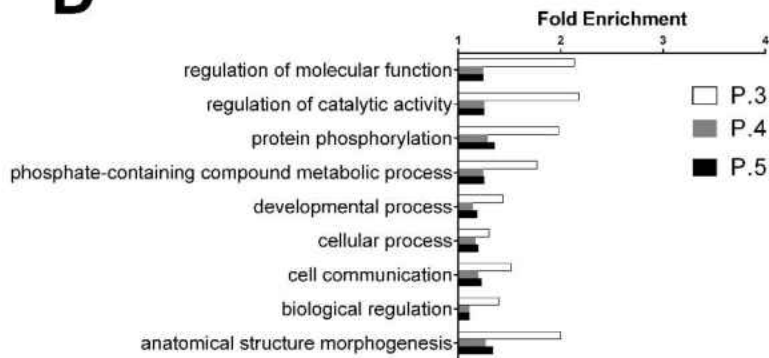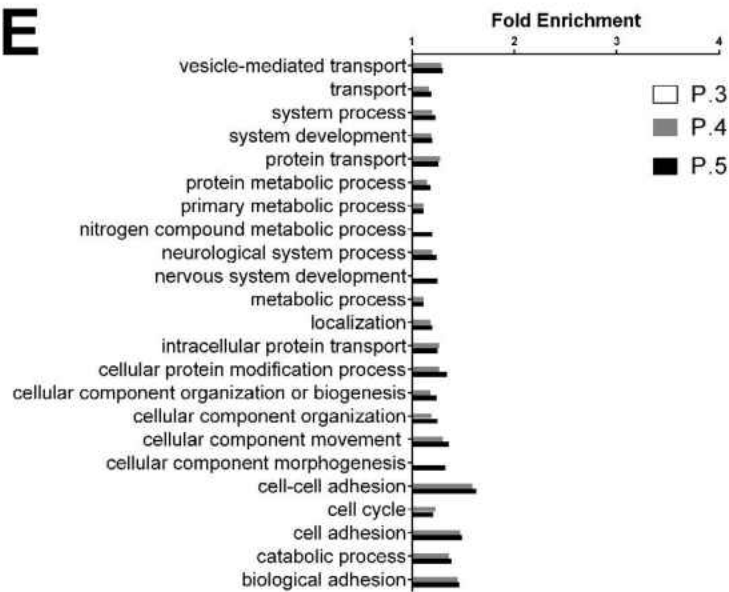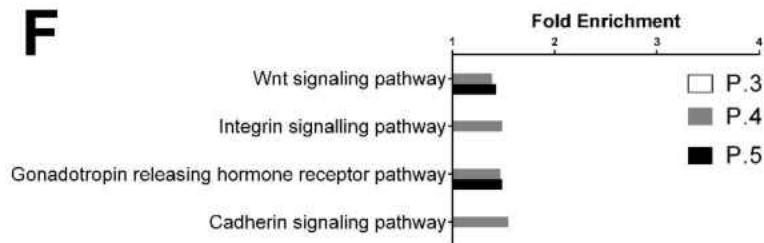
Figure 18 cont.

Schwann Cells
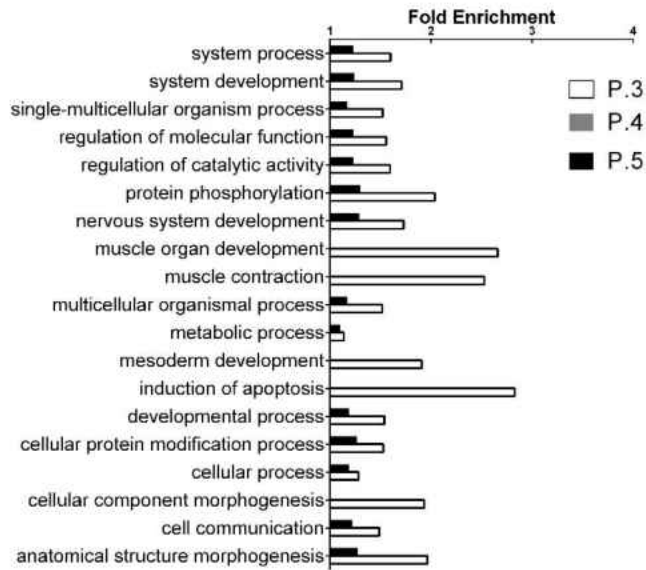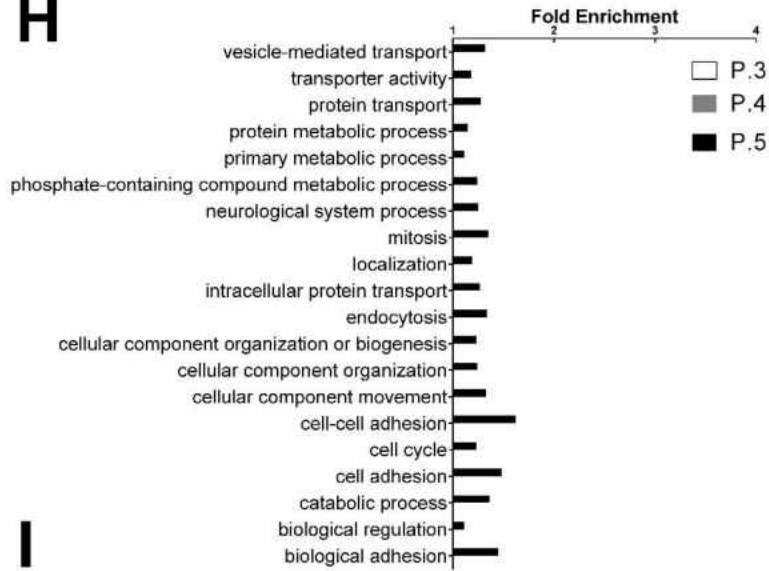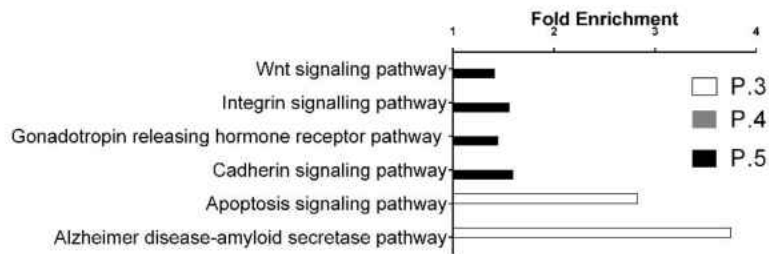
Figure 18 cont.

Figure 18 cont. Differentially methylated sites were characterized by genes that had at least one site differentially methylated. Gene lists for each passage and cell type were subjected to gene ontology analysis through the Panther database. Ontologies that were significantly overrepresented are represented.   Data also represent gene ontology analysis through each passage point, which display retention of ontology categories to late passages in each cell type. Biological process gene ontology represented by genes differentially methylated in early and late passages for astrocytes (A,B), brain vascular pericytes (D,E) and Schwann cells (G,H). Over-representation in pathway gene ontology of genes differentially methylated for astrocytes (C), brain vascular pericytes (F), and Schwann cells (I). Astrocytes, Brain Vascular Pericytes, and Schwann Cells have unique changes in DNA methylation but are over-represented in similar ontologies. There are unique over-representations of genes impacted bv changes in DNA methylation in each cell type.

CHAPTER VI

MATERNAL PARAQAUT EXPOSURE INDUCES PERSISTENT GENE EXPRESSION CHANGES IN NEONATE GLIAL CELLS THAT MAY DRIVE FUTURE DISEASE EVENTS

Introduction

Neural diseases that lack a clear genetic origin have been linked to being multifactorial diseases [287-289]. Few mutations exist that explain neurodegenerative diseases and the mutations that do exist fail to explain the majority of the disease pool [211, 290, 291]. Neural cancers are often low mutational load cancers and reside in a privileged environment protected by the blood brain barrier preventing effective treatment [292, 293]. Despite a clear genetic influence there does appear to be an influence from outside sources.

Environmental factors appear to have an epidemiological impact on both neurodegenerative disease and neural cancer [8-19]. There is a clear increase in risk of childhood brain tumors after maternal pesticide exposure [294]. However, adult exposure seems limited to an increased risk of neurological disorders and neurodegenerative diseases [295, 296]. There appears to be a critical window in which pesticide exposure can drive cancerous events after which only neurodegenerative events occur.

One such pathway that may define if such a window of susceptibility exists is epigenetics. Epigenetic remodeling events have been linked to environmental influence. We propose that pesticide exposure *in utero* will lead to significant transcriptional changes that may be regulated by epigenetic remodeling events.

In this study we used a current Paraquat induced parkinsonian model to assess the effect of early development pesticide exposure on progeny neuroglia. Here we show that Paraquat is retained in the adult brain tissue but not in the brain of pups (figures 20 and 21). Despite the absence of detectable Paraquat, we show that pup astrocytes and microglia have sustained differential gene expression after maternal Paraquat exposure. We also show these changes are cell type specific.

Intraperitoneal Paraquat exposure prior to and during gestation does not affect dam mass, gravidity or pup number

To effectively address chronic exposure of an environmental toxicant during development we utilized an *in vivo* model system where female mice are treated with Paraquat just prior to and during gestation (figure 19 A). This model allows us to address the effect of Paraquat in a naturally developing animal without the caveats of long term culture induced epigenetic changes. Additionally, the animal model allows for normal development and cellular interactions not present in *in vitro* modeling systems.

In our model system, female mice receive twice weekly injections of 10 mg/kg Paraquat for a total of six weeks. One week into the treatment schedule, the female mice were bred and exposures continued throughout gestation. Brain tissue of 1 to 3 day old pups were collected and cultured with the exception being a small subset of pups where the brain was retained for mass spectrometry and future histological analysis. Adults were carried out until 6 weeks at which point the animals were perfused and brain tissue collected for histological analysis as well as mass spectrometry. Injections of animals were performed intraperitoneally with 1 mg/mL Paraquat saline solutions made fresh prior to injections. Samples of injection stocks were saved and assessed for Paraquat

concentration by mass spectrometry (figure 19 B). Injection stocks were on average 1.15

mg /mL, slightly higher than our target concentration. This may be due to technical

errors. However, all animals were treated with the same stock on the same day; any

discrepancies in Paraquat exposure were across all animals.

With this injection schedule we assessed the mass of the adults prior to each

injection to determine a consistent 10 mg/kg Paraquat dosing schedule. We characterized

this data to assess the effect on the weight of animals (figure 19 C). This data indicates

that non-gravid mice did not lose mass throughout the dosing schedule. The gravid

females also did not lose any mass prior to breeding, nor was there a difference in mass

between Paraquat treated and saline treated gravid females indicating there were no

obvious or overt gross changes on the adult mice.

Additionally we recorded the number of mice that were gravid (figure 19 D) and

the pup yield for each gravid mouse (figure 19 E). In both of these characteristics there

was no significant difference between control and treatment groups. In the percent of

gravid mice there does appear to be a negative trend in the number of gravid mice in the

Paraquat treatment group, however the p-value is 0.117 indicating the reduced number of

gravid mice is not significant.

The characterization of the mice indicates no change in the treated animals

compared to the control group. Treatment of animals with a substantia nigra impacting

compound usually affects some motor and behavioral characteristics not assessed here.

Anecdotally the Paraquat treated animals appeared healthy and indistinguishable from

control animals. The Paraquat treated animals did not exhibit any changes that would

meet the criteria necessary for euthanasia.

Dam brains unable to clear Paraquat from intraperitoneal injections.

Blood samples were collected prior to cardiac perfusion with saline. Blood samples were centrifuged in heparin sulfate and sera collected. Brain tissue was removed after perfusion of approximately 10 mL of saline. Brains were dissected into hemispheres, snap frozen and pulverized to homogenize samples. Processed samples were submitted for mass spectrometry analysis. Adult brain tissues (figure 20 A) from Paraquat treated animals show significant increase in Paraquat levels with in the brain tissue compared at approximately 0.5 ng/mg tissue to control group animals with about 0 ng/mg tissue. This residual Paraquat is available in the brain tissue approximately 2-3 days after the last injection.

Paraquat is water soluble and 95% of Paraquat is cleared from the body in urine or feces within the first few hours of injection [297]. This indicates that Paraquat is retained within brain tissues after serum levels have cleared and may reflect an inability to effectively clear Paraquat from the brain tissue. However, of note is for the 10 mg/kg Paraquat injected, only a small amount of Paraquat is retained. This is reflected in the work of others; Paraquat is able to cross the blood brain barrier but only small amounts cross and are retained within the brain tissue [163]. Our study confirms that Paraquat is retained in the brain but does not address if brain Paraquat can be cleared over a slower time frame [163, 169].

Pup brains and serum are clear of Paraquat

We also sought to assess the level of Paraquat in pup tissues. Brain tissue from maternally Paraquat treated pups show no difference in Paraquat levels from control group pups (figure 21A). Pup sera also show no Paraquat availability in either control or Paraquat exposed animals. The lack of Paraquat in the neonate brain is markedly

different from the adult brain tissues and may be indicative of either an enhanced ability to clearance Paraquat or an inability for Paraquat to access the neonate brain tissues.

The lack of Paraquat in the neonate tissues indicate that Paraquat is unable to maintain a presence in the brain tissue indicating that any effect from Paraquat would have to be in single hit responses that correlate to the injection schedule. To assess if such an effect were occurring we assayed astrocytes and microglia cultured from neonate brains for changes in gene expression.

Maternal Paraquat exposure has no apparent effect on astrocyte enrichment or Glial Fibrillary Acidic Protein (GFAP) expression

In order to assess gene expression changes in cultures derived from neonate tissues, we first sought to characterize the cultures for astrocyte and microglia presence. Pup adherent brain cultures were cultured and assessed for astrocyte number with anti-GFAP antibody (figure 22 A). Images indicate that there are a number of positively stained cells for GFAP as well as unstained nuclei indicating a mixed population of cells. Positively stained cells display a fibrous astrocyte morphology but display no differences between treatment conditions in morphology or staining intensity. Morphology of stained cells indicate a fibrous astrocyte type as the GFAP staining is diffuse in a flat processes similar in morphology to a fibroblast [298]. Protoplasmic astrocytes exhibit spindle shaped processes in a stellate appearance and do not regularly appear in the images [299]. Protoplasmic astrocytes do not stain well for GFAP which may reduce the yield of GFAP positive cells in our cultures [300]. However, with the number of nuclei that do not stain within the images, there is a population of nuclei that cluster and are smaller than the stained astrocyte counterparts. These smaller nuclei indicate a completely different cell type and the size of the nuclei are suggestive of microglia.

111

Future co-staining with IBA-1 would be necessary to determine the level of microglia contamination in the astrocyte population.

Image counts were made by two independent and blinded investigators. The average of the results indicates a population of astrocytes enriched to about 55-65 percent of the total population. There is also no statistical difference between the treatment and control populations in the number of positively stained cells.

The similarity in GFAP positive cells in morphology and percentage of the population of cells between treatment conditions indicates the astrocyte composition is similar between treatment groups and that there is not a significant loss in one population over the other. Examination of the microglia from the same populations indicate a marked difference in treatment groups.

Maternal Paraquat exposure alters pup microglia Ionized Calcium-Binding Adaptor Molecule 1 (IBA1) expression

Microglia were collected from shaken flasks and cultured on poly-D-Lysine coated coverslips for 48 hours prior to fixation. Cells were stained for IBA1, a cytoskeletal marker of microglia and macrophages. Representative images (figure 23 A) show amoeboid shaped cells in control and Paraquat conditions. However, staining intensity of IBA1 is noticeably different between the treatment groups. Indeed the number of IBA1 cells is reduced in Paraquat exposed cells (figure 23 B) with approximately 25% drop in the percentage of IBA1 positive cells. Additionally the intensity ratio of IBA1 intensity to DAPI intensity in Paraquat treatment group is significantly lower than that of control treatment group (figure 23 C).

The difference in IBA1 is unexpected as IBA1 is present in matured microglia and the production of IBA1 is stimulated by macrophage colony stimulating factor,

which is secreted by the brain [301]. Microglia are not derived from neural precursors but from myeloid precursor cells and migrate to the central nervous system during development [302]. The presence of mCSF in the brain stimulates the migrating cells to mature into microglia [303]. In having reduced expression of IBA1 for the Paraquat treatment group, we raise the possibility that the microglia may not be fully matured. Another possibility also remains in that the microglia may be unhealthy and are simply dying. With the limited population of cells cultured from the pup brains we assessed gene expression data for changes that might give direction to response to Paraquat treatment.

Gene expression analysis shows experimental batch effect

In utero exposure treatments were completed in two separate experiments, an initial study with fewer animals and a second larger study with age matched animals. RNA was extracted from cultured pup brain tissue with adherent and non-adherent cells mechanically separated. RNA sequencing was performed on samples and differential gene expression analysis was completed. Distance clustering of all samples in both experiments was completed (figure 24).

Samples cluster out into two distinct clades based on cell type. The separation based on cell type are expected as different cell types have unique gene expression profiles. This does indicate that the mechanical separation effectively separated out two different populations of cells. However, the samples also cluster into two distinct clades based on experimental replicates. This indicates the two experiments are more dissimilar than control and treatment groups. When examining treatment and control groups within each experiment clade, the microglia samples cluster by treatment group while astrocyte

cultures cluster indifferently to treatment group. To assess the difference in treatment versus control as well as differences between the experiments we performed differential gene expression between Paraquat treatment and Control treatment for differences in treatment and differential gene expression between Control group from Experiment 1 and Control group from experiment 2.

Maternal Paraquat exposure experiments are unique from one another

Differential gene expression analysis of RNA sequencing data for treatment versus control conditions in astrocytes and microglia (figure 25A) indicate differentially expressed genes that are typically overexpressed in both cell populations. However, comparing control groups between the two experiments shows large differences between experiments, far greater number of changes than those attributed to Paraquat exposure. This indicates the experiments are very distinct from one another.

Further examination of the differences between the experiments identifies several points on which the two experiments are different from one another and should be analyzed separately. Experiment 1 animals are of varying ages and pups are from mostly older adults in the 4 to 7 month at the end of study age range (Table 4). However, Experiment 2 is comprised of age matched animals that are 3.5 months at the end of study. Additionally the representation of pups between treatment and control groups is more balanced in experiment 2 as pups were born to several mothers in both treatment groups. In experiment 1 pups were born to several control animals but only two treatment animals. In those treatment animals 6 were born to one female while 2 were born to another female. This disproportionately represents one dam in the treatment

group. Based on these results we analyzed differential gene expression separately for each experiment.

Repeat experiments have different patterns in gene expression changes

In splitting the analyses between the experiments there is an immediate difference in the pattern of differential gene expression. In experiment 1, the differential gene expression is largely overexpressed significantly differential expressed genes for the Paraquat treatment group in both astrocytes and microglia (figure 26 A, B); whereas the significantly differentially expressed genes are more split between over and under expressed genes for astrocytes and microglia in experiment 2 (figure 26 C, D). However the overlap of the genes is minimal between cell type and experiments. Despite the lack of cohesion between cell types or treatment groups in the differential gene expression we sought to identify if there were specific patterns to the types of genes affected and analyzed these gene sets for gene ontology to provide some insight.

Independent differential gene expression analysis identifies distinct differential gene expression patterns for each experiment. Experiment 1 shows mostly increased gene expression for differentially expressed genes while experiment 2 has both increased and decreased gene expression (Tables 5, 6, 7, 8,). Likely, this may be a reflection of the disproportionate representation of Paraquat samples from a single dam. With the understanding that these experiments are different in animal representation and that the second experiment has a larger sample population we characterized the differences in gene expression for experiment 2.

Gene expression data indicates a response in pup brain cells to maternal Paraquat exposure

We tested the similarity of samples within a cell population type using distance clustering methods. Paraquat samples have a tendency to cluster separately from the control groups (figure 27). Astrocyte clustering identifies a group of pup samples that cluster into two unique clades distinct from control clades (figure 27 A). Additionally we find that some pups from Paraquat treated mothers cluster in Paraquat clades while their littermates cluster into control clades. Microglia samples cluster more distinctly than astrocyte samples (figure 27 A,B). In microglia samples there are three distinct clades that are highly independent from one another. Again littermates do not cluster together into the same clades and in some cases cluster with control group samples.

The distance clustering results indicate that maternal Paraquat exposure differentially effects offspring. As some littermates cluster with Paraquat treatment and Control treatment, we note that not all samples are representative of a single pup. Future studies will require pups to be analyzed independently as pooling cells from multiple pups may mask littermate differences. Paraquat treatment also appears to generate unique clades indicating a unique response from each sample group or unique effects from Paraquat treatment on the same population.

Cellular adhesion and signaling ontologies are over-represented in differential gene expression of astrocyte cultures

To give us a general indication of processes and pathways affected by changes in gene expression we used Panther Gene Ontology analysis. Ontology analysis was used on differential gene expression lists (Table 7) to identify groups of genes and signaling pathways impacted by *in utero* Paraquaat exposure. Biological Process-Slim (figure 28 A) uses a reduced ontology gene list to help identify global changes in gene expression.

116

In astrocytes, the slim biological process identifies a number changed in gene expression grouped into categories involved in cell adhesion and signaling. Changes in gene expression are over-represented by approximately 2 to 10 fold indicating there are more genes identified in the ontology than we should expect. The top three categories are adhesion related ontologies indicating that *in utero* Paraquat exposure affects astrocyte adhesion genes and potentially properties.

While biological process allows for the overall identification of changes, focusing on other ontology characterizations allow us to identify in more detail the effect of differential gene expression from *in utero* Paraquat exposure. We next identified genes significantly over-represented in pathways (figure 28 B). Genes in the cadherin signaling pathway are significantly over-represented by 5.64 fold (Table 9). Genes in this pathway play an important role in cellular adhesion but also in cellular migration, stem cell maintenance, and cancer progression. Analysis of genes in the context of reactome pathway ontologies identifies genes over-represented in two pathways: collagen biosynthesis and modifying enzymes and Collagen Formation. These pathways may be important in matrix deposition and in the context of astrocytes; formation of glial scarring. Analysis of genes over-represented in protein classification ontologies (figure 28 D) identifies cell adhesion molecules and signaling molecules as major constituents in our differentially expressed genes for astrocyte cultures. Together these ontologies begin to identify that the astrocyte cultures are different in their ability to communicate and adhere to their surrounding cells and matrix. Identifying other groups of genes with similar functions may help define the role that a change in adhesion capabilities and cellular signaling may play.

**Comprehensive biological process ontology identifies additional developmental
ontologies in astrocyte cultures**

We sought to characterize the differentially expressed gene list for astrocyte

cultures further with the complete biological process ontology (Figure 29). Further

characterization would allow us to identify genes over-represented in additional ontology

groups clarifying the effect of environmental toxicant exposure. In astrocyte cultures, the

expanded analysis of differential gene expression identifies additional ontologies being

related to development. Genes in the newly identified ontologies are all over-represented

indicating we are seeing more genes in these ontologies than we should expect. Our

differential gene expression list is most over-represented in the hexose biosynthetic

process with greater than 20 fold over-representation. Hexose biosynthetic pocess

ontology involve genes that play a role in forming six carbon monosaccharides. This

ontology might be expected with the proposed role of Paraquat inhibiting mitochondrial

function. We next sought to characterize the changes in gene expression for microglia.

**Immune function and stimulation response ontologies are over-represented in
differential gene expression of microglia cultures**

We characterized *in utero* Paraquat exposure microglia differentially expressed

genes (Table 8) to identify processes and pathways affected by changes in gene

expression. In the slim biological process (figure 30A) genes are underrepresented in

ontology categories involving immune and sensory related processes. The under-

representation of immune related genes signifies that genes involved in immune function

might be protected in their expression as we identify fewer than expected genes in these

ontologies. Analysis in the reactome pathway ontologies (figure 30 B) finds

differentially expressed genes are overrepresented in ontologies being related to

translation and transcription. No other ontology characterizations had significant gene

representation. Paraquat exposure impacting some of the translation and transcriptional genes, as over-represented here, is in line with *in vitro* Paraquat studies initiating an unfolded protein response and altering translational and transcriptional activity [304, 305]. As the number of differentially expressed genes in microglia are greater than the number in astrocytes we again sought to characterize the differentially expressed genes with the Complete Biological Process ontology.

Comprehensive biological process ontology identifies numerous metabolic ontologies in microglia culture differential gene expression

Further characterization of differentially expressed genes in microglia identifies many metabolic and catabolic processes that may be disrupted with Paraquat exposure. Genes are over-represented many of the ontology groups (Table 10). However, genes are under-represented in three categories: neurological system process, G-protein coupled receptor signaling pathway, and sensory perception. The expanded analysis has identified a switch from under to over-representation in genes due to the expansion of the gene lists for each of ontology group, previous analysis did not incorporate all of the possible genes. The overrepresentation of genes in metabolic ontologies show a clear disruption of normal cellular processes in microglia exposed to Paraquat during development. Despite the number of metabolic processes impacted, genes are only over-represented in one ontology (regulation of cell cycle) that is potentially related to apoptosis or cell death. While the ontology analysis presented here offers a basic understanding of what processes and pathways are being impacted, incorporation of gene expression levels is critical in predicting the outcome of such changes

Astrocyte and microglia cultures have different predicted responses in activation of pathways

Gene ontology analysis offers an understanding of potential impact from differentially expressed genes, however, this type of analysis does not factor in expression patterns. To incorporate gene expression data we used Ingenuity Pathway Analysis which offers a predictive function in identifying pathway ontologies. Using the expression patterns within the gene set the algorithm predicts if the pathway would be active (orange, positive z-score), inactive (blue, negative z-score), unchanged (white, zero z-score) or no activity pattern available (gray) if activity of interacting genes in a pathway can be predicted from differential gene expression. No activity pattern available can be derived from conflicting gene expression data points or insufficient data points to make a conclusion.

Ingenuity Pathway analysis allows us to identify the pathways most likely to be involved with our differential gene expression lists and to predict the activation of a pathway. Ingenuity Pathway Analysis of experiment 2 indicates that the two cell types vary in the pathways affected by the differentially expressed genes with Ephrin A signaling and Circadian Rhythm Signaling being the only common pathways (figure 32). Both of these pathways are unpredicted in the pathway analysis.

In astrocyte pathway analysis (figure 32 A) the Wnt-b catenin signaling, Dopamine-DARRP32 feedback in cAMP signaling and glioblastoma multiforme signaling are predicted to be activated pathways. The NF-kB signaling pathway is predicted to be inactivated. Microglia pathway analysis (figure 32 B) displays several pathways predicted to be inactivated including: ETF2 signaling, p53 signaling, ATM signaling, and prolactin signaling. Both mTOR and AMPK signaling are predicted to be

activated. A majority of the pathways in both astrocytes and microglia were unpredicted in activity pattern. This may be due to a lack of consensus on the direction of changes in gene expression within the pathway. However, despite the lack of prediction available there are a number of signaling pathways and cancer related pathways that are significant. To identify constituents that may be playing a critical role in the response to *in utero* Paraquat exposure we expanded the pathways for select pathway ontologies.

Ingenuity pathway analysis identifies some potential proto-oncogenic pathways in Paraquat exposed astrocyte cultures

IPA analysis of *in utero* Paraquat exposed astrocyte cultures identified several potentially proto-oncogenic pathways with over-represented genes (figure 33). WNT/ b-catenin signaling is predicted to be activated (figure 32 A) and expansion of the pathway identifies the gene hits in our differentially expressed genes (figure 33 A). Two *Wnt* members are both increased in expression as well as a key transcription factor in the WNT canonical pathway, *Lef1*. *Frzb*, an antagonist of the canonical WNT signaling pathway, is also increased in gene expression. *Frzb* is reported to be silenced in glioblastoma multiforme but contradicting results indicate that *Frzb* is highly expressed in the nucleus of high grade astrocytoma patient samples [306, 307] indicating an ambiguous role in mediating the *Wnt* signaling pathway. A casein kinase *Csnk1g1* is increased in expression in Paraquat exposed astrocyte cultures. *Csnk1g1* is involved in mitotic spindle location and polarity [308]. *Gnao1*, encodes for Go subunits in signaling cascades [309], is found to be decreased in expression in Paraquat exposed astrocytes. In hepatocellular carcinoma, decreased *Gnao1* expression was found in patient samples and inhibiting *Gnao1* decreased cellular senescence [310]. Critical gene hits in Wnt/ β catenin signaling; *Wnt4, Wnt6*, and *Lef*, are also identified in three additional pathways:

121

Role of Wnt/GSK-3b signaling in the pathogenesis of influenza (figure 33 B), Human Embryonic stem cell pluripotency (figure 33 C) and Glioblastoma Mutliforme signaling (figure 33 D).

The Role of Wnt/Gsk-3b signaling in pathogenis of influenza pathway (figure 33 B) identifes Interferon alpha/beta receptor 1 (*Ifnar1*) which is overexpressed in Paraquat exposed samples. *Ifnar1* is involved in the signaling cascade of interferon signaling which regulates general immune responses [311]. However, *Ifnar1* signaling is also important in the ability of glioblastoma cells and glioblastoma stem-like cells to evade natural host immunity [312]. While *Ifnar1* gene expression compared to normal cells is not addressed in the study, the loss of *Ifnar1* mediates a loss in the signaling pathway down regulating MHC class proteins and increasing the ability of natural killer cells to target the glioblastoma cells.

In Human embryonic stem cell pluripotency pathway, which cannot be predicted in activity (figure 32 A), we see the addition of genes *Fgfr3* and *Fgfrl1*. *Fgfr3* has been implicated as a marker specific for astrocytes and involved in the regulation of morphology in reactive astrogliosis [313, 314]. Reduced *Fgfr3* induces a fibrous astrocyte phenotype and is associated with a reduced hypertrophic pathological response [313]. In our study *Fgfr3* has decreased in expression. *Fgfrl1* is also decreased in expression in our study. *Fgfrl1* overexpression induces cell adhesion in a transformed human embryonic kidney cell line [315], but can induce proliferation in esophageal squamous cell carcinoma by preventing cell cycle arrest [316].

The glioblastoma multiforme signaling pathway in Paraquat exposed astrocyte cultures is predicted to be activated. No new genes are incorporated in this list, but

important cell proliferation regulators are identified in the pathway. Important to note is that *Fgfr3* is downregulated but in glioblastoma lines *Fgfr3* is typically overexpressed. *Fgfr3* can control differentiation of chondrocytes and neuronal cells and is expressed in early astrocyte progenitor cells [313, 317, 318]. This suggests that *Fgfr3* signaling may play a role in the differentiation of astrocytes and would require further examination.

Ingenuity pathway analysis identifies some glial scarring and disrupted cellular signaling pathways in Paraquat exposed astrocyte cultures

We next expanded pathways that may have a role in glial scarring and cellular signaling. The Hepatic fibrosis/Stellate cell activation pathway (figure 34 A) could not be predicted in activity but, several collagen encoding genes are increased in expression as well as CD40. CD40 is involved astrocyte immune response in neuro-inflammation [319, 320]. CD40 has also been reported as a biomarker for better prognosis in glioma patients and enhancing expression can increase efficacy of antibody treatments in model systems [321]. *Igfbp5* is decreased in expression which may play a role in IGF signaling mediated inflammation [322]. Increased expression in genes coding for collagen and inflammatory mediators indicate a potential for an inflammatory glial scarring environment.

Additional evidence for an inflammatory glial scarring environment arise from the Axonal guidance signaling pathway (figure 34 B). While IPA analysis was unable to predict the activity of the axonal guidance signaling pathway, insight can be taken from the changes in gene expression of key genes. Within this data set *Robo1* and *Sema6a*, both repulsive cues in axonal guidance, are increased in expression. *Epha7* and *Efna2*, both increased in our study, are members of the ephrin signaling pathway and play a role in repulsion in axonal guidance [323, 324]. We also see changes in G-protein signaling

members *Gnaao1* and *Gng11*, with increased expression of *Gng11*; and a decrease in

Rgs3 which negatively regulates g protein signaling and can play a role in inhibiting

chemoattraction [325]. One additionally important member of this pathway is *Sema3f*,

shown to be decreased in expression. *Sema3f* plays a significant role in directing

neurons, there is also evidence that *Sema3f* plays a role in mTOR signaling [326, 327].

Considering that gene expression patterns indicate an increase in chemo-repulsive

genes and cellular signaling potentially involved in maintaining the axon repulsive

environment it would appear that the astrocyte cultures are producing an inhibitory

environment for neurons. This potential taken into account with the upregulation of

collagen coding genes and inflammatory modulators would suggest that the *in utero*

exposed Paraquat astrocyte cultures are developing a glial scarring environment. While

we do not see an increase in GFAP positive cells or intensity as we would expect in such

an environment (figure 22 A), we must take note of the fact that the expression changes

are small and may be subtly influencing the astrocytes.

Indeed, when we examine the NF-kB signaling pathway (figure 34 C), IPA

analysis predicts an inactivation of the pathway. NF-kB is a transcription factor that will

translocate to the nucleus after dissociation from IkB regulating inflammation pathways

[328]. A predicted inactivation of inflammatory pathways might be responsible for the

lack of a perceivable difference in *in utero* Paraquat exposed astrocytes. Il1rn is an Il1A

and Il1B antagonist and can deactivate the NF-kB signaling pathway [329]. *Il1rn* is

increased in expression for *in utero* Paraquat exposed astrocyte cultures potentially

driving down NF-kB signaling. *Irak3* is also increased in expression in the *in utero*

Paraquat exposed astrocytes. *Irak3* is primarily expressed in macrophages and

monocytes and serves to regulate the IL-1 signaling pathway and can also deactivate monocytes [330]. Data on function in astrocytes is limited, however, *Irak3* expression in glioblastoma tumors is prognostic of recurrence [331].

Additional signaling pathways are also disrupted. The dopamine-DARRP32 feed-back signaling pathway is predicted to be activated by IPA analysis (figure 34 D). In this pathway there are several ion channel genes affected by *in utero* Paraquat exposure. *Grin2a* which is overexpressed and Grina, under-expressed are both glutamate gated ion channels. Another ion channel *Cacna1c*, a calcium ion channel has slightly increased gene expression. Changes in ion channel signaling may alter signaling capabilities within the cell.

The glycerol 3-phosphate shuttle pathway is unpredicted in activation through IPA analysis but is involved in the shuttling of electrons into the electron transport chain by conversion of NADH to NAD+. Both *Gpd1* and *Gpd2* are decreased in expression. *Gpd1* and *Gpd2* encode for Glycerol-3-Phosphate Dehydrogenase in the cytosol and mitochondria respectively. The proteins encoded by these genes function to transport electrons from the cytosolic NADH into the electron transport chain. Transcriptional control of *Gpd2* is under thyroid hormone response elements. The role decreased expression of *Gpd1* and *Gpd2 in utero* Paraquat exposed astrocytes is unclear as there is limited evidence for physiologic response to changes in expression of *Gpd1* and *Gpd2*. By limiting the main enzymes in the glycerol-3-phosphate shuttle, the availability of cytosolic NADH might increase and subsequent ATP production limited, however, the malate aspartate shuttle may be able to compensate. The change in glycerol-3-phosphate

shuttle members warrant further investigation as metabolic dysregulation has been

implicated in a number of diseases.

Several DNA damage response genes and pathways are down regulated in Paraquat exposed microglia cultures

In microglia ingenuity pathway analysis we expanded pathways that play a role in DNA

damage response. Several of these pathways were in the top five represented pathways. Some

pathways are predictive in the nature of activation. The p53 Signaling pathway is predicted to

be inactivated (figure 32 B). There are several key members in the p53 signaling pathway that

are also represented in several other pathways (figure 35 A, B, C, E). *Atm* is decreased in

expression in our system. *Atm* plays a significant role in the DNA damage repair pathway [332].

Atm deficient models are prone to cancer development and neurodegeneration [333].

Additionally *Atm* silencing in glioma stem cells reduces the glioma stem cell capability to

proliferate [334] indicating a significant role in the ability of maintaining proliferation. Indeed

the *Atm* signaling pathway is predicted to be inactivated (figure 35 C) based on expression

changes. *Atr* is another DNA damage sensor and can act in concert with *Atm* [335]. Both *Atm*

and *Atr* are important in regulating apoptosis.

A confounding factor in the idea that DNA damage is down regulated is the Gadd45

Signaling pathway (figure 35 B), predicted to be inactive (Figure 32 B). *Gadd45b* is involved with

cell cycle check point regulation and cell growth [336] which we found to be increased in

expression. This indicates that some cell cycle arrest pathways may be activated while others

remain inactivated. However, *Gadd45b* may play a role in altering the DNA methylation profile

in the microglia as Gadd45b can induce DNA demethylation [337]. *Gadd45b* may also play a role

in proliferation and survival as overexpression has been reported to increase survival in serum

starved environments [338]. Additionally *Gadd45b* overexpressing cells were able to form tumors in NOD/SCID mice.

Additionally within the ATM Signaling pathway (Figure 35C) *Mdm2* is a critical member of the DNA damage response pathway as *Mdm2* inhibits p53 activating apoptotic pathways [339]. *Mdm2* also plays a role in proliferation of cancer cells [340] We report that *Mdm2* is increased in expression (Figure 35 A), indicating that there may be down regulation of apoptotic pathways in addition to the decreased DNA damage repair pathways. *Mdm2*, a ubiquitin ligase, facilitates ubiquitination of p53 and promotes degradation of p53 [341]. In addition to DNA damage repair pathways, *Mdm2* is critical in protein ubiquitination pathways [342].

We also report several genes associated with protein ubiquitination being differentially expressed (Figure 35D). Most differentially expressed ubiquitination genes (USP members) are decreased in expression. We also note that *Ubb* is increased in expression. Ubb knockout models find that *Ubb* plays a role in dysregulated differentiation in neural progenitor cells [343]. In the *Ubb* knockout models apoptosis was a regular occurrence. *Ubb* overexpression is found after forebrain ischemia within 24 hours but dissipates thereafter [344]. If *Ubb* expression translates to increased protein expression in the Paraquat impacted microglia *Ubb* may be facilitating a stress response pathway or may simply be targeting proteins for degradation. Some clue to the altered Protein Ubiquitination Pathway might be identified by expanding the eIF2 Signaling pathway. eIF2 Signaling is involved in transcriptional control and can facilitate apoptotic pathways [345]. The eIF2 Signaling pathway is predicted to be inactivated by ingenuity pathway analysis (Figure 32B). We report several ribosomal protein genes to be increased in expression (Figure 35E). We also report *Atf4*, a pro-survival factor activated after mitochondrial stress [346], to be increased in expression. *Atf5* acts as an anti-apoptotic transcription factor and plays a role in regulating mitochondrial dysfunction [347, 348]. We find

Atf5 increased in expression in Paraquat exposed mitochondria. These factors taken into account would suggest that the microglia are inducing a survival gene expression profile. We next decided to expand several proliferative and cell survival pathways over-represented from ingenuity pathway analysis.

Several cell proliferation and apoptosis pathways and genes are dysregulated in Paraquat exposed microglia cultures

We expanded several pathways that may have ties to cell survival and proliferation in microglia. mTOR signaling plays an important role in cell metabolism and apoptosis [349]. Ingenuity pathway analysis predicts mTOR signaling pathway to be activated in maternal Paraquat exposed microglia (figure 32 B). However, mTOR signaling is ambiguous in the effect on apoptotic signals [349] and requires further attention to genes affected to gain insight. One such gene *Ddit4*, has a significant role in the outcome of mTOR activation and function. In an energy depletion context *Ddit4* inhibits mTOR activation [350] in opposition to the predicted activation of mTOR Signaling pathway. However, high expression level of *Ddit4* correlates with poor prognosis in of glioblastoma multiforme [351] indicating that the role of *Ddit4* may be more ambiguous than initially understood. Indeed, in β-cells *Ddit4* blocked apoptotic signaling mechanisms [352] indicating that *Ddit4* mechanism is context dependent. Two additional genes that may have a significant role are *Irs2* and *Prkd3*. *Irs2* is reported to be involved in energy homeostasis [353] of the organism while *Prkd3* has a role in cancer migration and proliferation [354-356]. *Prkd3* is decreased in expression while *Irs2* is increased in expression lending the results to the idea that mTOR activation in the case of maternally exposed pup microglia to apoptotic events. However, *Rhod* is increased in expression in maternally exposed pup microglia. *Rhod* is a key member of cell cycle

progression and cell motility [357, 358] indicating that increased expression in the microglia could promote cell proliferation. It is clear that mTOR signaling pathway members have been affected, however, further investigation is warranted to establish to overall outcome of the differences in gene expression.

AMPK Signaling is predicted to be activated in microglia in maternal Paraquat exposed pups (Figure 36B). AMPK signaling may be important in our model as AMPK signaling has been reported to be upregulated in anti-neuroinflammatory models [359]. AMPK signaling is also upregulated in mitochondrial dysfunction promoting cell survival [360]. A key player may be *Adrb1* which is increased in gene expression. Signaling through *Adrb1*, (Adrenergic Beta Receptor 1) key to norepinephrine signaling, has been reported to reduce production of pro-inflammatory signaling cytokines [361, 362]. Studies in brown adipose tissue show *Adrb1* can modulate AMPK signaling. Activation of the *Adrb1* signaling pathway can reduce neuroinflammation and restore behavioral deficits in an Alzheimer's mouse model [363]. Modulation of the norepinephrine signaling pathways may help explain the difference in Iba1 expression (Figure 23) as Iba1 is a marker of microglial activation and inflammation [363, 364].

Another potentially critical gene identified is the bromodomain protein encoding gene *Brd7*. *Brd7* is critical during development as knockout models are embryonic lethal and show growth restriction [365]. *Brd7* may is reportedly involved in multiple models of senescence with changes in *Brd7* expression directly correlating with cellular senescence [366]. *Brd7* may play a role in modulating inflammation by inhibiting the NF-kB pathway [367]. In maternal Paraquat exposed Microglia, the expression level of *Brd7* is down. Decreased expression of *Brd7* may lead to inactivation of cellular

senescence pathways allowing the microglia to continue to proliferate. As we have already discussed *Atm* and *Atf4* are also identified and may be playing a role in promoting cell survival in line with *Brd7* expression and predicted activation of AMPK signaling.

We also report two additional categories from IPA analysis: Molecular Mechanisms in Cancer and Hereditary Breast Cancer Signaling (Figure 36 C, D). While activity of these pathways was not predicted, it is important to note that several constituents from previous pathways are also identified here as well. Additionally, that we are identifying changes in gene expression with ties to cancer is important. We wouldn't anticipate a microglial based cancer, however we might anticipate a protective role in the neural environment. We also expanded Nitric Oxide Signaling in the Cardiovascular System, which is predicted to be inactive (figure 32 B).

Several members of previous pathway ontologies are present in the Nitric Oxide Signaling Pathway in the Cardiovascular System as well. The production of nitric oxide can be detrimental to neurons [368, 369]. Nitric oxide plays a critical role in activation of microglia [370]. Activated microglia can overproduce nitric oxide negatively impacting neuronal survival [371]. The predicted inactivation of nitric oxide signaling offers evidence in support of a protective phenotype.

The effect on differential gene expression in both astrocyte cultures and microglia offers insight into the biological implications of maternal Paraquat exposure. However, changes in transcription levels offers a partial understanding of the impact of maternal Paraquat exposure. Future studies may allow us to examine effects at the protein level and potentially in long term ramifications from these changes. In light of recent advances

in sequencing analysis our study does lend itself to evaluating the effect of Paraquat maternal exposure on gene splicing events.

In utero Paraquat exposure alters RNA splicing in astrocyte and microglia cultures

Lastly we sought to characterize alternative splicing events (figure 37). Paraquat has been reported to induce a caloric restriction phenotype that induces alternative splicing. Considering we show a number of differentially expressed genes in microglia that may drive alternative splicing events (Figures 35E and 30B) paired end RNA sequencing data was analyzed with rMATs (Multivariate Analysis of Transcript Splicing). rMATs can determine the alternative splicing events based upon two criteria: Junction Counts Only that identifies reads that lie across exon splice points; and Junction Counts with Reads on Target, which adds the inference of relative reads around a splice site to the Junction Counts only. Alternative splicing events with a p-value significance <0.05 are displayed. rMATs accounts for five different splicing types: Skipped Exons (SE), Mutually Exclusive Exons (MXE), Alternative 5' Splice Site (A5SS), Alternative 3' Splice site (A3SS) and Retained Intron.

In astrocyte cultures and microglia the majority of alternative splicing events occurs in SE events. Maternal Paraquat exposure microglia have more alternative splicing events than the astrocyte cultures exposed to Paraquat. In both groups there are a few examples of RI which implies that the splicing machinery may be unable to function correctly in identifying correct splicing sites. Alternatively this may mean that transcription is occurring more quickly than splicing mechanisms can function. With so few significant examples of retained intron, there may be significance to the genes in this category. The MXE, A5SS, and A3SS have fewer significant events than SE in both cell

types but together comprise nearly as many events as SE. Further investigation into the splicing machinery may be necessary to determine the effect of Paraquat. Additionally evaluating the gene lists may highlight physiologic relevance for alternative splicing events. To illustrate the changes that are occurring in the individual samples we expanded Tensin 1 in astrocyte cultures.

As an example, tensin 1 in astrocytes is alternatively spliced in *in utero* Paraquat

Tensin 1, a focal adhesion molecule [372], has been reported to be alternatively spliced. We used Tensin 1 as a representative of alternative splicing in Paraqaut exposed astrocytes (figure 38). Control groups show multiple isoforms of Tensin 1 within a sample set. Some control samples preferentially selecting for only one isoform. Paraquat exposed samples preferentially select for one isoform with one sample present with both isoforms. This example highlights that further investigation is warranted into understanding the biological context of the alternative splicing events.

Tensin 1 is involved in cellular communications and focal adhesions [372, 373]. Cellular signaling can be achieved with specific protein domains that interact with tyrosine phosphatases present within the protein [374]. Tensin 1 plays a role in regulating proliferation and migration and the loss of which prevents migration and proliferation [373]. In our model system we show an alternatively spliced version which may impact the appropriate connections between cells. Further investigation is warranted for understanding the role one isoform plays over the other in cellular signaling as well as adherence capability of the astrocytes.

Discussion

We have shown that *in utero* Paraquat exposure induces changes in gene expression of glial cells from neonate tissues. We, however, also show discrepancies between the replicate experiments as we previously addressed. With the difference in

ages of animals giving birth between experiments we do not have true replicate experiments. We might conclude however, that there are differential gene expression changes based simply upon the age of the mothers that could warrant further investigation. There is evidence of neurological differences in pups born to advanced age mothers [375]. This may also provide an opportune investigation into the effect of environmental toxicants based on the age of animals during pregnancy. With the evidence of changes induced by age of the mothers and that the treatment group has fewer representative mothers in our initial experiment, we focused on the larger second study with younger females for most of our analyses.

The changes in gene expression are specific to each cell type as little overlap exists in differentially expressed genes as well as pathways and ontologies impacted. These changes are sustained changes as the cells were cultured for two weeks prior to harvest. The sustainable nature of the reported changes in gene expression imply we may have altered the epigenetic landscape. Additionally we report significant changes in splicing patterns in our experiment. While we do not report epigenetic remodeling events, ongoing studies in the laboratory include ATAC-sequencing to address the basic question of how we alter the chromatin landscape with *in utero* exposure to Paraquat. By evaluating the chromatin landscape we may be able to cross reference histone and polycomb ChIP data sets to find potential epigenetic remodeling targets. What remains clear is we have impacted these cell types and this impact could have long term ramifications.

The unique gene expression that occurs in each cell type indicates that different cells respond differently to Paraquat exposure. Analysis of differentially expressed genes

in astrocytes illustrates that astrocytes are predicted to be activated in glioblastoma signaling pathway while also have several pathways that could be tied to glial scarring and prevention of axonal growth. The cooperation of these pathways may signify that we may be inducing a precancerous phenotype as glioblastoma and other astrocytomas induce a glial scar like phenotype [376, 377]. What is interesting is that the Human Embryonic Stem Cell pathway is significant in represented genes but unpredicted in activity. This may also implicate a precancerous phenotype as glioblastoma populations typically do not share an identical expression profile with stem cells as they have a more differentiated phenotype, but do share proliferative gene expression profiles [378].

We also reported that the treatment astrocyte cultures are indistinguishable from control group astrocyte cultures. The lack of a phenotype change in the presence of the gene expression changes indicate that the altered astrocytes may be masked like normal cells and continue to incorporate further changes in gene expression. To evaluate this further we propose future studies to evaluate effects in neural cells of maternally exposed pups at later time points in life; for example 6 months, 12 months and 18 months. What might be the most interesting in such a long term study is to evaluate littermates. We report that littermates are unequally affected by maternal Paraquat exposure. Our data indicate that some littermates will cluster with Paraquat treatment groups while others cluster into control group. Additionally, within the Paraquat treatment groups there are distinct clades implying that Paraquat does not act uniformly in overall phenotypic outcome. Our current study was not designed to evaluate the condition of littermates as some littermates were pooled. Future studies would limit pooling of samples to evaluate specific changes within litters.

Microglia have a distinct response to Paraquat exposure as compared to astrocytes. In the astrocytes, gene expression changes suggest alterations to pathways which may promote increased proliferation and potential activation, where in the microglia the changes in gene expression are more ambiguous. Our *in vitro* culture staining show much reduced IBA1 staining indicating that Paraquat has had a clear phenotypic effect. One might propose that these cells are dying as the ontologies of differentially expressed genes are represented by metabolic functions and translational regulation as well as the IBA1 staining. IPA analysis indicates that DNA damage pathways are inactivated which would correlate with breakdown of DNA in cell death [379, 380]. However, we also have a predicted activation of the mTOR pathway which would indicate that these cells could be actively proliferating [381]. We also note that there are additional pathways tied to cancer signaling and activated translation and transcription that have been identified in these analyses. As we continue to delve deeper into the specific genes within the expanded pathways, the gene expression changes suggest that we have actively translating cells with reduced DNA damage signaling pathways and upregulated proliferation pathways. Indeed some regulators of apoptosis are decreased while others are increased. There is little evidence of microglia based cancers, but microglia may play a critical role in facilitating cancer initiation and progression [382]. Microglia are already reported to play a significant role in neurodegeneration [383-385]. Whether the microglia will play a role in either disease pathway is unclear, as is their ability to survive long term, but what remains clear is that the microglia are altered in our model and would likely be unable to function in a normal capacity. Future long term studies may help elucidate this function.

An interesting caveat to this data is that our study did not find measurable Paraquat in pup brain tissues by mass spectrometry. While we do see gene expression changes in two separate *in vivo in utero* Paraquat exposures (discussed later) we were unable to detect Paraquat in neonate tissues. We would not expect serum levels to contain Paraquat but we might expect to see Paraquat in the neonate brain tissues. What might explain this is the presence of the blood brain barrier. The blood brain barrier in developing organisms is not as leaky as is normally ascribed [386, 387]. Original data points to a fully functional blood brain barrier. Although the blood brain barrier may be complete and effective there are marked differences in the expression of transporters in endothelial cells of brain microvasculature. Notably the SLC family of proteins are overexpressed in developing embryos and neonates compared to adults [388, 389]. SLC family of proteins include organic cation transporters such as OCT3, known to play a role in internalization of Paraquat [167]. The absence of Paraquat may be due to the developing brain more effectively blocking or effluxing Paraquat from brain tissue. In order to isolate this effect, future studies can identify time of exposure in embryos as well as efficacy of blood brain barrier in our model system. Additionally we may be able to evaluate how effective Paraquat is at crossing the placental barrier. Some work has been done in this area which indicates that low levels of Paraquat can cross the placenta in monkeys [390].

It may be that the changes in gene expression in both the astrocyte cultures and the microglia is dependent upon the time frame of exposures. Astrocytes may be more protected after development of the blood brain barrier thereby limiting any further exposure to astrocytes. Microglia, however, do not enter the central nervous system

immediately as they are humoral in origin and migrate during development [302]. Consequently microglia may have additional exposure events driving the changes in gene expression we report here. This highlights that while these cells show significant difference in the effect of Paraquat, the differences may be a function of the number exposure events.
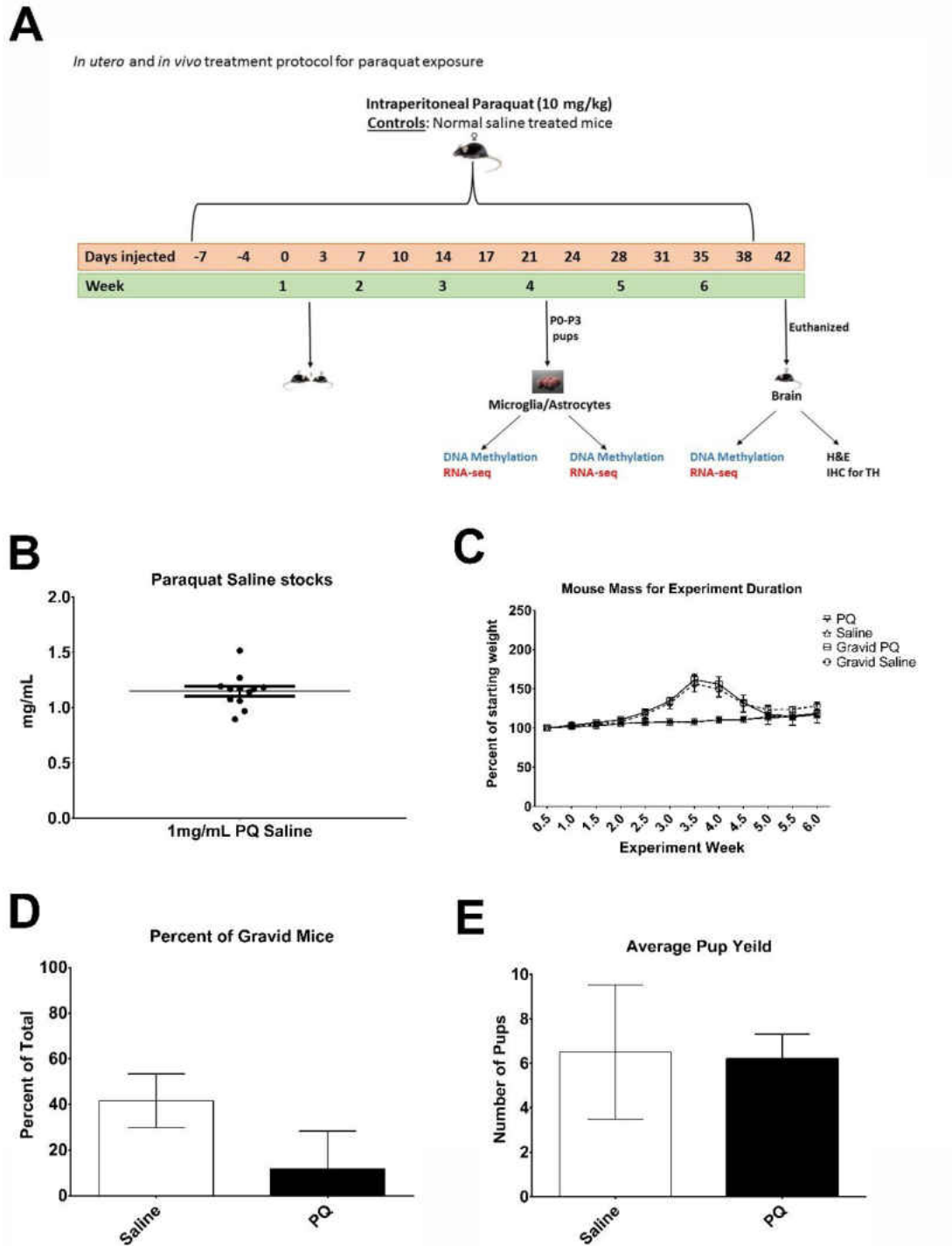
Figure 19. Intraperitoneal Paraquat exposure prior to and during gestation does not affect dam mass, gravidity or pup number. Schematic of experiment A). Adult female mice were exposed to Paraquat for six weeks with twice weekly intraperitoneal injections of 10 mg/kg of Paraquat and bred during exposure. Pups were carried to full term and sacrificed for whole brains as well as astrocytes and microglia. Injection stocks

Figure 19 cont. B) were made to 1 mg/mL for an injection schedule of 10 uL/g of adult weight. Paraquat stocks were assessed by liquid chromatography mass spectrometry. C) Mouse mass during experiment was not significantly different between control and Paraquat treated animals in either pregnant or non-pregnant animals (Two-way ANOVA with bonferroni's post test). D) Percent of mice that were gravid showed a decreased trend in Paraquat treated animals versus control animals although not significant (p-Value of 0.177 as determined by T-test). E) Average pup yield shows no difference between control and Paraquat treated groups (T-test).
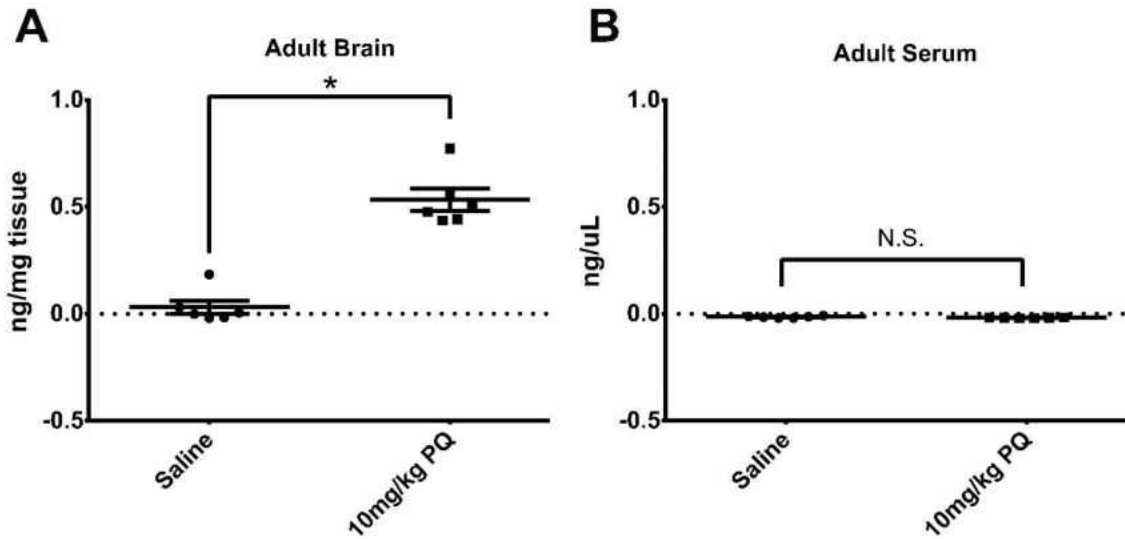
Figure 20. Dam brains unable to clear Paraquat from intraperitoneal injections.
Female mice were intraperitoneally treated with 10 mg/kg Paraquat for 6 weeks. Mice were sacrificed 3 days after last injection and blood was collected before transcardiace perfusion to flush the brain of blood. Brains were removed, snap frozen and pulverized for homogeneity. 10 ng of labelled Paraquat was added and samples were extracted with 80% methanol and sonication. Samples were centrifuged, and supernatant was washed with hexane twice. Samples were submitted for LC/LC mass spectrometry and normalized against internal standard. A) Adult brain tissues have a significant presence of Paraquat no longer present in B) adult serum. * indicates p-value < 0.5 as determined by T-test.
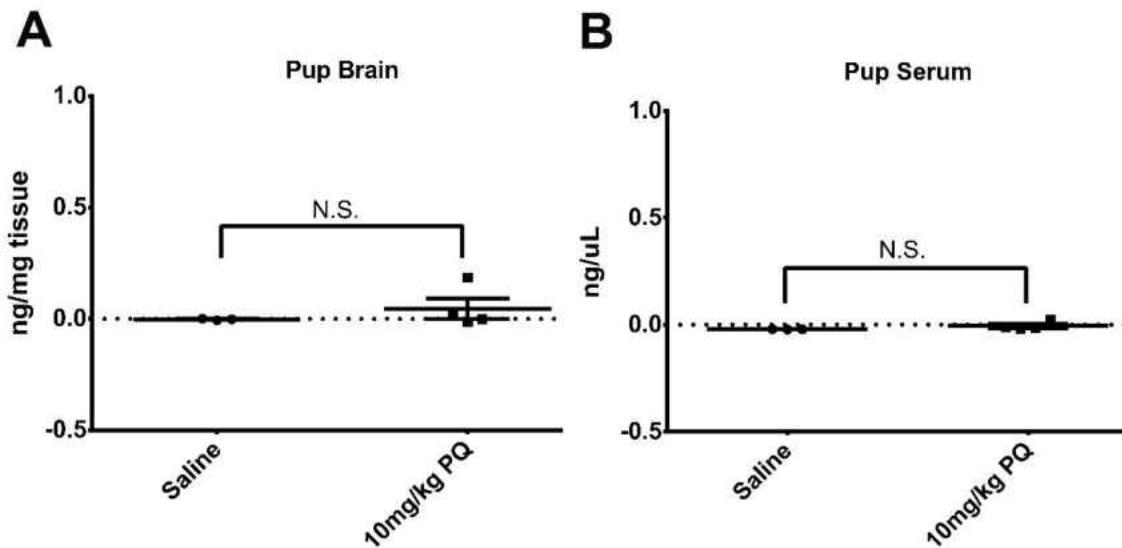
Figure 21. Pup brains and serum are clear of Paraquat. Pups were collected 1-3 days postnatal and sacrificed. Blood was collected after decapitation and brains were removed, snap frozen and pulverized for homogeneity. 10 ng of labelled Paraquat was added and samples were extracted with 80% methanol and sonication. Samples were centrifuged and supernatant washed twice in hexane. Samples were submitted for LC/LC mass spectrometry. A) Pup brains and B) sera had no significant levels of Paraquat (T-test).
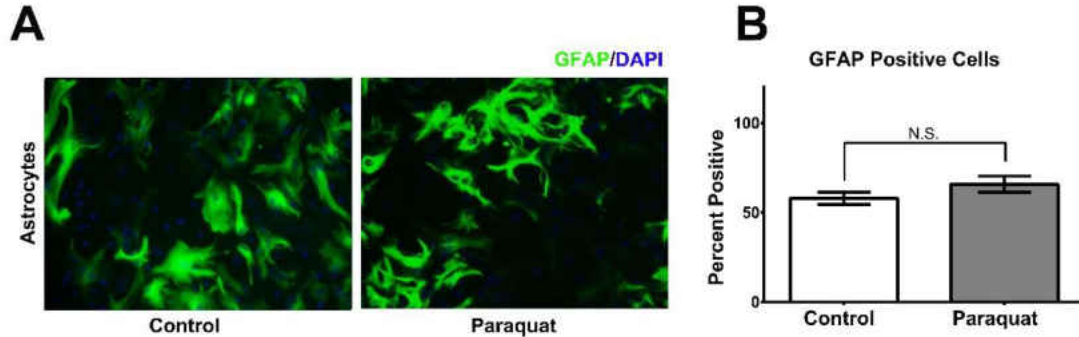
Figure 22. Maternal Paraquat exposure has no apparent effect on astrocyte enrichment or Glial Fibrillary Acidic Protein (GFAP) expression. Brains from 1 to 3 day old pups were cultured for two weeks at which point culture flasks were subjected to shaking at 200 rpm in an incubated shaker for 45 minutes. Medium was removed and cells were washed once in dissecting medium. Adherent cultures were treated with trypsin and suspended in complete medium. Cells were then reseeded onto poly-D-Lysine coated german glass coverslips. Cells were cultured for 48 hours prior to fixation in 4% paraformaldehyde. Coverslips were washed in PBS and incubated in blocking solution (3% Donkey serum, 2% Natural Goat Serum, 2% BSA, and 0.1% Triton X-100 in PBS with Ca^{++} and MG^{++}) for two hours. Coverslips were then incubated overnight at 4° C in blocking solution with 1:1000 anti-GFAP. Coverslips were then washed and incubated in blocking solution with alexa-fluor 555 secondary for two hours. Coverslips were washed and mounted with vectasheild mounting medium with DAPI. Coverslips were imaged (A) and counted (B) by two individuals for positively stained cells. The results were averaged and are represented in 6.3 B. A T-test was performed for statistical differences and no difference was found.
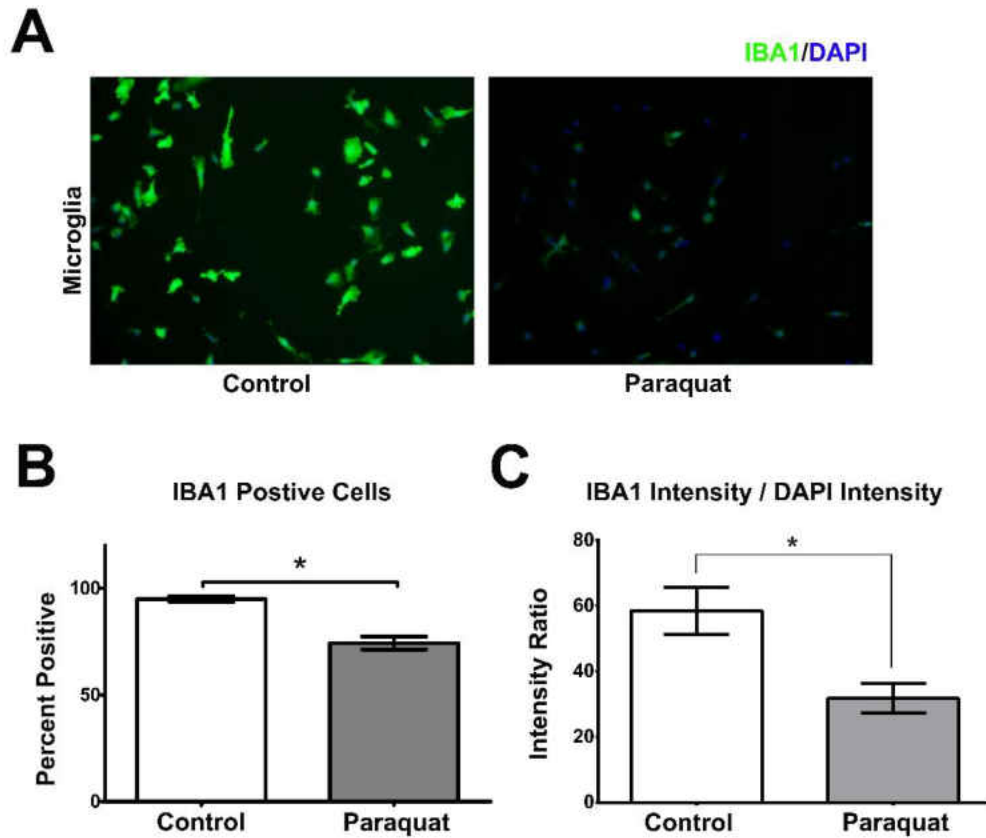
Figure 23. Maternal Paraquat exposure alters pup microglia Ionized Calcium-Binding Adaptor Molecule 1 (IBA1) expression. Brains from 1 to 3 day old pups were cultured for two weeks at which point culture flasks were subjected to shaking at 200 rpm in an incubated shaker for 45 minutes. Medium was removed and flasks were washed once in dissecting medium. Medium and Dissection Medium were collected and centrifuged to collect suspended cells. Cells were suspended in complete medium and then reseeded onto poly-D-Lysine coated german glass coverslips. Cells were cultured for 48 hours prior to fixation in 4% paraformaldehyde. Coverslips were washed in PBS and incubated in blocking solution (3% Donkey serum, 2% Natural Goat Serum, 2% BSA, and 0.1% Triton X-100 in PBS with Ca^{++} and MG^{++}) for two hours. Coverslips were then incubated overnight at 4° C in blocking solution with 1:200 anti-IBA1. Coverslips were then washed and incubated in blocking solution with alexa-fluor 555 secondary for two hours. Coverslips were washed and mounted with vectasheild mounting medium with DAPI. Coverslips were imaged (A) and counted (B) by two individuals for positive cells. The results were averaged and are represented in B. Intensity measurements (C) were performed for the DAPI and IBA1 channels and are displayed as an intensity ratio of IBA1/DAPI. * indicates p-value < 0.05 as determined by T-test.

143
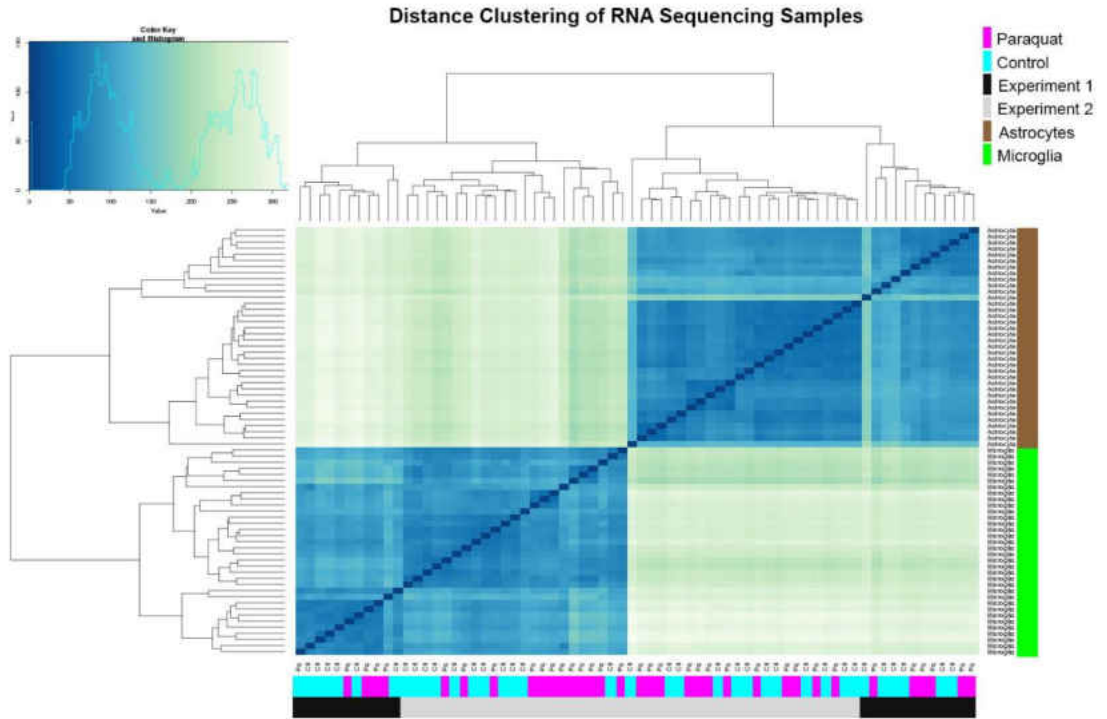
Figure 24. Gene expression analysis shows experimental batch effect. Distance clustering of the RNA sequencing results for microglia (green) and astrocyte (brown) samples from experiment 1 (black) and experiment 2 (grey) exposed to Paraquat (pink) or Saline (control, blue). Results indicate samples cluster according to cell type and followed by experiment.
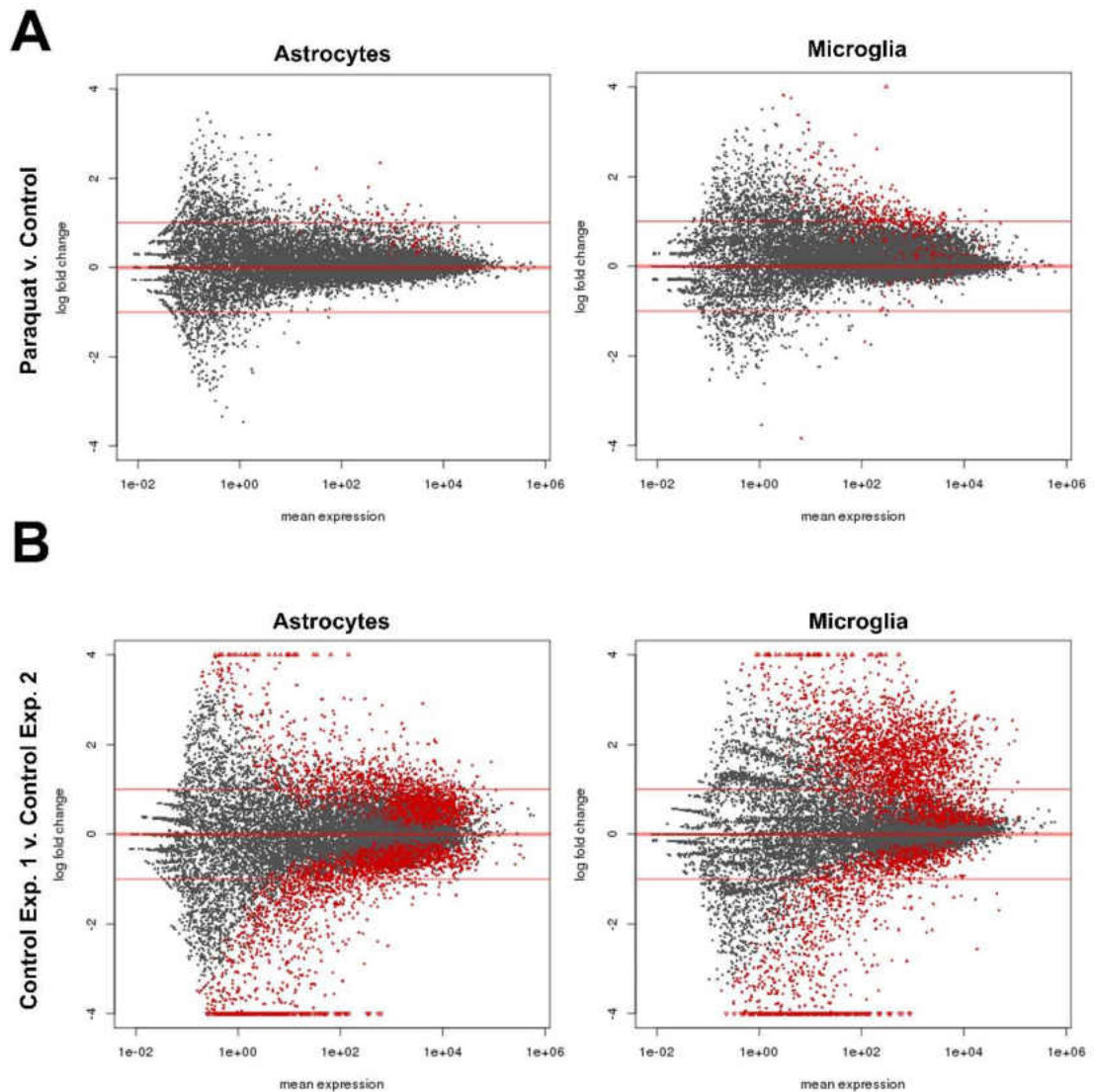
Figure 25. Maternal Paraquat exposure experiments are unique from one another. Differential gene expression between Paraquat and control for astrocytes and microglia combined for experiment 1 and 2 (A); and differential gene expression between control groups from experiment 1 and 2 (B) for astrocytes and microglia. Results are shown in MA plot format of mean expression versus log fold change. Each dot indicates the results for a gene locus; the further right indicates greater mean expression and away from the central axis indicate the greater the difference in expression between the two groups. Red dots indicate statistically significant difference in gene expression with an adjusted p-value < 0.05. Control conditions between the two experiments have significant number of differentially expressed genes that are greater in number than between the experimental conditions for both experiments combined. Reexamination of pup and dam populations in both experiments indicate that analysis should be conducted separately.

Figure 25 Cont. Dams in first experiment vary in age from 3 to 7 months at the end of experiment while the second experiment, dams were aged 3.5 months at the end of experiment. Additionally, pups from first experiment were from varied aged mothers in control group while treatment group were primarily from one mother at the age of 6 months. One mother in the Paraquat treatment group was aged 4 months at the end of the study but generated only two pups compared to 6 pups from the 6 month old mother. The second study had pups from multiple dams in both treatment groups.

TABLE 4. DIFFERENCES IN AGE OF MOTHERS AND PUP REPRESENTATION OF *IN VIVO* PARAQUAT EXPOSURE

EXPERIMENT 1

DAM	Age (end of study)	Number of pups
CONTROL		
A	4 Months	9
B	7 Months	10
C	6 Months	8
D	5 Months	8
PARAQUAT		
E	4 Months	2
F	6 Months	6

EXPERIMENT 2

DAM	Age (end of study)	Number of pups
CONTROL		
A	3.5 Months	2
B	3.5 Months	3
C	3.5 Months	8
D	3.5 Months	4
PARAQUAT		
E	3.5 Months	4
F	3.5 Months	4
G	3.5 Months	7
H	3.5 Months	7
I	3.5 Months	7
J	3.5 Months	7
K	3.5 Months	5
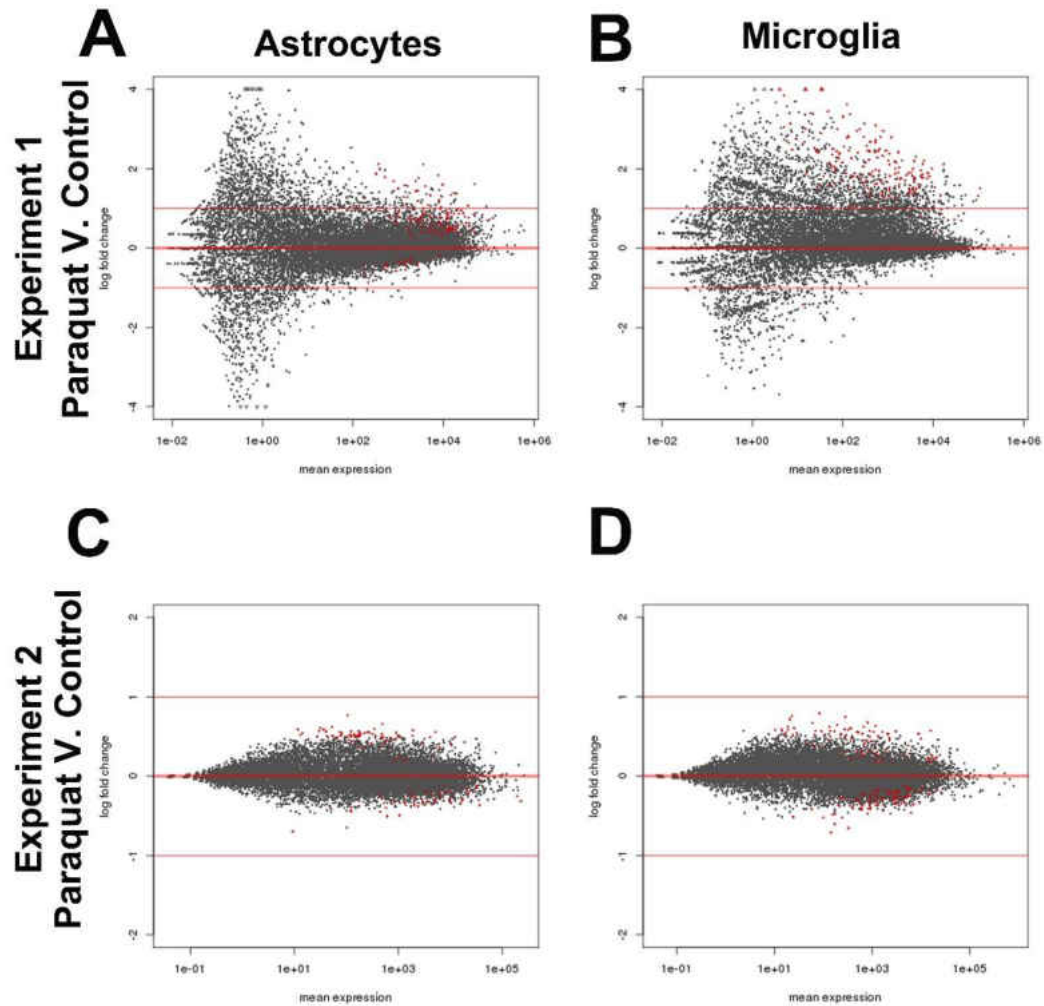
Figure 26. Repeat experiments have different patterns in gene expression changes.
Differential gene expression alaysis is displayed in MA plot format for differential gene
expression between Paraquat and Control groups for Astrocytes in experiment 1 (A) and
experiment 2 (C); and microglia in experiment 1 (B) and experiment 2 (D). Each dot
represents a gene locus with greatest difference between control and treatment group
furthest right and distal to central axis. Red dot indicates significant difference in gene
expression with an adjusted p-value < 0.05. Experiment 1 has differential gene
expression that is largely increased gene expression in both cultures whereas the second
experiment has a balance between increased and decreased gene expression in both
cultures.
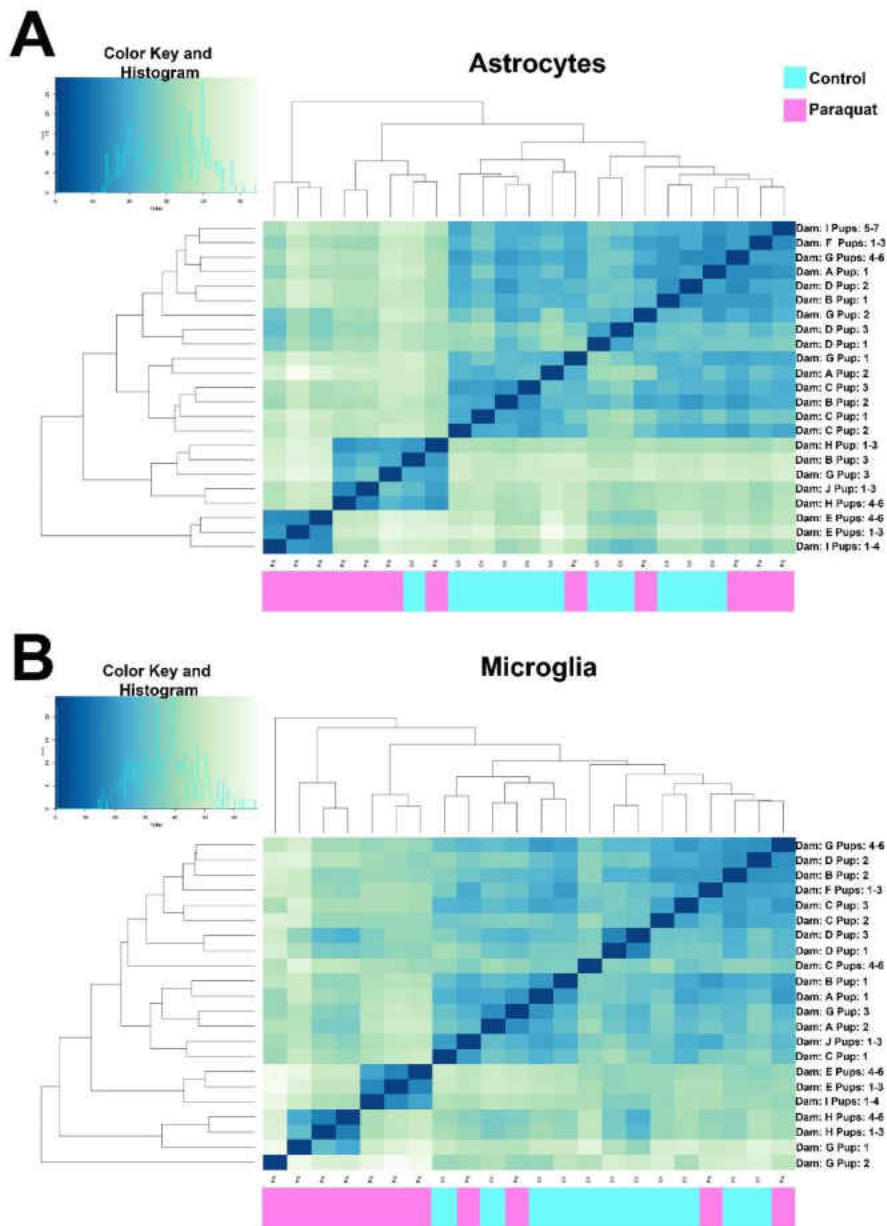
Figure 27. Gene expression data indicates a response in pup brain cells to maternal Paraquat exposure. Distance clustering of gene expression data sets are separated into A) astrocytes and B) microglia from the second experiment. Pups from Paraquat treated dams are differentially clustered with some pups clustered into the control groups in both astrocyte and microglia cultures. Some littermates do not cluster according to treatment group while others follow treatment groups.

Table 5. Experiment 1 astrocyte differential gene expression

Gene	Base mean	Fold change (log$_2$)	Lfcse	Stat	p-value	Adjusted p-value
A230072C01RIK	195.3009	-0.5321	0.1635	-3.255	0.0011	0.0455
A630001G21RIK	924.8758	0.5126	0.1553	3.3013	0.001	0.0427
ABCB10	1218.071	0.2473	0.0712	3.4712	0.0005	0.0306
ABCB7	2721.595	0.3768	0.1101	3.4238	0.0006	0.034
ACD	1467.72	-0.2938	0.092	-3.1939	0.0014	0.0495
ACVR1	1914.492	0.5833	0.1236	4.7205	0	0.0041
ACVRL1	852.0515	0.7915	0.2116	3.7414	0.0002	0.0199
ADAM10	16799.99	0.5327	0.1269	4.1968	0	0.0113
ADAM17	13550.44	0.5387	0.1423	3.7852	0.0002	0.0188
ADCK4	2674.018	-0.4368	0.126	-3.4671	0.0005	0.0307
ADH5	6600.139	-0.2266	0.0694	-3.2661	0.0011	0.0446
ADPRHL2	1198.513	-0.3543	0.1007	-3.5197	0.0004	0.0294
AGA	1537.543	0.2808	0.0879	3.1955	0.0014	0.0495
AKIP1	1116.054	-0.3865	0.1205	-3.2084	0.0013	0.049
AKR1E1	1935.482	-0.345	0.0923	-3.7388	0.0002	0.0199
ALDH16A1	1782.4	0.2893	0.09	3.2151	0.0013	0.049
ALG1	1368.435	0.2909	0.0848	3.4298	0.0006	0.034
ALG11	1440.983	0.3399	0.0956	3.5557	0.0004	0.028
ALG2	2460.809	0.3112	0.093	3.347	0.0008	0.0387
AOAH	3480.191	0.876	0.2505	3.497	0.0005	0.0299
APP	44525.44	0.5073	0.1469	3.4522	0.0006	0.0321
ARFIP2	2139.4	-0.2924	0.0887	-3.2959	0.001	0.0432
ARL3	2819.645	-0.2976	0.0922	-3.2266	0.0013	0.0483
ATF6B	3455.05	0.2322	0.071	3.2713	0.0011	0.0444
ATP11C	1962.929	0.3982	0.115	3.4609	0.0005	0.0313
ATP13A1	3089.343	0.3383	0.1021	3.3139	0.0009	0.0417
ATP2A2	26053.34	0.4474	0.1275	3.5081	0.0005	0.0298
ATP2B1	11288.16	0.6114	0.1833	3.3358	0.0009	0.0391
ATP6AP1	18666.66	0.3356	0.1045	3.2101	0.0013	0.049
ATP6AP2	13597.31	0.4013	0.1225	3.2762	0.0011	0.0439
ATP7A	4402.727	0.6084	0.1679	3.6231	0.0003	0.025
B3GLCT	1402.893	0.454	0.1197	3.7942	0.0001	0.0186
B4GALT1	8795.652	0.4872	0.1217	4.0023	0.0001	0.0152
BCAP31	6819.807	0.3337	0.094	3.5492	0.0004	0.0285
BTF3L4	5121.198	-0.2107	0.0563	-3.7417	0.0002	0.0199
C2CD2	1042.574	0.2686	0.0771	3.4865	0.0005	0.0302
C3AR1	34789.4	1.0594	0.3244	3.2658	0.0011	0.0446
C430049B03RIK	139.2193	-0.4529	0.1297	-3.4913	0.0005	0.0302
C5AR1	16713.56	0.8603	0.2442	3.5231	0.0004	0.0294

Table 5. Experiment 1 astrocyte differential gene expression

Gene	Base mean	Fold change (log$_2$)	Lfcse	Stat	p-value	Adjusted p-value
CALCRL	1024.469	0.8964	0.2308	3.8842	0.0001	0.0173
CALU	20149.08	0.5101	0.1483	3.4394	0.0006	0.0334
CANX	39879.08	0.4137	0.1146	3.6092	0.0003	0.026
CCDC88B	2981.955	0.6913	0.1736	3.9823	0.0001	0.0154
CCL3	19161.82	1.3696	0.3629	3.7741	0.0002	0.0195
CCL4	9547.414	1.5974	0.3337	4.7874	0	0.0041
CCRL2	794.1884	1.6785	0.4658	3.6034	0.0003	0.0261
CD40	183.9531	1.2576	0.3528	3.5649	0.0004	0.028
CD93	8790.698	1.3089	0.4049	3.2328	0.0012	0.0475
CDK5	1971.101	-0.3076	0.0745	-4.1267	0	0.0124
CFH	14731.47	1.3322	0.3494	3.8128	0.0001	0.0181
CHMP5	5878.114	-0.2852	0.078	-3.655	0.0003	0.0236
CKAP4	3707.037	0.5815	0.1631	3.5649	0.0004	0.028
CLEC4A2	933.3873	0.8477	0.2641	3.2093	0.0013	0.049
CLPTM1	9861.658	0.377	0.115	3.2787	0.001	0.0439
CMKLR1	3021.377	0.7944	0.2112	3.7622	0.0002	0.0199
CNPY3	3993.837	0.32	0.0875	3.6564	0.0003	0.0236
COL14A1	3564.542	0.9967	0.2961	3.3659	0.0008	0.0375
COL15A1	389.0267	1.9925	0.3517	5.665	0	0.0002
COL18A1	5116.197	1.3278	0.3884	3.4187	0.0006	0.0345
COL7A1	989.7385	1.4971	0.3811	3.928	0.0001	0.017
COMMD3	3807.594	-0.2749	0.0779	-3.5275	0.0004	0.0294
COMMD6	1532.15	-0.3604	0.1095	-3.2914	0.001	0.0434
COPZ1	8958.451	-0.205	0.0642	-3.1913	0.0014	0.0495
COX20	1109.286	-0.3893	0.1158	-3.3607	0.0008	0.0376
CPD	24174.18	0.6776	0.2001	3.3859	0.0007	0.0367
CRIPT	2717.822	-0.32	0.0852	-3.7547	0.0002	0.0199
CRTAP	2888.495	0.5213	0.1471	3.5436	0.0004	0.0286
CTSC	35438.14	0.766	0.1732	4.4223	0	0.0072
CUTC	309.7578	-0.448	0.1248	-3.59	0.0003	0.0269
CWC27	1204.131	-0.156	0.0467	-3.3396	0.0008	0.0389
CYB5RL	311.2579	-0.3769	0.0914	-4.1234	0	0.0124
CYBA	10220.45	0.5603	0.174	3.2196	0.0013	0.049
DCHS1	1013.114	0.8995	0.2822	3.188	0.0014	0.0496
DCPS	1402.558	-0.4135	0.1113	-3.7138	0.0002	0.0213
DCTN6	2315.876	-0.271	0.0683	-3.9678	0.0001	0.0158
DDOST	10934.29	0.4269	0.1115	3.8304	0.0001	0.0181
DERL1	8018.775	0.4006	0.1056	3.7941	0.0001	0.0186
DGCR2	5137.984	0.3249	0.0924	3.5172	0.0004	0.0294

Table 5. Experiment 1 astrocyte differential gene expression

Gene	Base mean	Fold change ($\log_2$)	Lfcse	Stat	p-value	Adjusted p-value
DHCR7	1649.84	0.4022	0.1095	3.6729	0.0002	0.023
DIEXF	685.7031	0.2853	0.0893	3.1959	0.0014	0.0495
DMAP1	900.4709	-0.3192	0.0985	-3.2409	0.0012	0.0466
DNAJB11	7392.899	0.4047	0.1243	3.257	0.0011	0.0455
DNAJC7	8110.152	-0.1793	0.0558	-3.2144	0.0013	0.049
DOCK10	3867.138	0.557	0.1665	3.3455	0.0008	0.0387
DOLK	1126.045	0.3476	0.0895	3.8863	0.0001	0.0173
DPH7	564.8091	-0.3512	0.1023	-3.4316	0.0006	0.0339
DSE	5699.122	0.5911	0.1678	3.5221	0.0004	0.0294
DYNC1I2	11074.47	-0.1477	0.0458	-3.2213	0.0013	0.049
E130308A19RIK	500.0205	0.2803	0.0856	3.2765	0.0011	0.0439
ECE1	1498.967	0.6907	0.1901	3.6324	0.0003	0.0246
EDEM1	16303.32	0.5362	0.1491	3.5952	0.0003	0.0267
EDEM3	4587.485	0.5111	0.1392	3.6708	0.0002	0.023
EHBP1L1	5408.712	0.4034	0.1224	3.294	0.001	0.0432
EHMT1	2529.755	0.2232	0.0643	3.4723	0.0005	0.0306
ELF4	3493.626	0.7022	0.1918	3.6605	0.0003	0.0235
EMC10	5454.196	0.2404	0.0712	3.376	0.0007	0.0372
EMC2	3596.058	-0.2835	0.0734	-3.8603	0.0001	0.0175
EMC3	5357.152	0.3346	0.0939	3.564	0.0004	0.028
EMILIN1	2720.479	1.1828	0.3455	3.4238	0.0006	0.034
EMILIN2	7921.403	1.2023	0.3106	3.871	0.0001	0.0175
EMR1	27153.69	0.8778	0.2622	3.348	0.0008	0.0387
ENG	408.0728	1.0139	0.2631	3.8533	0.0001	0.0175
ENPP1	2427.951	1.4304	0.2787	5.1324	0	0.0012
ERLIN1	3048.488	0.4262	0.1328	3.2089	0.0013	0.049
ERP29	11721.5	0.3548	0.1102	3.2197	0.0013	0.049
ERP44	4069.614	0.4037	0.0978	4.1284	0	0.0124
ESYT2	3178.01	0.3792	0.1134	3.3442	0.0008	0.0387
EXT2	4349.371	0.4552	0.1057	4.3065	0	0.0095
FAM103A1	2687.899	-0.3078	0.087	-3.5354	0.0004	0.0292
FAM129A	1042.007	0.7762	0.2421	3.2066	0.0013	0.049
FAM3C	3017.126	0.3039	0.0768	3.9574	0.0001	0.016
FASTKD2	1389.962	0.342	0.1052	3.2509	0.0012	0.0458
FBXW2	3215.126	-0.2123	0.058	-3.6605	0.0003	0.0235
FCF1	1595.481	-0.336	0.1046	-3.2127	0.0013	0.049
FES	5227.603	0.5863	0.1812	3.2366	0.0012	0.047
FNTA	5027.679	-0.2116	0.0587	-3.6026	0.0003	0.0261
FRG1	2067.485	-0.3112	0.0916	-3.398	0.0007	0.0364

Table 5. Experiment 1 astrocyte differential gene expression

Gene	Base mean	Fold change (log$_2$)	Lfcse	Stat	p-value	Adjusted p-value
FRRS1	2518.767	0.6612	0.207	3.1946	0.0014	0.0495
FUT8	2082.426	0.3559	0.1065	3.3406	0.0008	0.0389
GALNT1	10160.44	0.3104	0.0774	4.0084	0.0001	0.0152
GALNT12	842.2514	0.6795	0.2094	3.2448	0.0012	0.0463
GALNT2	7107.554	0.3683	0.0931	3.9559	0.0001	0.016
GALNT4	1730.21	0.38	0.1067	3.5625	0.0004	0.028
GANAB	12257.23	0.4326	0.1022	4.2349	0	0.0109
GLCE	1346.104	0.5984	0.1592	3.76	0.0002	0.0199
GLO1	7175.031	-0.1986	0.0601	-3.3051	0.0009	0.0426
GM6377	3904.936	1.5563	0.4007	3.8841	0.0001	0.0173
GPANK1	455.6793	-0.4837	0.145	-3.335	0.0009	0.0391
GPATCH11	781.2755	-0.2322	0.0707	-3.2832	0.001	0.0438
GPR180	1113.092	0.2589	0.0762	3.3962	0.0007	0.0365
GRN	104280.8	0.7218	0.2243	3.2174	0.0013	0.049
GUSB	31750.72	0.6288	0.1898	3.3124	0.0009	0.0418
GXYLT1	3039.154	0.5203	0.1483	3.5076	0.0005	0.0298
H2-M3	980.9927	0.5882	0.1654	3.5556	0.0004	0.028
H6PD	2492.987	0.699	0.1894	3.6912	0.0002	0.022
HDAC10	680.952	-0.315	0.0955	-3.298	0.001	0.043
HIATL1	4518.212	0.2807	0.0855	3.284	0.001	0.0438
HSPA13	3915.644	0.4053	0.1111	3.6478	0.0003	0.0241
IDH3B	6113.389	-0.1772	0.045	-3.9392	0.0001	0.0166
IDH3G	5382.453	-0.2383	0.0619	-3.8526	0.0001	0.0175
IFNAR1	9678.696	0.4328	0.1238	3.4969	0.0005	0.0299
IL13RA1	2340.843	0.7033	0.1839	3.8249	0.0001	0.0181
IL18RAP	118.1133	1.0702	0.3357	3.1878	0.0014	0.0496
IL21R	3447.091	0.82	0.2566	3.1951	0.0014	0.0495
IL2RG	1460.285	1.0865	0.2568	4.2316	0	0.0109
IMPAD1	5495.458	0.4523	0.1414	3.1981	0.0014	0.0495
ISCA2	1238.617	-0.3537	0.108	-3.2752	0.0011	0.0439
ITGA4	5130.182	0.9199	0.2803	3.282	0.001	0.0438
ITGA6	21184.41	0.5762	0.1625	3.5468	0.0004	0.0286
ITGA8	503.5242	1.7937	0.5144	3.4867	0.0005	0.0302
ITGA9	1981.366	0.7063	0.2144	3.2947	0.001	0.0432
ITGAM	24746.32	0.9502	0.2355	4.0342	0.0001	0.0152
ITGAV	12366.5	0.6432	0.1671	3.85	0.0001	0.0175
ITPRIPL2	5674.511	0.5019	0.1259	3.9867	0.0001	0.0154
JOSD2	976.6704	-0.3236	0.1006	-3.2182	0.0013	0.049
JRKL	520.5603	-0.6055	0.1796	-3.3718	0.0007	0.0373

Table 5. Experiment 1 astrocyte differential gene expression

Gene	Base mean	Fold change (log$_2$)	Lfcse	Stat	p-value	Adjusted p-value
KAT5	2090.07	-0.258	0.0605	-4.2615	0	0.0109
KCNK13	1822.596	0.776	0.2363	3.2842	0.001	0.0438
KCNK6	2355.364	0.6456	0.1982	3.2572	0.0011	0.0455
KCNN4	1300.014	1.2798	0.3944	3.2447	0.0012	0.0463
KDELR2	4894.537	0.4156	0.1247	3.3329	0.0009	0.0392
KLHL15	225.8867	0.4846	0.1332	3.6387	0.0003	0.0245
KREMEN1	2403.113	0.3545	0.0912	3.8862	0.0001	0.0173
LAMA1	367.8885	2.1206	0.545	3.8913	0.0001	0.0173
LAMA4	1402.364	1.5817	0.4828	3.2764	0.0011	0.0439
LAMC1	12371.84	0.8419	0.2254	3.7344	0.0002	0.02
LCMT1	1100.947	-0.292	0.0917	-3.1851	0.0014	0.0499
LEMD3	1292.685	0.365	0.0961	3.7988	0.0001	0.0186
LEPRE1	1333.03	0.5375	0.1454	3.6967	0.0002	0.0217
LGALS3BP	8398.49	0.752	0.2165	3.4738	0.0005	0.0306
LHFPL2	12282.17	0.778	0.2271	3.4252	0.0006	0.034
LMAN2	10273.98	0.4465	0.098	4.5581	0	0.0065
LPGAT1	5014.969	0.4222	0.1138	3.7113	0.0002	0.0213
LRP1	47331.02	0.848	0.2222	3.8171	0.0001	0.0181
LRP10	7731.231	0.3713	0.1093	3.3975	0.0007	0.0364
LRP5	6046.732	0.5663	0.1775	3.1907	0.0014	0.0495
LRRC25	2487.824	0.6944	0.1828	3.798	0.0001	0.0186
LTBR	4483.262	0.2747	0.0784	3.5024	0.0005	0.0298
LYN	12984.76	0.4525	0.1185	3.8182	0.0001	0.0181
LYRM2	1341.636	-0.4026	0.1074	-3.7471	0.0002	0.0199
MAGT1	5500.203	0.4634	0.1235	3.7509	0.0002	0.0199
MAN1A2	6429.679	0.3107	0.0941	3.3029	0.001	0.0426
MAN2A1	8285.93	0.984	0.241	4.0828	0	0.013
MANBA	4460.731	0.6957	0.1991	3.4937	0.0005	0.0302
MAP3K15	316.4611	0.5917	0.1657	3.5721	0.0004	0.0279
MED31	610.4451	-0.3774	0.1163	-3.2462	0.0012	0.0463
MESDC2	4584.407	0.3255	0.0909	3.5828	0.0003	0.0271
METTL10	960.2092	-0.3818	0.099	-3.8554	0.0001	0.0175
METTL17	642.2856	-0.3604	0.1012	-3.5607	0.0004	0.028
MFSD1	20364.69	0.5407	0.1542	3.5069	0.0005	0.0298
MGAT2	5369.618	0.3587	0.1	3.5881	0.0003	0.0269
MGAT4A	3240.102	0.5317	0.1527	3.4814	0.0005	0.0302
MIA3	5095.23	0.4318	0.1072	4.0295	0.0001	0.0152
MMP14	7945.334	0.6584	0.2003	3.2876	0.001	0.0437
MRGBP	549.8911	-0.2987	0.0935	-3.1964	0.0014	0.0495

Table 5. Experiment 1 astrocyte differential gene expression

Gene	Base mean	Fold change (log$_2$)	Lfcse	Stat	p-value	Adjusted p-value
MRPS33	2649.029	-0.3677	0.1153	-3.1899	0.0014	0.0495
MTCP1	311.8406	-0.4286	0.134	-3.1998	0.0014	0.0495
MTFMT	595.4192	-0.3666	0.0995	-3.6839	0.0002	0.0224
MTIF3	655.3098	-0.2924	0.0851	-3.435	0.0006	0.0336
NAE1	2024.557	-0.2724	0.0835	-3.2629	0.0011	0.045
NAGPA	3508.316	0.4979	0.1469	3.3897	0.0007	0.0367
NCLN	5196.686	0.3544	0.1006	3.5223	0.0004	0.0294
NCOR2	8393.79	0.4895	0.1443	3.3917	0.0007	0.0367
NCSTN	10341.39	0.421	0.1184	3.5551	0.0004	0.028
NIN	3647.378	0.5307	0.1277	4.1553	0	0.012
NIPA2	4946.151	0.3115	0.092	3.3844	0.0007	0.0367
NLRP3	4574.967	1.0899	0.2572	4.2379	0	0.0109
NPRL2	715.6184	-0.3113	0.0905	-3.4377	0.0006	0.0334
NRP1	21438.17	0.8646	0.1772	4.878	0	0.0034
NRP2	15104.98	0.7894	0.2275	3.4706	0.0005	0.0306
NRROS	12552.96	0.8931	0.2658	3.3596	0.0008	0.0376
NUCB1	12918.29	0.4492	0.1312	3.4241	0.0006	0.034
OSM	2739.486	1.753	0.4372	4.0096	0.0001	0.0152
OSTM1	5618.707	0.3419	0.1072	3.1901	0.0014	0.0495
OTUB1	4481.877	-0.2309	0.0633	-3.6461	0.0003	0.0241
P4HB	36182.08	0.5432	0.1321	4.1111	0	0.0124
PAGR1A	1422.095	-0.5559	0.1428	-3.8934	0.0001	0.0173
PCGF1	287.4089	-0.3889	0.1151	-3.3779	0.0007	0.0371
PDIA3	48632.65	0.4068	0.1249	3.256	0.0011	0.0455
PEF1	2431.798	-0.2495	0.0649	-3.8432	0.0001	0.0178
PELP1	2692.532	0.2592	0.0812	3.1921	0.0014	0.0495
PGAP3	307.4509	0.498	0.1153	4.3197	0	0.0094
PIGK	3666.926	0.3749	0.1172	3.1978	0.0014	0.0495
PIGN	3716.082	0.4244	0.1146	3.7041	0.0002	0.0215
PIGS	5057.106	0.3242	0.1012	3.2039	0.0014	0.0492
PIGT	8942.47	0.3408	0.1008	3.3817	0.0007	0.0367
PIGU	2159.139	0.3387	0.1026	3.3027	0.001	0.0426
PIK3R6	640.2297	0.8153	0.2336	3.4896	0.0005	0.0302
PIN4	930.7954	-0.4076	0.1211	-3.3651	0.0008	0.0375
PLOD1	11968.77	0.7851	0.1657	4.7392	0	0.0041
POFUT1	2835.486	0.3434	0.0883	3.8887	0.0001	0.0173
POFUT2	4048.77	0.3543	0.0866	4.0915	0	0.013
POLR1C	1527.871	-0.2688	0.0803	-3.3484	0.0008	0.0387
PPIL2	3733.749	-0.2102	0.0644	-3.2659	0.0011	0.0446

Table 5. Experiment 1 astrocyte differential gene expression

Gene	Base mean	Fold change (log$_2$)	Lfcse	Stat	p-value	Adjusted p-value
PRKCSH	6513.871	0.4808	0.1042	4.6133	0	0.0055
PROKR1	213.2612	0.6461	0.191	3.3828	0.0007	0.0367
PRSS36	163.599	-0.4516	0.1359	-3.3219	0.0009	0.0407
PSD4	2735.632	0.5863	0.1733	3.3826	0.0007	0.0367
PSEN1	5850.226	0.341	0.0951	3.5848	0.0003	0.0271
PTBP3	18674.18	0.437	0.1097	3.9828	0.0001	0.0154
PTPRC	10185.11	0.9065	0.2155	4.2062	0	0.0113
PUS3	567.4557	-0.3629	0.1136	-3.1943	0.0014	0.0495
QPCTL	920.8176	0.2812	0.0829	3.3931	0.0007	0.0367
QSOX1	3086.738	0.5552	0.148	3.7523	0.0002	0.0199
RAP2A	13356.74	0.3054	0.0908	3.3645	0.0008	0.0375
RBM48	419.9354	-0.3427	0.0983	-3.4854	0.0005	0.0302
REEP3	10627.55	0.5032	0.1529	3.2908	0.001	0.0434
REL	980.9194	0.8689	0.2482	3.5003	0.0005	0.0299
RGS1	7701.269	1.8377	0.4697	3.9127	0.0001	0.0172
RNF113A2	547.5429	-0.4368	0.128	-3.4111	0.0006	0.035
RNF149	5370.134	0.5457	0.1311	4.1626	0	0.012
RPN1	14886.6	0.5032	0.1428	3.5238	0.0004	0.0294
RRBP1	15760.78	0.4892	0.1305	3.7493	0.0002	0.0199
SCFD2	694.3512	-0.2418	0.074	-3.2658	0.0011	0.0446
SCNM1	1156.713	-0.3953	0.1166	-3.389	0.0007	0.0367
SCUBE1	323.346	1.8724	0.5169	3.6225	0.0003	0.025
SEC61A1	12593.95	0.4306	0.1126	3.8234	0.0001	0.0181
SELT	15910.02	0.2542	0.0711	3.5776	0.0003	0.0275
SEPN1	5584.832	0.3949	0.094	4.203	0	0.0113
SH3GLB2	2354.215	-0.2099	0.0563	-3.7282	0.0002	0.0202
SHISA5	8331.439	0.402	0.1153	3.4859	0.0005	0.0302
SKP1A	16355.09	-0.3139	0.0927	-3.3878	0.0007	0.0367
SLC16A10	3935.105	0.9064	0.2694	3.3638	0.0008	0.0375
SLC16A6	2398.814	0.5642	0.1609	3.5055	0.0005	0.0298
SLC20A2	2315.617	0.3727	0.0978	3.8127	0.0001	0.0181
SLC27A4	2544.628	0.2537	0.0755	3.3581	0.0008	0.0376
SLC29A1	2653.751	0.7363	0.1835	4.0117	0.0001	0.0152
SLC30A7	2964.695	0.4033	0.108	3.733	0.0002	0.02
SLC35C1	1973.678	0.3348	0.0963	3.4788	0.0005	0.0304
SLC35E1	4689.348	0.4362	0.1205	3.6191	0.0003	0.0252
SLC38A1	16627.57	0.4675	0.1387	3.3695	0.0008	0.0375
SLC38A10	11091.78	0.4208	0.1137	3.7009	0.0002	0.0216
SLC39A7	7170.347	0.3955	0.0968	4.0858	0	0.013

Table 5. Experiment 1 astrocyte differential gene expression

Gene	Base mean	Fold change (log$_2$)	Lfcse	Stat	p-value	Adjusted p-value
SLC7A8	11644.68	0.7271	0.1766	4.1175	0	0.0124
SLC9A6	1969.346	0.2992	0.0859	3.4823	0.0005	0.0302
SMIM11	1006.976	-0.3447	0.1068	-3.2266	0.0013	0.0483
SNHG3	503.1507	-0.532	0.1591	-3.3439	0.0008	0.0387
SNW1	5752.968	-0.169	0.0482	-3.5071	0.0005	0.0298
SNX1	7620.871	-0.2091	0.0637	-3.2833	0.001	0.0438
SP3	6227.712	0.2062	0.047	4.3906	0	0.0078
SPAG7	2411.116	-0.3085	0.0741	-4.1645	0	0.012
SPPL2A	8643.653	0.3622	0.1117	3.2421	0.0012	0.0466
SPTLC1	3468.398	0.3826	0.1054	3.6318	0.0003	0.0246
SPTLC2	5668.586	0.3589	0.1117	3.2148	0.0013	0.049
SRI	6607.079	-0.2311	0.0687	-3.3654	0.0008	0.0375
SRPR	6653.627	0.3343	0.101	3.3103	0.0009	0.0419
SSBP1	1501.318	-0.4168	0.1073	-3.8845	0.0001	0.0173
SSR1	13524.05	0.5052	0.1377	3.6693	0.0002	0.023
SSR3	21787.28	0.336	0.0866	3.8786	0.0001	0.0174
STK11	3820.487	-0.1985	0.0611	-3.2501	0.0012	0.0458
STT3A	11701.76	0.495	0.1263	3.9192	0.0001	0.017
SUDS3	4986.608	-0.1995	0.0569	-3.504	0.0005	0.0298
SUMO1	5342.998	-0.2905	0.0905	-3.2089	0.0013	0.049
SURF4	14765.49	0.4535	0.1011	4.4876	0	0.0072
SUSD1	896.6106	0.64	0.1918	3.3372	0.0008	0.039
SYF2	3528.691	-0.2387	0.0675	-3.5345	0.0004	0.0292
SYPL	8472.742	0.3041	0.0936	3.2504	0.0012	0.0458
TAGAP1	492.3484	-0.4524	0.1315	-3.4395	0.0006	0.0334
TGFB1	8369.635	0.6034	0.1631	3.6986	0.0002	0.0217
TGFBI	8673.343	1.0345	0.287	3.6047	0.0003	0.0261
TGFBR2	16001.84	0.5502	0.1632	3.3718	0.0007	0.0373
TLR13	14753	0.8835	0.2712	3.2571	0.0011	0.0455
TLR2	20841.62	0.9854	0.3071	3.2087	0.0013	0.049
TM9SF2	12249.12	0.4823	0.1103	4.3725	0	0.0078
TM9SF4	5997.882	0.3939	0.1125	3.5022	0.0005	0.0298
TMED5	6579.794	0.3991	0.1134	3.5195	0.0004	0.0294
TMED7	11970.08	0.3397	0.0866	3.9224	0.0001	0.017
TMED9	9185.515	0.3538	0.0963	3.6725	0.0002	0.023
TMEM104	5814.546	0.6047	0.1743	3.4697	0.0005	0.0306
TMEM131	5680.992	0.418	0.13	3.2158	0.0013	0.049
TMEM132A	1846.728	0.559	0.1466	3.8121	0.0001	0.0181
TMEM164	5159.286	0.3324	0.0935	3.5565	0.0004	0.028

Table 5. Experiment 1 astrocyte differential gene expression

Gene	Base mean	Fold change (log$_2$)	Lfcse	Stat	p-value	Adjusted p-value
TMEM19	3011.849	0.3331	0.0831	4.0065	0.0001	0.0152
TMEM2	2768.403	0.6281	0.1834	3.4245	0.0006	0.034
TMEM30A	12706	0.3364	0.0803	4.19	0	0.0113
TMEM57	2668.674	0.3358	0.0851	3.9436	0.0001	0.0166
TMEM64	3149	0.5357	0.1522	3.5202	0.0004	0.0294
TMEM68	1846.48	0.3147	0.0711	4.4237	0	0.0072
TMX3	6415.346	0.3752	0.0982	3.8206	0.0001	0.0181
TNF	2685.478	1.4428	0.341	4.2307	0	0.0109
TNKS2	14357.72	0.3336	0.0993	3.3587	0.0008	0.0376
TPST2	2584.03	0.3235	0.0839	3.8558	0.0001	0.0175
TRAM1	9466.617	0.3325	0.0973	3.4161	0.0006	0.0346
TRAPPC2	973.6465	-0.3002	0.0765	-3.925	0.0001	0.017
TRMU	463.9333	-0.3944	0.1055	-3.7385	0.0002	0.0199
TTC13	2953.259	0.3059	0.0932	3.2816	0.001	0.0438
TTYH3	16065.18	0.5298	0.1571	3.3721	0.0007	0.0373
TWSG1	5048.738	0.5117	0.1137	4.5015	0	0.0072
TXNDC11	1764.228	0.3478	0.0969	3.5884	0.0003	0.0269
TXNL4B	553.3604	-0.3406	0.0978	-3.4839	0.0005	0.0302
UBE2D1	1866.279	-0.3456	0.1019	-3.3901	0.0007	0.0367
UGGT1	7733.067	0.64	0.1442	4.4394	0	0.0072
UGT1A7C	1764.872	0.7477	0.2239	3.3396	0.0008	0.0389
UTP11L	1867.103	-0.3373	0.0844	-3.9945	0.0001	0.0154
VMP1	5199.738	-0.6321	0.1419	-4.4534	0	0.0072
VPS45	1440.364	-0.2842	0.0782	-3.6335	0.0003	0.0246
VPS4A	3608.722	-0.1682	0.0436	-3.8547	0.0001	0.0175
WBP1L	5235.345	0.2787	0.0724	3.8495	0.0001	0.0175
WDFY4	5028.03	0.7778	0.2403	3.237	0.0012	0.047
XRCC4	755.597	-0.3033	0.0646	-4.6974	0	0.0041
XXYLT1	1692.086	0.4572	0.1106	4.1329	0	0.0124
XYLT2	2935.113	0.7188	0.1401	5.1315	0	0.0012
ZBTB25	543.4528	-0.275	0.0782	-3.5165	0.0004	0.0294
ZBTB8OS	1140.782	-0.335	0.0982	-3.4119	0.0006	0.035
ZDHHC20	6570.417	0.4712	0.1171	4.0226	0.0001	0.0152
ZDHHC7	2457.302	0.2314	0.0653	3.544	0.0004	0.0286
ZFP330	1910.027	-0.2463	0.0732	-3.3626	0.0008	0.0376
ZFP386	1470.418	-0.3234	0.0932	-3.4689	0.0005	0.0306
ZFP706	8249.081	-0.1659	0.0466	-3.5643	0.0004	0.028
ZFP94	169.5686	-0.6248	0.1686	-3.7065	0.0002	0.0215
ZFYVE19	966.4367	-0.2197	0.0606	-3.623	0.0003	0.025

Table 5. Experiment 1 astrocyte differential gene expression

Gene	Base mean	Fold change (log$_2$)	Lfcse	Stat	p-value	Adjusted p-value
42800	7872.051	0.4196	0.128	3.2775	0.001	0.0439
0610009B22RIK	895.9714	-0.5822	0.1536	-3.7903	0.0002	0.0186
1110012L19RIK	775.7164	-0.3949	0.1032	-3.8264	0.0001	0.0181
1110034G24RIK	275.4704	-0.5444	0.1447	-3.763	0.0002	0.0199
1110059G10RIK	891.831	-0.4886	0.1303	-3.7496	0.0002	0.0199
1190007I07RIK	227.7795	-0.4425	0.138	-3.206	0.0013	0.049
2510039O18RIK	4894.173	0.3569	0.0877	4.0718	0	0.0134
2610306M01RIK	180.2548	-0.6463	0.1774	-3.6437	0.0003	0.0242
2700089E24RIK	3287.711	-0.2679	0.0836	-3.2062	0.0013	0.049
2810008D09RIK	279.8897	-1.0949	0.2506	-4.3694	0	0.0078
3830406C13RIK	1653.929	-0.3361	0.0953	-3.5261	0.0004	0.0294
4930486L24RIK	165.288	0.8332	0.2098	3.9715	0.0001	0.0158
9330151L19RIK	217.7894	-0.862	0.194	-4.4441	0	0.0072
9530068E07RIK	16125.63	0.353	0.0931	3.7903	0.0002	0.0186

Table 6. Experiment 1 Microglia Differential Gene Expression

Gene	Base mean	Fold change (log$_2$)	Lfcse	Stat	p-value	Adjusted p-value
A730017C20RIK	73.0021	2.4393	0.5876	4.1512	0	0.0097
ABLIM1	3743.775	1.3256	0.3745	3.5399	0.0004	0.0412
ACE2	125.0611	3.6259	0.7301	4.9662	0	0.0014
ADAMTS14	342.6756	1.239	0.3253	3.8084	0.0001	0.0228
ADCY1	1073.887	1.4615	0.3905	3.7428	0.0002	0.0271
ADRB1	863.2682	1.0133	0.249	4.0704	0	0.0118
ALDH1A2	1173.402	2.7949	0.6767	4.1302	0	0.0101
ALDH1A7	46.8158	3.4469	0.9661	3.5678	0.0004	0.0392
ANGPT1	1463.155	2.0042	0.561	3.5724	0.0004	0.0388
AP3B2	418.1542	1.3198	0.3812	3.4623	0.0005	0.0479
ARMC5	2066.559	0.3121	0.0715	4.3628	0	0.0062
BACE2	3868.033	1.7252	0.4666	3.6974	0.0002	0.0295
BC031361	143.995	1.0786	0.2864	3.7656	0.0002	0.0259
BC064078	836.2855	1.485	0.3879	3.8282	0.0001	0.0219
BHLHE22	26.841	2.4867	0.7162	3.4723	0.0005	0.0475
BICC1	1583.676	1.7668	0.4277	4.1306	0	0.0101
BMP6	3613.874	1.5421	0.4049	3.8087	0.0001	0.0228
CACNA1E	84.031	2.371	0.6477	3.6607	0.0003	0.0313
CACNA2D1	713.522	1.4391	0.3084	4.667	0	0.0028
CAMK4	314.8504	1.2966	0.3493	3.7117	0.0002	0.0288
CAMKV	33.3433	4.7324	0.8144	5.8105	0	0.0001
CCDC80	3533.582	1.9989	0.4335	4.6108	0	0.003
CCDC85A	453.6419	1.4551	0.3972	3.663	0.0002	0.0312
CD200	1725.909	1.3493	0.3877	3.4801	0.0005	0.0467
CDH23	29.1038	0.9503	0.269	3.5329	0.0004	0.042
CDH4	1414.445	1.2305	0.3526	3.4898	0.0005	0.0458
CDK5R2	9.4923	2.7579	0.7234	3.8126	0.0001	0.0228
CHST8	34.784	4.1442	0.9803	4.2275	0	0.008
CNKSR2	68.5533	1.6299	0.4669	3.4911	0.0005	0.0458
COL12A1	7295.101	1.7611	0.4582	3.8432	0.0001	0.0209
COL22A1	513.6226	2.423	0.5553	4.3634	0	0.0062
COL26A1	527.9782	2.6675	0.5678	4.6976	0	0.0027
COL4A1	17129.36	2.1169	0.4823	4.3894	0	0.0061
COL4A2	9102.346	2.0022	0.4842	4.1351	0	0.0101
COL4A6	5300.096	1.8328	0.4487	4.0842	0	0.0113
COL5A1	4609.233	1.6091	0.4599	3.499	0.0005	0.0452
COL6A3	905.7634	2.4516	0.5791	4.2335	0	0.008

Table 6. Experiment 1 Microglia Differential Gene Expression

Gene	Base mean	Fold change (log$_2$)	Lfcse	Stat	p-value	Adjusted p-value
CRTAC1	65.4142	1.9043	0.5231	3.6404	0.0003	0.0326
CYBRD1	5355.732	1.8173	0.5096	3.5662	0.0004	0.0392
DAB1	1427.766	1.2953	0.3403	3.8069	0.0001	0.0228
DBPHT2	63.6344	2.0597	0.5793	3.5556	0.0004	0.0399
DDN	37.4809	1.8147	0.515	3.5238	0.0004	0.0429
DENND5B	550.3831	0.6637	0.1774	3.7425	0.0002	0.0271
DIO2	393.1914	2.4419	0.5804	4.2073	0	0.0084
DUSP8	791.159	1.2719	0.343	3.7077	0.0002	0.0288
EDA	179.3621	1.5301	0.3979	3.8453	0.0001	0.0209
EFNA5	639.1167	1.7303	0.3556	4.8653	0	0.0019
EGFR	1100.873	1.8237	0.3994	4.5664	0	0.0033
F3	7337.277	1.249	0.3387	3.6876	0.0002	0.0302
FADS3	1402.469	0.6138	0.1653	3.7127	0.0002	0.0288
FAIM2	58.2132	2.3503	0.637	3.6897	0.0002	0.0302
FAM167A	3059.392	1.407	0.3381	4.162	0	0.0096
FAM189B	646.888	0.6988	0.153	4.5687	0	0.0033
FAM26E	424.2522	1.3924	0.4001	3.4799	0.0005	0.0467
FBLN7	752.5122	1.6441	0.4553	3.611	0.0003	0.0351
FGF12	352.9938	1.5167	0.4382	3.4613	0.0005	0.0479
FGF7	170.4306	1.8167	0.5244	3.4645	0.0005	0.0479
FHDC1	1054.209	1.3042	0.3468	3.7604	0.0002	0.0259
FNDC1	381.6169	2.2269	0.5596	3.9794	0.0001	0.0154
FOXF2	132.2251	2.8214	0.6298	4.4802	0	0.0046
FRMD6	2981.72	0.7892	0.212	3.7232	0.0002	0.028
GLI1	511.8623	1.611	0.4287	3.758	0.0002	0.0259
GM12992	77.1153	0.7027	0.1886	3.7268	0.0002	0.028
GM15698	7563.887	1.8977	0.5158	3.6788	0.0002	0.031
GM17359	50.6792	1.5755	0.3756	4.1941	0	0.0088
GM2027	6.5144	2.6555	0.7655	3.4689	0.0005	0.0478
GM4532	13.0828	-1.4243	0.3982	-3.5772	0.0003	0.0386
GM5124	15.7992	1.9001	0.5001	3.7994	0.0001	0.0232
GPR115	5.0011	3.0438	0.8302	3.6662	0.0002	0.0312
GPR123	1009.71	2.21	0.462	4.7835	0	0.0024
GPR153	348.9549	1.5166	0.4234	3.5824	0.0003	0.0383
GPR173	459.5778	1.3409	0.3697	3.6265	0.0003	0.0334
GREM2	14.813	4.4003	1.0705	4.1103	0	0.0108
GRIN1	51.0595	2.118	0.4872	4.3477	0	0.0062
GULP1	1445.241	1.3358	0.3636	3.6734	0.0002	0.0312
HAPLN1	145.9553	3.3711	0.6302	5.3493	0	0.0005

Table 6. Experiment 1 Microglia Differential Gene Expression

Gene	Base mean	Fold change (log$_2$)	Lfcse	Stat	p-value	Adjusted p-value
HECW1	4.0287	4.3915	1.0389	4.2272	0	0.008
HIC1	397.7564	1.8703	0.5153	3.6293	0.0003	0.0333
HPCAL4	137.7397	2.461	0.6885	3.5743	0.0004	0.0388
ID2	13952.38	0.847	0.2269	3.7323	0.0002	0.028
IGFBP3	14309.82	1.3288	0.3534	3.76	0.0002	0.0259
IGFBP5	108788.4	1.5185	0.4174	3.6376	0.0003	0.0327
IGFBP7	1673.65	2.4178	0.4908	4.9263	0	0.0016
IGSF1	1511.518	2.1669	0.5554	3.9014	0.0001	0.0185
INMT	530.03	3.0929	0.7407	4.1758	0	0.0093
IP6K3	7.6019	2.4873	0.7069	3.5184	0.0004	0.0431
ITIH3	3789.471	2.1965	0.4675	4.6983	0	0.0027
ITIH5	5848.005	2.1224	0.5328	3.9832	0.0001	0.0154
JPH2	350.3937	1.68	0.4095	4.1029	0	0.011
KANK4	650.0364	2.5025	0.4743	5.2765	0	0.0005
KCNE1L	769.3375	2.3287	0.5429	4.2896	0	0.0072
KCNF1	159.135	1.7872	0.5119	3.4911	0.0005	0.0458
KCNK2	3606.003	1.474	0.4163	3.5408	0.0004	0.0412
KCNK7	27.1935	1.4609	0.3308	4.4165	0	0.0056
KCNS1	124.2714	2.7718	0.7442	3.7244	0.0002	0.028
LAMA2	1052.258	2.1097	0.4457	4.7335	0	0.0026
LHFP	4927.776	1.5246	0.3863	3.9471	0.0001	0.0169
LMO7	319.6524	1.7141	0.3702	4.6298	0	0.0029
LMOD1	1682.484	1.9051	0.4069	4.6817	0	0.0028
LTBP2	2521.688	1.8347	0.471	3.8957	0.0001	0.0188
LUM	774.5171	2.9597	0.6558	4.5131	0	0.0041
MAL2	281.4064	1.6398	0.4581	3.5798	0.0003	0.0385
MATN4	101.4181	3.3148	0.7219	4.592	0	0.0032
MEDAG	295.0378	2.0529	0.5307	3.868	0.0001	0.0201
MEG3	8219.089	1.8175	0.4438	4.0949	0	0.0111
MEGF10	1784.407	2.0407	0.4747	4.299	0	0.0072
MFAP2	757.3667	1.4198	0.4059	3.4974	0.0005	0.0452
MFAP4	605.2943	2.4484	0.5626	4.3517	0	0.0062
MFAP5	75.2295	3.0096	0.7667	3.9256	0.0001	0.0174
MFSD2A	2798.267	1.8943	0.4953	3.8244	0.0001	0.0221
MME	1437.59	1.8741	0.4307	4.3515	0	0.0062
MPPED1	15.2467	3.0099	0.7564	3.9794	0.0001	0.0154
NDP	575.1154	2.2861	0.5745	3.9793	0.0001	0.0154
NECAB1	19.1154	3.4042	0.7944	4.285	0	0.0072
NID1	5254.111	1.9638	0.53	3.705	0.0002	0.0289

Table 6. Experiment 1 Microglia Differential Gene Expression

Gene	Base mean	Fold change (log$_2$)	Lfcse	Stat	p-value	Adjusted p-value
NPAS4	360.8875	2.4508	0.4824	5.0802	0	0.0009
NPPC	202.085	2.9561	0.5346	5.5296	0	0.0003
NPTX2	67.2354	1.9961	0.5482	3.641	0.0003	0.0326
NPVF	672.9517	2.798	0.6884	4.0645	0	0.0118
NPY1R	235.8728	3.0075	0.866	3.4728	0.0005	0.0475
NRGN	14.3936	2.6798	0.7303	3.6692	0.0002	0.0312
NTM	460.9907	1.9355	0.5312	3.6438	0.0003	0.0326
NTN4	2999.298	1.4727	0.4172	3.5298	0.0004	0.0423
NTNG1	116.8852	1.811	0.5154	3.5136	0.0004	0.0433
OGN	5942.034	1.8519	0.4292	4.315	0	0.007
PAK6	289.0081	1.4641	0.4039	3.6253	0.0003	0.0334
PCDH1	553.0089	1.0854	0.3089	3.5141	0.0004	0.0433
PDE1A	897.0164	1.6789	0.4568	3.6752	0.0002	0.0312
PDGFRB	1975.468	1.7586	0.3775	4.6582	0	0.0028
PI15	529.5914	2.7179	0.7067	3.8461	0.0001	0.0209
PIPOX	1848.177	1.7458	0.4414	3.9549	0.0001	0.0167
PLAGL1	3735.54	1.7658	0.3394	5.2028	0	0.0006
PLAT	5775.338	1.7744	0.4488	3.9535	0.0001	0.0167
PRKD1	1082.668	1.5227	0.3609	4.2196	0	0.0082
PROM1	3218.514	1.9088	0.4475	4.2651	0	0.0076
PRRT1	128.6237	1.5306	0.4058	3.7715	0.0002	0.0258
PRSS12	81.3551	2.2701	0.6023	3.7688	0.0002	0.0258
PTCH2	94.411	1.7266	0.4814	3.5868	0.0003	0.0379
PTPN13	3659.421	1.452	0.3964	3.6631	0.0002	0.0312
PTPRD	1356.39	1.1504	0.3085	3.7285	0.0002	0.028
RAB40C	1836.967	0.3117	0.0804	3.8793	0.0001	0.0198
RADIL	304.4651	1.4409	0.4061	3.5486	0.0004	0.0403
RASGEF1B	5144.28	0.8031	0.2263	3.5491	0.0004	0.0403
RASGEF1C	98.3201	2.1637	0.554	3.9054	0.0001	0.0184
RBM24	436.4542	1.8386	0.5013	3.6676	0.0002	0.0312
RBMS3	1011.575	1.3152	0.3168	4.1509	0	0.0097
RHOB	29397.12	0.7138	0.1712	4.1707	0	0.0094
RIAN	4132.306	1.4999	0.3816	3.9306	0.0001	0.0174
RND3	4150.046	1.3451	0.3158	4.2587	0	0.0076
RYR2	60.0668	2.5052	0.6157	4.0688	0	0.0118
SAMD5	560.3396	1.6204	0.4117	3.9357	0.0001	0.0173
SCG3	10611.28	1.533	0.4433	3.4583	0.0005	0.0482
SCHIP1	212.4639	2.4022	0.4627	5.1922	0	0.0006
SCN2A1	155.519	2.2688	0.4768	4.7583	0	0.0025

Table 6. Experiment 1 Microglia Differential Gene Expression

Gene	Base mean	Fold change (log$_2$)	Lfcse	Stat	p-value	Adjusted p-value
SCN2B	55.3216	2.0877	0.5316	3.9268	0.0001	0.0174
SEMA3C	2350.5	1.7006	0.4403	3.8627	0.0001	0.0203
SGIP1	747.9939	1.3553	0.3887	3.4868	0.0005	0.046
SH2D5	28.1419	1.0218	0.2875	3.5548	0.0004	0.0399
SH3RF2	106.1537	2.5558	0.5955	4.2916	0	0.0072
SH3RF3	230.5073	1.7665	0.4506	3.9199	0.0001	0.0176
SLC12A8	180.874	1.8909	0.4881	3.874	0.0001	0.02
SLC26A8	30.7562	1.5972	0.4151	3.8478	0.0001	0.0209
SLC44A3	85.0588	2.3914	0.5844	4.0919	0	0.0111
SLC6A11	288.2325	2.7971	0.7692	3.6361	0.0003	0.0327
SLCO1A5	860.0803	2.4542	0.5133	4.7813	0	0.0024
SNPH	677.4294	1.694	0.484	3.5002	0.0005	0.0452
SPARC	98824.16	1.3061	0.3771	3.4637	0.0005	0.0479
SPATA33	118.2393	1.8868	0.5445	3.465	0.0005	0.0479
SPHKAP	28.5643	2.4048	0.6216	3.8685	0.0001	0.0201
SPRN	6.8803	3.1424	0.892	3.5229	0.0004	0.0429
SSTR2	437.354	1.8371	0.5329	3.4475	0.0006	0.0499
SUCNR1	279.6469	1.8587	0.528	3.5201	0.0004	0.043
SVEP1	335.2602	2.5874	0.6975	3.7096	0.0002	0.0288
SYNPO	2929.554	1.3996	0.3299	4.2422	0	0.008
SYNPO2	1740.815	1.6004	0.4494	3.5611	0.0004	0.0397
TAGLN3	525.0871	1.9767	0.5417	3.6494	0.0003	0.0322
TENM3	3389.799	1.8332	0.41	4.4718	0	0.0046
THY1	1068.467	2.3795	0.5128	4.6406	0	0.0029
TMEM179	26.5128	2.4349	0.6097	3.9939	0.0001	0.0153
TMEM200A	630.7292	1.9441	0.4448	4.3707	0	0.0062
TMEM59L	32.472	2.897	0.6798	4.2618	0	0.0076
TRANK1	23.8336	2.5346	0.6275	4.0391	0.0001	0.0128
TSHR	403.0675	2.6772	0.6052	4.4234	0	0.0056
UNC13C	15.0141	4.0948	1.0124	4.0445	0.0001	0.0127
WFIKKN1	170.5624	1.0498	0.287	3.6586	0.0003	0.0313
WISP1	314.8719	2.1519	0.5574	3.8604	0.0001	0.0203
WNT10B	5.0584	3.8566	1.0749	3.5879	0.0003	0.0379
WSCD2	397.5781	1.29	0.3278	3.9348	0.0001	0.0173
ZFAND5	11274.92	0.4155	0.1168	3.5584	0.0004	0.0399

Table 7. Experiment 2 Astrocyte Differential Gene Expression

Gene	Base mean	Fold change (log$_2$)	Lfcse	Stat	p-value	Adjusted p-value
ADAMTSL4	2538.0	-0.2108	0.0589	-3.5787	0.0003	0.0415
AGRN	17294.6	-0.1554	0.0421	-3.6928	0.0002	0.0303
AKR1C14	10696.2	-0.2663	0.0683	-3.8996	0.0001	0.0223
AKTIP	6115.7	-0.2078	0.0599	-3.4682	0.0005	0.0491
ALX3	141.3	0.5246	0.1439	3.6458	0.0003	0.0352
APLP2	31875.3	-0.1221	0.0293	-4.1670	0.0000	0.0130
ARL8A	14719.7	-0.1581	0.0385	-4.1106	0.0000	0.0154
ATXN10	12340.1	-0.0679	0.0174	-3.9065	0.0001	0.0220
BC064078	1416.6	-0.3596	0.1041	-3.4544	0.0006	0.0492
BICC1	3089.1	0.2460	0.0643	3.8242	0.0001	0.0236
BOK	434.8	0.3643	0.0982	3.7094	0.0002	0.0286
BSN	179.3	0.3669	0.1040	3.5294	0.0004	0.0431
CACNA1B	77.4	0.5112	0.1178	4.3391	0.0000	0.0095
CACNA1C	914.7	0.4540	0.1214	3.7388	0.0002	0.0284
CACNG7	2441.4	-0.1693	0.0421	-4.0216	0.0001	0.0184
CACNG8	433.8	-0.2442	0.0697	-3.5046	0.0005	0.0451
CAPS2	275.7	-0.3205	0.0903	-3.5498	0.0004	0.0426
CCDC126	394.2	-0.1658	0.0481	-3.4472	0.0006	0.0492
CCDC141	1506.8	-0.2253	0.0632	-3.5671	0.0004	0.0421
CD40	54.0	0.5085	0.1456	3.4921	0.0005	0.0464
CD81	32753.2	-0.1466	0.0363	-4.0377	0.0001	0.0176
CDH4	2923.0	-0.3445	0.0977	-3.5260	0.0004	0.0431
CDHR1	314.7	0.5312	0.1431	3.7127	0.0002	0.0286
CELSR3	164.7	0.4905	0.1423	3.4473	0.0006	0.0492
CERS4	4719.8	-0.2956	0.0635	-4.6542	0.0000	0.0043
CHAMP1	2360.5	-0.1189	0.0330	-3.6073	0.0003	0.0384
CHCHD1	1117.8	0.1670	0.0450	3.7116	0.0002	0.0286
CHIL1	1053.1	-0.4952	0.1433	-3.4565	0.0005	0.0492
CHMP5	5993.5	-0.1431	0.0414	-3.4550	0.0006	0.0492
CHST15	724.5	0.4786	0.1122	4.2640	0.0000	0.0110
CLEC4A1	123.7	0.5149	0.1416	3.6363	0.0003	0.0356
CLEC4A2	107.5	0.7710	0.1244	6.1958	0.0000	0.0000
CLEC4N	171.7	0.5154	0.1359	3.7923	0.0001	0.0246
CMKLR1	539.9	0.4286	0.0873	4.9097	0.0000	0.0020
CNTNAP2	612.2	-0.5059	0.1263	-4.0055	0.0001	0.0184
COBLL1	2102.6	-0.2700	0.0765	-3.5284	0.0004	0.0431
COL15A1	478.8	0.4973	0.1439	3.4546	0.0006	0.0492
COL23A1	482.1	0.5310	0.1309	4.0559	0.0000	0.0171
COL26A1	1013.6	0.5142	0.1335	3.8521	0.0001	0.0228

Table 7. Experiment 2 Astrocyte Differential Gene Expression

Gene	Base mean	Fold change (log$_2$)	Lfcse	Stat	p-value	Adjusted p-value
COL27A1	479.3	0.3712	0.0963	3.8536	0.0001	0.0228
COL4A3	446.3	-0.4538	0.1217	-3.7296	0.0002	0.0284
COL7A1	1928.3	0.5805	0.1455	3.9907	0.0001	0.0184
CPM	146.8	0.5113	0.1455	3.5141	0.0004	0.0444
CSNK1G1	1366.5	0.2024	0.0473	4.2764	0.0000	0.0110
CTSC	6152.1	0.3523	0.0882	3.9960	0.0001	0.0184
CYFIP2	4281.5	-0.2306	0.0564	-4.0893	0.0000	0.0157
CYTIP	42.6	0.5106	0.1445	3.5339	0.0004	0.0431
DEFB1	100.8	-0.6499	0.1440	-4.5145	0.0000	0.0071
DLX6OS1	269.8	0.5513	0.1434	3.8437	0.0001	0.0228
DUSP6	4744.9	-0.2355	0.0590	-3.9921	0.0001	0.0184
E130308A19RIK	601.0	0.1679	0.0428	3.9202	0.0001	0.0214
EFNA2	146.6	0.4061	0.1094	3.7108	0.0002	0.0286
EMILIN2	911.6	0.5495	0.1429	3.8450	0.0001	0.0228
EPAS1	5275.8	-0.3102	0.0620	-5.0017	0.0000	0.0020
EPDR1	5425.4	-0.0991	0.0279	-3.5519	0.0004	0.0426
EPHA7	519.6	0.4954	0.1345	3.6830	0.0002	0.0312
ESYT3	40.7	0.5641	0.1453	3.8826	0.0001	0.0227
FAM124A	2038.4	-0.2355	0.0571	-4.1248	0.0000	0.0148
FAM19A5	4434.7	-0.1890	0.0517	-3.6577	0.0003	0.0342
FGFR3	4699.6	-0.1688	0.0474	-3.5599	0.0004	0.0426
FGFRL1	9790.8	-0.3023	0.0694	-4.3529	0.0000	0.0095
FOXF2	218.7	0.5413	0.1450	3.7325	0.0002	0.0284
FRZB	155.6	0.5098	0.1454	3.5058	0.0005	0.0451
G6PC3	2092.0	-0.1180	0.0301	-3.9150	0.0001	0.0216
GAD2	81.3	0.5442	0.1423	3.8258	0.0001	0.0236
GALNT18	590.3	-0.3980	0.0954	-4.1722	0.0000	0.0130
GARNL3	638.8	-0.2059	0.0580	-3.5504	0.0004	0.0426
GLDC	4609.9	-0.3468	0.0865	-4.0114	0.0001	0.0184
GM15698	12532.5	0.4908	0.1150	4.2693	0.0000	0.0110
GM5803	18.5	0.4624	0.1282	3.6067	0.0003	0.0384
GNAO1	17281.1	-0.2914	0.0769	-3.7909	0.0002	0.0246
GNG11	362.0	0.5124	0.1328	3.8573	0.0001	0.0228
GPC6	6233.2	0.3637	0.1055	3.4473	0.0006	0.0492
GPD1	1071.3	-0.2818	0.0757	-3.7207	0.0002	0.0286
GPD2	4763.0	-0.2486	0.0648	-3.8380	0.0001	0.0228
GRIN2A	11.8	0.5877	0.1452	4.0465	0.0001	0.0173
GRINA	9790.2	-0.1974	0.0514	-3.8376	0.0001	0.0228
GSTM1	36668.6	-0.3687	0.0987	-3.7355	0.0002	0.0284

Table 7. Experiment 2 Astrocyte Differential Gene Expression

Gene	Base mean	Fold change (log$_2$)	Lfcse	Stat	p-value	Adjusted p-value
HIGD2A	2799.8	-0.1666	0.0479	-3.4764	0.0005	0.0486
IFNAR1	4812.4	0.1343	0.0379	3.5417	0.0004	0.0426
IGFBP5	226472.7	-0.3154	0.0903	-3.4930	0.0005	0.0464
IGLON5	1361.6	-0.1644	0.0455	-3.6121	0.0003	0.0382
IL1RN	142.5	0.4960	0.1437	3.4523	0.0006	0.0492
IRAK3	181.0	0.5474	0.1303	4.1998	0.0000	0.0126
JAKMIP3	124.9	-0.4445	0.1148	-3.8716	0.0001	0.0227
JAZF1	1645.1	-0.1930	0.0532	-3.6281	0.0003	0.0362
KANK1	4046.8	-0.2763	0.0797	-3.4675	0.0005	0.0491
KCNMB4	162.1	0.3742	0.1059	3.5328	0.0004	0.0431
KCNQ1OT1	93.4	0.4336	0.1224	3.5419	0.0004	0.0426
KCTD12	5405.9	0.3573	0.0807	4.4272	0.0000	0.0076
KDM4C	2162.0	-0.1187	0.0282	-4.2116	0.0000	0.0123
KIFC3	4200.3	-0.2007	0.0490	-4.0974	0.0000	0.0157
LAMB2	21107.1	-0.1640	0.0472	-3.4727	0.0005	0.0487
LAMC3	175.5	0.5670	0.1441	3.9335	0.0001	0.0206
LEF1	121.8	0.5127	0.1454	3.5271	0.0004	0.0431
LEPREL1	2358.9	-0.2864	0.0803	-3.5672	0.0004	0.0421
LRP10	7715.3	-0.1010	0.0260	-3.8815	0.0001	0.0227
MAN1B1	5441.2	-0.0606	0.0163	-3.7115	0.0002	0.0286
MBTD1	2287.8	0.1653	0.0389	4.2509	0.0000	0.0110
MDK	1080.0	0.4954	0.1395	3.5518	0.0004	0.0426
MEDAG	588.5	0.4339	0.0975	4.4522	0.0000	0.0071
MGAT4A	1015.1	0.2478	0.0618	4.0116	0.0001	0.0184
MRGPRF	123.6	0.5628	0.1412	3.9872	0.0001	0.0184
MSC	27.8	0.4991	0.1444	3.4555	0.0005	0.0492
MYL6B	542.5	-0.3410	0.0764	-4.4622	0.0000	0.0071
MYO1E	8312.6	-0.2066	0.0505	-4.0940	0.0000	0.0157
NACC2	22214.8	-0.2159	0.0558	-3.8692	0.0001	0.0227
NDUFA7	2877.9	-0.0991	0.0250	-3.9576	0.0001	0.0195
NDUFB2	1117.8	0.1495	0.0398	3.7530	0.0002	0.0271
NKX6-1	67.4	0.4883	0.1411	3.4594	0.0005	0.0492
NNMT	104.6	0.4927	0.1237	3.9833	0.0001	0.0184
NREP	5184.4	0.5528	0.1131	4.8883	0.0000	0.0020
PANX2	121.5	-0.4230	0.1199	-3.5292	0.0004	0.0431
PCDHGB2	493.3	-0.2881	0.0744	-3.8698	0.0001	0.0227
PCX	6520.2	-0.2591	0.0710	-3.6490	0.0003	0.0351
PDE4A	848.2	-0.3251	0.0892	-3.6441	0.0003	0.0352
PEA15A	196585.1	-0.2511	0.0663	-3.7893	0.0002	0.0246

Table 7. Experiment 2 Astrocyte Differential Gene Expression

Gene	Base mean	Fold change (log$_2$)	Lfcse	Stat	p-value	Adjusted p-value
PHLPP1	6378.6	-0.2590	0.0647	-4.0027	0.0001	0.0184
PLA1A	172.4	0.5006	0.1428	3.5055	0.0005	0.0451
PNLIP	9.4	-0.6958	0.1399	-4.9726	0.0000	0.0020
PPP2R2A	3913.3	-0.0797	0.0184	-4.3212	0.0000	0.0099
PRDM16	2783.1	-0.2847	0.0647	-4.3965	0.0000	0.0084
PRSS16	13.1	0.5189	0.1453	3.5706	0.0004	0.0421
PTN	10305.8	0.4129	0.0978	4.2217	0.0000	0.0121
RAB4A	1014.0	-0.1020	0.0292	-3.4940	0.0005	0.0464
RARRES1	124.5	0.4382	0.1243	3.5249	0.0004	0.0431
RASGRP2	175.1	-0.3719	0.1068	-3.4817	0.0005	0.0480
RBFOX1	81.3	0.5307	0.1413	3.7549	0.0002	0.0271
RBFOX2	4559.8	0.2638	0.0745	3.5418	0.0004	0.0426
REL	232.4	0.3591	0.0942	3.8129	0.0001	0.0239
RGS3	2422.6	-0.3820	0.1107	-3.4505	0.0006	0.0492
RNF141	1177.7	-0.1580	0.0420	-3.7594	0.0002	0.0271
ROBO1	1887.5	0.5103	0.1219	4.1855	0.0000	0.0129
RPL31-PS12	44.9	0.4148	0.1076	3.8536	0.0001	0.0228
SALL3	2132.3	-0.2193	0.0567	-3.8688	0.0001	0.0227
SAP18	2004.9	-0.1943	0.0494	-3.9344	0.0001	0.0206
SCAP	7705.7	-0.1274	0.0308	-4.1320	0.0000	0.0147
SEMA3F	1288.3	-0.3209	0.0882	-3.6396	0.0003	0.0355
SEMA6A	4697.9	0.1583	0.0458	3.4562	0.0005	0.0492
SH3BGR	153.8	-0.3012	0.0807	-3.7304	0.0002	0.0284
SKP1A	23642.2	-0.1850	0.0516	-3.5883	0.0003	0.0404
SLC26A1	48.4	-0.3820	0.0961	-3.9745	0.0001	0.0188
SLC30A7	2647.7	0.1568	0.0436	3.5946	0.0003	0.0399
SLC32A1	14.4	0.5455	0.1452	3.7583	0.0002	0.0271
SMIM4	382.0	-0.1992	0.0525	-3.7951	0.0001	0.0246
SNAP47	5834.3	-0.1601	0.0369	-4.3416	0.0000	0.0095
SNED1	663.1	0.4276	0.1202	3.5573	0.0004	0.0426
SNX33	3464.6	-0.2165	0.0567	-3.8197	0.0001	0.0236
SOCS2	637.1	0.3515	0.0983	3.5753	0.0003	0.0417
SORL1	10447.0	-0.3368	0.0882	-3.8184	0.0001	0.0236
SP2	1308.5	-0.1165	0.0302	-3.8548	0.0001	0.0228
SP9	115.4	0.5201	0.1450	3.5875	0.0003	0.0404
SPRY2	3582.5	-0.3162	0.0624	-5.0708	0.0000	0.0020
SPRY4	2025.5	-0.3680	0.0750	-4.9066	0.0000	0.0020
SRPK2	6690.9	-0.1612	0.0356	-4.5317	0.0000	0.0071
SRPX2	75.8	0.5605	0.1424	3.9355	0.0001	0.0206

Table 7. Experiment 2 Astrocyte Differential Gene Expression

Gene	Base mean	Fold change (log$_2$)	Lfcse	Stat	p-value	Adjusted p-value
SYNE3	257.7	0.4415	0.0983	4.4897	0.0000	0.0071
SYNPO2	3508.3	-0.1901	0.0512	-3.7143	0.0002	0.0286
TCEAL3	1988.7	-0.3411	0.0989	-3.4495	0.0006	0.0492
TECR	6406.3	-0.1113	0.0274	-4.0600	0.0000	0.0171
TENM2	31.4	0.6047	0.1422	4.2516	0.0000	0.0110
TGFBI	4078.8	0.4913	0.1414	3.4746	0.0005	0.0487
TMEM200B	52.3	0.6192	0.1454	4.2586	0.0000	0.0110
TMEM56	1951.4	-0.2445	0.0616	-3.9698	0.0001	0.0189
TMX2	5585.2	-0.0603	0.0170	-3.5534	0.0004	0.0426
TNFRSF19	2983.9	0.4133	0.1110	3.7241	0.0002	0.0286
TPRGL	6440.3	-0.1308	0.0337	-3.8764	0.0001	0.0227
TSPAN7	16870.1	-0.3066	0.0865	-3.5436	0.0004	0.0426
UNC13C	30.3	0.5732	0.1230	4.6586	0.0000	0.0043
VASH2	249.8	0.5535	0.1238	4.4723	0.0000	0.0071
VAV2	1312.1	0.1960	0.0504	3.8882	0.0001	0.0227
VEPH1	124.6	-0.3908	0.1027	-3.8041	0.0001	0.0242
VSTM2A	350.0	0.5980	0.1335	4.4801	0.0000	0.0071
WBP2	8936.0	-0.1475	0.0384	-3.8385	0.0001	0.0228
WNK4	185.5	0.5142	0.1451	3.5442	0.0004	0.0426
WNT4	490.4	0.6603	0.1406	4.6976	0.0000	0.0042
WNT6	36.5	0.5891	0.1453	4.0537	0.0001	0.0171
ZBTB8A	209.6	0.3039	0.0803	3.7819	0.0002	0.0251
ZC3HAV1L	304.7	0.4134	0.0872	4.7415	0.0000	0.0038
ZFP282	847.1	0.1945	0.0391	4.9754	0.0000	0.0020
ZFP536	154.1	0.5005	0.1197	4.1812	0.0000	0.0129
ZIC4	704.2	0.4792	0.1258	3.8100	0.0001	0.0239
2900026A02RIK	2962.6	-0.1480	0.0408	-3.6291	0.0003	0.0362
5430417L22RIK	2462.8	-0.1885	0.0536	-3.5149	0.0004	0.0444

Table 8. Experiment 2 Microglia Differential Gene Expression

Gene	Base mean	Fold change (log$_2$)	Lfcse	Stat	p-value	Adjusted p-value
A3GALT2	18.9	0.5820	0.1658	3.5106	0.0004	0.0271
ABCA7	2545.8	-0.2382	0.0648	-3.6781	0.0002	0.0200
ABCB7	2884.3	-0.2114	0.0493	-4.2841	0.0000	0.0043
ABHD17A	1884.6	0.1379	0.0335	4.1158	0.0000	0.0070
ACBD3	3949.3	-0.1982	0.0584	-3.3944	0.0007	0.0343
ACBD6	999.9	0.2136	0.0531	4.0245	0.0001	0.0086
ACTR8	987.0	-0.2850	0.0655	-4.3535	0.0000	0.0035
ADRB1	60.9	0.6680	0.1487	4.4922	0.0000	0.0024
AGGF1	2817.1	-0.0919	0.0259	-3.5547	0.0004	0.0249
AGL	1831.5	-0.1882	0.0418	-4.5056	0.0000	0.0024
AHCYL1	5504.4	-0.1490	0.0415	-3.5909	0.0003	0.0240
AHSA2	1219.0	-0.1856	0.0474	-3.9174	0.0001	0.0113
AI314180	4233.0	-0.1797	0.0380	-4.7270	0.0000	0.0012
AIFM1	1790.2	-0.1948	0.0604	-3.2265	0.0013	0.0475
AKT1S1	1465.0	0.1829	0.0509	3.5947	0.0003	0.0239
ALKBH6	552.3	0.2434	0.0500	4.8690	0.0000	0.0007
ANAPC4	2273.0	-0.1482	0.0462	-3.2108	0.0013	0.0491
ANKRD26	474.0	-0.3034	0.0929	-3.2648	0.0011	0.0445
ANXA3	16718.3	-0.2183	0.0436	-5.0045	0.0000	0.0007
AP2B1	9163.2	-0.1202	0.0303	-3.9635	0.0001	0.0100
APPL1	2157.1	-0.1848	0.0519	-3.5611	0.0004	0.0247
ARG2	136.4	0.4938	0.1305	3.7832	0.0002	0.0151
ARHGAP30	10050.0	-0.1900	0.0569	-3.3399	0.0008	0.0388
ARID5A	805.7	0.6736	0.1654	4.0714	0.0000	0.0079
ARMC5	1948.8	0.1711	0.0425	4.0315	0.0001	0.0085
ARX	139.8	0.5682	0.1589	3.5755	0.0003	0.0247
ASNS	901.8	0.5685	0.1663	3.4187	0.0006	0.0332
ATF4	15609.4	0.5663	0.1568	3.6106	0.0003	0.0234
ATF5	850.0	0.3319	0.0917	3.6207	0.0003	0.0226
ATM	1270.0	-0.3023	0.0841	-3.5950	0.0003	0.0239
ATP11B	2630.8	-0.1929	0.0319	-6.0579	0.0000	0.0000
ATP2C1	5053.2	-0.1703	0.0434	-3.9209	0.0001	0.0112
ATP5D	5532.3	0.1839	0.0537	3.4282	0.0006	0.0328
ATP5G2	6991.2	0.1458	0.0397	3.6668	0.0002	0.0205
ATR	1108.8	-0.2275	0.0610	-3.7327	0.0002	0.0170
ATRX	4915.7	-0.2703	0.0705	-3.8359	0.0001	0.0132
B930041F14RIK	235.0	0.2746	0.0782	3.5104	0.0004	0.0271
BBC3	681.5	0.6168	0.1657	3.7221	0.0002	0.0176
BC005537	26016.8	-0.2069	0.0515	-4.0174	0.0001	0.0088

Table 8. Experiment 2 Microglia Differential Gene Expression

Gene	Base mean	Fold change (log$_2$)	Lfcse	Stat	p-value	Adjusted p-value
BDP1	1652.6	-0.2172	0.0593	-3.6628	0.0002	0.0206
BICD2	3447.1	-0.2860	0.0576	-4.9681	0.0000	0.0007
BRD7	3352.7	-0.2130	0.0646	-3.2955	0.0010	0.0418
CAAP1	453.2	-0.1562	0.0405	-3.8577	0.0001	0.0129
CAMKK2	1968.5	-0.2019	0.0598	-3.3779	0.0007	0.0356
CAMSAP1	2026.4	-0.2315	0.0702	-3.2972	0.0010	0.0416
CCDC171	57.9	-0.4177	0.1205	-3.4651	0.0005	0.0297
CCDC82	1197.1	-0.2623	0.0707	-3.7082	0.0002	0.0182
CCDC91	683.3	-0.2335	0.0599	-3.8954	0.0001	0.0119
CCRN4L	690.4	0.4473	0.1286	3.4798	0.0005	0.0285
CCSER2	1505.4	-0.1712	0.0489	-3.5045	0.0005	0.0272
CD180	19226.6	-0.1979	0.0599	-3.3031	0.0010	0.0412
CD2AP	4584.6	-0.1698	0.0381	-4.4579	0.0000	0.0027
CDK20	954.5	0.4402	0.1321	3.3325	0.0009	0.0392
CELF1	5028.4	-0.2329	0.0680	-3.4223	0.0006	0.0331
CENPF	1689.4	-0.4361	0.1226	-3.5572	0.0004	0.0247
CEP170	3018.9	-0.3309	0.0724	-4.5726	0.0000	0.0020
CEP250	3769.8	-0.2159	0.0588	-3.6703	0.0002	0.0204
CEP290	558.2	-0.3549	0.0704	-5.0446	0.0000	0.0006
CEPT1	2694.5	-0.2738	0.0822	-3.3325	0.0009	0.0392
CHAC1	375.6	0.4781	0.1194	4.0055	0.0001	0.0090
CHML	819.7	-0.1835	0.0503	-3.6473	0.0003	0.0213
CHORDC1	3205.7	-0.1779	0.0528	-3.3710	0.0007	0.0360
CIART	191.5	0.6441	0.1658	3.8843	0.0001	0.0122
CIRBP	884.0	0.4909	0.1348	3.6432	0.0003	0.0215
CKLF	878.6	-0.1929	0.0539	-3.5800	0.0003	0.0247
CLDN12	226.9	0.5192	0.1388	3.7391	0.0002	0.0169
CLOCK	1925.8	-0.1613	0.0502	-3.2123	0.0013	0.0491
CMAS	2381.3	-0.1481	0.0459	-3.2291	0.0012	0.0475
CNTRL	1752.9	-0.2540	0.0738	-3.4417	0.0006	0.0314
COPB1	7858.4	-0.1342	0.0308	-4.3654	0.0000	0.0034
CPM	15.8	0.5212	0.1573	3.3136	0.0009	0.0405
CRTC1	595.4	0.3019	0.0761	3.9682	0.0001	0.0099
CSPP1	567.6	-0.3052	0.0939	-3.2485	0.0012	0.0459
CTTNBP2NL	6958.5	-0.3567	0.1077	-3.3121	0.0009	0.0405
CUL2	2220.9	-0.1573	0.0390	-4.0362	0.0001	0.0085
CUL4A	3224.0	-0.1136	0.0355	-3.2004	0.0014	0.0499
CYTIP	324.1	0.5826	0.1663	3.5034	0.0005	0.0272
D330050I16RIK	42.2	0.4375	0.1092	4.0052	0.0001	0.0090

Table 8. Experiment 2 Microglia Differential Gene Expression

Gene	Base mean	Fold change (log$_2$)	Lfcse	Stat	p-value	Adjusted p-value
DDA1	2010.9	0.1586	0.0447	3.5497	0.0004	0.0249
DDIT3	1068.8	0.5555	0.1662	3.3432	0.0008	0.0385
DDIT4	131.4	0.6213	0.1648	3.7711	0.0002	0.0155
DDX19B	963.6	-0.1638	0.0494	-3.3157	0.0009	0.0405
DDX23	3607.0	-0.0938	0.0289	-3.2475	0.0012	0.0460
DENND2C	909.4	-0.4120	0.1041	-3.9569	0.0001	0.0100
DICER1	2972.9	-0.2462	0.0572	-4.3063	0.0000	0.0041
DIRAS2	19.1	0.6227	0.1663	3.7442	0.0002	0.0167
DOCK10	4503.9	-0.2689	0.0654	-4.1145	0.0000	0.0070
DOCK8	13878.9	-0.2310	0.0649	-3.5584	0.0004	0.0247
DOK7	11.2	0.4577	0.1330	3.4405	0.0006	0.0314
DPP8	5875.1	-0.1682	0.0479	-3.5142	0.0004	0.0271
DRD1A	22.6	0.7531	0.1655	4.5503	0.0000	0.0022
DROSHA	1843.4	0.1028	0.0314	3.2779	0.0010	0.0433
DSEL	619.2	-0.1620	0.0399	-4.0555	0.0001	0.0081
DUSP14	83.6	0.7880	0.1635	4.8184	0.0000	0.0009
DUSP8	284.4	0.7448	0.1663	4.4783	0.0000	0.0025
ECHDC1	1144.1	-0.1755	0.0368	-4.7699	0.0000	0.0011
EFTUD1	761.0	-0.1461	0.0450	-3.2455	0.0012	0.0460
EHBP1L1	5589.8	-0.2064	0.0641	-3.2199	0.0013	0.0484
EIF3K	4849.2	0.1605	0.0434	3.7014	0.0002	0.0186
EIF5B	7453.8	-0.1569	0.0287	-5.4630	0.0000	0.0001
EPC1	2254.3	0.4761	0.1354	3.5158	0.0004	0.0271
EPHA2	328.5	-0.6557	0.1553	-4.2220	0.0000	0.0054
ERCC1	464.0	0.2185	0.0550	3.9717	0.0001	0.0099
ESYT2	2031.5	-0.1948	0.0447	-4.3551	0.0000	0.0035
EXOC1	2373.2	-0.2029	0.0458	-4.4308	0.0000	0.0028
EYA4	821.1	-0.4711	0.1280	-3.6806	0.0002	0.0199
FADS3	292.2	0.4571	0.1084	4.2180	0.0000	0.0054
FAM167B	176.1	-0.4790	0.1316	-3.6388	0.0003	0.0217
FAM199X	634.7	-0.2334	0.0468	-4.9888	0.0000	0.0007
FAM73A	1064.8	-0.1725	0.0515	-3.3482	0.0008	0.0380
FAM78A	900.8	-0.3538	0.1046	-3.3812	0.0007	0.0356
FAM83F	11.0	0.4484	0.1375	3.2609	0.0011	0.0449
FAR1	5045.1	-0.2230	0.0625	-3.5654	0.0004	0.0247
FAU	16130.8	0.1832	0.0508	3.6066	0.0003	0.0235
FGFR1OP	1085.7	-0.2306	0.0696	-3.3122	0.0009	0.0405
FLT1	142.9	-0.7126	0.1659	-4.2964	0.0000	0.0042
FRAT2	104.3	0.5118	0.1566	3.2671	0.0011	0.0445

Table 8. Experiment 2 Microglia Differential Gene Expression

Gene	Base mean	Fold change (log$_2$)	Lfcse	Stat	p-value	Adjusted p-value
FRYL	2109.3	-0.2712	0.0810	-3.3480	0.0008	0.0380
G3BP2	9195.7	-0.1219	0.0246	-4.9594	0.0000	0.0007
GADD45B	523.8	0.5519	0.1658	3.3286	0.0009	0.0395
GBF1	2490.3	-0.2348	0.0545	-4.3061	0.0000	0.0041
GLCCI1	488.7	0.5603	0.1573	3.5619	0.0004	0.0247
GM10638	14.2	0.5864	0.1617	3.6274	0.0003	0.0222
GM14322	156.8	-0.4838	0.1219	-3.9690	0.0001	0.0099
GM15708	47.8	0.4116	0.1142	3.6043	0.0003	0.0235
GM3414	204.0	-0.3630	0.0949	-3.8270	0.0001	0.0134
GM4285	93.1	0.3706	0.1090	3.3988	0.0007	0.0341
GM6498	24.1	-0.5170	0.1393	-3.7114	0.0002	0.0182
GMCL1	822.0	-0.1879	0.0493	-3.8092	0.0001	0.0141
GOPC	1518.3	-0.2004	0.0560	-3.5768	0.0003	0.0247
GPR19	190.5	0.3217	0.0949	3.3888	0.0007	0.0349
H2AFJ	1262.9	0.1766	0.0523	3.3751	0.0007	0.0358
HCFC2	765.3	-0.2675	0.0749	-3.5722	0.0004	0.0247
HIATL1	3922.6	-0.1322	0.0413	-3.2011	0.0014	0.0499
HK2	2828.2	-0.3479	0.1029	-3.3829	0.0007	0.0355
HNRNPUL2	10451.4	-0.1543	0.0340	-4.5395	0.0000	0.0022
HOOK3	3705.1	-0.2809	0.0665	-4.2250	0.0000	0.0054
HPS3	2519.4	-0.2673	0.0824	-3.2422	0.0012	0.0463
HSD17B4	7442.0	-0.2042	0.0549	-3.7220	0.0002	0.0176
IBTK	2278.9	-0.2340	0.0659	-3.5528	0.0004	0.0249
IK	6794.4	-0.1887	0.0468	-4.0277	0.0001	0.0086
IKBIP	815.4	-0.2344	0.0551	-4.2533	0.0000	0.0049
IREB2	4470.8	-0.1319	0.0397	-3.3235	0.0009	0.0400
IRS2	1638.5	0.5601	0.1606	3.4872	0.0005	0.0282
ITPRIPL2	5828.5	-0.2513	0.0565	-4.4484	0.0000	0.0027
IWS1	2531.5	-0.1715	0.0424	-4.0464	0.0001	0.0083
JMY	1320.4	0.5016	0.1530	3.2794	0.0010	0.0432
KANSL1	5409.4	0.3860	0.1133	3.4080	0.0007	0.0338
KDM4C	1407.6	-0.2410	0.0723	-3.3343	0.0009	0.0392
KLHL20	915.7	-0.2869	0.0783	-3.6641	0.0002	0.0206
KLHL35	20.7	0.7122	0.1593	4.4699	0.0000	0.0026
KRCC1	3159.2	-0.2766	0.0657	-4.2105	0.0000	0.0054
LACTB2	1078.1	-0.2627	0.0564	-4.6568	0.0000	0.0015
LCORL	1008.2	-0.1966	0.0582	-3.3804	0.0007	0.0356
LNPEP	2834.1	-0.2984	0.0816	-3.6577	0.0003	0.0207
LPGAT1	4876.4	-0.1767	0.0433	-4.0794	0.0000	0.0077

Table 8. Experiment 2 Microglia Differential Gene Expression

Gene	Base mean	Fold change (log$_2$)	Lfcse	Stat	p-value	Adjusted p-value
LRRK2	313.3	-0.3093	0.0805	-3.8410	0.0001	0.0132
LTN1	2692.0	-0.2063	0.0439	-4.6951	0.0000	0.0014
MAFK	1307.0	0.4336	0.1273	3.4053	0.0007	0.0338
MANBAL	1164.1	0.1948	0.0596	3.2665	0.0011	0.0445
MBD1	1934.6	0.2669	0.0812	3.2879	0.0010	0.0424
MCM3AP	1783.6	-0.1997	0.0451	-4.4272	0.0000	0.0028
MCRS1	1908.1	0.1938	0.0602	3.2189	0.0013	0.0484
MDM2	8869.8	0.5307	0.1656	3.2054	0.0013	0.0497
MED1	2008.7	-0.1112	0.0338	-3.2876	0.0010	0.0424
MED16	1677.0	0.2095	0.0598	3.5063	0.0005	0.0272
MED25	2180.0	0.1665	0.0296	5.6301	0.0000	0.0001
MFN1	1796.6	-0.1268	0.0281	-4.5134	0.0000	0.0024
MIA3	4051.5	-0.1894	0.0456	-4.1549	0.0000	0.0062
MKLN1	3059.5	-0.1881	0.0379	-4.9621	0.0000	0.0007
MORC3	4464.5	-0.3390	0.0960	-3.5311	0.0004	0.0262
MOSPD3	947.6	0.1607	0.0398	4.0401	0.0001	0.0084
MPHOSPH8	1217.0	-0.3371	0.0668	-5.0491	0.0000	0.0006
MT1	10115.1	0.4713	0.1192	3.9544	0.0001	0.0100
MT2	3038.4	0.5639	0.1657	3.4028	0.0007	0.0338
MTMR6	7181.9	-0.2036	0.0577	-3.5263	0.0004	0.0265
MXD1	629.8	0.5299	0.1534	3.4546	0.0006	0.0304
NAA30	1291.2	-0.1559	0.0483	-3.2266	0.0013	0.0475
NAIP6	395.2	-0.3904	0.1157	-3.3727	0.0007	0.0359
NDUFA7	2045.0	0.1810	0.0540	3.3512	0.0008	0.0378
NEMF	1943.0	-0.1862	0.0339	-5.4920	0.0000	0.0001
NINL	841.1	-0.2887	0.0891	-3.2386	0.0012	0.0463
NKAP	1275.1	-0.2039	0.0522	-3.9073	0.0001	0.0115
NLRP1A	425.3	-0.3091	0.0902	-3.4265	0.0006	0.0328
NPEPPS	5192.0	-0.2558	0.0666	-3.8388	0.0001	0.0132
NR1D1	273.5	0.5888	0.1645	3.5799	0.0003	0.0247
OPA1	3778.9	-0.1791	0.0376	-4.7612	0.0000	0.0011
P4HA1	7052.0	-0.2586	0.0588	-4.3981	0.0000	0.0030
PANK2	1821.3	-0.2802	0.0869	-3.2265	0.0013	0.0475
PBRM1	4726.8	-0.2308	0.0471	-4.9040	0.0000	0.0007
PCIF1	1772.6	0.1818	0.0396	4.5889	0.0000	0.0019
PCM1	3399.0	-0.2493	0.0652	-3.8219	0.0001	0.0136
PCNT	1767.0	-0.1997	0.0569	-3.5117	0.0004	0.0271
PEX14	1275.7	0.1927	0.0577	3.3379	0.0008	0.0390
PGLS	2630.7	0.1637	0.0505	3.2408	0.0012	0.0463

Table 8. Experiment 2 Microglia Differential Gene Expression

Gene	Base mean	Fold change (log$_2$)	Lfcse	Stat	p-value	Adjusted p-value
PIGT	5806.1	0.1205	0.0340	3.5500	0.0004	0.0249
PIM3	593.8	0.3185	0.0995	3.2005	0.0014	0.0499
PJA2	3308.2	-0.2935	0.0828	-3.5464	0.0004	0.0251
PLCXD2	362.1	0.6025	0.1625	3.7078	0.0002	0.0182
PLEKHA2	4626.2	-0.2821	0.0712	-3.9607	0.0001	0.0100
POLR2I	610.2	0.2306	0.0650	3.5509	0.0004	0.0249
POU3F1	25.3	0.6062	0.1661	3.6500	0.0003	0.0213
PPIG	4992.1	-0.1408	0.0385	-3.6602	0.0003	0.0207
PPIP5K2	2901.8	-0.1386	0.0360	-3.8511	0.0001	0.0129
PPM1B	2281.1	-0.1345	0.0313	-4.2919	0.0000	0.0042
PPP1R32	17.1	0.5391	0.1653	3.2609	0.0011	0.0449
PRCC	1722.5	0.2032	0.0622	3.2648	0.0011	0.0445
PRKD3	3941.6	-0.1444	0.0430	-3.3576	0.0008	0.0372
PRKDC	643.1	-0.3680	0.0907	-4.0561	0.0000	0.0081
PROS1	5055.9	-0.2530	0.0786	-3.2176	0.0013	0.0484
PRPF38B	3041.9	-0.2152	0.0514	-4.1858	0.0000	0.0059
PRPF4B	3678.2	-0.1361	0.0382	-3.5658	0.0004	0.0247
PRR3	466.1	0.2994	0.0711	4.2099	0.0000	0.0054
PRRC1	2338.1	-0.1761	0.0500	-3.5225	0.0004	0.0268
PSME4	4651.0	-0.1743	0.0401	-4.3509	0.0000	0.0035
PSMF1	1640.7	0.2727	0.0714	3.8190	0.0001	0.0137
PTBP3	22203.0	-0.1389	0.0390	-3.5608	0.0004	0.0247
PTPRC	12970.4	-0.1783	0.0489	-3.6459	0.0003	0.0213
PTPRE	2343.5	-0.2013	0.0600	-3.3561	0.0008	0.0373
RAB11B	5346.6	0.1345	0.0382	3.5176	0.0004	0.0271
RAB14	16198.8	-0.1740	0.0497	-3.4988	0.0005	0.0274
RAB3GAP1	2769.7	-0.1897	0.0564	-3.3604	0.0008	0.0369
RALGAPB	2983.1	-0.2352	0.0522	-4.5029	0.0000	0.0024
RAP1GDS1	10200.3	-0.1031	0.0318	-3.2394	0.0012	0.0463
RAP2A	14651.6	-0.2315	0.0695	-3.3336	0.0009	0.0392
RBM15B	1149.5	0.1948	0.0590	3.3008	0.0010	0.0414
RBM25	5363.1	-0.1752	0.0460	-3.8075	0.0001	0.0141
RBM26	1467.0	-0.2981	0.0675	-4.4151	0.0000	0.0029
RBM42	2703.8	0.1705	0.0498	3.4258	0.0006	0.0328
RBM4B	284.2	0.2952	0.0842	3.5076	0.0005	0.0272
RBPMS2	23.6	0.5138	0.1512	3.3970	0.0007	0.0341
RHOD	291.0	0.5092	0.1571	3.2415	0.0012	0.0463
RIN1	65.7	0.5197	0.1383	3.7575	0.0002	0.0161
RLF	1713.8	-0.1889	0.0573	-3.2979	0.0010	0.0416

Table 8. Experiment 2 Microglia Differential Gene Expression

Gene	Base mean	Fold change (log$_2$)	Lfcse	Stat	p-value	Adjusted p-value
RNF113A1	69.7	0.5669	0.1571	3.6086	0.0003	0.0234
RNF170	1134.9	-0.1716	0.0519	-3.3049	0.0009	0.0411
RNF20	2551.1	-0.1274	0.0214	-5.9566	0.0000	0.0000
RNF220	2692.3	0.1469	0.0372	3.9454	0.0001	0.0102
ROCK2	4415.6	-0.2061	0.0367	-5.6203	0.0000	0.0001
RPL10A	14543.3	0.1959	0.0562	3.4828	0.0005	0.0284
RPL18A	21153.7	0.2392	0.0538	4.4471	0.0000	0.0027
RPL23A	11958.4	0.1714	0.0491	3.4885	0.0005	0.0282
RPL28	14100.4	0.2233	0.0535	4.1764	0.0000	0.0060
RPL29	5126.6	0.2484	0.0597	4.1587	0.0000	0.0062
RPL36	6392.9	0.2275	0.0636	3.5747	0.0004	0.0247
RPL41	20083.8	0.2197	0.0646	3.4024	0.0007	0.0338
RPS15	16405.0	0.2576	0.0558	4.6133	0.0000	0.0018
RPS20	15239.4	0.1832	0.0536	3.4197	0.0006	0.0332
RPS5	17877.2	0.2077	0.0603	3.4439	0.0006	0.0314
RRM2B	581.6	-0.1970	0.0607	-3.2465	0.0012	0.0460
RSBN1	814.1	-0.2526	0.0750	-3.3680	0.0008	0.0361
RSBN1L	2244.1	-0.1894	0.0429	-4.4129	0.0000	0.0029
SAP30BP	1309.6	0.2500	0.0714	3.5017	0.0005	0.0273
SCAND1	1232.3	0.2979	0.0399	7.4693	0.0000	0.0000
SEC23A	2231.2	-0.1312	0.0404	-3.2502	0.0012	0.0458
SESN2	1179.7	0.6301	0.1656	3.8047	0.0001	0.0142
SETD3	5514.8	-0.1340	0.0384	-3.4896	0.0005	0.0282
SETX	2821.4	-0.2555	0.0524	-4.8779	0.0000	0.0007
SF3A2	2690.2	0.2959	0.0857	3.4537	0.0006	0.0304
SGMS2	91.9	0.5648	0.1660	3.4020	0.0007	0.0338
SHPRH	1196.8	-0.3742	0.1048	-3.5714	0.0004	0.0247
SIKE1	1494.0	-0.1824	0.0447	-4.0795	0.0000	0.0077
SLC25A17	1538.2	0.1199	0.0350	3.4214	0.0006	0.0331
SLC25A53	62.5	0.3871	0.1083	3.5737	0.0004	0.0247
SLC35A3	3109.8	-0.1654	0.0499	-3.3144	0.0009	0.0405
SLC4A7	1805.6	-0.3777	0.0771	-4.8974	0.0000	0.0007
SLC7A5	2094.4	0.5310	0.1650	3.2185	0.0013	0.0484
SLC9A6	1350.5	-0.1572	0.0408	-3.8529	0.0001	0.0129
SLCO4A1	244.6	-0.5276	0.1611	-3.2742	0.0011	0.0437
SLMAP	3785.4	-0.1744	0.0376	-4.6329	0.0000	0.0017
SMCHD1	3735.9	-0.2014	0.0628	-3.2089	0.0013	0.0493
SMG9	1904.1	0.3303	0.0978	3.3776	0.0007	0.0356
SMIM15	3767.8	-0.2393	0.0722	-3.3147	0.0009	0.0405

Table 8. Experiment 2 Microglia Differential Gene Expression

Gene	Base mean	Fold change (log$_2$)	Lfcse	Stat	p-value	Adjusted p-value
SNAPC2	800.5	0.1719	0.0483	3.5613	0.0004	0.0247
SOGA1	4987.0	-0.3742	0.0802	-4.6681	0.0000	0.0015
SP1	4197.5	-0.2523	0.0769	-3.2833	0.0010	0.0428
SP9	103.5	0.5032	0.1546	3.2536	0.0011	0.0458
SPPL2A	8627.3	-0.1626	0.0453	-3.5914	0.0003	0.0240
SPPL2B	1134.5	0.1555	0.0442	3.5187	0.0004	0.0271
SPRED1	9411.1	-0.2011	0.0538	-3.7386	0.0002	0.0169
SPTBN1	5214.9	-0.1930	0.0603	-3.2021	0.0014	0.0499
SRP54A	580.8	-0.1465	0.0388	-3.7720	0.0002	0.0155
STAG2	5332.5	-0.1409	0.0336	-4.1958	0.0000	0.0057
STX7	12355.2	-0.1411	0.0357	-3.9571	0.0001	0.0100
SWT1	371.1	-0.3224	0.0944	-3.4152	0.0006	0.0335
SYPL	8007.0	-0.1475	0.0448	-3.2890	0.0010	0.0424
SYS1	1668.6	0.1753	0.0490	3.5779	0.0003	0.0247
SYT12	10.3	0.5776	0.1657	3.4857	0.0005	0.0282
TAF1	2375.4	-0.1943	0.0394	-4.9331	0.0000	0.0007
TAF1C	656.0	0.2632	0.0647	4.0691	0.0000	0.0079
TBC1D8B	905.7	-0.2487	0.0658	-3.7772	0.0002	0.0154
TEP1	3184.6	-0.3459	0.0732	-4.7235	0.0000	0.0012
THADA	890.2	-0.1834	0.0558	-3.2858	0.0010	0.0426
THOC2	3254.1	-0.1948	0.0487	-3.9977	0.0001	0.0091
THUMPD3	1306.5	-0.2526	0.0671	-3.7637	0.0002	0.0159
TIAM2	229.1	0.5362	0.1616	3.3188	0.0009	0.0404
TJAP1	1016.1	0.2847	0.0731	3.8919	0.0001	0.0120
TLR3	844.5	-0.3379	0.0899	-3.7578	0.0002	0.0161
TMED8	2057.7	-0.1910	0.0592	-3.2261	0.0013	0.0475
TMEM158	169.1	0.5635	0.1553	3.6287	0.0003	0.0222
TMEM164	5260.5	-0.1367	0.0401	-3.4099	0.0006	0.0338
TMEM199	1085.7	-0.2277	0.0669	-3.4066	0.0007	0.0338
TMEM245	1314.1	-0.2278	0.0701	-3.2519	0.0011	0.0458
TMEM259	3388.2	0.1320	0.0317	4.1617	0.0000	0.0062
TMEM30A	10613.4	-0.1481	0.0422	-3.5057	0.0005	0.0272
TMEM55B	4131.6	0.2618	0.0741	3.5352	0.0004	0.0260
TMEM68	1828.5	-0.1970	0.0496	-3.9680	0.0001	0.0099
TMF1	3882.0	-0.3462	0.0764	-4.5333	0.0000	0.0022
TMUB1	343.7	0.1793	0.0552	3.2500	0.0012	0.0458
TMX3	5573.2	-0.1445	0.0393	-3.6811	0.0002	0.0199
TNFAIP6	28.6	0.5461	0.1535	3.5580	0.0004	0.0247
TOP1	7011.0	-0.1570	0.0409	-3.8357	0.0001	0.0132

**Table 8. Experiment 2 Microglia Differential Gene Expression**

Gene	Base mean	Fold change (log$_2$)	Lfcse	Stat	p-value	Adjusted p-value
TPR	9536.8	-0.1946	0.0540	-3.6040	0.0003	0.0235
TRIB3	289.9	0.5221	0.1322	3.9501	0.0001	0.0101
TRIM23	634.7	-0.2176	0.0628	-3.4673	0.0005	0.0296
TRIP11	1537.8	-0.3139	0.0826	-3.8002	0.0001	0.0143
TRIP4	1338.4	-0.1845	0.0541	-3.4112	0.0006	0.0338
TROVE2	1251.7	-0.1982	0.0597	-3.3178	0.0009	0.0404
TTC37	902.7	-0.2926	0.0712	-4.1097	0.0000	0.0070
UAP1	1632.1	-0.2625	0.0633	-4.1455	0.0000	0.0063
UBA3	2868.3	-0.1615	0.0430	-3.7550	0.0002	0.0161
UBALD1	1671.0	0.2901	0.0843	3.4422	0.0006	0.0314
UBB	6584.5	0.3693	0.1140	3.2383	0.0012	0.0463
UBE3A	2353.9	-0.2248	0.0582	-3.8653	0.0001	0.0127
UEVLD	1097.4	-0.3178	0.0943	-3.3685	0.0008	0.0361
UFL1	1578.5	-0.2804	0.0862	-3.2518	0.0011	0.0458
UIMC1	1305.6	-0.2348	0.0600	-3.9135	0.0001	0.0114
USP12	3255.2	-0.2066	0.0585	-3.5319	0.0004	0.0262
USP2	1263.9	0.2587	0.0528	4.9015	0.0000	0.0007
USP25	4348.5	-0.1227	0.0375	-3.2705	0.0011	0.0442
USP42	526.1	-0.3139	0.0809	-3.8810	0.0001	0.0122
USP45	1555.1	-0.2181	0.0545	-4.0007	0.0001	0.0091
USP9X	7816.3	-0.1951	0.0607	-3.2168	0.0013	0.0484
UTP3	2510.7	-0.1840	0.0573	-3.2103	0.0013	0.0491
VPS13A	874.6	-0.3750	0.0697	-5.3807	0.0000	0.0001
VPS13C	6226.6	-0.4661	0.1216	-3.8321	0.0001	0.0132
VPS37A	2018.2	-0.2077	0.0583	-3.5628	0.0004	0.0247
VSIG4	101.7	-0.5245	0.1611	-3.2563	0.0011	0.0455
WAPAL	4614.6	-0.1410	0.0408	-3.4602	0.0005	0.0300
WDR37	1497.6	-0.1514	0.0473	-3.2021	0.0014	0.0499
WDR83OS	1737.5	0.2104	0.0641	3.2825	0.0010	0.0428
XIAP	4600.3	-0.1983	0.0539	-3.6761	0.0002	0.0200
XKR8	253.4	-0.2792	0.0802	-3.4811	0.0005	0.0285
YLPM1	2199.8	-0.2242	0.0659	-3.4029	0.0007	0.0338
YTHDC2	687.0	-0.3399	0.0882	-3.8530	0.0001	0.0129
YY1	3485.8	-0.1233	0.0297	-4.1535	0.0000	0.0062
ZBTB2	2097.9	0.5256	0.1506	3.4912	0.0005	0.0281
ZBTB41	958.1	-0.1708	0.0491	-3.4765	0.0005	0.0287
ZC3H13	1752.6	-0.1857	0.0448	-4.1475	0.0000	0.0063
ZCCHC7	543.1	-0.3132	0.0808	-3.8756	0.0001	0.0123
ZDHHC4	788.2	0.1564	0.0431	3.6288	0.0003	0.0222

**Table 8. Experiment 2 Microglia Differential Gene Expression**

| Gene	Base mean	Fold change ($\log_2$)	Lfcse	Stat	p-value	Adjusted p-value
ZFML	2576.7	-0.2874	0.0688	-4.1748	0.0000	0.0060
ZFP143	941.4	-0.2461	0.0630	-3.9056	0.0001	0.0115
ZFP318	1184.0	-0.2559	0.0753	-3.3968	0.0007	0.0341
ZFP518B	563.0	-0.2352	0.0706	-3.3308	0.0009	0.0394
ZFP52	598.5	-0.4250	0.1124	-3.7831	0.0002	0.0151
ZFP597	601.9	-0.4043	0.1169	-3.4586	0.0005	0.0301
ZFP628	1199.2	0.3423	0.0882	3.8787	0.0001	0.0122
ZFP7	157.0	-0.3553	0.0925	-3.8412	0.0001	0.0132
ZFP771	373.9	0.2167	0.0565	3.8337	0.0001	0.0132
ZFP777	698.3	0.2538	0.0768	3.3055	0.0009	0.0411
ZFP871	3033.3	-0.2739	0.0754	-3.6345	0.0003	0.0219
ZFP930	247.0	-0.2787	0.0828	-3.3681	0.0008	0.0361
ZFP956	135.3	-0.2831	0.0852	-3.3211	0.0009	0.0402
ZFPL1	940.7	0.1538	0.0455	3.3785	0.0007	0.0356
ZFYVE16	1321.2	-0.3688	0.0957	-3.8540	0.0001	0.0129
ZKSCAN8	353.9	-0.3741	0.1156	-3.2349	0.0012	0.0467
ZMIZ2	4745.3	0.2161	0.0634	3.4084	0.0007	0.0338
ZRANB2	3119.4	-0.2091	0.0560	-3.7359	0.0002	0.0169
0610010K14RIK	1528.9	0.1573	0.0442	3.5625	0.0004	0.0247
1700066M21RIK	565.6	-0.2805	0.0690	-4.0629	0.0000	0.0080
1810011O10RIK	171.1	-0.6053	0.1561	-3.8786	0.0001	0.0122
2410006H16RIK	690.0	0.4070	0.1131	3.5978	0.0003	0.0239
2510009E07RIK	9556.5	-0.3395	0.0826	-4.1100	0.0000	0.0070
3000002C10RIK	133.2	0.4163	0.1202	3.4642	0.0005	0.0297
3930402G23RIK	14.1	0.5671	0.1614	3.5136	0.0004	0.0271
4931440P22RIK	66.5	0.3813	0.1155	3.3027	0.0010	0.0412
5830417I10RIK	411.6	-0.2755	0.0850	-3.2401	0.0012	0.0463
8430427H17RIK	832.4	-0.4101	0.1234	-3.3234	0.0009	0.0400
9130221H12RIK	215.7	-0.2762	0.0839	-3.2936	0.0010	0.0419
9630033F20RIK	911.0	-0.2927	0.0886	-3.3052	0.0009	0.0411
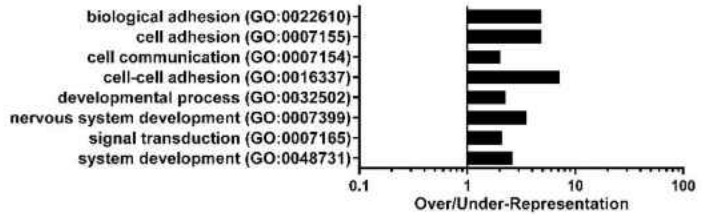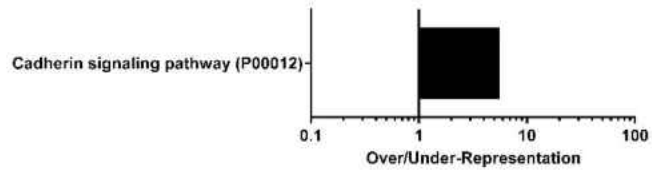
Figure 28. Cellular adhesion and signaling ontologies are over-represented in differential gene expression of astrocyte cultures. Differentially expressed gene lists were subjected for statistical overrepresentation in four gene ontology groups: A) Biological process – slim, B) Pathway, C) Reactome Pathway, and D) Protein Classification. Results represent gene expression changes with over/under-representation in notated ontologies with a p-value of less than 0.05. Results indicate there are a number of gene expression changes that play a role in cell signaling and adherence. All expression changes are overrepresented by their group signifying there are more genes in these categories in the differentially expressed gene list than would be expected based on the number of genes on the list.
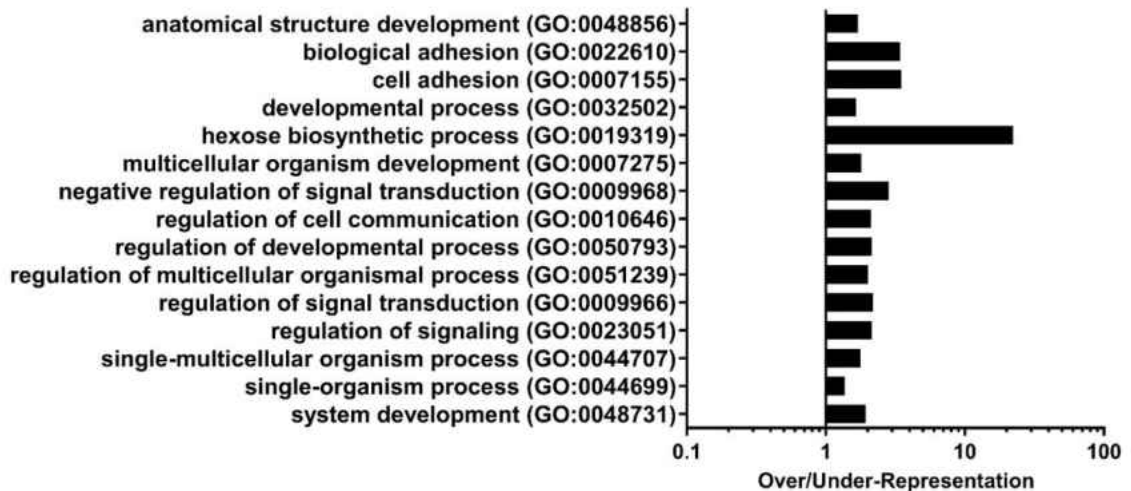
Figure 29. Comprehensive biological process ontology identifies additional developmental ontologies in astrocyte cultures. Differentially expressed gene lists were subjected for statistical overrepresentation in Biological process – complete. The complete biological process ontology accounts for all ontologies and more genes in each ontology than the slim biological process ontology. Results represent gene expression changes with over/under-representation and with a p-value of less than 0.05. Results indicate there are a number of gene expression changes that play a role in cell signaling and adherence. There are also several gene expression changes in developmental categories. All gene expression changes are overrepresented by their group signifying there are more genes in these categories in the differentially expressed gene list than would be expected based on the number of genes in the list.

Table 9. Experiment 2 Astrocyte Differential Gene Expression Gene Ontology

	Reference list gene number	Observed genes	Expected gene number	Over/ Under	Fold enrichment	P-value
PANTHER GO-SLIM BIOLOGICAL PROCESS						
CELL-CELL ADHESION (GO:0016337)	310	18	2.5	+	7.2	2.68E-08
CELL ADHESION (GO:0007155)	486	19	3.92	+	4.85	4.85E-06
BIOLOGICAL ADHESION (GO:0022610)	486	19	3.92	+	4.85	4.85E-06
NERVOUS SYSTEM DEVELOPMENT (GO:0007399)	668	19	5.39	+	3.53	5.78E-04
SYSTEM DEVELOPMENT (GO:0048731)	1084	23	8.74	+	2.63	5.83E-03
DEVELOPMENTAL PROCESS (GO:0032502)	2027	37	16.35	+	2.26	5.00E-04
SIGNAL TRANSDUCTION (GO:0007165)	2728	46	22	+	2.09	1.91E-04
CELL COMMUNICATION (GO:0007154)	3008	49	24.26	+	2.02	2.03E-04
UNCLASSIFIED (UNCLASSIFIED)	9053	53	73	-	0.73	0.00E+00
GO BIOLOGICAL PROCESS COMPLETE						
HEXOSE BIOSYNTHETIC PROCESS (GO:0019319)	28	5	0.23	+	22.14	3.22E-02
CELL ADHESION (GO:0007155)	747	21	6.02	+	3.49	6.87E-03
BIOLOGICAL ADHESION (GO:0022610)	757	21	6.1	+	3.44	8.47E-03
NEGATIVE REGULATION OF SIGNAL TRANSDUCTION (GO:0009968)	1048	24	8.45	+	2.84	3.77E-02
REGULATION OF SIGNAL TRANSDUCTION (GO:0009966)	2432	43	19.61	+	2.19	4.85E-03
REGULATION OF SIGNALING (GO:0023051)	2778	48	22.4	+	2.14	1.70E-03
REGULATION OF DEVELOPMENTAL PROCESS (GO:0050793)	2331	40	18.8	+	2.13	2.80E-02
REGULATION OF CELL COMMUNICATION (GO:0010646)	2756	47	22.22	+	2.11	3.48E-03

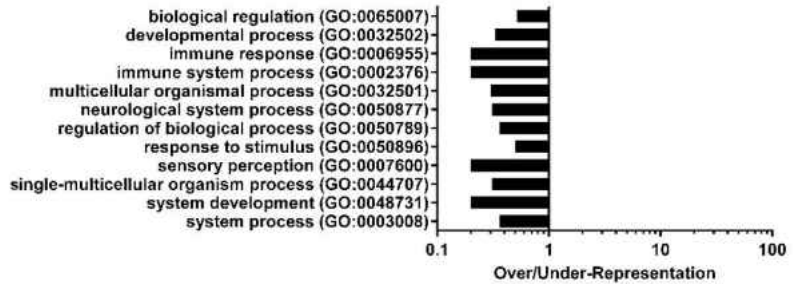**Table 9. Experiment 2 Astrocyte Differential Gene Expression Gene Ontology**

	Reference list gene number	Observed genes	Expected gene number	Over/ Under	Fold enrichment	P-value
GO BIOLOGICAL PROCESS COMPLETE CONT.						
REGULATION OF MULTICELLULAR ORGANISMAL PROCESS (GO:0051239)	2711	44	21.86	+	2.01	3.41E-02
SYSTEM DEVELOPMENT (GO:0048731)	3909	61	31.52	+	1.94	7.77E-04
MULTICELLULAR ORGANISM DEVELOPMENT (GO:0007275)	4474	65	36.08	+	1.8	3.49E-03
SINGLE-MULTICELLULAR ORGANISM PROCESS (GO:0044707)	5145	74	41.49	+	1.78	4.53E-04
ANATOMICAL STRUCTURE DEVELOPMENT (GO:0048856)	4796	66	38.67	+	1.71	1.97E-02
DEVELOPMENTAL PROCESS (GO:0032502)	5119	68	41.28	+	1.65	4.52E-02
SINGLE-ORGANISM PROCESS (GO:0044699)	12063	133	97.27	+	1.37	2.82E-04
UNCLASSIFIED (UNCLASSIFIED)	1777	4	14.33	-	0.28	0.00E+00
PANTHER PROTEIN CLASS						
CELL ADHESION MOLECULE (PC00069)	496	14	4	+	3.5	1.18E-02
SIGNALING MOLECULE (PC00207)	1079	21	8.7	+	2.41	3.73E-02
UNCLASSIFIED (UNCLASSIFIED)	10995	64	88.66	-	0.72	0.00E+00
PANTHER PATHWAYS						
CADHERIN SIGNALING PATHWAY (P00012)	154	7	1.24	+	5.64	4.49E-02
UNCLASSIFIED (UNCLASSIFIED)	19715	134	158.98	-	0.84	0.00E+00

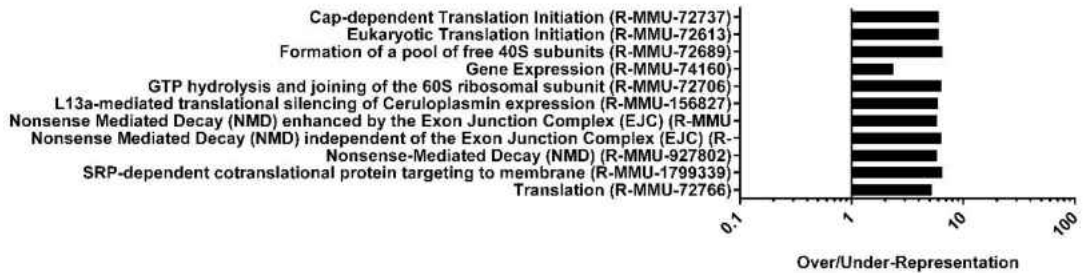**Table 9. Experiment 2 Astrocyte Differential Gene Expression Gene Ontology**

	Reference list gene number	Observed genes	Expected gene number	Over/ Under	Fold enrichment	P-value
REACTOME PATHWAYS						
COLLAGEN BIOSYNTHESIS AND MODIFYING ENZYMES (R-MMU-1650814)	62	7	0.5	+	14	1.34E-03
COLLAGEN FORMATION (R-MMU-1474290)	89	7	0.72	+	9.75	1.40E-02
UNCLASSIFIED (UNCLASSIFIED)	14500	90	116.93	-	0.77	0.00E+00

Gene Ontology Over-Representation - Microglia Culture
Experiment 2

A Biological Process

biological regulation (GO:0065007)
developmental process (GO:0032502)
immune response (GO:0006955)
immune system process (GO:0002376)
multicellular organismal process (GO:0032501)
neurological system process (GO:0050877)
regulation of biological process (GO:0050789)
response to stimulus (GO:0050896)
sensory perception (GO:0007600)
single-multicellular organism process (GO:0044707)
system development (GO:0048731)
system process (GO:0003008)

0.1   1   10   100
Over/Under-Representation

B Reactome Pathway

Cap-dependent Translation Initiation (R-MMU-72737)
Eukaryotic Translation Initiation (R-MMU-72613)
Formation of a pool of free 40S subunits (R-MMU-72689)
Gene Expression (R-MMU-74160)
GTP hydrolysis and joining of the 60S ribosomal subunit (R-MMU-72706)
L13a-mediated translational silencing of Ceruloplasmin expression (R-MMU-156827)
Nonsense Mediated Decay (NMD) enhanced by the Exon Junction Complex (EJC) (R-MMU-
Nonsense Mediated Decay (NMD) independent of the Exon Junction Complex (EJC) (R-
Nonsense-Mediated Decay (NMD) (R-MMU-927802)
SRP-dependent cotranslational protein targeting to membrane (R-MMU-1799339)
Translation (R-MMU-72766)

0.1   1   10   100
Over/Under-Representation
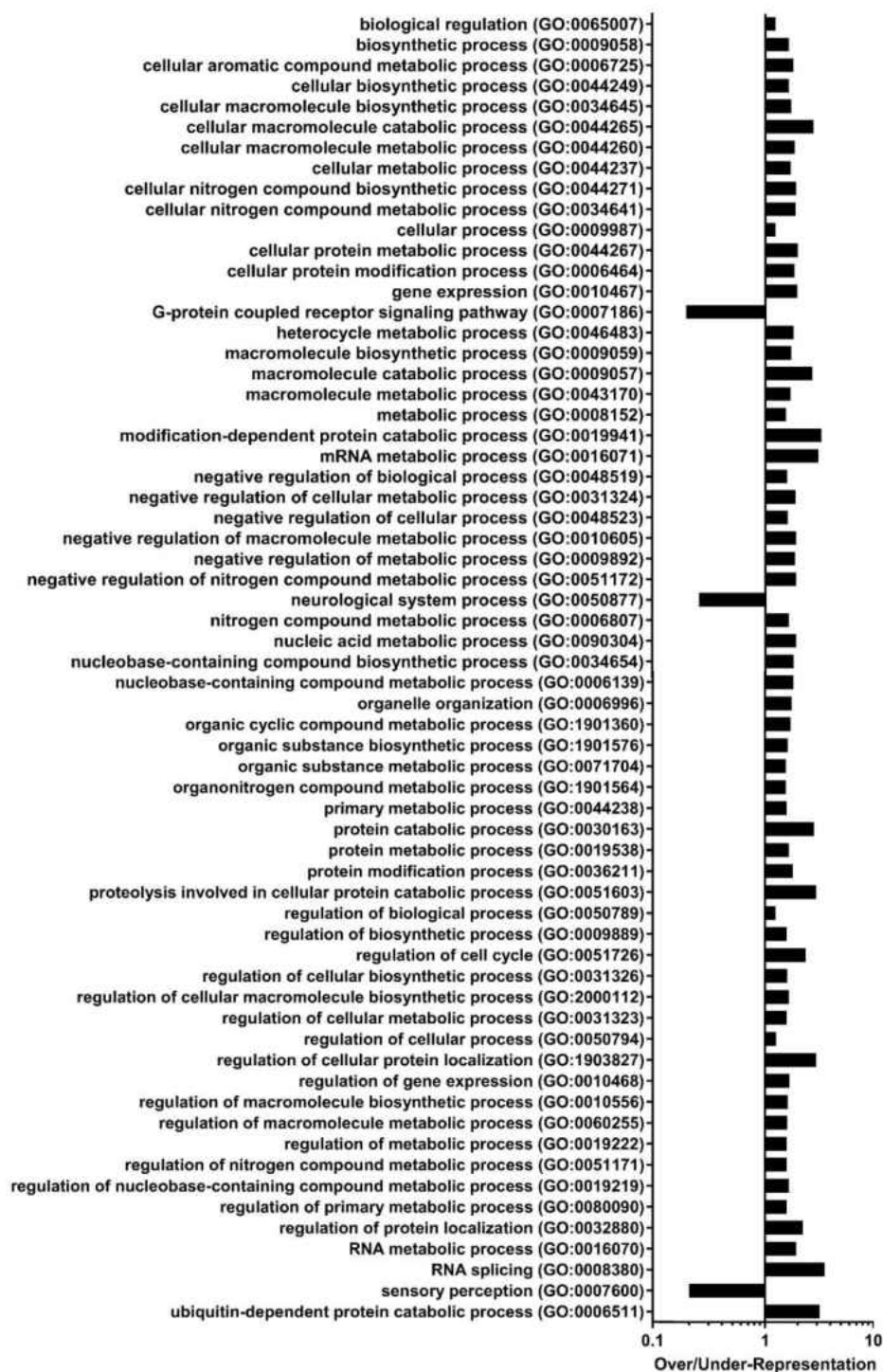
0

Figure 30. Immune function and stimulation response ontologies are over-represented in differential gene expression of microglia cultures. Differentially expressed gene lists were subjected for statistical overrepresentation in two gene ontology groups: A) Biological process – slim and B) Reactome Pathway. Results represent gene ontologies with over/under-representation with a p-value of less than 0.05. Results indicate there are a number of gene groups that play a role in immune function and stimulation response. Gene expression changes are under-represented in biological process and over-represented in reactome pathway ontologies. No gene expression changes were represented in either pathway or protein classification ontology groups.

185

Microglia Biological Process Gene Ontology Over-representation - Comprehensive
Experiment 2

Figure 31. Comprehensive biological process ontology identifies numerous metabolic ontologies in microglia culture differential gene expression. Differentially

186

13   **Figure 31 cont.** expressed gene lists were subjected for statistical overrepresentation in
14   Biological process – complete. Results represent gene expression changes with
15   over/under-representation in ontologies and with a p-value of less than 0.05. Results
16   indicate there are a number of gene expression changes that play a role in transcription
17   and metabolic and catabolic processes. Most expression changes are overrepresented
18   with some being underrepresented in ontology groups.

Table 10. Experiment 2 Microglia Differential Gene Expression Gene Ontology

	Reference list gene number	Observed genes	Expected gene number	Over/ Under	Fold enrichment	P-value
PANTHER GO-SLIM BIOLOGICAL PROCESS						
UNCLASSIFIED (UNCLASSIFIED)	9053	174	150.46	+	1.16	0.00E+00
BIOLOGICAL REGULATION (GO:0065007)	3021	26	50.21	-	0.52	1.23E-02
RESPONSE TO STIMULUS (GO:0050896)	3345	28	55.6	-	0.5	2.40E-03
REGULATION OF BIOLOGICAL PROCESS (GO:0050789)	2647	16	43.99	-	0.36	8.37E-05
SYSTEM PROCESS (GO:0003008)	1992	12	33.11	-	0.36	2.89E-03
DEVELOPMENTAL PROCESS (GO:0032502)	2027	11	33.69	-	0.33	6.10E-04
SINGLE-MULTICELLULAR ORGANISM PROCESS (GO:0044707)	2527	13	42	-	0.31	1.14E-05
NEUROLOGICAL SYSTEM PROCESS (GO:0050877)	1770	9	29.42	-	0.31	1.41E-03
MULTICELLULAR ORGANISMAL PROCESS (GO:0032501)	2628	13	43.68	-	0.3	3.00E-06
IMMUNE SYSTEM PROCESS (GO:0002376)	1354	4	22.5	-	< 0.2	3.21E-04
SYSTEM DEVELOPMENT (GO:0048731)	1084	3	18.02	-	< 0.2	3.04E-03
SENSORY PERCEPTION (GO:0007600)	1283	2	21.32	-	< 0.2	1.95E-05
IMMUNE RESPONSE (GO:0006955)	800	1	13.3	-	< 0.2	4.69E-03
GO BIOLOGICAL PROCESS COMPLETE						
RNA SPLICING (GO:0008380)	304	18	5.05	+	3.56	4.19E-02
UBIQUITIN-DEPENDENT PROTEIN CATABOLIC PROCESS (GO:0006511)	396	21	6.58	+	3.19	3.74E-02
MODIFICATION-DEPENDENT PROTEIN CATABOLIC PROCESS (GO:0019941)	403	21	6.7	+	3.14	4.86E-02

Table 10. Experiment 2 Microglia Differential Gene Expression Gene Ontology

	Reference list gene number	Observed genes	Expected gene number	Over/ Under	Fold enrichment	P-value
GO BIOLOGICAL PROCESS COMPLETE CONT.						
MRNA METABOLIC PROCESS (GO:0016071)	488	24	8.11	+	2.96	2.78E-02
PROTEOLYSIS INVOLVED IN CELLULAR PROTEIN CATABOLIC PROCESS (GO:0051603)	468	23	7.78	+	2.96	4.51E-02
REGULATION OF CELLULAR PROTEIN LOCALIZATION (GO:1903827)	570	28	9.47	+	2.96	4.29E-03
PROTEIN CATABOLIC PROCESS (GO:0030163)	531	25	8.83	+	2.83	3.67E-02
CELLULAR MACROMOLECULE CATABOLIC PROCESS (GO:0044265)	630	28	10.47	+	2.67	2.87E-02
MACROMOLECULE CATABOLIC PROCESS (GO:0009057)	711	31	11.82	+	2.62	1.26E-02
REGULATION OF CELL CYCLE (GO:0051726)	862	34	14.33	+	2.37	3.37E-02
REGULATION OF PROTEIN LOCALIZATION (GO:0032880)	996	37	16.55	+	2.24	4.78E-02
CELLULAR PROTEIN METABOLIC PROCESS (GO:0044267)	2662	86	44.24	+	1.94	9.19E-06
RNA METABOLIC PROCESS (GO:0016070)	2642	85	43.91	+	1.94	1.44E-05
GENE EXPRESSION (GO:0010467)	2942	94	48.9	+	1.92	2.07E-06
NEGATIVE REGULATION OF MACROMOLECULE METABOLIC PROCESS (GO:0010605)	2206	69	36.66	+	1.88	2.06E-03
NUCLEIC ACID METABOLIC PROCESS (GO:0090304)	3070	96	51.02	+	1.88	3.93E-06
NEGATIVE REGULATION OF NITROGEN COMPOUND METABOLIC PROCESS (GO:0051172)	2079	65	34.55	+	1.88	5.03E-03
CELLULAR NITROGEN COMPOUND BIOSYNTHETIC PROCESS (GO:0044271)	2568	80	42.68	+	1.87	2.06E-04

Table 10. Experiment 2 Microglia Differential Gene Expression Gene Ontology

	Reference list gene number	Observed genes	Expected gene number	Over/ Under	Fold enrichment	P-value
GO BIOLOGICAL PROCESS COMPLETE CONT.						
NEGATIVE REGULATION OF CELLULAR METABOLIC PROCESS (GO:0031324)	2229	69	37.05	+	1.86	3.02E-03
CELLULAR NITROGEN COMPOUND METABOLIC PROCESS (GO:0034641)	4053	125	67.36	+	1.86	5.44E-09
NEGATIVE REGULATION OF METABOLIC PROCESS (GO:0009892)	2446	75	40.65	+	1.84	1.20E-03
NUCLEOBASE-CONTAINING COMPOUND METABOLIC PROCESS (GO:0006139)	3522	107	58.54	+	1.83	1.38E-06
CELLULAR MACROMOLECULE METABOLIC PROCESS (GO:0044260)	5333	161	88.64	+	1.82	1.09E-12
CELLULAR PROTEIN MODIFICATION PROCESS (GO:0006464)	2156	65	35.83	+	1.81	1.73E-02
PROTEIN MODIFICATION PROCESS (GO:0036211)	2156	65	35.83	+	1.81	1.73E-02
HETEROCYCLE METABOLIC PROCESS (GO:0046483)	3648	108	60.63	+	1.78	4.91E-06
NUCLEOBASE-CONTAINING COMPOUND BIOSYNTHETIC PROCESS (GO:0034654)	2133	63	35.45	+	1.78	4.92E-02
CELLULAR AROMATIC COMPOUND METABOLIC PROCESS (GO:0006725)	3702	109	61.53	+	1.77	5.40E-06
ORGANELLE ORGANIZATION (GO:0006996)	2674	78	44.44	+	1.76	4.68E-03
ORGANIC CYCLIC COMPOUND METABOLIC PROCESS (GO:1901360)	3890	111	64.65	+	1.72	2.15E-05
CELLULAR MACROMOLECULE BIOSYNTHETIC PROCESS (GO:0034645)	2652	75	44.08	+	1.7	2.57E-02
MACROMOLECULE BIOSYNTHETIC PROCESS (GO:0009059)	2690	76	44.71	+	1.7	2.25E-02

Table 10. Experiment 2 Microglia Differential Gene Expression Gene Ontology

|	Reference list gene number	Observed genes	Expected gene number	Over/ Under	Fold enrichment	P-value
GO BIOLOGICAL PROCESS COMPLETE CONT.						
REGULATION OF GENE EXPRESSION (GO:0010468)	3786	106	62.92	+	1.68	1.63E-04
CELLULAR METABOLIC PROCESS (GO:0044237)	7037	196	116.96	+	1.68	1.40E-13
MACROMOLECULE METABOLIC PROCESS (GO:0043170)	6040	168	100.39	+	1.67	3.71E-10
REGULATION OF CELLULAR MACROMOLECULE BIOSYNTHETIC PROCESS (GO:2000112)	3429	95	56.99	+	1.67	1.97E-03
PROTEIN METABOLIC PROCESS (GO:0019538)	3396	94	56.44	+	1.67	2.44E-03
REGULATION OF NUCLEOBASE-CONTAINING COMPOUND METABOLIC PROCESS (GO:0019219)	3558	98	59.14	+	1.66	1.55E-03
ORGANIC SUBSTANCE BIOSYNTHETIC PROCESS (GO:1901576)	3455	93	57.42	+	1.62	9.96E-03
REGULATION OF MACROMOLECULE BIOSYNTHETIC PROCESS (GO:0010556)	3533	95	58.72	+	1.62	7.64E-03
NITROGEN COMPOUND METABOLIC PROCESS (GO:0006807)	6709	180	111.51	+	1.61	6.09E-10
BIOSYNTHETIC PROCESS (GO:0009058)	3519	94	58.49	+	1.61	1.19E-02
CELLULAR BIOSYNTHETIC PROCESS (GO:0044249)	3372	90	56.04	+	1.61	2.25E-02
REGULATION OF CELLULAR BIOSYNTHETIC PROCESS (GO:0031326)	3717	99	61.78	+	1.6	6.33E-03
REGULATION OF MACROMOLECULE METABOLIC PROCESS (GO:0060255)	5221	139	86.77	+	1.6	7.40E-06

Table 10. Experiment 2 Microglia Differential Gene Expression Gene Ontology

	Reference list gene number	Observed genes	Expected gene number	Over/ Under	Fold enrichment	P-value
GO BIOLOGICAL PROCESS COMPLETE CONT.						
NEGATIVE REGULATION OF CELLULAR PROCESS (GO:0048523)	4158	110	69.11	+	1.59	1.59E-03
REGULATION OF NITROGEN COMPOUND METABOLIC PROCESS (GO:0051171)	5070	134	84.27	+	1.59	3.01E-05
REGULATION OF CELLULAR METABOLIC PROCESS (GO:0031323)	5302	140	88.12	+	1.59	1.09E-05
REGULATION OF PRIMARY METABOLIC PROCESS (GO:0080090)	5196	137	86.36	+	1.59	2.07E-05
REGULATION OF METABOLIC PROCESS (GO:0019222)	5657	149	94.02	+	1.58	2.43E-06
PRIMARY METABOLIC PROCESS (GO:0044238)	7292	192	121.2	+	1.58	2.20E-10
REGULATION OF BIOSYNTHETIC PROCESS (GO:0009889)	3772	99	62.69	+	1.58	1.24E-02
NEGATIVE REGULATION OF BIOLOGICAL PROCESS (GO:0048519)	4545	118	75.54	+	1.56	1.24E-03
ORGANONITROGEN COMPOUND METABOLIC PROCESS (GO:1901564)	4214	109	70.04	+	1.56	5.76E-03
ORGANIC SUBSTANCE METABOLIC PROCESS (GO:0071704)	7618	197	126.61	+	1.56	4.47E-10
METABOLIC PROCESS (GO:0008152)	8101	205	134.64	+	1.52	7.13E-10
REGULATION OF CELLULAR PROCESS (GO:0050794)	10161	212	168.88	+	1.26	3.89E-02
REGULATION OF BIOLOGICAL PROCESS (GO:0050789)	10723	223	178.22	+	1.25	1.70E-02
BIOLOGICAL REGULATION (GO:0065007)	11220	230	186.48	+	1.23	3.01E-02
CELLULAR PROCESS (GO:0009987)	13608	278	226.17	+	1.23	7.83E-05
UNCLASSIFIED (UNCLASSIFIED)	1777	15	29.53	-	0.51	0.00E+00

Table 10. Experiment 2 Microglia Differential Gene Expression Gene Ontology

	Reference list gene number	Observed genes	Expected gene number	Over/ Under	Fold enrichment	P-value
GO BIOLOGICAL PROCESS COMPLETE CONT.						
NEUROLOGICAL SYSTEM PROCESS (GO:0050877)	2107	9	35.02	-	0.26	5.56E-04
G-PROTEIN COUPLED RECEPTOR SIGNALING PATHWAY (GO:0007186)	1805	6	30	-	0.2	4.27E-04
SENSORY PERCEPTION (GO:0007600)	1761	4	29.27	-	< 0.2	2.29E-05
PANTHER PROTEIN CLASS						
UNCLASSIFIED (UNCLASSIFIED)	10995	186	182.74	+	1.02	0.00E+00
PANTHER PATHWAYS						
UNCLASSIFIED (UNCLASSIFIED)	19715	329	327.67	+	1	0.00E+00
REACTOME PATHWAYS						
FORMATION OF A POOL OF FREE 40S SUBUNITS (R-MMU-72689)	92	10	1.53	+	6.54	6.55E-03
SRP-DEPENDENT COTRANSLATIONAL PROTEIN TARGETING TO MEMBRANE (R-MMU-1799339)	83	9	1.38	+	6.52	2.00E-02
GTP HYDROLYSIS AND JOINING OF THE 60S RIBOSOMAL SUBUNIT (R-MMU-72706)	103	11	1.71	+	6.43	2.59E-03
NONSENSE MEDIATED DECAY (NMD) INDEPENDENT OF THE EXON JUNCTION COMPLEX (EJC) (R-MMU-975956)	85	9	1.41	+	6.37	2.41E-02
CAP-DEPENDENT TRANSLATION INITIATION (R-MMU-72737)	109	11	1.81	+	6.07	4.42E-03

Table 10. Experiment 2 Microglia Differential Gene Expression Gene Ontology

	Reference list gene number	Observed genes	Expected gene number	Over/ Under	Fold enrichment	P-value
REACTOME PATHWAYS CONT.						
EUKARYOTIC TRANSLATION INITIATION (R-MMU-72613)	110	11	1.83	+	6.02	4.81E-03
L13A-MEDIATED TRANSLATIONAL SILENCING OF CERULOPLASMIN EXPRESSION (R-MMU-156827)	102	10	1.7	+	5.9	1.59E-02
NONSENSE MEDIATED DECAY (NMD) ENHANCED BY THE EXON JUNCTION COMPLEX (EJC) (R-MMU-975957)	104	10	1.73	+	5.79	1.87E-02
NONSENSE-MEDIATED DECAY (NMD) (R-MMU-927802)	104	10	1.73	+	5.79	1.87E-02
TRANSLATION (R-MMU-72766)	126	11	2.09	+	5.25	1.70E-02
GENE EXPRESSION (R-MMU-74160)	1088	43	18.08	+	2.38	2.74E-04
UNCLASSIFIED (UNCLASSIFIED)	14500	214	241	-	0.89	0.00E+00

20
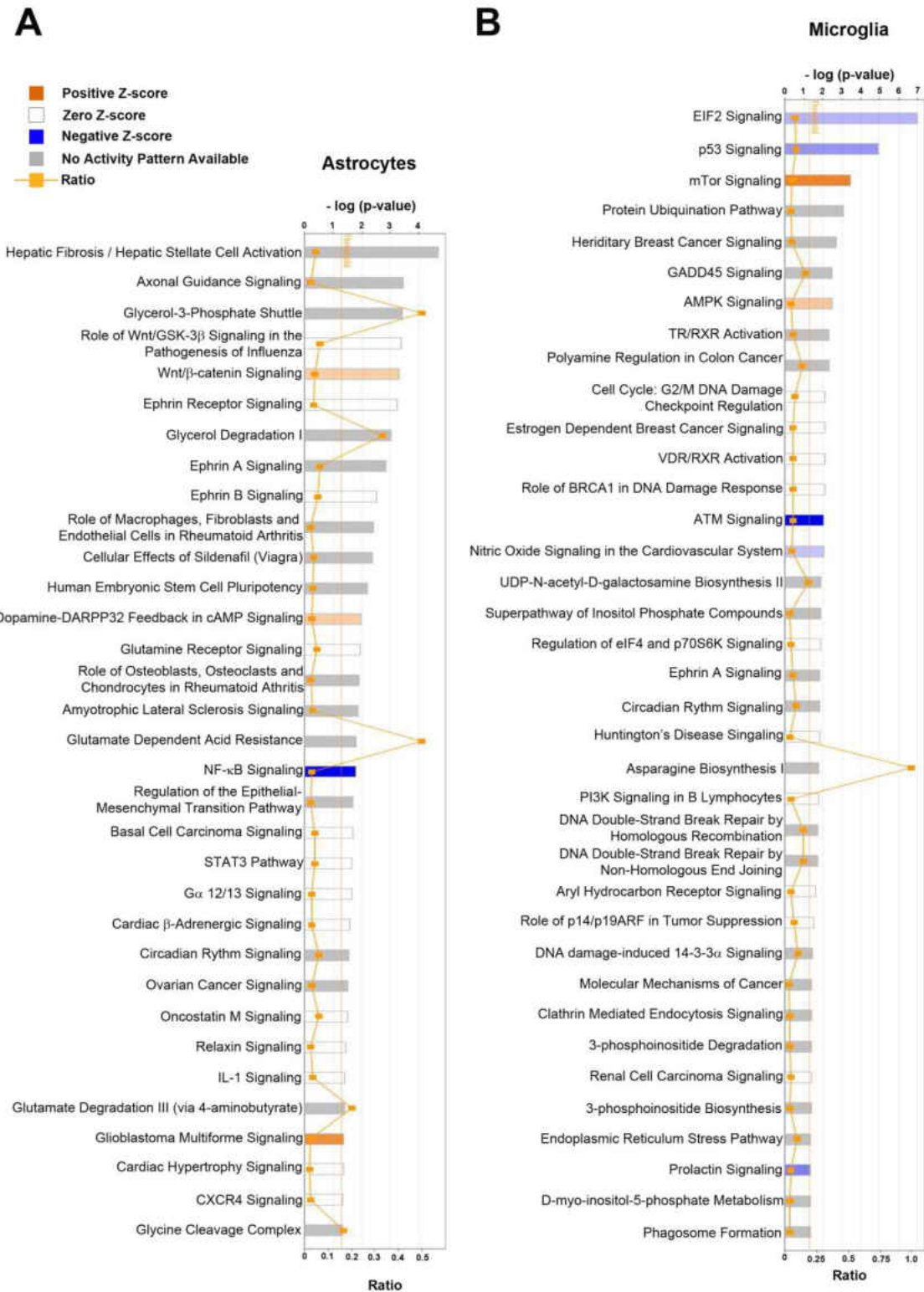
Figure 32. Astrocyte and microglia cultures have different predicted responses in activation of pathways. Differentially expressed gene lists were subjected to Ingenuity

Figure 32 cont. Pathway Analysis and results are displayed in bar chart format for astrocytes (A) and microglia (B). Bar charts for ingenuity pathway analysis display p-value (top horizontal axis) in length of the bar. Color of the bar indicates the predicted activation of the pathway based upon z-score (calculations incorporate differential gene expression) to be activated (orange), no change (white), deactivated (blue) or no activity pattern detected (gray). The ratio line (orange line with square points) indicates the ratio (bottom horizontal axis) of the number of submitted genes to the total genes available in the pathway.
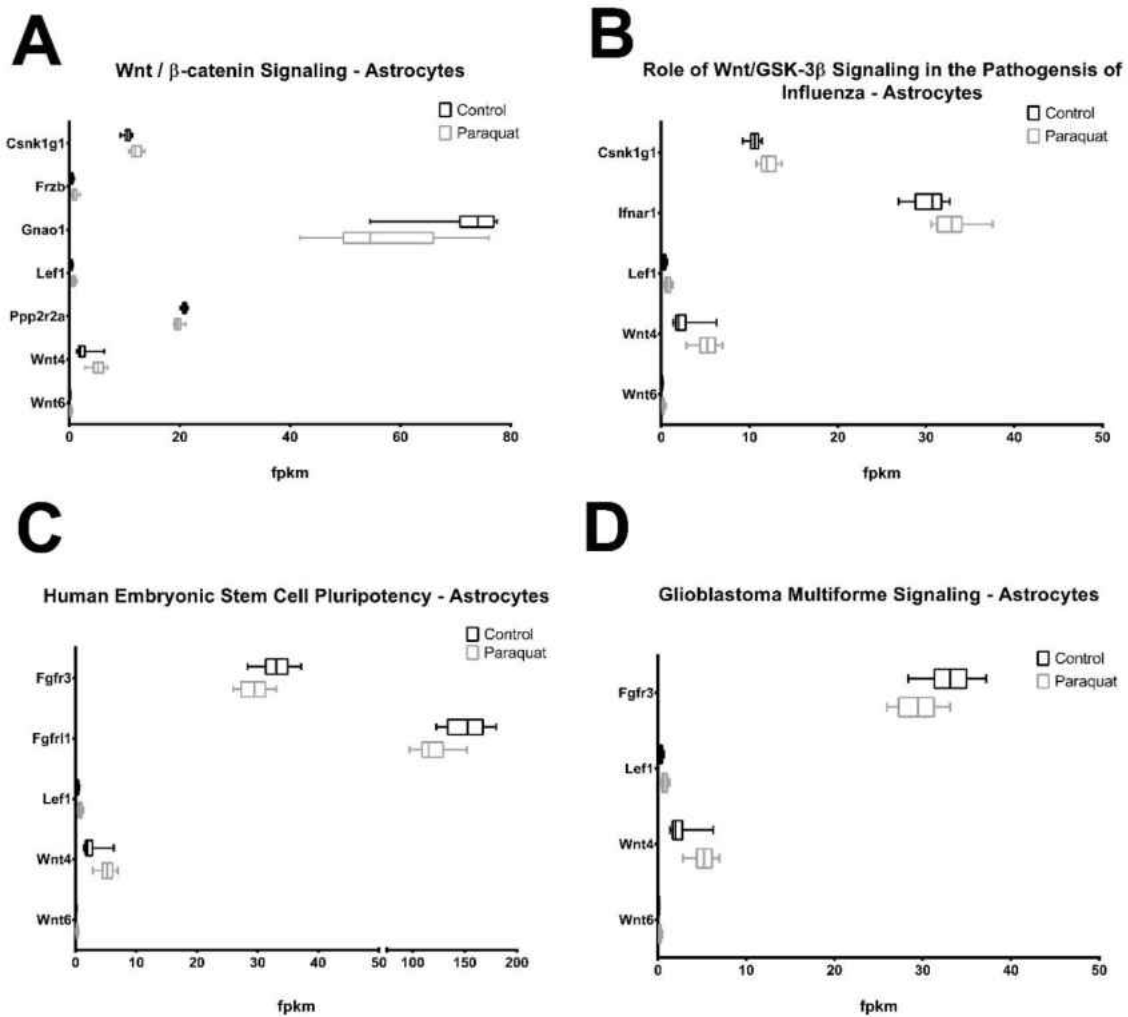
Figure 33. Ingenuity pathway analysis identifies some potential proto-oncogenic pathways in Paraquat exposed astrocyte cultures. Graphs represent expansion of pathways impacted by changes in gene expression identified in ingenuity pathway analysis. A) Wnt/b catenin signaling, p-value: 5.01×10^{-4}; B) Role of Wnt/Gsk-b in the pathogenesis of influenza, p-value: 3.98×10^{-4}; C) Human embryonic stem cell pluripotency, p-value: 6.46×10^{-3}, and D) Glioblastoma multiforme signaling, p-value: 4.17×10^{-2} are expanded for hits in differentially expressed genes of selected ontologies. Expanded ontologies have implications in cancer development and progression. Individual genes within the expanded lists, such as *Lef1*, *Wnt 4* and *Ppp2r2a* have altered expression patterns in gliomas and glioblastoma.
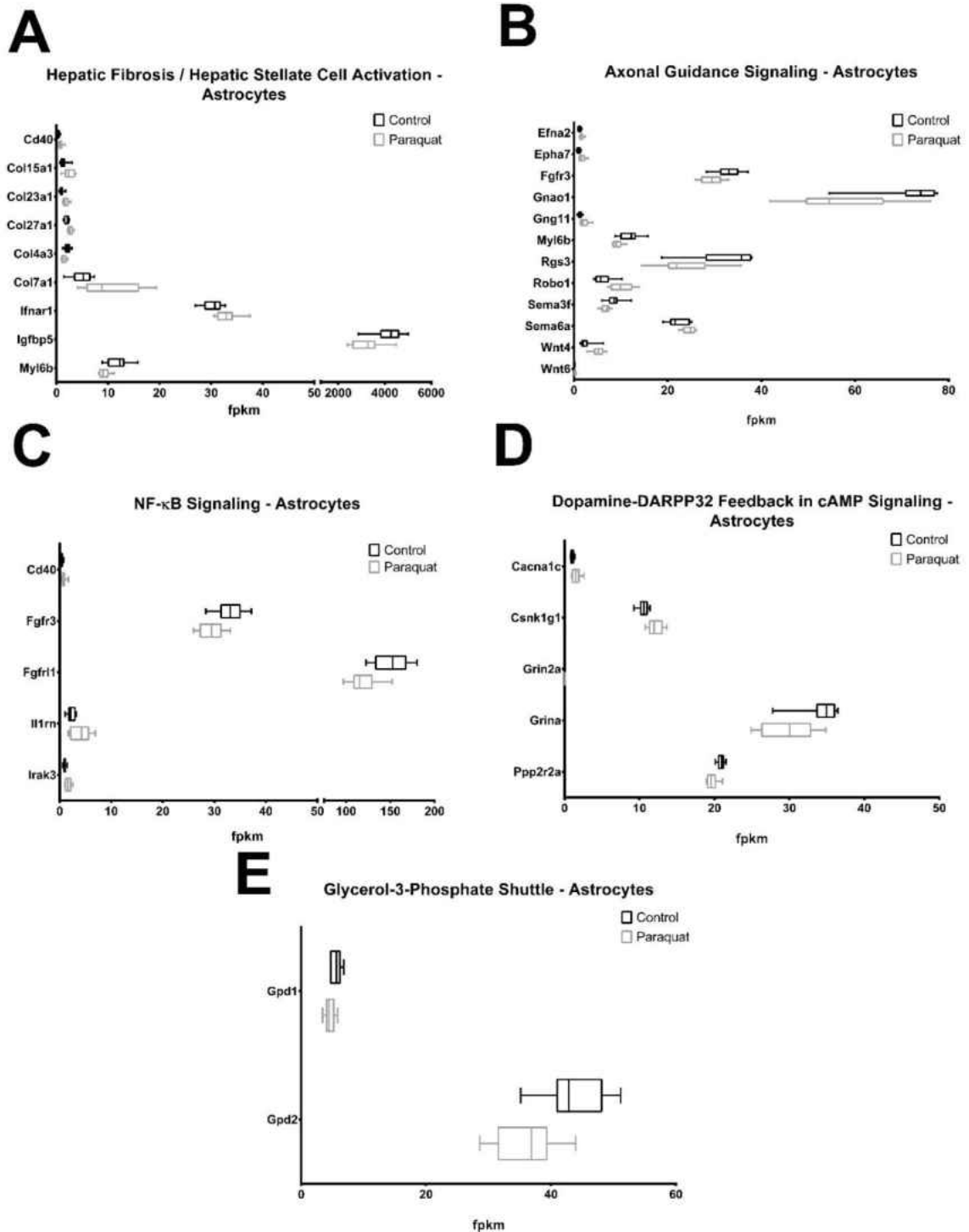
Figure 34. Ingenuity pathway analysis identifies some glial scarring and disrupted cellular signaling pathways in Paraquat exposed astrocyte cultures. Represented here are pathways identified by ingenuity pathway analysis that identify genes and pathways indicative of glial scarring as well as disrupted cell signaling. A) Hepatic fibrosis/hepatic stellate cell activation, p-value: 2.09 x 10^{-5}; B) Axonal guidance

Figure 34 Cont. signaling, p-value: 3.39×10^{-4}; C) NF-kB signaling, p-value: 1.66×10^{-2}, D) Dopamine-DARRP32 feedback in cAMP signaling, p-value: 1.07×10^{-2} and E) Glycerol-3-phosphate shuttle, p-value: 3.98×10^{-4} are expanded for hits in differentially expressed genes of selected ontologies.
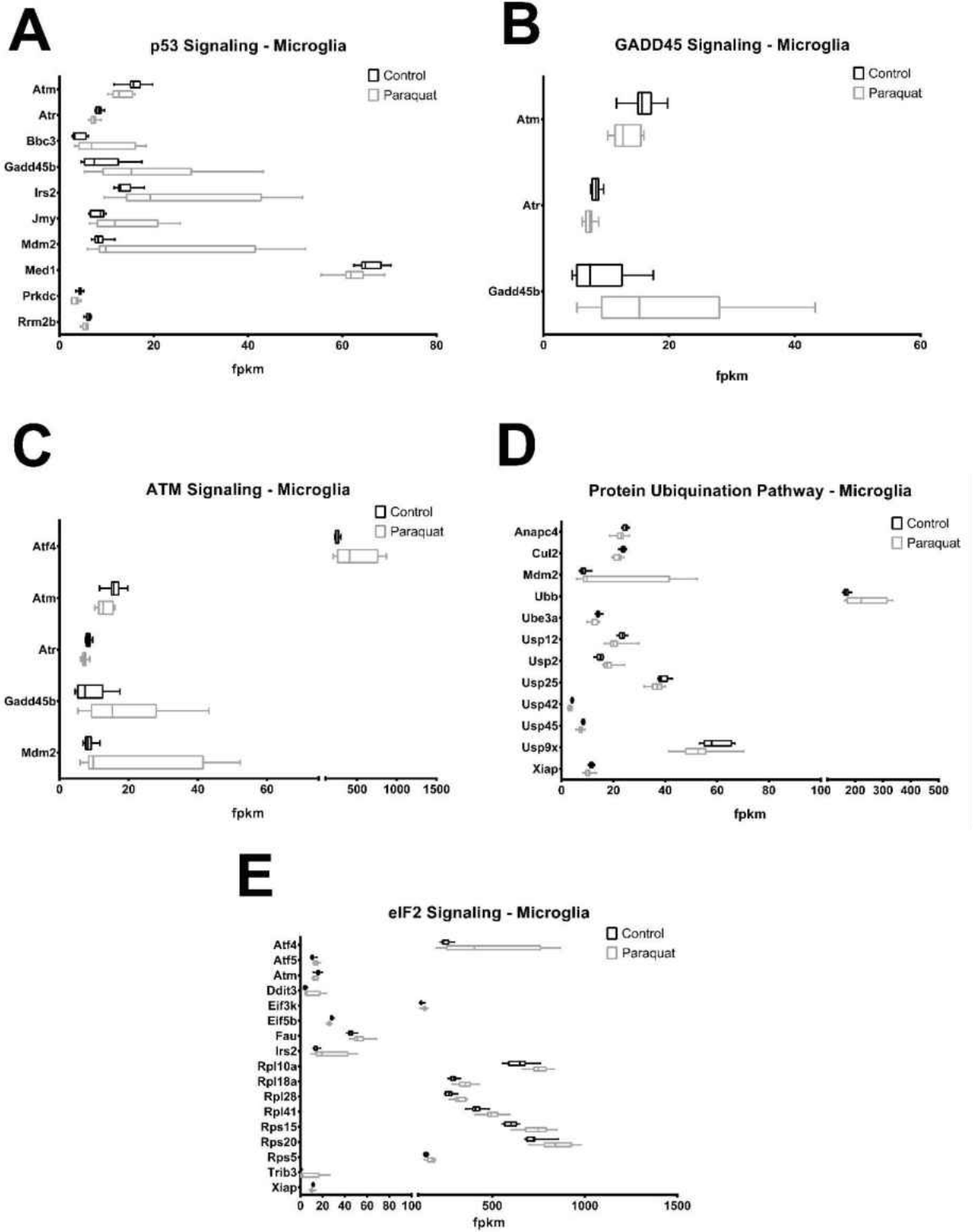
Figure 35. Several DNA damage response genes and pathways are down regulated in Paraquat exposed microglia cultures. Selected IPA pathway ontologies were expanded to identify constituents differentially expressed in pup microglia cultures from

Figure 35 cont. maternal Paraquat exposure. A) p53 signaling, p-value: 1.12×10^{-5}; B) GADD45 signaling, p-value: 3.24×10^{-3}; C) ATM signaling, p-value: 8.91×10^{-3}, D) Protein ubiquination pathway, p-value: 8.32×10^{-4} and E) eIF2 signaling, p-value: 1.02×10^{-7}. Pathways and gene constituents indicate a general decrease in expression of DNA damage sensors and repair mechanisms as well as an increase in transcription initiators.
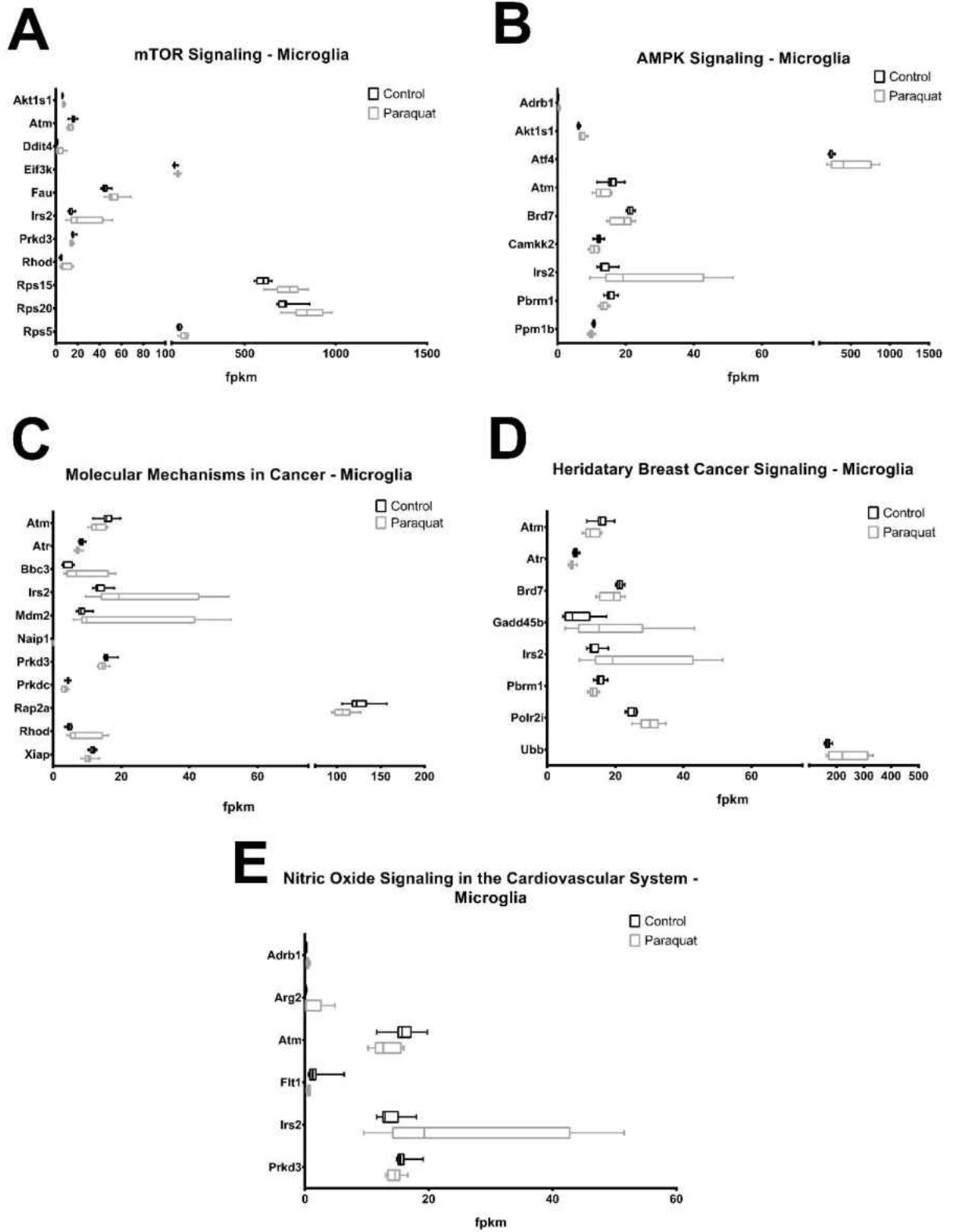
Figure 36. Several cell proliferation and apoptosis pathways and genes are dysregulated in Paraquat exposed microglia cultures. Selected IPA pathway

Figure 36 cont. ontologies were expanded to identify constituents differentially expressed in pup microglia cultures from maternal Paraquat exposure. A) mTOR signaling, p-value: 3.63×10^{-3}; B) AMPK signaling, p-value: 3.39×10^{-3}; C) Molecular mechanisms in cancer, p-value: 3.80×10^{-2}, D) Hereditary breast cancer signaling, p-value: 2.00×10^{-3} and E) Nitric oxide signaling in the cardiovascular system, p-value: 9.55×10^{-3}. Pathways and gene constituents indicate dysregulated proliferation and cell survival genes as well as apoptotic regulators.
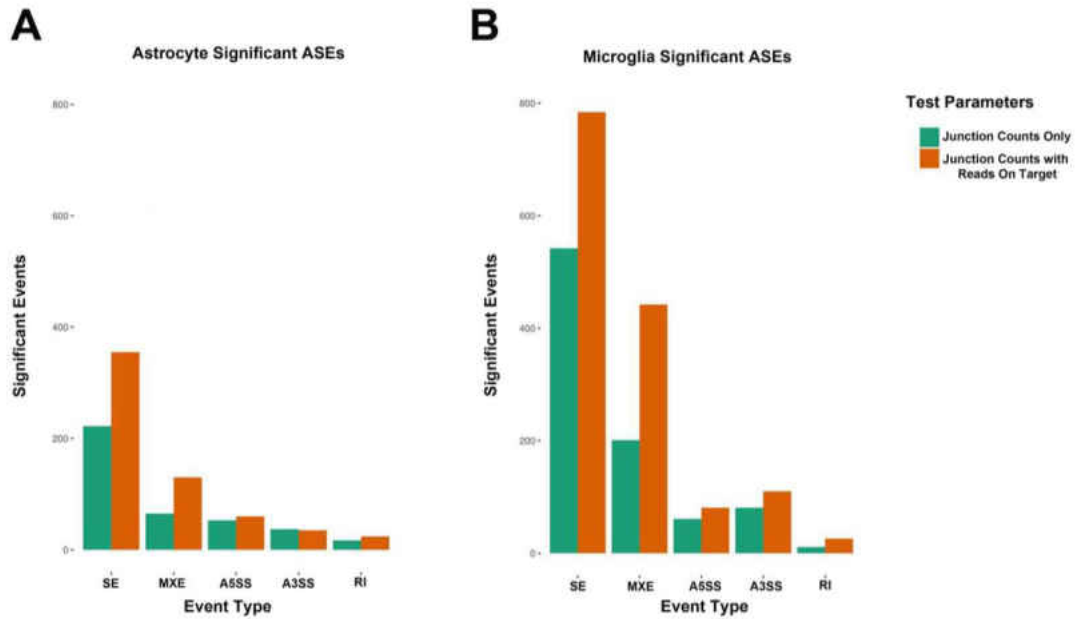
Figure 37. *In utero* **Paraquat exposure alters RNA splicing in astrocyte and microglia cultures.** Paired end RNA sequencing data was subjected to Multivariate Analysis for Transcript Splicing for A) astrocyte and B) microglia cultures. Data are represented as junction counts only and junction counts with reads on target, which indicate read events that span the junction (junction counts only) and read events which span the junction and additionally are inferred from reads on exons involved in alternative splicing events (junction counts with reads on target). Astrocyte cultures exhibited fewer alternative splicing events than that of microglia cultures, with most alternative splicing events being skipped exons. Microglia also exhibit mostly skipped exon events. Each culture type also has alternative splicing events in each event category. SE: Skipped Exon; MXE: Mutually Exclusive Exons; A5SS: Alternative 5' Splice Site; A3SS: Alternative 3' Splice Site; RI: Retained Intron.
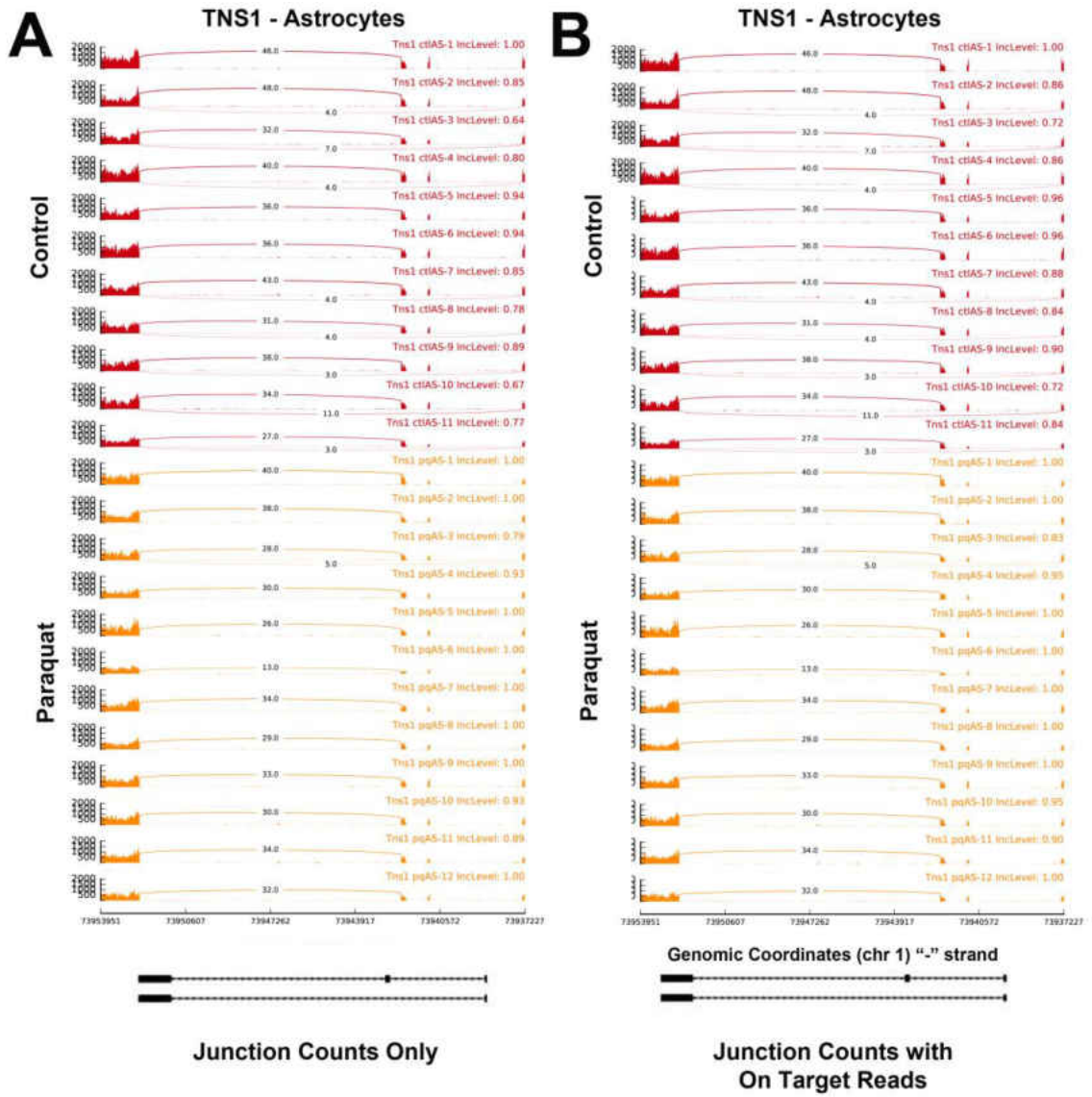
Figure 38. As an example, tensin 1 in astrocytes is alternatively spliced in *in utero* Paraquat exposure. Sashimi plots of tensin 1 gene for astrocyte culture alternative splicing data. A) Junction reads only; B) Junction reads with on target reads of tensin 1 in astrocyte cultures show cultures from maternal Paraquat exposure have preference for longer transcript of tensin 1. Some samples in control show preferential selection for longer isoform while some in Paraquat show mixed isoform selection.

CHAPTER VII

DISCUSSION

We set out to establish an early development environmental toxicant model to evaluate if a window of opportunity exists for epigenetic remodeling events that may drive future disease events. Our data reflects many of the technical difficulties in establishing such a model. We found that primary cells can have changes in DNA methylation through long term culture. These culture induced changes are important to the field as previous investigations have only noted changes in pluripotent cells [267, 269, 270, 284]. Identifying these changes may offer insight into the *in vitro* fertilization and therapeutic cell expansion fields. We propose future investigations that may help to identify how these changes occur.

We also report that different cells respond differently to an environmental toxicant in both *in vitro* and *in vivo* models. While we were only able to test two parameters in our *in vitro* models, we were able to note differences dependent on cell type. This was corroborated in the *in vivo* model as two distinct cell types had unique gene expression profiles in response to Paraquat exposure even though both cell types came from the same animal. Differential cell response to toxicants is important to understand when evaluating pharmacological effects; the heterogeneous population needs to be considered in understanding specific mechanisms. We also report that an immortalized cell line has a more robust response to a toxicant than the primary counterpart. This highlights the importance of studying primary cell cultures. Our work lays the groundwork for future studies evaluating the effect of toxicants in brain cells and continued work in evaluating Paraquat in primary cell types.

Finally we report significant and persistent changes in gene expression of neonate glial cells. Despite the absence of Paraquat in the tissues at the time of measurement, there are subtle changes that we interpret to have a potential impact driving future oncogenic events. We also begin to address the effect of a toxicant after differentiation from a pluripotent state. This work may help to define the boundaries of the window of opportunity for epigenetic remodeling if identifying a senescent or apoptotic cell population. This is important in the field of oncology in identifying from which population of cells the low mutational load cancers arise. This may also help to define the idea that environmental toxicants play a significant role in the development of disease. We can also begin to identify that segments of the population are at risk of neural disease due to environmental exposure.

We highlighted that primary cells undergo epigenetic changes induced by culture. We also presented data that astrocyte cultures respond differently to Paraquat exposure in as little as on culture event. Some of the *in vitro* work was based upon cultures that had been passaged at least once which should be repeated with fresh primary cultures to confirm the data we have found. We reported a batch effect in gene expression of *in vitro* astrocyte cultures, which could be due to different culture states, and repeating RNA sequencing would be of significant value if the culturing conditions can be controlled sufficiently. Additionally this data should be sequenced paired-end to evaluate alternative splicing events in a differentiated cell type.

We also reported differences in the two *in vivo* Paraquat exposure experiments. We outlined the differences previously, but the underrepresentation of ages in Paraquat treated animals prevents us from fully evaluating the first study. Having controlled for

the age of the animals in the second study prevented a repeat of skewed representation, but also prevented us from evaluating differences in age during pregnancy. We were also unable to evaluate the differences in littermates during maternal Paraquat exposure. The finding that littermates are not affected equally may be of significance becoming a missed opportunity. Additionally, by pooling the pups and not sexing the animals we also missed an opportunity to identify gender differences in our study. Finally having only just established the model in our lab, we were unable to identify how much we could assess in a single experiment. One critical piece of information that would direct future epigenetic studies is the accessibility of chromatin. With this data we would be able to define regions of interest and identify epigenetic targets that may play a significant role in that region.

Future Directions

Our study has yielded significant results but leaves room for further investigation. We have highlighted future directions in each individual model, but there are additional directions we could assess. One key factor that we may have identified in our model system is that maternal age in pregnancy may play a significant role in the impact of toxicant exposure. Studying the difference in maternal age in addition to environmental exposure may identify potential risk factors in developing a cancerous or neurodegenerative phenotype. Developed countries are facing advanced maternal age in bearing children, studying the effect in maternal age will have significant societal reward [391, 392].

Another area that we did not address were other tissues. We proposed that the astrocyte cultures may be more protected by the blood brain barrier thereby limiting their

exposure compared to microglia which may play a role in the differential gene expression. However, if this is true we might expect to find similar gene expression patterns in other unprotected cell types. We did not evaluate other tissues or cell types to this effect. Understanding the dichotomy between the unique tissue types may further advance our understanding of the impact of environmental toxicants in disease. This would also help to define the idea that different cells respond differently and what the difference in the cells is that defines their response.

The final future direction we will address here is the impact of additional toxicants in developmental exposure. Paraquat is not unique in its ability to inhibit mitochondrial function nor to produce reactive oxygen species. Our *in vitro* data indicate that at low concentrations, Paraquat had little impact on mitochondrial function and reactive oxygen species response was undetectable. By expanding the toxicant library we may be able to define the biological process that is most impacted by environmental toxicant exposure providing an avenue for future therapeutics. Addressing different toxicants may also define if each toxicant is unique in its own right or if there are classes of toxicants that can drive epigenetic remodeling events.

In using Paraquat as a model toxicant we offer a glimpse into developmental changes that have potential to drive future disease states. We also offer a straightforward model to address unanswered questions in environmental exposures and potentially aberrant epigenetic remodeling events.

REFERENCES

1. Raizer JJ, Fitzner KA, Jacobs DI, Bennett CL, Liebling DB, Luu TH, Trifilio SM, Grimm SA, Fisher MJ, Haleem MS *et al*: **Economics of Malignant Gliomas: A Critical Review**. *J Oncol Pract* 2015, **11**(1):e59-65.
2. Society AC: **Cancer Facts & Figures 2015**. In*.* Atlanta: American Cancer Society; 2015.
3. Kowal SL, Dall TM, Chakrabarti R, Storm MV, Jain A: **The current and projected economic burden of Parkinson's disease in the United States**. *Mov Disord* 2013, **28**(3):311-318.
4. Johnson DR, O'Neill BP: **Glioblastoma survival in the United States before and during the temozolomide era**. *J Neurooncol* 2012, **107**(2):359-364.
5. Grossman SA, Ye X, Piantadosi S, Desideri S, Nabors LB, Rosenfeld M, Fisher J: **Survival of patients with newly diagnosed glioblastoma treated with radiation and temozolomide in research studies in the United States**. *Clin Cancer Res* 2010, **16**(8):2443-2449.
6. Talacchi A, Santini B, Savazzi S, Gerosa M: **Cognitive effects of tumour and surgical treatment in glioma patients**. *J Neurooncol* 2011, **103**(3):541-549.
7. Scheibel RS, Meyers CA, Levin VA: **Cognitive dysfunction following surgery for intracerebral glioma: influence of histopathology, lesion location, and treatment**. *J Neurooncol* 1996, **30**(1):61-69.
8. Greenop KR, Peters S, Bailey HD, Fritschi L, Attia J, Scott RJ, Glass DC, de Klerk NH, Alvaro F, Armstrong BK *et al*: **Exposure to pesticides and the risk of childhood brain tumors**. *Cancer Causes Control* 2013, **24**(7):1269-1278.
9. Chen S, Gu S, Wang Y, Yao Y, Wang G, Jin Y, Wu Y: **Exposure to pyrethroid pesticides and the risk of childhood brain tumors in East China**. *Environmental Pollution* 2016, **218**:1128-1134.
10. Kunkle B, Bae S, Singh KP, Roy D: **INCREASED RISK OF CHILDHOOD BRAIN TUMORS AMONG CHILDREN WHOSE PARENTS HAD FARM-RELATED PESTICIDE EXPOSURES DURING PREGNANCY**. *JP J Biostat* 2014, **11**(2):89-101.
11. Sioen I, Den Hond E, Nelen V, Van de Mieroop E, Croes K, Van Larebeke N, Nawrot TS, Schoeters G: **Prenatal exposure to environmental contaminants and behavioural problems at age 7–8 years**. *Environment International* 2013, **59**:225-231.
12. Rohlman DS, Ismail AA, Abdel-Rasoul G, Lasarev M, Hendy O, Olson JR: **Characterizing exposures and neurobehavioral performance in Egyptian adolescent pesticide applicators**. *Metab Brain Dis* 2014, **29**(3):845-855.
13. Roberts JR, Karr CJ: **Pesticide exposure in children**. *Pediatrics* 2012, **130**(6):e1765-1788.
14. Kim SA, Lee YM, Lee HW, Jacobs DR, Jr., Lee DH: **Can Inconsistent Association between Hypertension and Cognition in Elders be Explained by Levels of Organochlorine Pesticides?** *PLoS One* 2015, **10**(12):e0144205.
15. Povey AC, McNamee R, Alhamwi H, Stocks SJ, Watkins G, Burns A, Agius R: **Pesticide exposure and screen-positive neuropsychiatric disease in British sheep farmers**. *Environmental Research* 2014, **135**:262-270.
16. Minkemeyer V, Wellman C, Goebel L: **The Impact of Alzheimer's Disease in an Aging Rural Population**. *W V Med J* 2016, **112**(3):90-93.
17. Yue W, Wang X-D, Shi Z, Wang Y, Liu S, Liu S, Zhang Y, Zhang Y, Lu H, Su W *et al*: **The prevalence of dementia with Lewy bodies in a rural area of China**. *Parkinsonism & Related Disorders* 2016, **29**:72-77.
18. Pezzoli G, Cereda E: **Exposure to pesticides or solvents and risk of Parkinson disease**. *Neurology* 2013, **80**(22):2035-2041.

19. Ritz BR, Paul KC, Bronstein JM: **Of Pesticides and Men: a California Story of Genes and Environment in Parkinson's Disease**. *Curr Environ Health Rep* 2016, **3**(1):40-52.

20. Cabré R, Naudí A, Dominguez-Gonzalez M, Ayala V, Jové M, Mota-Martorell N, Piñol-Ripoll G, Gil-Villar MP, Rué M, Portero-Otín M *et al*: **Sixty years old is the breakpoint of human frontal cortex aging**. *Free Radical Biology and Medicine* 2017, **103**:14-22.

21. Bartesaghi S, Graziano V, Galavotti S, Henriquez NV, Betts J, Saxena J, Minieri V, A D, Karlsson A, Martins LM *et al*: **Inhibition of oxidative metabolism leads to p53 genetic inactivation and transformation in neural stem cells**. *Proc Natl Acad Sci U S A* 2015, **112**(4):1059-1064.

22. Rinaldi M, Caffo M, Minutoli L, Marini H, Abbritti RV, Squadrito F, Trichilo V, Valenti A, Barresi V, Altavilla D *et al*: **ROS and Brain Gliomas: An Overview of Potential and Innovative Therapeutic Strategies**. *Int J Mol Sci* 2016, **17**(6).

23. Barker DJ: **The fetal and infant origins of adult disease**. *Bmj* 1990, **301**(6761):1111.

24. Smith CJ, Ryckman KK: **Epigenetic and developmental influences on the risk of obesity, diabetes, and metabolic syndrome**. *Diabetes Metab Syndr Obes* 2015, **8**:295-302.

25. Besson AA, Guerreiro R, Bellenger J, Ragot K, Faivre B, Sorci G: **Parental experience of a risky environment leads to improved offspring growth rate**. *J Exp Biol* 2014, **217**(Pt 15):2734-2739.

26. Malta A, de Moura EG, Ribeiro TA, Tofolo LP, Abdennebi-Najar L, Vieau D, Barella LF, de Freitas Mathias PC, Lisboa PC, de Oliveira JC: **Protein-energy malnutrition at mid-adulthood does not imprint long-term metabolic consequences in male rats**. *Eur J Nutr* 2016, **55**(4):1423-1433.

27. Baxi DB, Singh PK, Vachhrajani KD, Ramachandran AV: **Neonatal corticosterone programs for thrifty phenotype adult diabetic manifestations and oxidative stress: countering effect of melatonin as a deprogrammer**. *J Matern Fetal Neonatal Med* 2012, **25**(9):1574-1585.

28. Xie SH, Lagergren J: **A Possible Link between Famine Exposure in Early Life and Future Risk of Gastrointestinal Cancers: Implications from Age-Period-Cohort Analysis**. *Int J Cancer* 2016.

29. Demetriou CA, van Veldhoven K, Relton C, Stringhini S, Kyriacou K, Vineis P: **Biological embedding of early-life exposures and disease risk in humans: a role for DNA methylation**. *Eur J Clin Invest* 2015, **45**(3):303-332.

30. Sweatt JD: **The Emerging Field of Neuroepigenetics**. *Neuron* 2013, **80**(3):624-632.

31. Gardiner-Garden M, Frommer M: **CpG islands in vertebrate genomes**. *J Mol Biol* 1987, **196**(2):261-282.

32. Esteller M: **CpG island hypermethylation and tumor suppressor genes: a booming present, a brighter future**. *Oncogene* 2002, **21**(35):5427-5440.

33. Edgar R, Tan PP, Portales-Casamar E, Pavlidis P: **Meta-analysis of human methylomes reveals stably methylated sequences surrounding CpG islands associated with high gene expression**. *Epigenetics Chromatin* 2014, **7**(1):28.

34. Irizarry RA, Ladd-Acosta C, Wen B, Wu Z, Montano C, Onyango P, Cui H, Gabo K, Rongione M, Webster M *et al*: **The human colon cancer methylome shows similar hypo- and hypermethylation at conserved tissue-specific CpG island shores**. *Nat Genet* 2009, **41**(2):178-186.

35. Doi A, Park IH, Wen B, Murakami P, Aryee MJ, Irizarry R, Herb B, Ladd-Acosta C, Rho J, Loewer S *et al*: **Differential methylation of tissue- and cancer-specific CpG island shores distinguishes human induced pluripotent stem cells, embryonic stem cells and fibroblasts**. *Nat Genet* 2009, **41**(12):1350-1353.

36. Merlo A, Herman JG, Mao L, Lee DJ, Gabrielson E, Burger PC, Baylin SB, Sidransky D: **5' CpG island methylation is associated with transcriptional silencing of the tumour suppressor p16/CDKN2/MTS1 in human cancers**. *Nat Med* 1995, **1**(7):686-692.

37. Herman JG, Merlo A, Mao L, Lapidus RG, Issa JP, Davidson NE, Sidransky D, Baylin SB: **Inactivation of the CDKN2/p16/MTS1 gene is frequently associated with aberrant DNA methylation in all common human cancers**. *Cancer Res* 1995, **55**(20):4525-4530.

38. Gonzalez-Zulueta M, Bender CM, Yang AS, Nguyen T, Beart RW, Van Tornout JM, Jones PA: **Methylation of the 5' CpG island of the p16/CDKN2 tumor suppressor gene in normal and transformed human tissues correlates with gene silencing**. *Cancer Res* 1995, **55**(20):4531-4535.

39. Maurano Matthew T, Wang H, John S, Shafer A, Canfield T, Lee K, Stamatoyannopoulos John A: **Role of DNA Methylation in Modulating Transcription Factor Occupancy**. *Cell Reports* 2015, **12**(7):1184-1195.

40. Hing B, Ramos E, Braun P, McKane M, Jancic D, Tamashiro KL, Lee RS, Michaelson JJ, Druley TE, Potash JB: **Adaptation of the targeted capture Methyl-Seq platform for the mouse genome identifies novel tissue-specific DNA methylation patterns of genes involved in neurodevelopment**. *Epigenetics* 2015, **10**(7):581-596.

41. Spiers H, Hannon E, Schalkwyk LC, Smith R, Wong CC, O'Donovan MC, Bray NJ, Mill J: **Methylomic trajectories across human fetal brain development**. *Genome Res* 2015, **25**(3):338-352.

42. Shelton AL, Cornish KM, Kolbe S, Clough M, Slater HR, Li X, Kraan CM, Bui QM, Godler DE, Fielding J: **Brain structure and intragenic DNA methylation are correlated, and predict executive dysfunction in fragile X premutation females**. *Transl Psychiatry* 2016, **6**(12):e984.

43. Meissner A, Mikkelsen TS, Gu H, Wernig M, Hanna J, Sivachenko A, Zhang X, Bernstein BE, Nusbaum C, Jaffe DB *et al*: **Genome-scale DNA methylation maps of pluripotent and differentiated cells**. *Nature* 2008, **454**(7205):766-770.

44. Amir RE, Van den Veyver IB, Wan M, Tran CQ, Francke U, Zoghbi HY: **Rett syndrome is caused by mutations in X-linked MECP2, encoding methyl-CpG-binding protein 2**. *Nat Genet* 1999, **23**(2):185-188.

45. Smrt RD, Pfeiffer RL, Zhao X: **Age-dependent expression of MeCP2 in a heterozygous mosaic mouse model**. *Hum Mol Genet* 2011, **20**(9):1834-1843.

46. Garg SK, Lioy DT, Cheval H, McGann JC, Bissonnette JM, Murtha MJ, Foust KD, Kaspar BK, Bird A, Mandel G: **Systemic delivery of MeCP2 rescues behavioral and cellular deficits in female mouse models of Rett syndrome**. *J Neurosci* 2013, **33**(34):13612-13620.

47. Szulwach KE, Li X, Li Y, Song CX, Wu H, Dai Q, Irier H, Upadhyay AK, Gearing M, Levey AI *et al*: **5-hmC-mediated epigenetic dynamics during postnatal neurodevelopment and aging**. *Nat Neurosci* 2011, **14**(12):1607-1616.

48. Jin B, Li Y, Robertson KD: **DNA methylation: superior or subordinate in the epigenetic hierarchy?** *Genes Cancer* 2011, **2**(6):607-617.

49. Tahiliani M, Koh KP, Shen Y, Pastor WA, Bandukwala H, Brudno Y, Agarwal S, Iyer LM, Liu DR, Aravind L *et al*: **Conversion of 5-methylcytosine to 5-hydroxymethylcytosine in mammalian DNA by MLL partner TET1**. *Science* 2009, **324**(5929):930-935.

50. Guo JU, Su Y, Zhong C, Ming GL, Song H: **Hydroxylation of 5-methylcytosine by TET1 promotes active DNA demethylation in the adult brain**. *Cell* 2011, **145**(3):423-434.

51. Kriaucionis S, Heintz N: **The nuclear DNA base 5-hydroxymethylcytosine is present in Purkinje neurons and the brain**. *Science* 2009, **324**(5929):929-930.

52. Yildirim O, Li R, Hung JH, Chen PB, Dong X, Ee LS, Weng Z, Rando OJ, Fazzio TG: **Mbd3/NURD complex regulates expression of 5-hydroxymethylcytosine marked genes in embryonic stem cells**. *Cell* 2011, **147**(7):1498-1510.

53. Li S, Papale LA, Zhang Q, Madrid A, Chen L, Chopra P, Keleş S, Jin P, Alisch RS: **Genome-wide alterations in hippocampal 5-hydroxymethylcytosine links plasticity genes to acute stress**. *Neurobiology of Disease* 2016, **86**:99-108.

54. Li W, Liu M: **Distribution of 5-hydroxymethylcytosine in different human tissues**. *J Nucleic Acids* 2011, **2011**:870726.

55. Valinluck V, Sowers LC: **Endogenous Cytosine damage products alter the site selectivity of human DNA methyltransferase DNMT1**. *Cancer Research* 2007, **67**:946-950.

56. Chuang LS, Ian HI, Koh TW, Ng HH, Xu G, Li BF: **Human DNA-(cytosine-5) methyltransferase-PCNA complex as a target for p21WAF1**. *Science* 1997, **277**(5334):1996-2000.

57. Chin HG, Ponnaluri VK, Zhang G, Esteve PO, Schaus SE, Hansen U, Pradhan S: **Transcription factor LSF-DNMT1 complex dissociation by FQI1 leads to aberrant DNA methylation and gene expression**. *Oncotarget* 2016.

58. Niu Y, DesMarais TL, Tong Z, Yao Y, Costa M: **Oxidative stress alters global histone modification and DNA methylation**. *Free Radical Biology and Medicine* 2015, **82**:22-28.

59. Zhao B, Yang Y, Wang X, Chong Z, Yin R, Song SH, Zhao C, Li C, Huang H, Sun BF *et al*: **Redox-active quinones induces genome-wide DNA methylation changes by an iron-mediated and Tet-dependent mechanism**. *Nucleic Acids Res* 2014, **42**(3):1593-1605.

60. Park SY, Kim KS, Lee YM, Kim MJ, Jacobs DR, Jr., Porta M, Kim DS, Lee DH: **Persistent organic pollutants and promoter hypermethylation of the O(6)-methylguanine-DNA methyltransferase gene**. *Biomarkers* 2015, **20**(2):136-142.

61. Zhang X, Wallace AD, Du P, Kibbe WA, Jafari N, Xie H, Lin S, Baccarelli A, Soares MB, Hou L: **DNA methylation alterations in response to pesticide exposure in vitro**. *Environ Mol Mutagen* 2012, **53**(7):542-549.

62. Long HK, King HW, Patient RK, Odom DT, Klose RJ: **Protection of CpG islands from DNA methylation is DNA-encoded and evolutionarily conserved**. *Nucleic Acids Res* 2016.

63. Valinluck-Lao V, Herring JL, Kim CH, Darwanto A, Soto U, Sowers LC: **Incorporation of 5-chlorocytosine into mammalian DNA results in heritable gene silencing and altered cytosine methylation patterns**. *Carcinogenesis* 2009, **30**(5):886-893.

64. Whiteman A, Jenner A, Halliwell B: **Hypochlorous acid-induced base modifications in isolated calf thymus DNA**. *Chemical Research in Toxicology* 1997, **10**:1240-1246.

65. Fedeles BI, Freudenthal BD, Yau E, Singh V, Chang SC, Li D, Delaney JC, Wilson SH, Essigmann JM: **Intrinsic mutagenic properties of 5-chlorocytosine: A mechanistic connection between chronic inflammation and cancer**. *Proc Natl Acad Sci U S A* 2015, **112**(33):E4571-4580.

66. Jin J, Lian T, Gu C, Yu K, Gao YQ, Su XD: **The effects of cytosine methylation on general transcription factors**. *Sci Rep* 2016, **6**:29119.

67. Zhang D, Wu B, Wang P, Wang Y, Lu P, Nechiporuk T, Floss T, Greally JM, Zheng D, Zhou B: **Non-CpG methylation by DNMT3B facilitates REST binding and gene silencing in developing mouse hearts**. *Nucleic Acids Res* 2016.

68. Guo JU, Su Y, Shin JH, Shin J, Li H, Xie B, Zhong C, Hu S, Le T, Fan G *et al*: **Distribution, recognition and regulation of non-CpG methylation in the adult mammalian brain**. *Nat Neurosci* 2014, **17**(2):215-222.

69. Lister R, Mukamel EA, Nery JR, Urich M, Puddifoot CA, Johnson ND, Lucero J, Huang Y, Dwork AJ, Schultz MD *et al*: **Global epigenomic reconfiguration during mammalian brain development**. *Science* 2013, **341**(6146):1237905.

70. Kinde B, Wu DY, Greenberg ME, Gabel HW: **DNA methylation in the gene body influences MeCP2-mediated gene repression**. *Proc Natl Acad Sci U S A* 2016.

71. Grimaud C, Negre N, Cavalli G: **From genetics to epigenetics: the tale of Polycomb group and trithorax group genes**. *Chromosome Res* 2006, **14**(4):363-375.

72. Ku M, Koche RP, Rheinbay E, Mendenhall EM, Endoh M, Mikkelsen TS, Presser A, Nusbaum C, Xie X, Chi AS *et al*: **Genomewide analysis of PRC1 and PRC2 occupancy identifies two classes of bivalent domains**. *PLoS Genet* 2008, **4**(10):e1000242.

73. Cao R, Wang L, Wang H, Xia L, Erdjument-Bromage H, Tempst P, Jones RS, Zhang Y: **Role of histone H3 lysine 27 methylation in Polycomb-group silencing**. *Science* 2002, **298**(5595):1039-1043.

74. Bernstein BE, Mikkelsen TS, Xie X, Kamal M, Huebert DJ, Cuff J, Fry B, Meissner A, Wernig M, Plath K *et al*: **A Bivalent Chromatin Structure Marks Key Developmental Genes in Embryonic Stem Cells**. *Cell* 2006, **125**(2):315-326.

75. Oliviero G, Brien GL, Waston A, Streubel G, Jerman E, Andrews D, Doyle B, Munawar N, Wynne K, Crean J *et al*: **Dynamic Protein Interactions of the Polycomb Repressive Complex 2 during Differentiation of Pluripotent Cells**. *Mol Cell Proteomics* 2016, **15**(11):3450-3460.

76. Margueron R, Reinberg D: **The Polycomb complex PRC2 and its mark in life**. *Nature* 2011, **469**(7330):343-349.

77. Satijn DP, Otte AP: **RING1 interacts with multiple Polycomb-group proteins and displays tumorigenic activity**. *Mol Cell Biol* 1999, **19**(1):57-68.

78. de Napoles M, Mermoud JE, Wakao R, Tang YA, Endoh M, Appanah R, Nesterova TB, Silva J, Otte AP, Vidal M *et al*: **Polycomb Group Proteins Ring1A/B Link Ubiquitylation of Histone H2A to Heritable Gene Silencing and X Inactivation**. *Developmental Cell* 2004, **7**(5):663-676.

79. Taherbhoy AM, Huang OW, Cochran AG: **BMI1-RING1B is an autoinhibited RING E3 ubiquitin ligase**. *Nat Commun* 2015, **6**:7621.

80. Gray F, Cho HJ, Shukla S, He S, Harris A, Boytsov B, Jaremko L, Jaremko M, Demeler B, Lawlor ER *et al*: **BMI1 regulates PRC1 architecture and activity through homo- and hetero-oligomerization**. *Nat Commun* 2016, **7**:13343.

81. Abdouh M, Facchino S, Chatoo W, Balasingam V, Ferreira J, Bernier G: **BMI1 sustains human glioblastoma multiforme stem cell renewal**. *J Neurosci* 2009, **29**(28):8884-8896.

82. Molofsky AV, He S, Bydon M, Morrison SJ, Pardal R: **Bmi-1 promotes neural stem cell self-renewal and neural development but not mouse growth and survival by repressing the p16Ink4a and p19Arf senescence pathways**. *Genes Dev* 2005, **19**(12):1432-1437.

83. Abdouh M, Chatoo W, El Hajjar J, David J, Ferreira J, Bernier G: **Bmi1 is down-regulated in the aging brain and displays antioxidant and protective activities in neurons**. *PLoS One* 2012, **7**(2):e31870.

84. von Schimmelmann M, Feinberg PA, Sullivan JM, Ku SM, Badimon A, Duff MK, Wang Z, Lachmann A, Dewell S, Ma'ayan A *et al*: **Polycomb repressive complex 2 (PRC2) silences genes responsible for neurodegeneration**. *Nat Neurosci* 2016, **19**(10):1321-1330.

85. Zemke M, Draganova K, Klug A, Schöler A, Zurkirchen L, Gay MH-P, Cheng P, Koseki H, Valenta T, Schübeler D *et al*: **Loss of Ezh2 promotes a midbrain-to-forebrain identity**

switch by direct gene derepression and Wnt-dependent regulation. *BMC Biology* 2015, **13**(1):1.

86. Kuzmichev A, Nishioka K, Erdjument-Bromage H, Tempst P, Reinberg D: **Histone methyltransferase activity associated with a human multiprotein complex containing the Enhancer of Zeste protein**. *Genes Dev* 2002, **16**(22):2893-2905.

87. Sarma K, Margueron R, Ivanov A, Pirrotta V, Reinberg D: **Ezh2 requires PHF1 to efficiently catalyze H3 lysine 27 trimethylation in vivo**. *Mol Cell Biol* 2008, **28**(8):2718-2731.

88. Zhao L, Li J, Ma Y, Wang J, Pan W, Gao K, Zhang Z, Lu T, Ruan Y, Yue W *et al*: **Ezh2 is involved in radial neuronal migration through regulating Reelin expression in cerebral cortex**. *Sci Rep* 2015, **5**:15484.

89. Xie H, Xu J, Hsu Jessie H, Nguyen M, Fujiwara Y, Peng C, Orkin Stuart H: **Polycomb Repressive Complex 2 Regulates Normal Hematopoietic Stem Cell Function in a Developmental-Stage-Specific Manner**. *Cell Stem Cell* 2014, **14**(1):68-80.

90. Ura H, Usuda M, Kinoshita K, Sun C, Mori K, Akagi T, Matsuda T, Koide H, Yokota T: **STAT3 and Oct-3/4 control histone modification through induction of Eed in embryonic stem cells**. *J Biol Chem* 2008, **283**(15):9713-9723.

91. Hirabayashi Y, Suzki N, Tsuboi M, Endo TA, Toyoda T, Shinga J, Koseki H, Vidal M, Gotoh Y: **Polycomb Limits the Neurogenic Competence of Neural Precursor Cells to Promote Astrogenic Fate Transition**. *Neuron* 2009, **63**(5):600-613.

92. O'Hagan H, Wang W, Sen S, Sheilds CD, Lee SS, Zhang YW, Clements EG, Cai Y, Neste LV, Easwaran H *et al*: **Oxidative damage targets complexes containing DNA methyltransferases, SIRT1 and polycomb members to promoter CpG islands**. *Cancer Cell* 2011, **5**(20):606-619.

93. Lu L, Luo F, Liu Y, Liu X, Shi L, Lu X, Liu Q: **Posttranscriptional silencing of the lncRNA MALAT1 by miR-217 inhibits the epithelial–mesenchymal transition via enhancer of zeste homolog 2 in the malignant transformation of HBE cells induced by cigarette smoke extract**. *Toxicology and Applied Pharmacology* 2015, **289**(2):276-285.

94. Pandey M, Sahay S, Tiwari P, Upadhyay DS, Sultana S, Gupta KP: **Involvement of EZH2, SUV39H1, G9a and associated molecules in pathogenesis of urethane induced mouse lung tumors: Potential targets for cancer control**. *Toxicology and Applied Pharmacology* 2014, **280**(2):296-304.

95. Stern S, Snir O, Mizrachi E, Galili M, Zaltsman I, Soen Y: **Reduction in maternal Polycomb levels contributes to transgenerational inheritance of a response to toxic stress in flies**. *J Physiol* 2014, **592**(11):2343-2355.

96. Doherty LF, Bromer JG, Zhou Y, Aldad TS, Taylor HS: **In utero exposure to diethylstilbestrol (DES) or bisphenol-A (BPA) increases EZH2 expression in the mammary gland: an epigenetic mechanism linking endocrine disruptors to breast cancer**. *Horm Cancer* 2010, **1**(3):146-155.

97. Zhou M, Pasa-Tolic L, Stenoien DL: **Profiling of Histone Post-Translational Modifications in Mouse Brain with High-Resolution Top-Down Mass Spectrometry**. *J Proteome Res* 2016.

98. Song C, Kanthasamy A, Jin H, Anantharam V, Kanthasamy AG: **Paraquat induces epigenetic changes by promoting histone acetylation in cell culture models of dopaminergic degeneration**. *NeuroToxicology* 2011, **32**(5):586-595.

99. Jia H, Wang Y, Morris CD, Jacques V, Gottesfeld JM, Rusche JR, Thomas EA: **The Effects of Pharmacological Inhibition of Histone Deacetylase 3 (HDAC3) in Huntington's Disease Mice**. *PLoS One* 2016, **11**(3):e0152498.

100.   Qin HT, Li HQ, Liu F: **Selective histone deacetylase small molecule inhibitors: recent progress and perspectives**. *Expert Opin Ther Pat* 2017, **27**(5):621-636.

101.   Pinho BR, Reis SD, Guedes-Dias P, Leitão-Rocha A, Quintas C, Valentão P, Andrade PB, Santos MM, Oliveira JMA: **Pharmacological modulation of HDAC1 and HDAC6 in vivo in a zebrafish model: Therapeutic implications for Parkinson's disease**. *Pharmacological Research* 2016, **103**:328-339.

102.   Sanchez-Arias JA, Rabal O, Cuadrado-Tejedor M, de Miguel I, Perez-Gonzalez M, Ugarte A, Saez E, Espelosin M, Ursua S, Haizhong T *et al*: **Impact of Scaffold Exploration on Novel Dual-Acting Histone Deacetylases and Phosphodiesterase 5 Inhibitors for the Treatment of Alzheimer's Disease**. *ACS Chem Neurosci* 2016.

103.   Rougeulle C, Navarro P, Avner P: **Promoter-restricted H3 Lys 4 di-methylation is an epigenetic mark for monoallelic expression**. *Hum Mol Genet* 2003, **12**(24):3343-3348.

104.   Hayashi A, Yamauchi N, Shibahara J, Kimura H, Morikawa T, Ishikawa S, Nagae G, Nishi A, Sakamoto Y, Kokudo N *et al*: **Concurrent activation of acetylation and tri-methylation of H3K27 in a subset of hepatocellular carcinoma with aggressive behavior**. *PLoS One* 2014, **9**(3):e91330.

105.   Tian B, Zhao Y, Sun H, Zhang Y, Yang J, Brasier AR: **BRD4 mediates NF-kappaB-dependent epithelial-mesenchymal transition and pulmonary fibrosis via transcriptional elongation**. *Am J Physiol Lung Cell Mol Physiol* 2016, **311**(6):L1183-l1201.

106.   Wang B, Sun J, Shi J, Guo Q, Tong X, Zhang J, Hu N, Hu Y: **Small-Activating RNA Can Change Nucleosome Positioning in Human Fibroblasts**. *J Biomol Screen* 2016, **21**(6):634-642.

107.   Kusevic D, Kudithipudi S, Iglesias N, Moazed D, Jeltsch A: **Clr4 specificity and catalytic activity beyond H3K9 methylation**. *Biochimie* 2017, **135**:83-88.

108.   Minoux M, Holwerda S, Vitobello A, Kitazawa T, Kohler H, Stadler MB, Rijli FM: **Gene bivalency at Polycomb domains regulates cranial neural crest positional identity**. *Science* 2017, **355**(6332).

109.   Harikumar A, Meshorer E: **Chromatin remodeling and bivalent histone modifications in embryonic stem cells**. *EMBO Rep* 2015, **16**(12):1609-1619.

110.   Yakovlev A, Khafizova M, Abdullaev Z, Loukinov D, Kondratyev A: **Epigenetic regulation of caspase-3 gene expression in rat brain development**. *Gene* 2010, **450**(1–2):103-108.

111.   Buttner N, Johnsen SA, Kugler S, Vogel T: **Af9/Mllt3 interferes with Tbr1 expression through epigenetic modification of histone H3K79 during development of the cerebral cortex**. *Proc Natl Acad Sci U S A* 2010, **107**(15):7042-7047.

112.   Zhang J, Parvin J, Huang K: **Redistribution of H3K4me2 on neural tissue specific genes during mouse brain development**. *BMC Genomics* 2012, **13 Suppl 8**:S5.

113.   Pekowska A, Benoukraf T, Ferrier P, Spicuglia S: **A unique H3K4me2 profile marks tissue-specific gene regulation**. *Genome Res* 2010, **20**(11):1493-1502.

114.   Luo C, Lancaster MA, Castanon R, Nery JR, Knoblich JA, Ecker JR: **Cerebral Organoids Recapitulate Epigenomic Signatures of the Human Fetal Brain**. *Cell Reports* 2016, **17**(12):3369-3384.

115.   Zhang Q, Xue P, Li H, Bao Y, Wu L, Chang S, Niu B, Yang F, Zhang T: **Histone modification mapping in human brain reveals aberrant expression of histone H3 lysine 79 dimethylation in neural tube defects**. *Neurobiology of Disease* 2013, **54**:404-413.

116.   Ullah M, Pelletier N, Xiao L, Zhao SP, Wang K, Degerny C, Tahmasebi S, Cayrou C, Doyon Y, Goh SL *et al*: **Molecular architecture of quartet MOZ/MORF histone acetyltransferase complexes**. *Mol Cell Biol* 2008, **28**(22):6828-6843.

117. You L, Zou J, Zhao H, Bertos NR, Park M, Wang E, Yang XJ: **Deficiency of the chromatin regulator BRPF1 causes abnormal brain development**. *J Biol Chem* 2015, **290**(11):7114-7129.

118. Tyler CR, Hafez AK, Solomon ER, Allan AM: **Developmental exposure to 50 parts-per-billion arsenic influences histone modifications and associated epigenetic machinery in a region- and sex-specific manner in the adult mouse brain**. *Toxicology and Applied Pharmacology* 2015, **288**(1):40-51.

119. Gadhia SR, O'Brien D, Barile FA: **Cadmium affects mitotically inherited histone modification pathways in mouse embryonic stem cells**. *Toxicology in Vitro* 2015, **30**(1, Part B):583-592.

120. Veazey KJ, Parnell SE, Miranda RC, Golding MC: **Dose-dependent alcohol-induced alterations in chromatin structure persist beyond the window of exposure and correlate with fetal alcohol syndrome birth defects**. *Epigenetics Chromatin* 2015, **8**:39.

121. Song C, Kanthasamy A, Anantharam V, Sun F, Kanthasamy AG: **Environmental neurotoxic pesticide increases histone acetylation to promote apoptosis in dopaminergic neuronal cells: relevance to epigenetic mechanisms of neurodegeneration**. *Mol Pharmacol* 2010, **77**(4):621-632.

122. Jorgenson JL: **Aldrin and dieldrin: a review of research on their production, environmental deposition and fate, bioaccumulation, toxicology, and epidemiology in the United States**. *Environ Health Perspect* 2001, **109 Suppl 1**:113-139.

123. Ravindra KC, Trudel LJ, Wishnok JS, Wogan GN, Tannenbaum SR, Skipper PL: **Hydroxyphenylation of Histone Lysines: Post-translational Modification by Quinone Imines**. *ACS Chem Biol* 2016, **11**(5):1230-1237.

124. Taouis M: **MicroRNAs in the hypothalamus**. *Best Practice & Research Clinical Endocrinology & Metabolism* 2016, **30**(5):641-651.

125. Giraldez AJ, Cinalli RM, Glasner ME, Enright AJ, Thomson JM, Baskerville S, Hammond SM, Bartel DP, Schier AF: **MicroRNAs regulate brain morphogenesis in zebrafish**. *Science* 2005, **308**(5723):833-838.

126. Kasai A, Kakihara S, Miura H, Okada R, Hayata-Takano A, Hazama K, Niu M, Shintani N, Nakazawa T, Hashimoto H: **Double In situ Hybridization for MicroRNAs and mRNAs in Brain Tissues**. *Front Mol Neurosci* 2016, **9**:126.

127. Rao YS, Pak TR: **microRNAs and the adolescent brain: Filling the knowledge gap**. *Neuroscience & Biobehavioral Reviews* 2016, **70**:313-322.

128. Ragan C, Patel K, Edson J, Zhang ZH, Gratten J, Mowry B: **Small non-coding RNA expression from anterior cingulate cortex in schizophrenia shows sex specific regulation**. *Schizophr Res* 2016.

129. Abrajano JJ, Qureshi IA, Gokhan S, Zheng D, Bergman A, Mehler MF: **REST and CoREST modulate neuronal subtype specification, maturation and maintenance**. *PLoS One* 2009, **4**(12):e7936.

130. Tyler CR, Labrecque MT, Solomon ER, Guo X, Allan AM: **Prenatal arsenic exposure alters REST/NRSF and microRNA regulators of embryonic neural stem cell fate in a sex-dependent manner**. *Neurotoxicology and Teratology*.

131. Nechiporuk T, McGann J, Mullendorff K, Hsieh J, Wurst W, Floss T, Mandel G: **The REST remodeling complex protects genomic integrity during embryonic neurogenesis**. *Elife* 2016, **5**:e09584.

132. Lu T, Aron L, Zullo J, Pan Y, Kim H, Chen Y, Yang TH, Kim HM, Drake D, Liu XS *et al*: **REST and stress resistance in ageing and Alzheimer's disease**. *Nature* 2014, **507**(7493):448-454.

133. Huang M, Lou D, Wang Y-P, Cai Q, Li H-h: **Paraquat inhibited differentiation in human neural progenitor cells (hNPCs) and down regulated miR-200a expression by targeting CTNNB1**. *Environmental Toxicology and Pharmacology* 2016, **42**:205-211.

134. Disayabutr S, Kim EK, Cha SI, Green G, Naikawadi RP, Jones KD, Golden JA, Schroeder A, Matthay MA, Kukreja J *et al*: **miR-34 miRNAs Regulate Cellular Senescence in Type II Alveolar Epithelial Cells of Patients with Idiopathic Pulmonary Fibrosis**. *PLoS One* 2016, **11**(6):e0158367.

135. Marques TM, Kuiperij HB, Bruinsma IB, van Rumund A, Aerts MB, Esselink RA, Bloem BR, Verbeek MM: **MicroRNAs in Cerebrospinal Fluid as Potential Biomarkers for Parkinson's Disease and Multiple System Atrophy**. *Mol Neurobiol* 2016.

136. Moustaka J, Moustakas M: **Photoprotective mechanism of the non-target organism Arabidopsis thaliana to paraquat exposure**. *Pesticide Biochemistry and Physiology* 2014, **111**:1-6.

137. Zhou DC, Zhang H, Luo ZM, Zhu QX, Zhou CF: **Prognostic value of hematological parameters in patients with paraquat poisoning**. *Sci Rep* 2016, **6**:36235.

138. Cha ES, Khang YH, Lee WJ: **Mortality from and incidence of pesticide poisoning in South Korea: findings from National Death and Health Utilization Data between 2006 and 2010**. *PLoS One* 2014, **9**(4):e95299.

139. Weng CH, Hu CC, Lin JL, Lin-Tan DT, Huang WH, Hsu CW, Yen TH: **Sequential organ failure assessment score can predict mortality in patients with paraquat intoxication**. *PLoS One* 2012, **7**(12):e51743.

140. Kitahara J, Yamanaka K, Kato K, Lee YW, Klein CB, Costa M: **Mutagenicity of cobalt and reactive oxygen producers**. *Mutat Res* 1996, **370**(3-4):133-140.

141. Posecion NC, Ostrea EM, Bielawski DM: **Quantitative determination of paraquat in meconium by sodium borohydride-nickel chloride chemical reduction and gas chromatography/mass spectrometry (GC/MS)**. *Journal of Chromatography B* 2008, **862**(1–2):93-99.

142. Huang C, Zhang X, Jiang Y, Li G, Wang H, Tang X, Wang Q: **Paraquat-induced convulsion and death: a report of five cases**. *Toxicol Ind Health* 2013, **29**(8):722-727.

143. !!! INVALID CITATION !!!

144. Rudyk C, Litteljohn D, Syed S, Dwyer Z, Hayley S: **Paraquat and psychological stressor interactions as pertains to Parkinsonian co-morbidity**. *Neurobiology of Stress* 2015, **2**:85-93.

145. McCormack AL, Thiruchelvam M, Manning-Bog AB, Thiffault C, Langston JW, Cory-Slechta DA, Di Monte D: **Environmental risk factors and Parkinson's disease: Selective degeneration of nigral dopaminergic neurons caused by the herbicide paraquat**. *Neurobiology of Disease* 2002, **10**:119-127.

146. Barbeau A, Dallaire L, Buu NT, Poirier J, Rucinska E: **Comparative behavioral, biochemical and pigmentary effects of MPTP, MPP+ and paraquat in Rana pipiens**. *Life Sci* 1985, **37**(16):1529-1538.

147. Mann VM, Cooper JM, Daniel SE, Srai K, Jenner P, Marsden CD, Schapira AH: **Complex I, iron, and ferritin in Parkinson's disease substantia nigra**. *Ann Neurol* 1994, **36**(6):876-881.

148. Richardson JR, Quan Y, Sherer TB, Greenamyre JT, Miller GW: **Paraquat Neurotoxicity is distinct from that of MPTP and Rotenone**. *Toxicological Sciences* 2005, **88**(1):193-201.

149. de Oliveira MR, Ferreira GC, Schuck PF: **Protective effect of carnosic acid against paraquat-induced redox impairment and mitochondrial dysfunction in SH-SY5Y cells: Role for PI3K/Akt/Nrf2 pathway**. *Toxicology in Vitro* 2016, **32**:41-54.

150. Kim E, Leverage WT, Liu Y, Panzella L, Alfieri ML, Napolitano A, Bentley WE, Payne GF: **Paraquat-Melanin Redox-Cycling: Evidence from Electrochemical Reverse Engineering**. *ACS Chem Neurosci* 2016, **7**(8):1057-1067.

151. Lei S, Zavala-Flores L, Garcia-Garcia A, Nandakumar R, Huang Y, Madayiputhiya N, Stanton RC, Dodds ED, Powers R, Franco R: **Alterations in energy/redox metabolism induced by mitochondrial and environmental toxins: a specific role for glucose-6-phosphate-dehydrogenase and the pentose phosphate pathway in paraquat toxicity**. *ACS Chem Biol* 2014, **9**(9):2032-2048.

152. Aliaga ME, Carrasco-Pozo C, López-Alarcón C, Olea-Azar C, Speisky H: **Superoxide-dependent reduction of free Fe3+ and release of Fe2+ from ferritin by the physiologically-occurring Cu(I)–glutathione complex**. *Bioorganic & Medicinal Chemistry* 2011, **19**(1):534-541.

153. Thompson JW, Narayanan SV, Perez-Pinzon MA: **Redox signaling pathways involved in neuronal ischemic preconditioning**. *Curr Neuropharmacol* 2012, **10**(4):354-369.

154. Wang W, Liu Z, Zhao L, Sun J, He Q, Yan W, Lu Z, Wang A: **Hexokinase 2 enhances the metastatic potential of tongue squamous cell carcinoma via the SOD2-H2O2 pathway**. *Oncotarget* 2016.

155. Huang CL, Chao CC, Lee YC, Lu MK, Cheng JJ, Yang YC, Wang VC, Chang WC, Huang NK: **Paraquat Induces Cell Death Through Impairing Mitochondrial Membrane Permeability**. *Mol Neurobiol* 2015.

156. Bonneh-Barkay D, Reaney SH, Langston WJ, Di Monte DA: **Redox cycling of the herbicide paraquat in microglial cultures**. *Molecular Brain Research* 2005(134):52-56.

157. Chinta SJ, Rane A, Poksay KS, Bredesen DE, Andersen JK, Rao RV: **Coupling endoplasmic reticulum stress to the cell death program in dopaminergic cells: effect of paraquat**. *Neuromolecular Med* 2008, **10**(4):333-342.

158. Huang C-L, Lee Y-C, Yang Y-C, Kuo T-Y, Huang N-K: **Minocycline prevents paraquat-induced cell death through attenuating endoplasmic reticulum stress and mitochondrial dysfunction**. *Toxicology Letters* 2012, **209**(3):203-210.

159. McCormack AL, Atienza JG, Johnston LC, Anderson JK, Vu S, Di Monte DA: **Role of oxidative stress in paraquat-induced dopaminergic cell degeneration**. *Journal of Neurochemistry* 2005, **93**:1030-1037.

160. Miller RL, Sun GY, Sun AY: **Cytotoxicity of paraquat in microglial cells: Involvement of pKC and ERK1/2 dependent NADPH oxidase**. *Brain Research* 2007, **1167**:129-139.

161. Castello PR, Dreschel DA, Patel M: **Mitochondria are a major source of paraquat-induced reactive oxygen species in the brain**. *Journal of Biological Chemistry* 2007, **382**(19):14186-14193.

162. Silva R, Carmo H, Vilas-Boas V, Barbosa DJ, Monteiro M, de Pinho PG, de Lourdes Bastos M, Remião F: **Several transport systems contribute to the intestinal uptake of Paraquat, modulating its cytotoxic effects**. *Toxicology Letters* 2015, **232**(1):271-283.

163. Shimizu K, Ohtaki K, Matsubara K, Aoyama K, Uezono T, Saito O, Suno M, Ogawa K, Hayase N, Kimura K *et al*: **Carrier-mediated processes in blood-brain barrier penetration and neural uptake of paraquat**. *Brain Research* 2001, **906**:135-402.

164. Lotharius J, Dugan LL, O'Malley KL: **Distinct mechanisms underlie neurotoxin-mediated cell death in cultured dopaminergic neurons**. *J Neurosci* 1999, **19**(4):1284-1293.

165. Mogi M, Harada M, Kondo T, Mizuno Y, Narabayashi H, Riederer P, Nagatsu T: **bcl-2 protein is increased in the brain from parkinsonian patients**. *Neurosci Lett* 1996, **215**(2):137-139.

166.	Kim RH, Smith PD, Aleyasin H, Hayley S, Mount MP, Pownall S, Wakeham A, You-Ten AJ, Kalia SK, Horne P *et al*: **Hypersensitivity of DJ-1-deficient mice to 1-methyl-4-phenyl-1,2,3,6-tetrahydropyrindine (MPTP) and oxidative stress**. *Proc Natl Acad Sci U S A* 2005, **102**(14):5215-5220.

167.	Rappold PM, Cui M, Chesser AS, Tibbett J, Grima JC, Duan L, Sen N, Javitch JA, Tieu K: **Paraquat neurotoxicity is mediated by the dopamine transporter and organic cation transporter-3**. *Proc Natl Acad Sci U S A* 2011, **108**(51):20766-20771.

168.	Nisar R, Hanson PS, He L, Taylor RW, Blain PG, Morris CM: **Diquat causes caspase-independent cell death in SH-SY5Y cells by production of ROS independently of mitochondria**. *Arch Toxicol* 2015.

169.	Breckenridge CB, Sturgess NC, Butt M, Wolf JC, Zadory D, Beck M, Mathews JM, Tisdel MO, Minnema D, Travis KZ *et al*: **Pharmacokinetic, neurochemical, stereological and neuropathological studies on the potential effects of paraquat in the substantia nigra pars compacta and striatum of male C57BL/6J mice**. *NeuroToxicology* 2013, **37**(0):1-14.

170.	Thiruchelvam M, Richfield EK, Goodman BM, Baggs RB, Cory-Slechta DA: **Developmental Exposure to the Pesticides Paraquat and Maneb and the Parkinson's Disease Phenotype**. *NeuroToxicology* 2002, **23**(4–5):621-633.

171.	Garbarino VR, Orr ME, Rodriguez KA, Buffenstein R: **Mechanisms of oxidative stress resistance in the brain: Lessons learned from hypoxia tolerant extremophilic vertebrates**. *Archives of Biochemistry and Biophysics* 2015, **576**:8-16.

172.	Yadav SK, Prakash J, Chouhan S, Singh SP: **Mucuna pruriens seed extract reduces oxidative stress in nigrostriatl tissue and improves neurobehavioral activity in paraquat-induced parkinsonian model**. *Neurochemistry International* 2013, **62**:1039-1047.

173.	Purisai MG, L. MA, Cumine S, Li J, Isla MZ, Di Monte DA: **Microglial activation as a priming event leading to paraquat-induced dopaminergic cell degeneration**. *Neurobiology of Disease* 2007, **25**:392-400.

174.	Minnema DJ, Travis KZ, Breckenridge CB, Sturgess NC, Butt M, Wolf JC, Zadory D, Beck MJ, Mathews JM, Tisdel MO *et al*: **Dietary administration of paraquat for 13 weeks does not result in a loss of dopaminergic neurons in the substantia nigra of C57BL/6J mice**. *Regulatory Toxicology and Pharmacology* 2014, **68**(2):250-258.

175.	Dey MS, Breeze RG, Hayton WL, Karara AH, Krieger RI: **Paraquat pharmacokinetics using a subcutaneous toxic low dose in the rat**. *Fundam Appl Toxicol* 1990, **14**(1):208-216.

176.	Lee S-J, Hwang AB, Kenyon C: **Inhibition of Respiration Extends C. elegans Life Span via Reactive Oxygen Species that Increase HIF-1 Activity**. *Current Biology* 2010, **20**(23):2131-2136.

177.	Yang W, Hekimi S: **A mitochondrial superoxide signal triggers increased longevity in Caenorhabditis elegans**. *PLoS Biol* 2010, **8**(12):e1000556.

178.	Hekimi S, Wang Y, Noe A: **Mitochondrial ROS and the Effectors of the Intrinsic Apoptotic Pathway in Aging Cells: The Discerning Killers!** *Front Genet* 2016, **7**:161.

179.	Merkwirth C, Jovaisaite V, Durieux J, Matilainen O, Jordan Sabine D, Quiros Pedro M, Steffen Kristan K, Williams Evan G, Mouchiroud L, Tronnes Sarah U *et al*: **Two Conserved Histone Demethylases Regulate Mitochondrial Stress-Induced Longevity**. *Cell* 2016, **165**(5):1209-1223.

180.	Schriner SE, Linford NJ, Martin GM, Treuting P, Ogburn CE, Emond M, Coskun PE, Ladiges W, Wolf N, Van Remmen H *et al*: **Extension of murine life span by overexpression of catalase targeted to mitochondria**. *Science* 2005, **308**(5730):1909-1911.

181.   Rea SL, Ventura N, Johnson TE: **Relationship between mitochondrial electron transport chain dysfunction, development, and life extension in Caenorhabditis elegans**. *PLoS Biol* 2007, **5**(10):e259.

182.   Sandström von Tobel J, Zoia D, Althaus J, Antinori P, Mermoud J, Pak HS, Scherl A, Monnet-Tschudi F: **Immediate and delayed effects of subchronic Paraquat exposure during an early differentiation stage in 3D-rat brain cell cultures**. *Toxicology Letters* 2014, **230**(2):188-197.

183.   Cherry C, Thompson B, Saptarshi N, Wu J, Hoh J: **2016: A 'Mitochondria' Odyssey**. *Trends in Molecular Medicine* 2016, **22**(5):391-403.

184.   Wang H, Dharmalingam P, Vasquez V, Mitra J, Boldogh I, Rao KS, Kent TA, Mitra S, Hegde ML: **Chronic oxidative damage together with genome repair deficiency in the neurons is a double whammy for neurodegeneration: Is damage response signaling a potential therapeutic target?** *Mechanisms of Ageing and Development*.

185.   He W, Cui L, Zhang C, Zhang X, He J, Xie Y, Chen Y: **Sonic hedgehog promotes neurite outgrowth of cortical neurons under oxidative stress: Involving of mitochondria and energy metabolism**. *Experimental Cell Research* 2017, **350**(1):83-90.

186.   Tian Y, Garcia G, Bian Q, Steffen Kristan K, Joe L, Wolff S, Meyer Barbara J, Dillin A: **Mitochondrial Stress Induces Chromatin Reorganization to Promote Longevity and UPRmt**. *Cell* 2016, **165**(5):1197-1208.

187.   Doynova MD, Berretta A, Jones MB, Jasoni CL, Vickers MH, O'Sullivan JM: **Interactions between mitochondrial and nuclear DNA in mammalian cells are non-random**. *Mitochondrion* 2016, **30**:187-196.

188.   Garcia-Prat L, Martinez-Vicente M, Perdiguero E, Ortet L, Rodriguez-Ubreva J, Rebollo E, Ruiz-Bonilla V, Gutarra S, Ballestar E, Serrano AL *et al*: **Autophagy maintains stemness by preventing senescence**. *Nature* 2016, **529**(7584):37-42.

189.   Liu B, Du Q, Chen L, Fu G, Li S, Fu L, Zhang X, Ma C, Bin C: **CpG methylation patterns of human mitochondrial DNA**. *Sci Rep* 2016, **6**:23421.

190.   Iacobazzi V, Castegna A, Infantino V, Andria G: **Mitochondrial DNA methylation as a next-generation biomarker and diagnostic tool**. *Molecular Genetics and Metabolism* 2013, **110**(1–2):25-34.

191.   Pawar T, Eide L: **Pitfalls in mitochondrial epigenetics**. *Mitochondrial DNA A DNA Mapp Seq Anal* 2016:1-10.

192.   Infantino V, Castegna A, Iacobazzi F, Spera I, Scala I, Andria G, Iacobazzi V: **Impairment of methyl cycle affects mitochondrial methyl availability and glutathione level in Down's syndrome**. *Molecular Genetics and Metabolism* 2011, **102**(3):378-382.

193.   Dzitoyeva S, Chen H, Manev H: **Effect of aging on 5-hydroxymethylcytosine in brain mitochondria**. *Neurobiology of Aging* 2012, **33**(12):2881-2891.

194.   Shock LS, Thakkar PV, Peterson EJ, Moran RG, Taylor SM: **DNA methyltransferase 1, cytosine methylation, and cytosine hydroxymethylation in mammalian mitochondria**. *Proc Natl Acad Sci U S A* 2011, **108**(9):3630-3635.

195.   Byun HM, Colicino E, Trevisi L, Fan T, Christiani DC, Baccarelli AA: **Effects of Air Pollution and Blood Mitochondrial DNA Methylation on Markers of Heart Rate Variability**. *J Am Heart Assoc* 2016, **5**(4).

196.   Mawlood SK, Dennany L, Watson N, Dempster J, Pickard BS: **Quantification of global mitochondrial DNA methylation levels and inverse correlation with age at two CpG sites**. *Aging (Albany NY)* 2016, **8**(4):636-641.

197. Choi YS, Hoon Jeong J, Min HK, Jung HJ, Hwang D, Lee SW, Kim Pak Y: **Shot-gun proteomic analysis of mitochondrial D-loop DNA binding proteins: identification of mitochondrial histones**. *Mol Biosyst* 2011, **7**(5):1523-1536.
198. Chatterjee A, Seyfferth J, Lucci J, Gilsbach R, Preissl S, Böttinger L, Mårtensson CU, Panhale A, Stehle T, Kretz O *et al*: **MOF Acetyl Transferase Regulates Transcription and Respiration in Mitochondria**. *Cell* 2016, **167**(3):722-738.e723.
199. Buenrostro JD, Wu B, Chang HY, Greenleaf WJ: **ATAC-seq: A Method for Assaying Chromatin Accessibility Genome-Wide**. *Curr Protoc Mol Biol* 2015, **109**:21.29.21-29.
200. Hui L, Chen X, Haughey NJ, Geiger JD: **Role of endolysosomes in HIV-1 Tat-induced neurotoxicity**. *ASN Neuro* 2012, **4**(4):243-252.
201. Assenov Y, Müller F, Lutsik P, Walter J, Lengauer T, Bock C: **Comprehensive analysis of DNA methylation data with RnBeads**. *Nature Methods* 2014, **11**:1138-1140.
202. Kim D, Langmead B, Salzberg SL: **HISAT: a fast spliced aligner with low memory requirements**. *Nat Methods* 2015, **12**(4):357-360.
203. Liao Y, Smyth GK, Shi W: **The Subread aligner: fast, accurate and scalable read mapping by seed-and-vote**. *Nucleic Acids Res* 2013, **41**(10):e108.
204. Shen S, Park JW, Lu ZX, Lin L, Henry MD, Wu YN, Zhou Q, Xing Y: **rMATS: robust and flexible detection of differential alternative splicing from replicate RNA-Seq data**. *Proc Natl Acad Sci U S A* 2014, **111**(51):E5593-5601.
205. Riemens RJM, Soares ES, Esteller M, Delgado-Morales R: **Stem Cell Technology for (Epi)genetic Brain Disorders**. *Adv Exp Med Biol* 2017, **978**:443-475.
206. Daulatzai MA: **Dysfunctional Sensory Modalities, Locus Coeruleus, and Basal Forebrain: Early Determinants that Promote Neuropathogenesis of Cognitive and Memory Decline and Alzheimer's Disease**. *Neurotox Res* 2016, **30**(3):295-337.
207. Gu J, Liu Y, Kyritsis AP, Bondy ML: **Molecular epidemiology of primary brain tumors**. *Neurotherapeutics* 2009, **6**(3):427-435.
208. Schapira AHV, Chaudhuri KR, Jenner P: **Non-motor features of Parkinson disease**. *Nat Rev Neurosci* 2017.
209. Levin BE, Tomer R, Rey GJ: **Cognitive impairments in Parkinson's disease**. *Neurol Clin* 1992, **10**(2):471-485.
210. Bauckneht M, Arnaldi D, Nobili F, Aarsland D, Morbelli S: **New tracers and new perspectives for molecular imaging in Lewy body diseases**. *Curr Med Chem* 2017.
211. Giesert F, Glasl L, Zimprich A, Ernst L, Piccoli G, Stautner C, Zerle J, Hölter SM, Vogt Weisenhorn DM, Wurst W: **The pathogenic LRRK2 R1441C mutation induces specific deficits modeling the prodromal phase of Parkinson's disease in the mouse**. *Neurobiology of Disease*.
212. Erer S, Egeli U, Zarifoglu M, Tezcan G, Cecener G, Tunca B, Ak S, Demirdogen E, Kenangil G, Kaleagası H *et al*: **Mutation analysis of the PARKIN, PINK1, DJ1, and SNCA genes in Turkish early-onset Parkinson's patients and genotype-phenotype correlations**. *Clinical Neurology and Neurosurgery* 2016, **148**:147-153.
213. Martin JE, Nguyen TT, Grunseich C, Nofziger JH, Lee PR, Fields D, Fischbeck KH, Foran E: **Decreased Motor Neuron Support by SMA Astrocytes due to Diminished MCP1 Secretion**. *J Neurosci* 2017, **37**(21):5309-5318.
214. Pan M-R, Peng G, Hung W-C, Lin S-Y: **Monoubiquitination of H2AX Protein Regulates DNA Damage Response Signaling**. 2011.
215. Singh I, Ozturk N, Cordero J, Mehta A, Hasan D, Cosentino C, Sebastian C, Kruger M, Looso M, Carraro G *et al*: **High mobility group protein-mediated transcription requires DNA damage marker gamma-H2AX**. *Cell Res* 2015, **25**(7):837-850.

216. Gonzalez-Hunt CP, Leung MC, Bodhicharla RK, McKeever MG, Arrant AE, Margillo KM, Ryde IT, Cyr DD, Kosmaczewski SG, Hammarlund M *et al*: **Exposure to mitochondrial genotoxins and dopaminergic neurodegeneration in Caenorhabditis elegans**. In: *PLoS One. Volume 9*, edn. United States; 2014: e114459.

217. Shitasako S, Ito Y, Ito R, Ueda Y, Shimizu Y, Ohshima T: **Wnt and Shh signals regulate neural stem cell proliferation and differentiation in the optic tectum of adult zebrafish**. *Dev Neurobiol* 2017.

218. Galloway DA, Williams JB, Moore CS: **Effects of fumarates on inflammatory human astrocyte responses and oligodendrocyte differentiation**. *Ann Clin Transl Neurol* 2017, **4**(6):381-391.

219. Wlodarczyk A, Cedile O, Jensen KN, Jasson A, Mony JT, Khorooshi R, Owens T: **Pathologic and Protective Roles for Microglial Subsets and Bone Marrow- and Blood-Derived Myeloid Cells in Central Nervous System Inflammation**. *Front Immunol* 2015, **6**:463.

220. Etchevers HC, Vincent C, Le Douarin NM, Couly GF: **The cephalic neural crest provides pericytes and smooth muscle cells to all blood vessels of the face and forebrain**. *Development* 2001, **128**(7):1059-1068.

221. Trost A, Lange S, Schroedl F, Bruckner D, Motloch KA, Bogner B, Kaser-Eichberger A, Strohmaier C, Runge C, Aigner L *et al*: **Brain and Retinal Pericytes: Origin, Function and Role**. *Front Cell Neurosci* 2016, **10**:20.

222. Smolders SM, Swinnen N, Kessels S, Arnauts K, Smolders S, Le Bras B, Rigo JM, Legendre P, Brone B: **Age-specific function of alpha5beta1 integrin in microglial migration during early colonization of the developing mouse cortex**. *Glia* 2017, **65**(7):1072-1088.

223. Shi H, Gong Y, Qiang L, Li X, Zhang S, Gao J, Li K, Ji X, Tian L, Gu X *et al*: **Derivation of Schwann cell precursors from neural crest cells resident in bone marrow for cell therapy to improve peripheral nerve regeneration**. *Biomaterials* 2016, **89**:25-37.

224. Jessen KR, Mirsky R: **The origin and development of glial cells in peripheral nerves**. *Nat Rev Neurosci* 2005, **6**(9):671-682.

225. Adamsky A, Goshen I: **Astrocytes in memory function: Pioneering findings and future directions**. *Neuroscience*.

226. Liu B, Teschemacher AG, Kasparov S: **Astroglia as a cellular target for neuroprotection and treatment of neuro-psychiatric disorders**. *Glia* 2017.

227. Paolicelli RC, Ferretti MT: **Function and Dysfunction of Microglia during Brain Development: Consequences for Synapses and Neural Circuits**. *Front Synaptic Neurosci* 2017, **9**:9.

228. Yin Z, Raj D, Saiepour N, Van Dam D, Brouwer N, Holtman IR, Eggen BJL, Möller T, Tamm JA, Abdourahman A *et al*: **Immune hyperreactivity of Aβ plaque-associated microglia in Alzheimer's disease**. *Neurobiology of Aging* 2017, **55**:115-122.

229. Shinozaki Y, Shibata K, Yoshida K, Shigetomi E, Gachet C, Ikenaka K, Tanaka KF, Koizumi S: **Transformation of Astrocytes to a Neuroprotective Phenotype by Microglia via P2Y1 Receptor Downregulation**. *Cell Rep* 2017, **19**(6):1151-1164.

230. Kawabe K, Takano K, Moriyama M, Nakamura Y: **Microglia Endocytose Amyloid beta Through the Binding of Transglutaminase 2 and Milk Fat Globule EGF Factor 8 Protein**. *Neurochem Res* 2017.

231. Osorio-Querejeta I, Saenz-Cuesta M, Munoz-Culla M, Otaegui D: **Models for Studying Myelination, Demyelination and Remyelination**. *Neuromolecular Med* 2017.

232. Jackson S, ElAli A, Virgintino D, Gilbert MR: **Blood-brain barrier pericyte importance in malignant gliomas: what we can learn from stroke and Alzheimer's disease**. *Neuro Oncol* 2017.

233. Domev H, Milkov I, Itskovitz-Eldor J, Dar A: **Immunoevasive pericytes from human pluripotent stem cells preferentially modulate induction of allogeneic regulatory T cells**. *Stem Cells Transl Med* 2014, **3**(10):1169-1181.

234. Monif M, Reid CA, Powell KL, Drummond KJ, O'Brien TJ, Williams DA: **Interleukin-1beta has trophic effects in microglia and its release is mediated by P2X7R pore**. *J Neuroinflammation* 2016, **13**(1):173.

235. Mendiola AS, Cardona AE: **The IL-1beta phenomena in neuroinflammatory diseases**. *J Neural Transm (Vienna)* 2017.

236. Bocchini V, Mazzolla R, Barluzzi R, Blasi E, Sick P, Kettenmann H: **An immortalized cell line expresses properties of activated microglial cells**. *J Neurosci Res* 1992, **31**(4):616-621.

237. Asanuma M, Miyazaki I, Murakami S, Diaz-Corrales FJ, Ogawa N: **Striatal astrocytes act as a reservoir for L-DOPA**. *PLoS One* 2014, **9**(9):e106362.

238. Xu J, Dong H, Qian Q, Zhang X, Wang Y, Jin W, Qian Y: **Astrocyte-derived CCL2 participates in surgery-induced cognitive dysfunction and neuroinflammation via evoking microglia activation**. *Behavioural Brain Research* 2017, **332**:145-153.

239. Dobson-Belaire WN, Cochrane A, Ostrowski MA, Gray-Owen SD: **Differential Response of Primary and Immortalized CD4+ T Cells to Neisseria gonorrhoeae-Induced Cytokines Determines the Effect on HIV-1 Replication**. In: *PLoS One. Volume 6*, edn.; 2011.

240. Unger RE, Krump-Konvalinkova V, Peters K, Kirkpatrick CJ: **In Vitro Expression of the Endothelial Phenotype: Comparative Study of Primary Isolated Cells and Cell Lines, Including the Novel Cell Line HPMEC-ST1.6R**. *Microvascular Research* 2002, **64**(3):384-397.

241. Pan C, Kumar C, Bohl S, Klingmueller U, Mann M: **Comparative Proteomic Phenotyping of Cell Lines and Primary Cells to Assess Preservation of Cell Type-specific Functions**. 2009.

242. Hidema S, Fukuda T, Date S, Tokitake Y, Matsui Y, Sasaki H, Nishimori K: **Transgenic expression of Telomerase reverse transcriptase (Tert) improves cell proliferation of primary cells and enhances reprogramming efficiency into the induced pluripotent stem cell**. *http://dxdoiorg/101080/0916845120161191330* 2016.

243. Birck C, Koncina E, Heurtaux T, Glaab E, Michelucci A, Heuschling P, Grandbarbe L: **Transcriptomic analyses of primary astrocytes under TNFα treatment**. *Genomics Data* 2016, **7**:7-11.

244. Chen C, Jin J, Lee GA, Silva E, Donoghue M: **Cross-species functional analyses reveal shared and separate roles for Sox11 in frog primary neurogenesis and mouse cortical neuronal differentiation**. 2016.

245. Gnad F, Doll S, Manning G, Arnott D, Zhang Z: **Bioinformatics analysis of thousands of TCGA tumors to determine the involvement of epigenetic regulators in human cancer**. *BMC Genomics* 2015, **16**(8):1.

246. Ryotokuji T, Yamaguchi H, Ueki T, Usuki K, Kurosawa S, Kobayashi Y, Kawata E, Tajika K, Gomi S, Kanda J *et al*: **Clinical characteristics and prognosis of acute myeloid leukemia associated with DNA-methylation regulatory gene mutations**. 2016.

247. Das Partha P, Hendrix David A, Apostolou E, Buchner Alice H, Canver Matthew C, Beyaz S, Ljuboja D, Kuintzle R, Kim W, Karnik R *et al*: **PRC2 Is Required to Maintain Expression**

of the Maternal Gtl2-Rian-Mirg Locus by Preventing De Novo DNA Methylation in Mouse Embryonic Stem Cells. *Cell Reports* 2015, **12**(9):1456-1470.

248.   Rush M, Appanah R, Lee S, Lam LL, Goyal P, Lorincz MC: **Targeting of EZH2 to a defined genomic site is sufficient for recruitment of Dnmt3a but not de novo DNA methylation**. *http://dxdoiorg/104161/epi469392* 2009.

249.   Shu L, Sun W, Li L, Xu Z, Lin L, Xie P, Shen H, Huang L, Xu Q, Jin P *et al*: **Genome-wide alteration of 5-hydroxymenthylcytosine in a mouse model of Alzheimer's disease**. *BMC Genomics* 2016, **17**(1):1.

250.   Dong E, Tueting P, Matrisciano F, Grayson DR, Guidotti A: **Behavioral and molecular neuroepigenetic alterations in prenatally stressed mice: relevance for the study of chromatin remodeling properties of antipsychotic drugs**. *Translational Psychiatry* 2016, **6**(1).

251.   Haque MM, Nilsson EE, Holder LB, Skinner MK: **Genomic Clustering of differential DNA methylated regions (epimutations) associated with the epigenetic transgenerational inheritance of disease and phenotypic variation**. *BMC Genomics* 2016, **17**(1):1.

252.   Li E, Bestor TH, Jaenisch R: **Targeted mutation of the DNA methyltransferase gene results in embryonic lethality**. *Cell* 1992, **69**(6):915-926.

253.   Haruta M, Shimada M, Nishiyama A, Johmura Y, Le Tallec B, Debatisse M, Nakanishi M: **Loss of maintenance DNA methylation results in abnormal DNA origin firing during DNA replication**. *Biochemical and Biophysical Research Communications* 2016, **469**(4):960-966.

254.   Koya J, Kataoka K, Sato T, Bando M, Kato Y, Tsuruta-Kishino T, Kobayashi H, Narukawa K, Miyoshi H, Shirahige K *et al*: **DNMT3A R882 mutants interact with polycomb proteins to block haematopoietic stem and leukaemic cell differentiation**. *Nature Communications* 2016, **7**.

255.   Branco Miguel R, King M, Perez-Garcia V, Bogutz Aaron B, Caley M, Fineberg E, Lefebvre L, Cook Simon J, Dean W, Hemberger M *et al*: **Maternal DNA Methylation Regulates Early Trophoblast Development**. *Developmental Cell* 2016, **36**(2):152-163.

256.   Ooi SKT, Qiu C, Bernstein E, Li K, Jia D, Yang Z, Erdjument-Bromage H, Tempst P, Lin S-P, Allis CD *et al*: **DNMT3L connects unmethylated lysine 4 of histone H3 to de novo methylation of DNA**. *Nature* 2007, **448**(7154):714-717.

257.   von Meyenn F, Iurlaro M, Habibi E, Liu Ning Q, Salehzadeh-Yazdi A, Santos F, Petrini E, Milagre I, Yu M, Xie Z *et al*: **Impairment of DNA Methylation Maintenance Is the Main Cause of Global Demethylation in Naive Embryonic Stem Cells**. *Molecular Cell*.

258.   Tahiliani M, Koh KP, Shen Y, Pastor WA, Bandukwala H, Brudno Y, Agarwal S, Iyer LM, Liu DR, Aravind L *et al*: **Conversion of 5-Methylcytosine to 5-Hydroxymethylcytosine in Mammalian DNA by MLL Partner TET1**. 2009.

259.   Ito S, Shen L, Dai Q, Wu SC, Collins LB, Swenberg JA, He C, Zhang Y: **Tet Proteins Can Convert 5-Methylcytosine to 5-Formylcytosine and 5-Carboxylcytosine**. 2011.

260.   Ito S, Shen L, Dai Q, Wu SC, Collins LB, Swenberg JA, He C, Zhang Y: **Tet proteins can convert 5-methylcytosine to 5-formylcytosine and 5-carboxylcytosine**. *Science* 2011, **333**(6047):1300-1303.

261.   He Y-F, Li B-Z, Li Z, Liu P, Wang Y, Tang Q, Ding J, Jia Y, Chen Z, Li L *et al*: **Tet-Mediated Formation of 5-Carboxylcytosine and Its Excision by TDG in Mammalian DNA**. 2011.

262.   Mahmud N, Petro B, Baluchamy S, Li X, Taioli S, Lavelle D, Quigley JG, Suphangul M, Araki H: **Differential Effects of Epigenetic Modifiers on the Expansion and Maintenance of Human Cord Blood Stem/Progenitor Cells**. *Biology of Blood and Marrow Transplantation* 2014, **20**(4):480-489.

263. de Waal E, Mak W, Calhoun S, Stein P, Ord T, Krapp C, Coutifaris C, Schultz RM, Bartolomei MS: **In vitro culture increases the frequency of stochastic epigenetic errors at imprinted genes in placental tissues from mouse concepti produced through assisted reproductive technologies**. *Biol Reprod* 2014, **90**(2):22.

264. Lee PT, Li WJ: **Chondrogenesis of Embryonic Stem Cell-Derived Mesenchymal Stem Cells Induced by TGFbeta1 and BMP7 through Increased TGFbeta Receptor Expression and Endogenous TGFbeta1 Production**. *J Cell Biochem* 2016.

265. Pourgholaminejad A, Aghdami N, Baharvand H, Moazzeni SM: **The effect of pro-inflammatory cytokines on immunophenotype, differentiation capacity and immunomodulatory functions of human mesenchymal stem cells**. *Cytokine* 2016, **85**:51-60.

266. Ye D, Li T, Heraud P, Parnpai R: **Effect of Chromatin-Remodeling Agents in Hepatic Differentiation of Rat Bone Marrow-Derived Mesenchymal Stem Cells In Vitro and In Vivo**. *Stem Cells Int* 2016, **2016**:3038764.

267. Zhu Y, Song X, Wang J, Li Y, Yang Y, Yang T, Ma H, Wang L, Zhang G, Cho WC *et al*: **Placental mesenchymal stem cells of fetal origin deposit epigenetic alterations during long-term culture under serum-free condition**. *Expert Opin Biol Ther* 2015, **15**(2):163-180.

268. Horvath S: **DNA methylation age of human tissues and cell types**. *Genome Biology* 2013, **14**(10):1.

269. Koch CM, Joussen S, Schellenberg A, Lin Q, Zenke M, Wagner W: **Monitoring of cellular senescence by DNA-methylation at specific CpG sites**. *Aging Cell* 2012, **11**(2):366-369.

270. Weidner CI, Walenda T, Lin Q, Wölfler MM, Denecke B, Costa IG, Zenke M, Wagner W: **Hematopoietic Stem and Progenitor Cells Acquire Distinct DNA-Hypermethylation During in vitro Culture**. *Scientific Reports, Published online: 28 November 2013; | doi:101038/srep03372* 2013.

271. Grace CE, Kim SJ, Rogers JM: **Maternal influences on epigenetic programming of the developing hypothalamic-pituitary-adrenal axis**. *Birth Defects Res A Clin Mol Teratol* 2011, **91**(8):797-805.

272. Lardenoije R, Iatrou A, Kenis G, Kompotis K, Steinbusch HWM, Mastroeni D, Coleman P, Lemere CA, Hof PR, van den Hove DLA *et al*: **The epigenetics of aging and neurodegeneration**. *Progress in Neurobiology* 2015, **131**:21-64.

273. Jeyapalan JN, Doctor GT, Jones TA, Alberman SN, Tep A, Haria CM, Schwalbe EC, Morley IC, Hill AA, LeCain M *et al*: **DNA methylation analysis of paediatric low-grade astrocytomas identifies a tumour-specific hypomethylation signature in pilocytic astrocytomas**. *Acta Neuropathol Commun* 2016, **4**(1):54.

274. Lu J, Cowperthwaite MC, Burnett MG, Shpak M: **Molecular Predictors of Long-Term Survival in Glioblastoma Multiforme Patients**. *PLoS One* 2016, **11**(4):e0154313.

275. Masliah E, Dumaop W, Glasako D, Desplats P: **Distinctive patterns of DNA methylation associated with Parkinson's disease Identification of concordant epigenetic changes in brain and peripheral blood leukocytes**. *Epigenetics* 2013, **8**(10):103-1038.

276. Coppieters N, Dieriks BV, Lill C, Faull RLM, Curtis MA, Dragunow M: **Global changes in DNA methylation and hydroxymethylation in Alzheimer's disease human brain**. *Neurobiology of Aging* 2014, **35**(6):1334-1344.

277. Zhang Y, Sloan SA, Clarke LE, Caneda C, Plaza CA, Blumenthal PD, Vogel H, Steinberg GK, Edwards MS, Li G *et al*: **Purification and Characterization of Progenitor and Mature Human Astrocytes Reveals Transcriptional and Functional Differences with Mouse**. *Neuron* 2016, **89**(1):37-53.

278. Pieper C, Marek JJ, Unterberg M, Schwerdtle T, Galla HJ: **Brain capillary pericytes contribute to the immune defense in response to cytokines or LPS in vitro**. *Brain Res* 2014, **1550**:1-8.

279. Mata M, Alessi D, Fink DJ: **S100 is preferentially distributed in myelin-forming Schwann cells**. *J Neurocytol* 1990, **19**(3):432-442.

280. Haimoto H, Hosoda S, Kato K: **Differential distribution of immunoreactive S100-alpha and S100-beta proteins in normal nonnervous human tissues**. *Lab Invest* 1987, **57**(5):489-498.

281. Triolo D, Dina G, Lorenzetti I, Malaguti M, Morana P, Carro UD, Comi G, Messing A, Quattrini A, Previtali SC: **Loss of glial fibrillary acidic protein (GFAP) impairs Schwann cell proliferation and delays nerve regeneration after damage**. 2006.

282. Langevin SM, Eliot M, Butler RA, Cheong A, Zhang X, McClean MD, Koestler DC, Kelsey KT: **CpG island methylation profile in non-invasive oral rinse samples is predictive of oral and pharyngeal carcinoma**. *Clin Epigenetics* 2015, **7**:125.

283. Moarii M, Boeva V, Vert JP, Reyal F: **Changes in correlation between promoter methylation and gene expression in cancer**. *BMC Genomics* 2015, **16**(1):873.

284. Izadpanah R, Kaushal D, Kriedt C, Tsien F, Patel B, Dufour J, Bunnell BA: **Long-term In vitro Expansion Alters the Biology of Adult Mesenchymal Stem Cells**. 2008.

285. Nakamura T, Hosoyama T, Murakami J, Samura M, Ueno K, Kurazumi H, Suzuki R, Mikamo A, Hamano K: **Age-related increase in Wnt inhibitor causes a senescence-like phenotype in human cardiac stem cells**. *Biochemical and Biophysical Research Communications* 2017, **487**(3):653-659.

286. Petrini S, Borghi R, D'Oria V, Restaldi F, Moreno S, Novelli A, Bertini E, Compagnucci C: **Aged induced pluripotent stem cell (iPSCs) as a new cellular model for studying premature aging**. *Aging (Albany NY)* 2017, **9**(5):1453-1469.

287. Pavlou MAS, Outeiro TF: **Epigenetics in Parkinson's Disease**. *Adv Exp Med Biol* 2017, **978**:363-390.

288. Morgan S, Shatunov A, Sproviero W, Jones AR, Shoai M, Hughes D, Al Khleifat A, Malaspina A, Morrison KE, Shaw PJ *et al*: **A comprehensive analysis of rare genetic variation in amyotrophic lateral sclerosis in the UK**. *Brain* 2017, **140**(6):1611-1618.

289. Nesi G, Sestito S, Digiacomo M, Rapposelli S: **Oxidative Stress, Mitochondrial Abnormalities and Proteins Deposition: Multitarget Approaches in Alzheimer's Disease**. *Curr Top Med Chem* 2017.

290. Nock TG, Chouinard-Watkins R, Plourde M: **Carriers of an apolipoprotein E epsilon 4 allele are more vulnerable to a dietary deficiency in omega-3 fatty acids and cognitive decline**. *Biochimica et Biophysica Acta (BBA) - Molecular and Cell Biology of Lipids*.

291. Karaca I, Wagner H, Ramirez A: **[Search for risk genes in Alzheimer's disease]**. *Nervenarzt* 2017, **88**(7):744-750.

292. Alexandrov LB, Nik-Zainal S, Wedge DC, Aparicio SA, Behjati S, Biankin AV, Bignell GR, Bolli N, Borg A, Borresen-Dale AL *et al*: **Signatures of mutational processes in human cancer**. *Nature* 2013, **500**(7463):415-421.

293. El-Ayadi M, Ansari M, Sturm D, Gielen GH, Warmuth-Metz M, Kramm CM, von Bueren AO: **High-grade glioma in very young children: a rare and particular patient population**. *Oncotarget* 2017.

294. Chen M, Chang CH, Tao L, Lu C: **Residential Exposure to Pesticide During Childhood and Childhood Cancers: A Meta-Analysis**. *Pediatrics* 2015, **136**(4):719-729.

295. Allen MT, Levy LS: **Parkinson's disease and pesticide exposure--a new assessment**. *Crit Rev Toxicol* 2013, **43**(6):515-534.

296. Yan D, Zhang Y, Liu L, Yan H: **Pesticide exposure and risk of Alzheimer's disease: a systematic review and meta-analysis**. *Sci Rep* 2016, **6**:32222.

297. Vettorazzi G: **International Regulatory Aspects for Pesticide**

Chemicals. In., vol. I: CRC Press; 1979.

298. Raff MC, Abney ER, Cohen J, Lindsay R, Noble M: **Two types of astrocytes in cultures of developing rat white matter: differences in morphology, surface gangliosides, and growth characteristics**. *J Neurosci* 1983, **3**(6):1289-1300.

299. Bushong EA, Martone ME, Ellisman MH: **Maturation of astrocyte morphology and the establishment of astrocyte domains during postnatal hippocampal development**. *International Journal of Developmental Neuroscience* 2004, **22**(2):73-86.

300. Miller RH, Raff MC: **Fibrous and protoplasmic astrocytes are biochemically and developmentally distinct**. *J Neurosci* 1984, **4**(2):585-592.

301. Thery C, Hetier E, Evrard C, Mallat M: **Expression of macrophage colony-stimulating factor gene in the mouse brain during development**. *J Neurosci Res* 1990, **26**(1):129-133.

302. Elmore Monica RP, Najafi Allison R, Koike Maya A, Dagher Nabil N, Spangenberg Elizabeth E, Rice Rachel A, Kitazawa M, Matusow B, Nguyen H, West Brian L *et al*: **Colony-Stimulating Factor 1 Receptor Signaling Is Necessary for Microglia Viability, Unmasking a Microglia Progenitor Cell in the Adult Brain**. *Neuron* 2014, **82**(2):380-397.

303. Horiuchi M, Wakayama K, Itoh A, Kawai K, Pleasure D, Ozato K, Itoh T: **Interferon regulatory factor 8/interferon consensus sequence binding protein is a critical transcription factor for the physiological phenotype of microglia**. *J Neuroinflammation* 2012, **9**:227.

304. Pellegrino MW, Nargund AM, Haynes CM: **Signaling the mitochondrial unfolded protein response**. *Biochimica et Biophysica Acta (BBA) - Molecular Cell Research* 2013, **1833**(2):410-416.

305. Yang W, Tiffany-Castiglioni E, Koh HC, Son I-H: **Paraquat activates the IRE1/ASK1/JNK cascade associated with apoptosis in human neuroblastoma SH-SY5Y cells**. *Toxicology Letters* 2009, **191**(2):203-210.

306. Pecina-Slaus N, Kafka A, Varosanec AM, Markovic L, Krsnik Z, Njiric N, Mrak G: **Expression patterns of Wnt signaling component, secreted frizzledrelated protein 3 in astrocytoma and glioblastoma**. *Mol Med Rep* 2016, **13**(5):4245-4251.

307. Schiefer L, Visweswaran M, Perumal V, Arfuso F, Groth D, Newsholme P, Warrier S, Dharmarajan A: **Epigenetic regulation of the secreted frizzled-related protein family in human glioblastoma multiforme**. *Cancer Gene Ther* 2014, **21**(7):297-303.

308. Panbianco C, Weinkove D, Zanin E, Jones D, Divecha N, Gotta M, Ahringer J: **A Casein Kinase 1 and PAR Proteins Regulate Asymmetry of a PIP2 Synthesis Enzyme for Asymmetric Spindle Positioning**. *Developmental Cell* 2008, **15**(2):198-208.

309. Strathmann M, Wilkie TM, Simon MI: **Alternative splicing produces transcripts encoding two forms of the alpha subunit of GTP-binding protein Go**. *Proc Natl Acad Sci U S A* 1990, **87**(17):6477-6481.

310. Pei X, Zhang J, Wu L, Lu B, Zhang X, Yang D, Liu J: **The down-regulation of GNAO1 and its promoting role in hepatocellular carcinoma**. *Biosci Rep* 2013, **33**(5).

311. Main BS, Zhang M, Brody KM, Ayton S, Frugier T, Steer D, Finkelstein D, Crack PJ, Taylor JM: **Type-1 interferons contribute to the neuroinflammatory response and disease progression of the MPTP mouse model of Parkinson's disease**. *Glia* 2016, **64**(9):1590-1604.

312. Silginer M, Nagy S, Happold C, Schneider H, Weller M, Roth P: **Autocrine activation of the IFN signaling pathway may promote immune escape in glioblastoma**. *Neuro Oncol* 2017.

313. Kang K, Lee SW, Han JE, Choi JW, Song MR: **The complex morphology of reactive astrocytes controlled by fibroblast growth factor signaling**. *Glia* 2014, **62**(8):1328-1344.

314. Pringle NP, Yu WP, Howell M, Colvin JS, Ornitz DM, Richardson WD: **Fgfr3 expression by astrocytes and their precursors: evidence that astrocytes and oligodendrocytes originate in distinct neuroepithelial domains**. *Development* 2003, **130**(1):93-102.

315. Yang X, Steinberg F, Zhuang L, Bessey R, Trueb B: **Receptor FGFRL1 does not promote cell proliferation but induces cell adhesion**. *Int J Mol Med* 2016, **38**(1):30-38.

316. Tsuchiya S, Fujiwara T, Sato F, Shimada Y, Tanaka E, Sakai Y, Shimizu K, Tsujimoto G: **MicroRNA-210 regulates cancer cell proliferation through targeting fibroblast growth factor receptor-like 1 (FGFRL1)**. *J Biol Chem* 2011, **286**(1):420-428.

317. Saarimaki-Vire J, Peltopuro P, Lahti L, Naserke T, Blak AA, Vogt Weisenhorn DM, Yu K, Ornitz DM, Wurst W, Partanen J: **Fibroblast growth factor receptors cooperate to regulate neural progenitor properties in the developing midbrain and hindbrain**. *J Neurosci* 2007, **27**(32):8581-8592.

318. Su N, Yang J, Xie Y, Du X, Lu X, Yin Z, Yin L, Qi H, Zhao L, Feng J *et al*: **Gain-of-function mutation of FGFR3 results in impaired fracture healing due to inhibition of chondrocyte differentiation**. *Biochem Biophys Res Commun* 2008, **376**(3):454-459.

319. Kim DY, Hong GU, Ro JY: **Signal pathways in astrocytes activated by cross-talk between of astrocytes and mast cells through CD40-CD40L**. *J Neuroinflammation* 2011, **8**:25.

320. Michels M, Danieslki LG, Vieira A, Florentino D, Dall'Igna D, Galant L, Sonai B, Vuolo F, Mina F, Pescador B *et al*: **CD40–CD40 Ligand Pathway Is a Major Component of Acute Neuroinflammation and Contributes to Long-term Cognitive Dysfunction after Sepsis**. In: *Mol Med. Volume 21*, edn.; 2015: 219-226.

321. Chonan M, Saito R, Shoji T, Shibahara I, Kanamori M, Sonoda Y, Watanabe M, Kikuchi T, Ishii N, Tominaga T: **CD40/CD40L expression correlates with the survival of patients with glioblastomas and an augmentation in CD40 signaling enhances the efficacy of vaccinations against glioma models**. *Neuro Oncol* 2015, **17**(11):1453-1462.

322. Ogundele OM, Ebenezer PJ, Lee CC, Francis J: **Stress-altered synaptic plasticity and DAMP signaling in the hippocampus-PFC axis; elucidating the significance of IGF-1/IGF-1R/CaMKIIα expression in neural changes associated with a prolonged exposure therapy**. *Neuroscience* 2017, **353**:147-165.

323. Takeuchi S, Katoh H, Negishi M: **Eph/ephrin reverse signalling induces axonal retraction through RhoA/ROCK pathway**. *J Biochem* 2015, **158**(3):245-252.

324. Kullander K, Klein R: **Mechanisms and functions of Eph and ephrin signalling**. *Nat Rev Mol Cell Biol* 2002, **3**(7):475-486.

325. Lu Q, Sun EE, Klein RS, Flanagan JG: **Ephrin-B reverse signaling is mediated by a novel PDZ-RGS protein and selectively inhibits G protein-coupled chemoattraction**. *Cell* 2001, **105**(1):69-79.

326. Tamamaki N, Fujimori K, Nojyo Y, Kaneko T, Takauji R: **Evidence that Sema3A and Sema3F regulate the migration of GABAergic neurons in the developing neocortex**. *J Comp Neurol* 2003, **455**(2):238-248.

327. Nakayama H, Bruneau S, Kochupurakkal N, Coma S, Briscoe DM, Klagsbrun M: **Regulation of mTOR Signaling by Semaphorin 3F-Neuropilin 2 Interactions In Vitro and In Vivo**. *Sci Rep* 2015, **5**:11789.

328.   Li YH, Fu HL, Tian ML, Wang YQ, Chen W, Cai LL, Zhou XH, Yuan HB: **Neuron-derived FGF10 ameliorates cerebral ischemia injury via inhibiting NF-kappaB-dependent neuroinflammation and activating PI3K/Akt survival signaling pathway in mice**. *Sci Rep* 2016, **6**:19869.

329.   Stanimirovic D, Zhang W, Howlett C, Lemieux P, Smith C: **Inflammatory gene transcription in human astrocytes exposed to hypoxia: roles of the nuclear factor-kappaB and autocrine stimulation**. *J Neuroimmunol* 2001, **119**(2):365-376.

330.   del Fresno C, Otero K, Gomez-Garcia L, Gonzalez-Leon MC, Soler-Ranger L, Fuentes-Prior P, Escoll P, Baos R, Caveda L, Garcia F *et al*: **Tumor cells deactivate human monocytes by up-regulating IL-1 receptor associated kinase-M expression via CD44 and TLR4**. *J Immunol* 2005, **174**(5):3032-3040.

331.   Varghese RT, Liang Y, Guan T, Franck CT, Kelly DF, Sheng Z: **Survival kinase genes present prognostic significance in glioblastoma**. *Oncotarget* 2016, **7**(15):20140-20151.

332.   Choy KR, Watters DJ: **Neurodegeneration in ataxia-telangiectasia: Multiple roles of ATM kinase in cellular homeostasis**. *Dev Dyn* 2017.

333.   Quek H, Luff J, Cheung K, Kozlov S, Gatei M, Lee CS, Bellingham MC, Noakes PG, Lim YC, Barnett NL *et al*: **Rats with a missense mutation in Atm display neuroinflammation and neurodegeneration subsequent to accumulation of cytosolic DNA following unrepaired DNA damage**. *J Leukoc Biol* 2017, **101**(4):927-947.

334.   Li Y, Li L, Wu Z, Wang L, Wu Y, Li D, Ma U, Shao J, Yu H, Wang D: **Silencing of ATM expression by siRNA technique contributes to glioma stem cell radiosensitivity in vitro and in vivo**. *Oncol Rep* 2017.

335.   Tomimatsu N, Mukherjee B, Harris JL, Boffo FL, Hardebeck M, Potts PR, Khanna KK, Burma S: **DNA damage-induced Degradation of EXO1 Limits DNA End Resection to Ensure Accurate DNA Repair**. *J Biol Chem* 2017.

336.   Vairapandi M, Balliet AG, Hoffman B, Liebermann DA: **GADD45b and GADD45g are cdc2/cyclinB1 kinase inhibitors with a role in S and G2/M cell cycle checkpoints induced by genotoxic stress**. *J Cell Physiol* 2002, **192**(3):327-338.

337.   Ma DK, Jang MH, Guo JU, Kitabatake Y, Chang ML, Pow-Anpongkul N, Flavell RA, Lu B, Ming GL, Song H: **Neuronal activity-induced Gadd45b promotes epigenetic DNA demethylation and adult neurogenesis**. *Science* 2009, **323**(5917):1074-1077.

338.   Engelmann A, Speidel D, Bornkamm GW, Deppert W, Stocking C: **Gadd45 beta is a pro-survival factor associated with stress-resistant tumors**. *Oncogene* 2008, **27**(10):1429-1438.

339.   Nomura K, Klejnot M, Kowalczyk D, Hock AK, Sibbet GJ, Vousden KH, Huang DT: **Structural analysis of MDM2 RING separates degradation from regulation of p53 transcription activity**. *Nat Struct Mol Biol* 2017.

340.   Saji S, Nakashima S, Hayashi S, Toi M, Nozawa Y: **Overexpression of MDM2 in MCF-7 promotes both growth advantage and p53 accumulation in response to estradiol**. *Jpn J Cancer Res* 1999, **90**(2):210-218.

341.   Haupt Y, Maya R, Kazaz A, Oren M: **Mdm2 promotes the rapid degradation of p53**. *Nature* 1997, **387**(6630):296-299.

342.   Sun Y, Cao L, Sheng X, Chen J, Zhou Y, Yang C, Deng T, Ma H, Feng P, Liu J *et al*: **WDR79 promotes the proliferation of non-small cell lung cancer cells via USP7-mediated regulation of the Mdm2-p53 pathway**. *Cell Death Dis* 2017, **8**(4):e2743.

343.   Kim M, Ryu K-Y: **Regulation of REST levels overcomes dysregulation of neural stem cell differentiation caused by disruption of polyubiquitin gene Ubb**. *Biochemical and Biophysical Research Communications* 2017, **486**(1):171-177.

344. Noga M, Hayashi T: **Ubiquitin gene expression following transient forebrain ischemia**. *Molecular Brain Research* 1996, **36**(2):261-267.

345. Tao YK, Yu PL, Bai YP, Yan ST, Zhao SP, Zhang GQ: **Role of PERK/eIF2alpha/CHOP Endoplasmic Reticulum Stress Pathway in Oxidized Low-density Lipoprotein Mediated Induction of Endothelial Apoptosis**. *Biomed Environ Sci* 2016, **29**(12):868-876.

346. Quiros PM, Prado MA, Zamboni N, D'Amico D, Williams RW, Finley D, Gygi SP, Auwerx J: **Multi-omics analysis identifies ATF4 as a key regulator of the mitochondrial stress response in mammals**. *J Cell Biol* 2017.

347. Fiorese Christopher J, Schulz Anna M, Lin Y-F, Rosin N, Pellegrino Mark W, Haynes Cole M: **The Transcription Factor ATF5 Mediates a Mammalian Mitochondrial UPR**. *Current Biology* 2016, **26**(15):2037-2043.

348. Persengiev SP, Devireddy LR, Green MR: **Inhibition of apoptosis by ATFx: a novel role for a member of the ATF/CREB family of mammalian bZIP transcription factors**. *Genes Dev* 2002, **16**(14):1806-1814.

349. Castedo M, Ferri KF, Kroemer G: **Mammalian target of rapamycin (mTOR): pro- and anti-apoptotic**. *Cell Death Differ* 2002, **9**(2):99-100.

350. Sofer A, Lei K, Johannessen CM, Ellisen LW: **Regulation of mTOR and cell growth in response to energy stress by REDD1**. *Mol Cell Biol* 2005, **25**(14):5834-5845.

351. Pinto JA, Rolfo C, Raez LE, Prado A, Araujo JM, Bravo L, Fajardo W, Morante ZD, Aguilar A, Neciosup SP *et al*: **In silico evaluation of DNA Damage Inducible Transcript 4 gene (DDIT4) as prognostic biomarker in several malignancies**. *Sci Rep* 2017, **7**(1):1526.

352. Yang Z, Liu F, Qu H, Wang H, Xiao X, Deng H: **1, 25(OH)2D3 protects β cell against high glucose-induced apoptosis through mTOR suppressing**. *Molecular and Cellular Endocrinology* 2015, **414**:111-119.

353. Pardini AW, Nguyen HT, Figlewicz DP, Baskin DG, Williams DL, Kim F, Schwartz MW: **Distribution of insulin receptor substrate-2 in brain areas involved in energy homeostasis**. *Brain Research* 2006, **1112**(1):169-178.

354. Chen J, Deng F, Singh SV, Wang QJ: **Protein kinase D3 (PKD3) contributes to prostate cancer cell growth and survival through a PKCepsilon/PKD3 pathway downstream of Akt and ERK 1/2**. *Cancer Res* 2008, **68**(10):3844-3853.

355. Chen J, Shen Q, Labow M, Gaither LA: **Protein kinase D3 sensitizes RAF inhibitor RAF265 in melanoma cells by preventing reactivation of MAPK signaling**. *Cancer Res* 2011, **71**(12):4280-4291.

356. He JH, Li BX, Han ZP, Zou MX, Wang L, Lv YB, Zhou JB, Cao MR, Li YG, Zhang JZ: **Snail-activated long non-coding RNA PCA3 up-regulates PRKD3 expression by miR-1261 sponging, thereby promotes invasion and migration of prostate cancer cells**. *Tumour Biol* 2016.

357. Kyrkou A, Soufi M, Bahtz R, Ferguson C, Bai M, Parton RG, Hoffmann I, Zerial M, Fotsis T, Murphy C: **RhoD participates in the regulation of cell-cycle progression and centrosome duplication**. *Oncogene* 2013, **32**(14):1831-1842.

358. Blom M, Reis K, Heldin J, Kreuger J, Aspenström P: **The atypical Rho GTPase RhoD is a regulator of actin cytoskeleton dynamics and directed cell migration**. *Experimental Cell Research* 2017, **352**(2):255-264.

359. Park SY, Jin ML, Ko MJ, Park G, Choi YW: **Anti-neuroinflammatory Effect of Emodin in LPS-Stimulated Microglia: Involvement of AMPK/Nrf2 Activation**. *Neurochem Res* 2016, **41**(11):2981-2992.

360. Zhao B, Qiang L, Joseph J, Kalyanaraman B, Viollet B, He Y-Y: **Mitochondrial dysfunction activates the AMPK signaling and autophagy to promote cell survival**. *Genes & Diseases* 2016, **3**(1):82-87.

361. Mori K, Ozaki E, Zhang B, Yang L, Yokoyama A, Takeda I, Maeda N, Sakanaka M, Tanaka J: **Effects of norepinephrine on rat cultured microglial cells that express α1, α2, β1 and β2 adrenergic receptors**. *Neuropharmacology* 2002, **43**(6):1026-1034.

362. Tanaka KF, Kashima H, Suzuki H, Ono K, Sawada M: **Existence of functional beta1- and beta2-adrenergic receptors on microglia**. *J Neurosci Res* 2002, **70**(2):232-237.

363. Ardestani PM, Evans AK, Yi B, Nguyen T, Coutellier L, Shamloo M: **Modulation of neuroinflammation and pathology in the 5XFAD mouse model of Alzheimer's disease using a biased and selective beta-1 adrenergic receptor partial agonist**. *Neuropharmacology* 2017, **116**:371-386.

364. Ito D, Imai Y, Ohsawa K, Nakajima K, Fukuuchi Y, Kohsaka S: **Microglia-specific localisation of a novel calcium binding protein, Iba1**. *Molecular Brain Research* 1998, **57**(1):1-9.

365. Kim Y, Andres Salazar Hernandez M, Herrema H, Delibasi T, Park SW: **The role of BRD7 in embryo development and glucose metabolism**. *J Cell Mol Med* 2016, **20**(8):1561-1570.

366. Heo JI, Kim W, Choi KJ, Bae S, Jeong JH, Kim KS: **XIAP-associating factor 1, a transcriptional target of BRD7, contributes to endothelial cell senescence**. *Oncotarget* 2016, **7**(5):5118-5130.

367. Zhao R, Liu Y, Wang H, Yang J, Niu W, Fan S, Xiong W, Ma J, Li X, Phillips JB *et al*: **BRD7 plays an anti-inflammatory role during early acute inflammation by inhibiting activation of the NF-small ka, CyrillicB signaling pathway**. *Cell Mol Immunol* 2016.

368. D'Antoni S, Ranno E, Spatuzza M, Cavallaro S, Catania MV: **Endothelin-1 Induces Degeneration of Cultured Motor Neurons Through a Mechanism Mediated by Nitric Oxide and PI3K/Akt Pathway**. *Neurotox Res* 2017.

369. Asiimwe N, Yeo SG, Kim MS, Jung J, Jeong NY: **Nitric Oxide: Exploring the Contextual Link with Alzheimer's Disease**. *Oxid Med Cell Longev* 2016, **2016**:7205747.

370. Xu P, Huang MW, Xiao CX, Long F, Wang Y, Liu SY, Jia WW, Wu WJ, Yang D, Hu JF *et al*: **Matairesinol Suppresses Neuroinflammation and Migration Associated with Src and ERK1/2-NF-kappaB Pathway in Activating BV2 Microglia**. *Neurochem Res* 2017.

371. Takano K, Ishida N, Kawabe K, Moriyama M, Hibino S, Choshi T, Hori O, Nakamura Y: **A dibenzoylmethane derivative inhibits lipopolysaccharide-induced NO production in mouse microglial cell line BV-2**. *Neurochemistry International*.

372. Chen H, Ishii A, Wong WK, Chen LB, Lo SH: **Molecular characterization of human tensin**. *Biochem J* 2000, **351 Pt 2**:403-411.

373. Shih Y-P, Sun P, Wang A, Lo SH: **Tensin1 positively regulates RhoA activity through its interaction with DLC1**. *Biochimica et Biophysica Acta (BBA) - Molecular Cell Research* 2015, **1853**(12):3258-3265.

374. Haynie DT, Xue B: **Superdomains in the protein structure hierarchy: The case of PTP-C2**. *Protein Sci* 2015, **24**(5):874-882.

375. Sampino S, Stankiewicz AM, Zacchini F, Goscik J, Szostak A, Swiergiel AH, Drago G, Modlinski JA, Ptak GE: **Pregnancy at Advanced Maternal Age Affects Behavior and Hippocampal Gene Expression in Mouse Offspring**. *J Gerontol A Biol Sci Med Sci* 2017.

376. Silver DJ, Steindler DA: **Common astrocytic programs during brain development, injury and cancer**. *Trends in Neurosciences* 2009, **32**(6):303-311.

377. Faria J, Romão L, Martins S, Alves T, Mendes FA, de Faria GP, Hollanda R, Takiya C, Chimelli L, Morandi V *et al*: **Interactive properties of human glioblastoma cells with brain neurons in culture and neuronal modulation of glial laminin organization**. *Differentiation* 2006, **74**(9):562-572.

378. Ben-Porath I, Thomson MW, Carey VJ, Ge R, Bell GW, Regev A, Weinberg RA: **An embryonic stem cell-like gene expression signature in poorly differentiated aggressive human tumors**. *Nat Genet* 2008, **40**(5):499-507.

379. Gavrieli Y, Sherman Y, Ben-Sasson SA: **Identification of programmed cell death in situ via specific labeling of nuclear DNA fragmentation**. *J Cell Biol* 1992, **119**(3):493-501.

380. Roos WP, Kaina B: **DNA damage-induced cell death by apoptosis**. *Trends in Molecular Medicine* 2006, **12**(9):440-450.

381. Laplante M, Sabatini David M: **mTOR Signaling in Growth Control and Disease**. *Cell* 2012, **149**(2):274-293.

382. Ye XZ, Xu SL, Xin YH, Yu SC, Ping YF, Chen L, Xiao HL, Wang B, Yi L, Wang QL *et al*: **Tumor-associated microglia/macrophages enhance the invasion of glioma stem-like cells via TGF-beta1 signaling pathway**. *J Immunol* 2012, **189**(1):444-453.

383. Yang R, Liu S, Zhou J, Bu S, Zhang J: **Andrographolide attenuates microglia-mediated Abeta neurotoxicity partially through inhibiting NF-kappaB and JNK MAPK signaling pathway**. *Immunopharmacol Immunotoxicol* 2017:1.

384. Yang HM, Yang S, Huang SS, Tang BS, Guo JF: **Microglial Activation in the Pathogenesis of Huntington's Disease**. *Front Aging Neurosci* 2017, **9**:193.

385. He Q, Wang Q, Yuan C, Wang Y: **Downregulation of miR-7116-5p in microglia by MPP+ sensitizes TNF-alpha production to induce dopaminergic neuron damage**. *Glia* 2017, **65**(8):1251-1263.

386. Ribatti D, Nico B, Crivellato E, Artico M: **Development of the blood-brain barrier: a historical point of view**. *Anat Rec B New Anat* 2006, **289**(1):3-8.

387. Goasdoué K, Miller SM, Colditz PB, Björkman ST: **Review: The blood-brain barrier; protecting the developing fetal brain**. *Placenta* 2017, **54**:111-116.

388. Bernacki J, Dobrowolska A, Nierwinska K, Malecki A: **Physiology and pharmacological role of the blood-brain barrier**. *Pharmacol Rep* 2008, **60**(5):600-622.

389. Saunders NR, Daneman R, Dziegielewska KM, Liddelow SA: **Transporters of the blood–brain and blood–CSF interfaces in development and in the adult**. *Molecular Aspects of Medicine* 2013, **34**(2):742-752.

390. Bartlett RM, Holden JE, Nickles RJ, Murali D, Barbee DL, Barnhart TE, Christian BT, DeJesus OT: **Paraquat is excluded by the blood brain barrier in rhesus macaque: An in vivo pet study**. *Brain Research* 2009, **1259**:74-79.

391. Kurtovic-Kozaric A, Mehinovic L, Malesevic R, Mesanovic S, Jaros T, Stomornjak-Vukadin M, Mackic-Djurovic M, Ibrulj S, Kurtovic-Basic I, Kozaric M: **Ten-year trends in prevalence of Down syndrome in a developing country: impact of the maternal age and prenatal screening**. *European Journal of Obstetrics & Gynecology and Reproductive Biology* 2016, **206**:79-83.

392. Bayrampour H, Heaman M: **Advanced maternal age and the risk of cesarean birth: a systematic review**. *Birth* 2010, **37**(3):219-226.